SYNTHESIS OF FOLATE- TARGETED POLY(ETHYLENE GLYCOL)-BASED CONJUGATES AND THEIR PRECURSORS

A Dissertation

Presented to

The Graduate Faculty of The University of Akron

In Partial Fulfillment

of the Requirements for the Degree

Doctor of Philosophy

Prajakatta Mulay

December, 2019

SYNTHESIS OF FOLATE-TARGETED POLY(ETHYLENE GLYCOL)-BASED CONJUGATES AND THEIR PRECURSORS

Prajakatta Mulay

Dissertation

Approved:	Accepted:
_____	_____
Advisor Dr Lingyun Liu	Department Chair Dr. H. Michael Cheung
_____	_____
Committee Member Dr. Jie Zheng	Dean of College Dr. Craig Menzemer
_____	_____
Committee Member Dr. Rebecca Kuntz Willits	Dean of the Graduate School Dr. Chand Midha
_____	_____
Committee Member Dr. Chrys Wesdemiotis	Date
_____	
Committee Member Dr. Mark Soucek	

ABSTRACT

Breast Cancer is the most common cancer among women and nearly 1 in every 8 American women suffer from it. Triple negative breast cancer, a type of breast cancer that can be only treated using chemotherapy, affects nearly 20% of the breast cancer diagnosed women. Early detection of breast cancer increases survival rates among patients. This dissertation discusses the development of a new two-functional folate-targeted poly(ethylene glycol)(PEG)-based fluorescein-labeled conjugate (FA-FL-PEG-FL-FA) for potential applications in selective diagnosis of triple negative breast cancer.

Since folate, or vitamin B_9, receptors (FRs) are overexpressed in breast cancer cells, the diagnosis of these cells is targeted by using a γ-thiolated folic acid (FA-γ-SH) as the targeting precursor. α-carboxyl group present on folate is necessary for binding with the FRs, therefore, exclusive γ-thiolation was achieved by using *n*-butyllithium that selectively forms the lithium salt (FA-γ-Li) at the γ-carboxyl position due to its higher pKa. The subsequent thiolation was achieved by reducing FA-γ-S-S-γ-FA, which was prepared by reacting a dibrominated disulphide compound (Br-S-S-Br, synthesized via enzyme-catalyzed transesterification) with FA-γ-Li. To increase the retention time in the body and improve the solubility of the agent in water, functionalized PEGs were used as the hydrophilic linkers. Diamine, dithiol, and dibromide functionalization of PEGs were achieved using novel enzyme (*Candida antartica* Lipase B)-catalyzed esterifications and transesterifications.

Specifically, three strategies to synthesize FA-FL-PEG-FL-FA were investigated for their synthetic convenience and feasibility. Strategy 1 used diamine-functionalized PEG (H_2N-PEG-NH_2), Strategy 2 used dithiol-functionalized PEG (HS-PEG-SH), and Strategy 3 used dibromide-functionalized PEG (Br-PEG-Br) as the precursors. The first strategy and the third strategy were not successful owing to not quantitatively yielding the intermediate products. Two-functional folate-targeted PEG-based fluorescein-labeled conjugates (FA-FL-PEG-FL-FA) with tetraethylene glycol, PEG with M_n = 1000 g/mol and 2050 g/mol, and discreet PEG (MW = 898 g/mol, Đ = 1) as the hydrophilic linkers were successfully synthesized using the second strategy.

The enzyme-catalyzed Michael addition of thiol-functionalized PEGs to Sefose and the synthesis of cyclic polydisulfide polymers made using Reversible Redox Ring Polymerization (R3P) was also investigated and is discussed in this dissertation. In addition, my NSF-sponsored internship report is also presented in the appendices.

DEDICATION

This dissertation is dedicated to my family: my constant source of strength, support, and love; my father, Balkrishna Mulay; my mother, Nayana Mulay; and my lovely sister, Kasturi; for always believing in me.

ACKNOWLEDGEMENTS

I offer my profound gratitude to Dr. Judit E. Puskas for giving me an opportunity to pursue this research. I gratefully acknowledge her guidance, which helped me during the course of my project completion. It is because of her efforts that I received an opportunity to pursue an internship at Philpott Rubber Company. I also wish to thank her for providing me a chance to work on multiple projects of inter-disciplinary nature.

I would also like to thank my committee members, Dr. Lingyun Liu, Dr. Jie Zheng, Dr. Rebecca Willits, Dr. Chrys Wesdemiotis, and Dr. Mark Soucek for providing encouraging and constructive feedback. I am indebted to Dr. Shivakumar Sastry for his constant kind support and invaluable mentorship during my graduate studies.

Additionally, I would like to thank all my past and present hard-working group members; their positive attitude inspired me not to give up. I would like to specially thank Dr Sanghamitra Sen for her invaluable guidance, insightful discussions, and her friendship. Thank you Andrew, Jozsef, Gayatri, and Aditya for the help, support, and wonderful memories that made this journey easier.

Finally, I am grateful to my parents and all of my friends, for their unconditional love, generosity, and support. Thank you Krutika, my roommate for 5 years, for constantly inspiring me, motivating me, and always being there. I would also like to thank Rishabh, for constantly providing me support from a distance. And finally, thank you Amal for your unconditional support and care in the crucial times. Thank you all!

TABLE OF CONTENTS

Page

LIST OF FIGURES

LIST OF TABLES

CHAPTER I

INTRODUCTION

The motivation of this dissertation is to develop a diagnostic agent that has a potential to diagnose triple negative breast cancer (TNBC). The principal objective of this investigation is to synthesize 2-functional folate-targeted poly(ethylene glycol)-based agents with a potential for TNBC diagnosis. This dissertation primarily discusses the chemo-enzymatic synthesis and characterization of functionalized poly(ethylene glycol)s and thiol-functionalized folic acid as precursors in the development of these agents.

Cancer caused nearly 600,000 deaths in the US in 2018. Among them, breast cancer has the highest number of occurrences in women followed closely by lung cancer. Breast cancer resulted in over 40,000 deaths in 2016 and nearly 330,000 new cases are expected in 2019 in the US.[1] We decided to focus on TNBC in which the tumor cells overexpress folate receptors (FRs), that are responsible for metabolizing folic acid (FA), on their surface. However, other cancers may also be targeted.

The delivery of protein conjugated imaging molecules to cancer cells via FR-mediated endocytosis was first investigated in 1991, after which research on the targeted delivery of folic acid conjugated imaging agents and drugs to FR-overexpressing cancer cells was reported extensively.[2] In addition, folic acid was also conjugated with synthetic polymers in order to make folic acid conjugated agents hydrophilic, increase their circulation time in the body, and also confer multivalency to it.[3] The efficacy of multivalent folic acid-conjugated agents was evaluated

thoroughly with poly(amido amine) (PAMAM)-base. When an average of 2.6 folic acid molecules were attached to PAMAM-based diagnostic and therapeutic agent, a 2500-fold enhancement in binding to FRs was observed over free folic acid. Maximum efficiency was achieved at about 5 folate groups per molecule, but the improvement from 2 to 5 was much less than from 1 to two.[4]

Against this background, our group investigated the *in vitro* performance of a diagnostic agent with PEG-base and two folic acid molecules attached to it (FA-FL-PEG-FL-FA). Poly(ethylene glycol) (PEG) is a hydrophilic, non-toxic, and bio-compatible polymer that is well-suited as a linker. Our group demonstrated that the solubility of folic acid increases by 2000 times when a PEG molecule is attached to it.[5] In case of imaging agents, fluorescein is widely used for *in vitro* testing of diagnostic agents.[6] Fluorescein (FL) has high quantum efficiency in aqueous media that makes it convenient for application in *in vitro* screenings. FA-FL-PEG-FL-FA was compared with diagnostic agents without PEG-base and with two folic acid molecules (FA-FL) and one folic acid molecule (FA-FL) attached to it. FA-FL-PEG-FL-FA had the best performance (unpublished data). Based on this preliminary screening, we designed more effective synthetic routes for the synthesis of PEG-based compounds. Specifically, we synthesized FA-FL-PEG_{2000}-FL-FA, FA-FL-PEG_{1000}-FL-FA, and FA-FL-$dPEG_{898}$-FL-FA where dPEG ("discreet PEG") is a monodisperse polymer. We used chemo-enzymatic processes that were pioneered by the Puskas group.[7-15]

The synthetic strategy developed is shown in Figure 1.1. In this strategy, PEG-dithiol (HS-PEG-SH) is reacted with 2 equivalents of Fluorescein-*o*-acrylate (FLA) via enzyme-catalyzed Michael addition and subsequent acrylation to obtain an acrylated fluorescein-labeled PEG (Ac-FL-PEG-FL-Ac). The Ac-FL-PEG-FL-Ac is

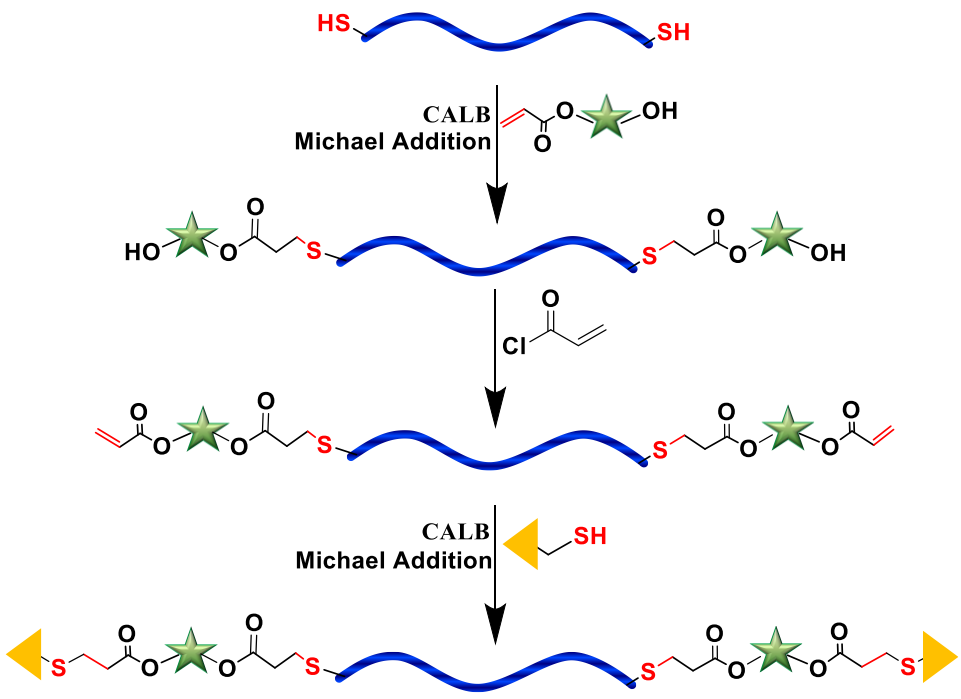

Figure 1.1 Synthetic strategy for two-functional PEG-based folate-targeted diagnostic agent

then reacted with 2 equivalents of a thiol-functionalized folic acid (FA-SH) via *Candida antartica* Lipase B (CALB)-catalyzed Michael addition to obtain FA-FL-PEG-FL-FA.

My thesis is focused on the synthesis of thiol-functionalized PEGs and FA, and my participation in the syntheses of the compounds listed above in close collaboration with my group-mate Gayatri Shrikhande. I also developed a new method to synthesize amine-functionalized PEG. I will also discuss the enzyme-catalyzed Michael addition of thiol-functionalized PEGs to Sefose, a multifunctional fatty acid provided by Dr. Dean Webster from North Dakota State University. I also participated in the synthesis of polydisulfide rings from dithiols, a project sponsored by the Department of Energy (DOE). The Appendix will present the results of my NSF-sponsored internship with Philpott Rubber Company. The Background section will present relevant literature data.

CHAPTER II

BACKGROUND

This chapter will present background information on folate-targeted diagnostic agents, sucrose ester of soybean oil, and cyclic polydisulfide polymers.

2.1. Folate-targeted Cancer Diagnostic Agents

This section will provide background information pertaining to folate-targeted cancer diagnostic agents that includes elaboration on types of breast cancer known, using folic acid as the targeting molecule for selectively targeting cancer cells, and literature reported on folate-targeted diagnostic agents. Background information explaining multivalent folate-targeting and its application in diagnostics and chemotherapy with polymers, based on which the objective of this dissertation is formed, will also be discussed. This section will also elaborate on our group's pioneering work in enzyme-catalyzed functionalization of poly(ethylene glycol)s, a technique that was used to prepare the polymer backbone of the diagnostic agents. The synthetic strategy and *in vitro* testing performed at the Cleveland Clinic pertaining to one PEG-based diagnostic agent with two folate targeting groups, in comparison with folate-containing small molecules will also be discussed.

2.1.1. Types of Breast Cancer

Breast cancer can be molecularly sub-classified into hormone receptor-positive and hormone-receptor negative breast cancer, which is also known as Triple Negative Breast Cancer (TNBC). Hormone-receptor positive breast cancer cells are over-expressed in hormone-receptors such as estrogen, progesterone, and human epidermal growth factor receptor-2 and are treated using hormone therapy.[1] However, TNBC, that comprises about 20% of all breast cancer types, does not over-express these hormone-receptors and is treated using traditional chemotherapy that also affects healthy cells.[16] Therefore, development of effective targeted diagnostics and therapies is desirable. Even though the hormone-receptors are not over-expressed on TNBC tumor cells, vitamin receptors are over-expressed because the tumor cells require nutrients such as riboflavin (vitamin B_2), biotin (vitamin B_7), folic acid (vitamin B_9), and cobalamin (vitamin B_{12}) to facilitate their rapid growth.[17] These vitamin receptors can act as biomarkers or targets for selective targeting of tumor cells with diagnostic molecules. Folate receptors (FRs) were reported to be over-expressed in 86% of the TNBC cases.[18] Therefore, FR qualify as a good potential biomarker for targeted diagnostics of TNBC.

2.1.2. Folic Acid as Targeting Molecule

FA has a high affinity for FR with an extremely low dissociation constant of 0.01 nM.[4] FA is internalized in the living cells via folate-mediated endocytosis. The TNBC cells aggressively compete with the normal cells to internalize the FA due to the over-expression of FRs on TNBC cells.[19] Therefore, FA offers an avenue for its use as a targeting agent in diagnostic and therapeutic molecules to treat breast cancer.

Leamon and Low were the pioneers in using FA as a targeting agent.[20] They studied the uptake of folate-conjugated proteins, which are inherently macromolecular in nature, by KB (FR-positive human epidermal carcinoma) cells. They reported that any protein can be non-destructively delivered to a living cell by a natural vitamin endocytosis pathway by covalently attaching FA to it. FA was covalently conjugated to ribonuclease (RNase, 13.7 kDa), horseradish peroxidase (HRP, 40 kDa), bovine serum albumin (BSA, 68 kDa), and IgG (160 kDa) using 1-ethyl-3-(3-dimethylaminopropyl)carbodiimide (EDC) catalyst and subsequently reacting it with the polypeptide backbone of the protein to produce an amide bond. They observed spectrophotometrically that nearly 1-10 FA molecules were covalently conjugated to each protein molecule. Fluorescein isothiocyanate (FITC) and ^{125}I were conjugated with these proteins for fluorescent labelling and radio-labelling, respectively. KB cells were treated with FA- conjugated-FITC labelled bovine IgG (IgG-FITC-folate) and just FITC labelled IgG (IgG-FITC). IgG-FITC-folate was observed to bind readily to the tumor cell surface within 5 minutes of incubation and gradual internalization was observed over a period of several hours. In contrast, FITC-IgG did not show binding or internalization with the cells when treated for the same time.

They also studied the binding and internalization of folate-conjugated ^{125}I-BSA to KB tumor cells. They reported that ^{125}I-BSA-folate at 10 μg/ml concentration demonstrated nearly 300% increase in binding to the KB cells when compared to ^{125}I-BSA. To verify whether proteins retain their activity after internalizing into the living cells by folate-mediated endocytosis, HRP-folate conjugate and HRP alone was incubated with KB cells. They observed that the cells treated with HRP-folate conjugate

were stained whereas the cells treated with HRP alone remained colorless when staining was performed for detection of HRP. Therefore, they concluded that internalized proteins retain their activity in the KB cells when they enter via folate-mediated endocytosis pathway.

Lee and Low[21] extended this work by tethering FA to a lipid bilayer that forms liposomes, via PEG spacer ($M_n \cong$ 3.35K g/mol), to demonstrate that liposome-encapsulated molecules can also be used for targeting KB tumor cells. This was the first example of conjugating FA to a synthetic polymer (PEG), although its function was that of a spacer. The folate-PEG-liposome with fluorescent calcein conjugate contained on the average ~365 covalently attached folates and exhibited a 66 ± 13 nm mean diameter. They reported that the KB cells did not uptake the liposome in the absence of FA conjugation. However, free FA competed with FA-conjugated liposomes and prevented its binding completely at 0.1 M FA concentration.

FA offers multiple advantages to use as a targeting agent. It is stable during storage, has low immunogenicity and small size (Formula Weight FW = 441.4 g/mol), and is readily available inexpensively.[22] FA has two sites available for conjugation, i.e., the α- and the γ-carboxyl sites that are illustrated in Figure 2.1. The two carboxyl sites can be distinguished by their pKa values, which are 2.5 (α-) and 4.5 (γ-).[23] The γ-carboxyl site has to be reacted for further attachment to a drug or an imaging agent. This is because when the α-carboxyl site is conjugated to a diagnostic agent or drug, it leaves the FA-conjugated agent bio-inactive.[24]

Figure 2.2 shows the number of FA molecules bound per KB cell when deferroxamine (DF) drug is conjugated to FA either at the α-carboxyl position or the γ-

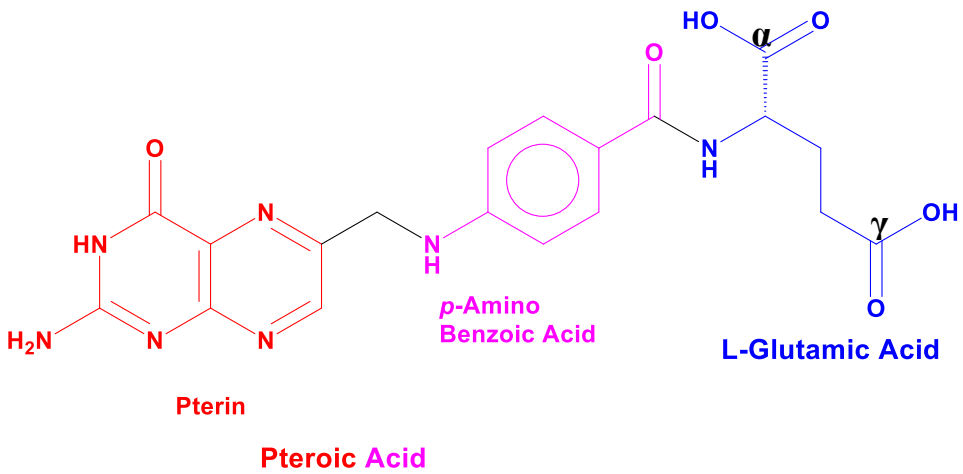

Figure 2.1. Folic Acid Structure

carboxyl position. Wang *et al* covalently conjugated deferroxamine (DF) drug to folic acid at the α-carboxyl position and the γ-carboxyl position separately and they incubated the DF-α-folate and DF-γ-folate with KB cancer cells.[25] They reported that DF-α-folate demonstrated nearly negligible binding affinity to tumor cells. Therefore, for effective FR binding FA needs to be conjugated at its γ-carboxyl group.[25]

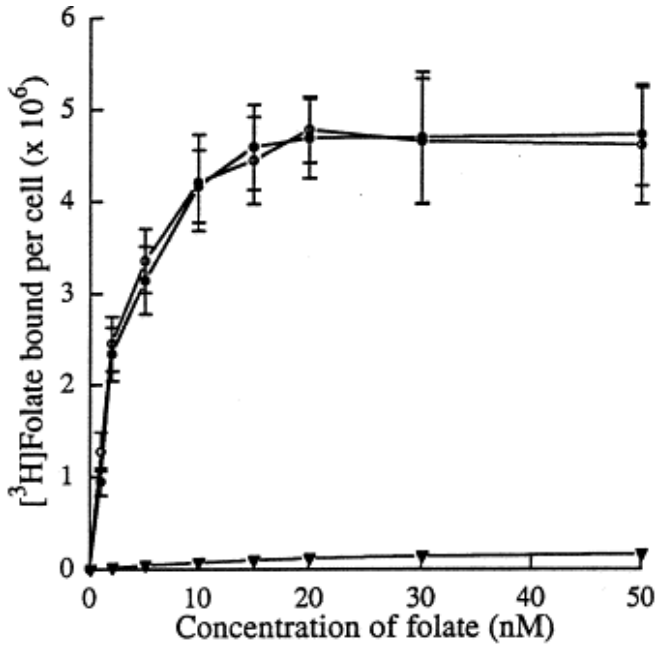

Figure 2.2 Affinities of the tritium-labeled DF-folate(α)(▾), DF-folate(γ) (•), and folic acid (○) for FRs on KB cells. Reprinted with permission from *Journal of Controlled Release* **1998**, *53(1)*, 39-48

2.1.3. Folic Acid Conjugated Diagnostic Agents

Folate-conjugated molecules have been reported for selective diagnosis of breast cancer cells. Overall, they can be classified into monovalent folate-targeted diagnostics and multivalent folate-targeted diagnostics.

In monovalent folate targeted diagnostics, one FA molecule is attached to an imaging molecule via a spacer. This spacer can be either a small molecule or it can be a polymer. Based on the type of spacer, the monovalent folate targeted diagnostics can be further classified into (i) folate-small molecule conjugates and (ii) folate-polymer conjugates which are discussed below.

In folate-conjugated diagnostic molecules, the imaging agent or the polymer may be tethered via a disulphide, an ester bond, or an amide bond. The disulphide bond is cleaved via its reduction done by the thiol group containing molecules (glutathione) already present inside the cytoplasm to release the imaging molecule or the polymer.26 The most synthetically convenient method to tether an imaging molecule or a polymer is via a carboxylic ester linker or an amide linker. The ester bonds release the diagnostic agent or drug through its hydrolysis done by the hydrolysing endosomes present inside the cell.[26, 27] The amide bond is stronger and is not as easily broken as the ester bond. Thus, the release of amide-linked molecules is more difficult. Therefore, the attachment of an imaging agent or the polymer in folate-conjugated diagnostic molecules via a disulphide bond or an ester bond is desirable. However, the majority of papers report conjugation via amide bonds.

2.1.3.1. Folate-Small Molecule Conjugates

Folate-small molecule conjugates have been reported in the literatures that were in human clinical trials for imaging purposes (Figure 2.3A).[2] These trials were discontinued owing to unsuccessful results, and these are discussed below.

A folate-small molecule imaging conjugate that was recently in human clinical trial for breast cancer diagnosis is EC17 (an Endocyte™ product). It is a FA-conjugated fluorescein compound. This trial is completed; however, it yielded unsuccessful results. Figure 2.4 shows the intraoperative fluorescent image of breast cancer metastases from a European (Netherlands) clinical trial of EC17. The surrounding tissues caused autofluorescence due to which the distinguishability of the tumor was suboptimal.[28]

The other folate-small molecule imaging conjugates that were in human clinical trials are ^{111}In-DTPA-folate and ^{99m}Tc-DTPA-folate where Indium (^{111}In) and Technetium (^{99m}Tc) are the imaging moieties for radioimaging.[2] ^{111}In-DTPA-folate is a folate-linked Indium complex conjugate whose uptake in ovarian cancer patients was observed in both the cancer tumor cells and kidneys. In healthy patients only kidney uptake was observed. However, this trial was terminated.[29] ^{99m}Tc-DTPA-folate (EC20/ Etarfolatide, an Endocyte ™ product) is a folate-linked Technetium complex conjugate which was used in more than 13 clinical studies in patients with different types of cancers. It has been administered to more than 1000 patients and was developed as the imaging agent to be used with folate-targeted therapeutic agents Vintafolide (EC145, Figure 2.3B; PROCEED Phase III, an Endocyte ™ product) and EC1456 (folate-tubulysin, Figure 2.3B, an Endocyte ™ product). EC145 is a hydrophilic conjugate of FA and vinca alkaloid desacetylvinblastine (drug) with a peptide spacer in between linked via

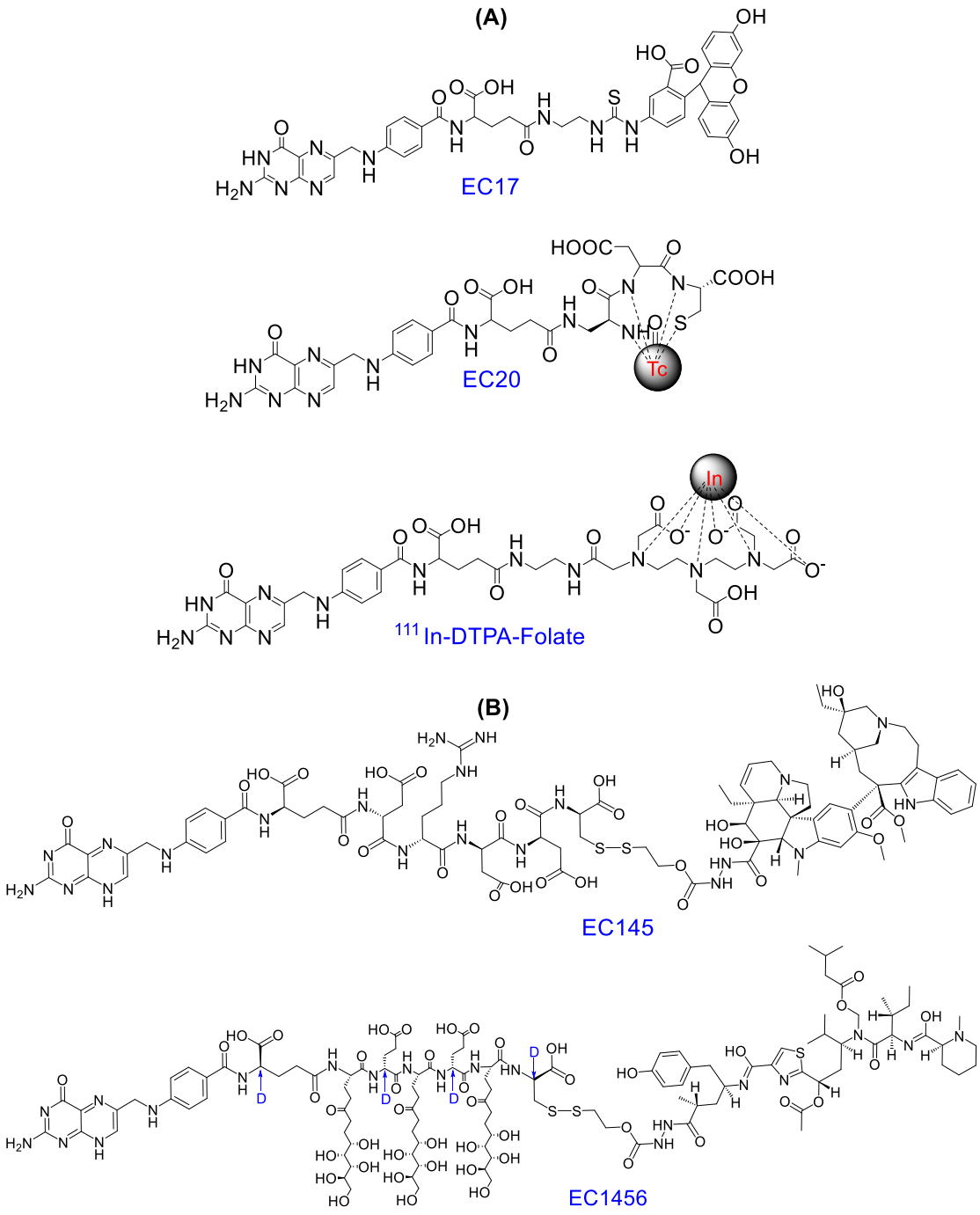

Figure 2.3. Folate-small molecule (A) imaging conjugates and (B) drug conjugates previously in human clinical trials

a reducible disulphide bond. The trials with Vintafolide for Triple Negative Breast Cancer (TNBC) were withdrawn in 2014 since the conjugated drug did not show the promised improvements in efficacy.[30] Synthesizing the folate-small molecule conjugates

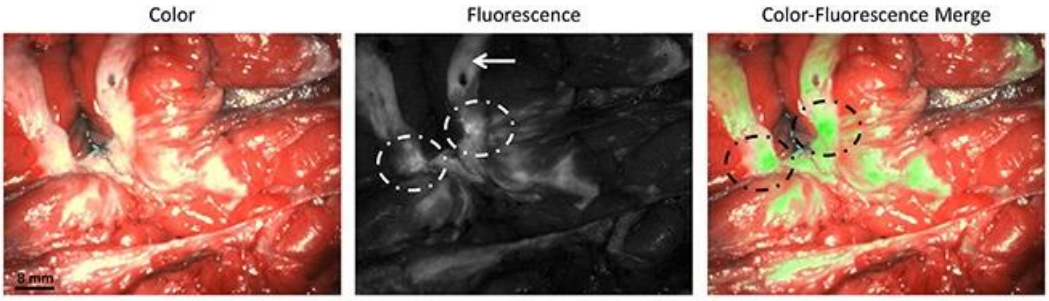

Figure 2.4. Identification of a bisected primary breast cancer lesion using fluorescence imaging (dashed circles). The arrow indicated auto-fluorescence signal from normal breast tissue. Reprinted with permission from *Oncotarget* **2016**, *7(22)*, 32144

is complicated and expensive, and they allow for only monovalent binding since one conjugate contains only one targeting folate ligand.

2.1.3.2. Folate-Polymer Conjugates

The first monovalent folate-polymer conjugate was reported by Aronov *et al* in 2003.[31] They conjugated FA with PEG (M_n = 3K g/mol) and reported that 65% of the conjugate had PEG attached to the γ-position of FA. This conjugate was later attached to Fluorescein IsoThioCyanate (FITC, imaging agent) to obtain FA-PEG-FITC for diagnosing folate-receptor enriched M109 tumor cells. While FA-PEG-FITC demonstrated three times more efficient (not quantified) cellular uptake over non-targeted PEG-FITC using fluorescent flow cytometry, free folic acid reduced the uptake.

Rhenium (I)[32] and Gallium (III)[33] complex based monovalent folate-PEG conjugates were developed by Viola-Villegas *et al*. Complexes of Rhenium (I)(Re^{I}) and Gallium (III)(Ga^{III}) are radiopharmaceuticals known to have anti-cancer properties. In both cases the uptake of the targeted compounds was higher than the non-targeted compounds. In case of the FA-PEG-Re^{I} complex, however, free FA blocked the uptake of the compound so the Gallium (III)[33] complex was tested in FA-free medium. This latter was shown to be inefficient anti-cancer agent.

Technetium (^{99m}Tc) complex based monovalent FA-PEG conjugates with covalently attached Doxorubicin were synthesized and their biodistribution in various organs investigated *in vivo* in Albino Wistar rats.[34] They have reported selected accumulation in FA-rich tissues (prostate) with 160 as the target/non-target ratio (prostate/muscle) at 60 minutes. However, after 120 minutes barely any uptake was found in the prostate, even though the conjugates were shown no be stable for 3 hours.

In summary, monovalent FA-targeted delivery research has controversial data, and the clinical trials had also less than satisfactory results.

2.1.4. Multivalent Folate-Targeting

In multivalent folate-targeted diagnostics, multiple FA molecules are connected to an imaging molecule/s via polymer arms. Multivalency was shown to have improved selectivity for tumor cells. Low's original work involved multivalency where they attached 1 – 10 FA molecules to proteins.[20] The potential of multivalency was investigated in detail by Baker and co-workers by synthesizing dendrimers that have multiple arms to attach multiple FA, imaging, and drug molecules.[35, 36] Dendrimers are branched polymers that are synthesized to obtain a spherical shape with 1-10 nm diameters, depending on the generation. The number of generations or layers of the dendrimers determine the molecular weight, size and the number of terminal groups of the polymer.[37] Another feature of the dendrimers is that they mimic the structure of globular proteins.[38] Poly(amidoamine) (PAMAM) dendrimers are used extensively among all the dendrimer types.[37]

Baker *et al* synthesized a FA-targeted generation 5 PAMAM dendrimer that had an average of five folic acid molecules, 5 FITC and 5 Methotrexate (MTX) that demonstrated nearly 71,400 fold better binding than free FA molecules.[4] Though the association constant was comparable to that of the free FA, however, the dissociation constant was nearly 1000 times less in magnitude than that of free FA. Figure 2.5 demonstrates that K_A increases with increasing number of FA molecules. K_A of the FA-targeted dendrimers was measured using surface plasmon resonance spectroscopy on folate binding proteins.[4] A higher association constant means that once the conjugate is attached, it is less likely to detach. When an average of 2.6 FA molecules were attached to this dendrimer, a 2500-fold enhancement in binding to FRs was observed over free FA. The increase in K_A is seen to saturate after attaching more than an average of 4.7 molecules of FA to each dendrimer. The highest K_A ($3 \pm 2 \times 10^{10}$ M^{-1}) is observed when an average of 13.7 FA molecules are attached per dendrimer, however, when an average of 4.7 molecules of FA are attached, K_A of $4 \pm 3 \times 10^{10}$ M^{-1} is observed. This K_A is merely 28 times higher than the K_A ($2 \pm 1 \times 10^{8}$

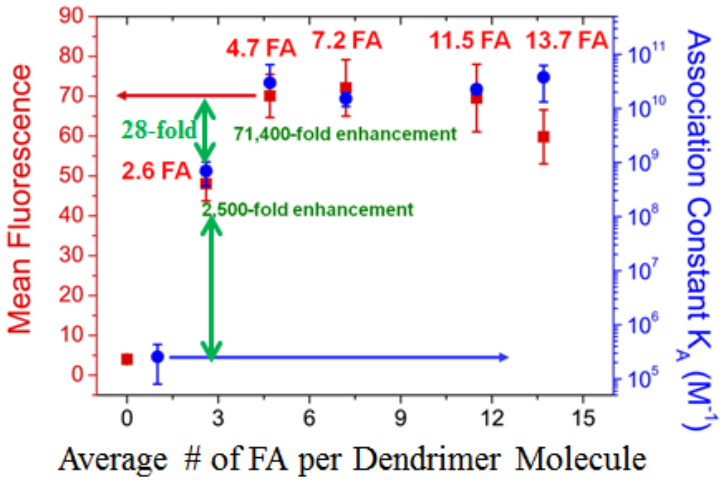

Figure 2.5 Effect of the number of FA molecules per dendrimer molecule upon the overall association constant K_A at equilibrium. Reprinted with permission from *Chemistry & Biology* **2007**, *14(1)*, 107-115. Copyright © 2007 Elsevier

M^{-1}) observed for a dendrimer with an average of 2.6 folic acid molecules attached to it. This jump in the K_A is not very significant.

A schematic representation of multivalent targeting having better selectivity towards malignant cells through lower dissociation constant is shown in Figure 2.6. Malignant cells are over-expressed in FRs and thus they trap the multiple FA molecules on one single diagnostic agent. This increases the chances of internalization of the multivalent agent better than the monovalent agent, thereby reducing the chances of dissociation of the multivalent agent from the FRs.

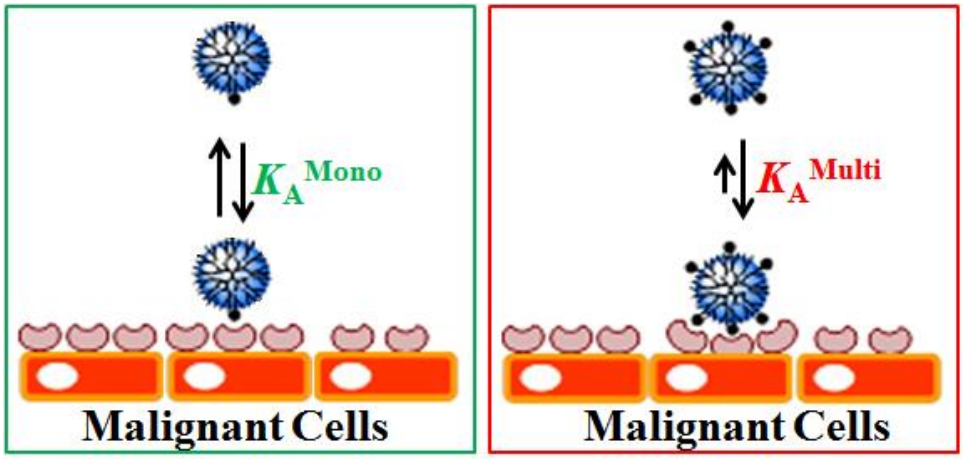

Figure 2.6 Schematic representation of multivalent targeting

As mentioned before, the folate-targeted G5 PAMAM dendrimer was conjugated with 5 molecules of FITC (Fluorescein isothiocynate), an imaging agent, to form the G5-FITC-FA conjugate and subsequently to a Methotrexate (MTX), a drug molecule, to form the G5-FITC-FA-MTX conjugate.[35] These conjugates were synthesized to study their *in vitro* cellular uptake by KB cells (FR-positive human epidermal carcinoma) by flow cytometry at a conjugate concentration of 10 - 15 nM or nearly 0.395 μg/ml. These conjugates demonstrated a dose-dependent binding towards the tumor cells with 50% binding. The highest binding (% not reported) was reported at 100 nM concentration of the

conjugate used. Non-folate targeted dendrimer (G5-FITC) did not show any cellular uptake.[39]

The therapeutic performance of the G5-FITC-FA-MTX conjugate was evaluated *in vivo* in mice with human FR-positive KB tumor xenografts. They compared its therapeutic performance with equivalent doses of free MTX.[38] G5-FITC-FA-MTX demonstrated significantly lower toxicity and ten times better binding with the FR when compared with the free MTX (5 mg/kg dose) at an equal cumulative dose. The FA-conjugated dendrimer demonstrated excellent selectivity towards the cancer cells. The tumor volume reduced twice as much with the dendrimer than with free MTX. Similar tumor reduction was achieved at much higher free MTX dose. The mice treated with free MTX lost all their hair, appeared sicker and died within 30 days, while the mice treated with MTX conjugated to folate-targeted dendrimer retained all their hair and did not lose weight.[38] Therefore, G5-FITC-FA-MTX showed great promise for selectively targeting tumor cells both *in vitro* and *in vivo* but they posed two major design challenges. First, the G5 PAMAM dendrimer has an average of 128±20 $-NH_2$ groups in the outer corona that induce toxicity into the structure so they need to be blocked.[35] Second, the FA molecules are conjugated to the dendrimer randomly; therefore, every dendrimer molecule does not have a precise number of FA molecules leading to a wide distribution of FA molecules present in every dendrimer molecule. To verify this, an HPLC characterization of the conjugate with an average of 2.6 folic acid molecules was performed and each fraction was analyzed using ^{1}H-NMR. It was observed that only 13 wt% of the dendrimer had 3 FA molecules conjugated to it, 16 wt% of the dendrimer demonstrated no FA conjugation, 22 wt% of the dendrimer had only 1 FA

conjugated to it, and the rest of the dendrimer had more than 3 FA molecules conjugated to it.[40] Therefore, nearly 40% of the dendrimer did not demonstrate multivalency.

Hence, there is a need of generating a good synthesis strategy for producing multivalent folate-polymer conjugates with more precise structure, i.e., having precise number of FA molecules conjugated to each polymer molecule. It was discussed previously that the K_A observed for an average of 4.7 folic acid molecules attached to the dendrimer is merely 28 times higher than the K_A observed for a conjugate with an average of 2.6 folic acid molecules. In addition, the K_A observed for the dendrimer with an average of 2.6 FA molecules is nearly 2500 higher than the K_A observed for free FA. Therefore, the K_A did not significantly increase after the attachment of more than an average of 2.6 FA molecules to the conjugate. Therefore, to maintain the multivalency and to produce a folate-polymer conjugate that gives a precise structure, we decided to attach two FA molecules to our diagnostic agent. We developed three strategies to synthesize these two-functional folate-polymer conjugates and they will be discussed in detail in Chapter IV.

2.1.5. Cleveland Clinic Trials (Submitted for Publication)

Baker *et al* reported a 2500-fold improvement in the binding of folate-targeted dendrimer when nearly two FAs were attached to it instead of one FA. Since the highest increase in binding avidity was observed from attaching 2 FAs, a two-functional folate-targeted fluorescein-labeled PEG-based diagnostic agent (FA-FL-PEG-FL-FA) was synthesized in the Puskas lab for *in vitro* screening in TNBC cell lines and it was compared with two other controls, a two-functional folate-targeted fluorescein-labeled diagnostic

agent (FA-FL-FA) and a mono-functional folate-targeted fluorescein-labeled diagnostic agent (FA-FL) as shown in Figure 2.7.

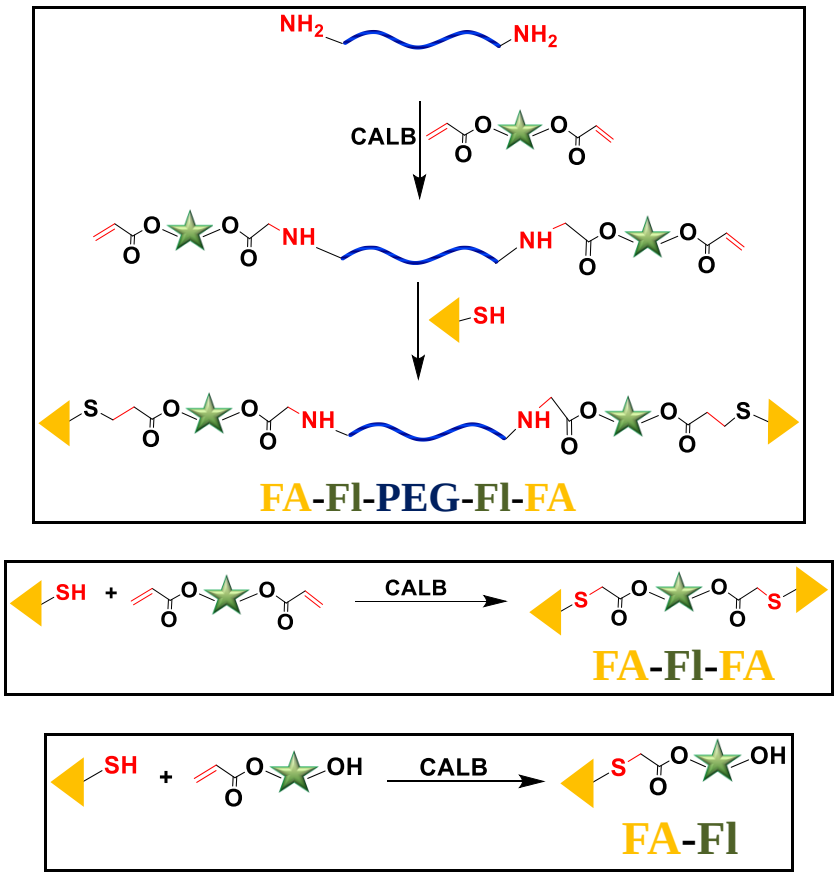

Figure 2.7 Synthetic strategies for FA-FL-PEG-FL-FA, FA-FL-FA and FA-FL

The cytotoxicity and bioavailability of these agents was evaluated inn human TNBC cell lines MDA_MB_231 (epithelial cells_HTB26_adenocarcinoma_patient ethnicity Caucasian) (MB_231) and MDA_MB_468 (epithelial cells HTB 132_adenocarcinoma_patient ethnicity African-American) (MB_468) at three different doses of each agent at 5, 10 and 30 μg/ml. These agents were incubated with these cell lines for two hours and were then harvested for flow cytometry analyses. Before that, immunocytochemistry was performed to determine the FR expression on these cell lines as shown in Figure 2.8 where FR is represented in green. This test was not quantitative;

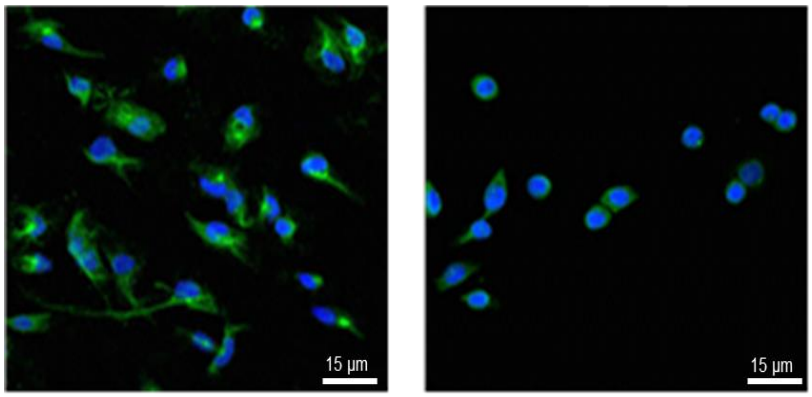

Figure 2.8 Comparison of MD-MB-231 (left) and MD-MB-468 (right) TNBC cells for FR-expression. Blue: cell nuclei; green: fluorescent secondary antibody attached to the primary FR-specific antibody

however, it was observed that MB_231 showed more intensive green staining, demonstrating higher level of FR expression.

Figure 2.9 to Figure 2.11 show the MB_231 cellular uptake and cytotoxicity data from flow cytometry and compound localization by confocal microscopy after 2 hours incubation with FA-FL, FA-FL-FA, and FA-FL-PEG-FL-FA respectively. FA-FL (10µg/ml, 0.01mM) had the simplest design among the three agents, and it was easily taken by the MB_231 TNBC cells. However, it did not show dose-dependency of uptake (Figure 2.9A). This behavior might be caused due to its small size, and only 1 FA targeting molecule, which may lead to an uptake through passive diffusion. Flow cytometry does not provide information on cellular uptake mechanism, that is, it cannot distinguish whether the uptake occurred via the intended FR-targeted endocytosis or by adherence to cell surface due to excessive dosage or incubation. Therefore, confocal microscopy and Z-stack imaging were performed to confirm the intracellular localization. Figure 2.9B shows bright green spots within the blue stained nuclei confirming the intracellular localization of FA-FL.

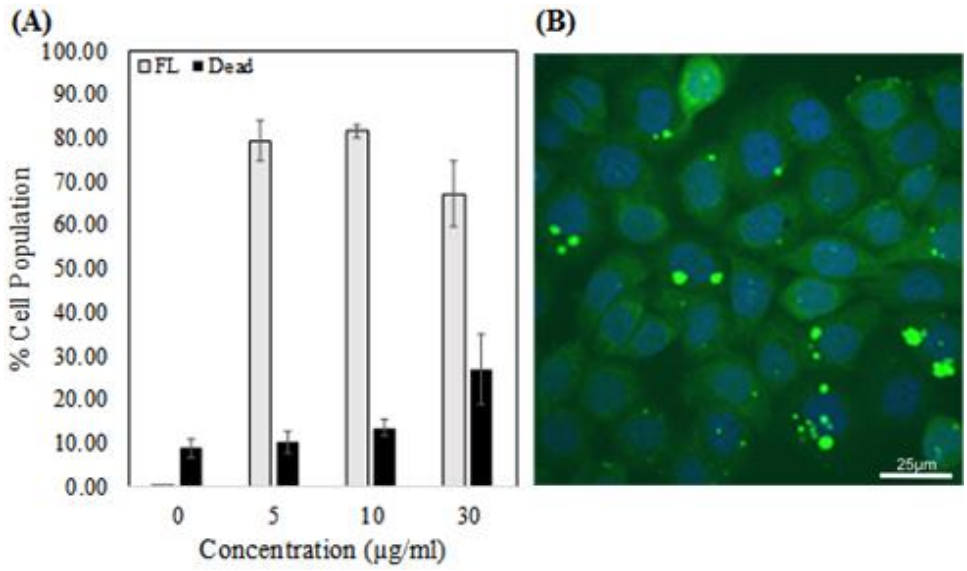

Figure 2.9 (A) FL-FA uptake and cytotoxicity in MDA_MB_231 TNBC cells (B) Confocal microscope image. Blue: cell nuclei; green: FL-FA

FA-FL-FA (10µg/ml, 0.006mM) had two FA molecules and it showed strong dose dependency of uptake as shown in Figure 2.10A. Figure 2.10B shows more bright green spots within the blue nuclei than Figure 2.9B, indicating higher FR-specificity of

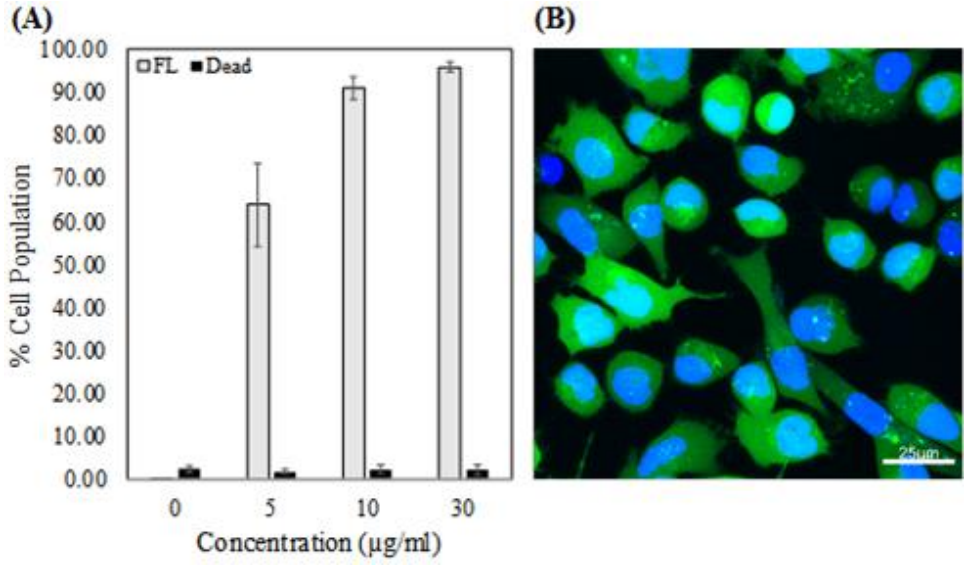

Figure 2.10 (A) FL-FA_FL uptake and cytotoxicity in MDA_MB_231 TNBC cells (B) Confocal microscopy image. Blue: cell nuclei; green: FA-FL-FA

FA-FL-FA. Therefore, the diagnostic agent having two FA molecules demonstrated higher specificity towards the FRs at a lower concentration.

FA-FL-PEG-FL-FA (10µg/ml, 0.002mM) had two FA molecules with a PEG backbone. It demonstrated strong dose dependency of uptake as shown in Figure 2.11A along with higher water solubility. Figure 2.11B shows bright green across the whole cytosol with no blue stain visible, indicating high FR-specificity by FA-FL-PEG-FL-FA. Therefore, the diagnostic agent having two FA molecules with a PEG backbone demonstrated higher specificity towards the FRs and higher water solubility at three times lower concentration than FA-FL-FA.

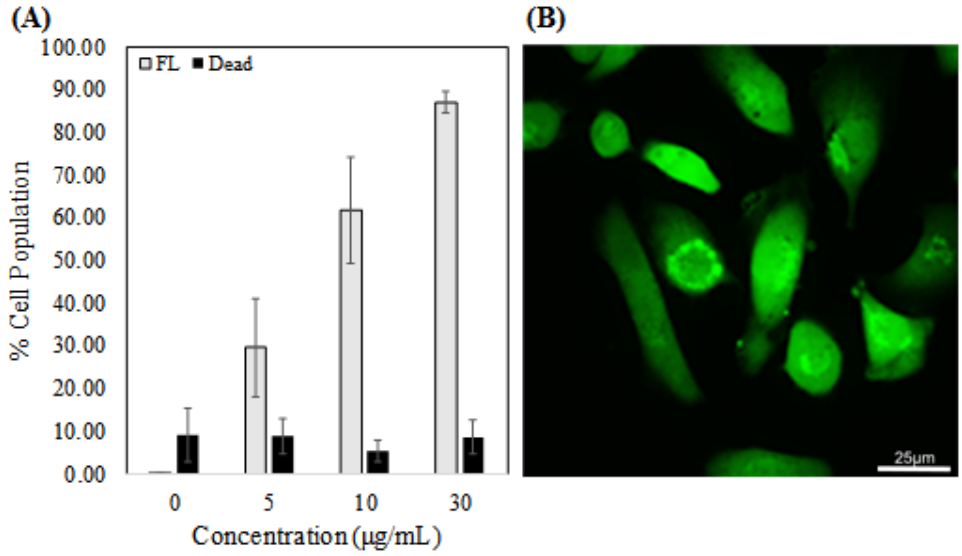

Figure 2.11 (A) FA-FL-PEG-FL-FA uptake and cytotoxicity in MDA-MB-231 cells (B) Confocal microscopy image. Green: FA-FL-PEG-FL-FA

The Cleveland Clinic also performed *in vivo* analysis of FA-FL-PEG-FL-FA in a rat model with liver cancer.[41] Two animals were injected with FA-FL-PEG-FL-FA intra-arterially (IA) while three were given intravenous (IV) injection of the same agent. They reported that when the compound was injected directly into an artery feeding the liver of the experimental rat, the compound was uptaken by the tumor cells in the liver as shown

in Figure 2.12A. Animals given a tail vein injection (IV) were imaged similarly and only a weak, diffuse liver area specific signal was detected (Figure 2.12B). This indicates that the IA approach is better than IV for targeted delivery. Fluorescent urine was detected post-injection in some of the animals indicating that the FA-FL-PEG-FL-FA is metabolized and eliminated by the kidneys.

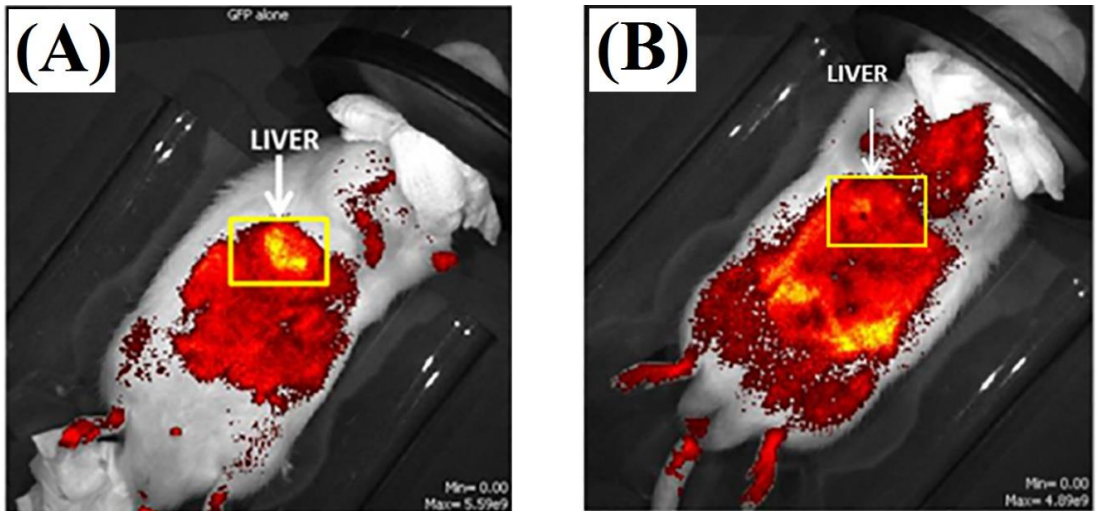

Figure 2.12 (A) Intra-arterial and (B) Intra-venous injection of FA-FL-PEG-FL-FA in liver cancer rat model. Reprinted with permission from *Journal of Biomedical Materials Research Part A* **2019**, *107(11)*, 2522-2535. Copyright © 2019 Wiley Periodicals, Inc

Against this background, we developed three strategies to synthesize two-functional folate-receptor targeted fluorescein-labeled PEG-based conjugates and evaluated them for their synthetic convenience and feasibility.

In the first strategy presented in Figure 2.13, Poly(ethylene glycol)(PEG)-diamine (H_2N-PEG-NH_2) is reacted with 2 equivalents of Fluorescein-*o*-acrylate (FLA) via an enzyme (*Candida antartica* Lipase B, CALB)-catalyzed Michael addition to ultimately obtain an acrylated fluorescein-labeled PEG (Ac-FL-PEG-FL-Ac). The Ac-FL-PEG-FL-Ac is then reacted with 2 equivalents of a thiol-functionalized Folic Acid (FA-SH) through CALB-catalyzed Michael addition for obtaining 2-functional folate-targeted poly(ethylene glycol)-based agent (FA-FL-PEG-FL-FA). The first section in Chapter IV,

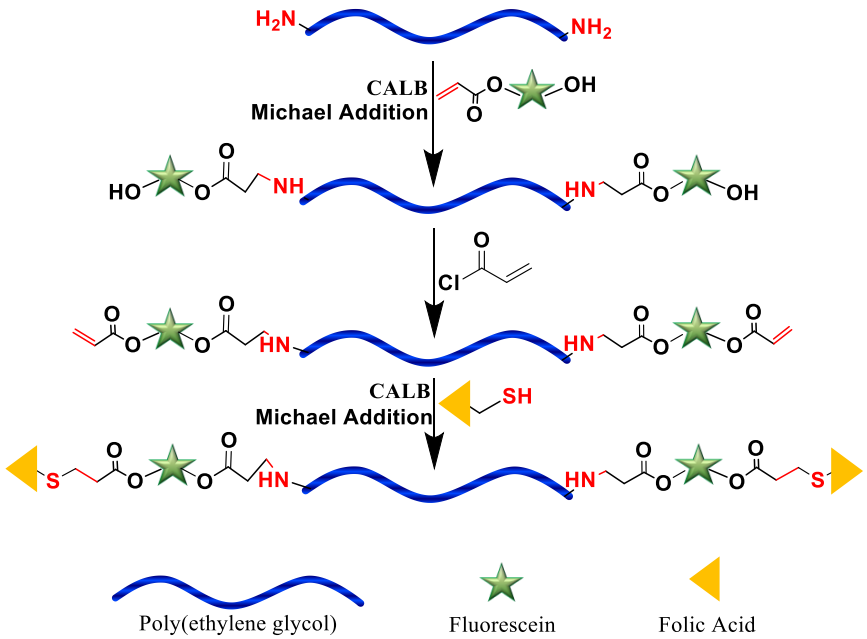

Figure 2.13 Strategy 1 for synthesizing folate-targeted PEG-based conjugate

Results and Discussion, describes the novel synthesis of H_2N-PEG-NH_2 via CALB-catalyzed esterification of *tert*-butyloxycarbonyl protected Alanine (*t*BOC-Al) with PEG and the subsequent de-protection of the *t*BOC group. This section also describes the modified synthesis of FA-SH that was developed earlier in our lab. FA-SH was synthesized by lithiation of folic acid (FA) using 1 molar equivalent of *n*-butyllithium (*n*-BuLi) and its subsequent reaction with 1 equivalent of a bis(2-ethyl 4-bromobutanoate) disulfide (Br-S-S-Br) compound to form FA-γ-bis(2-ethyl bromobutanoate) disulfide (FA-S-S-FA) and then cleavage of the disulphide bond with dithiothreitol (DTT).

In the second strategy presented in Figure 2.14, PEG-dithiol (HS-PEG-SH) is reacted with 2 equivalents of Fluorescein-*o*-acrylate (FLA) via CALB-catalyzed Michael addition and subsequent acrylation to obtain an acrylated fluorescein-labeled PEG (Ac-FL-PEG-FL-Ac). The Ac-FL-PEG-FL-Ac is then reacted with 2 equivalents of FA-SH through CALB-catalyzed Michael addition for obtaining FA-FL-PEG-FL-FA. The second section in Chapter IV, Results and Discussion, discusses a new synthesis method

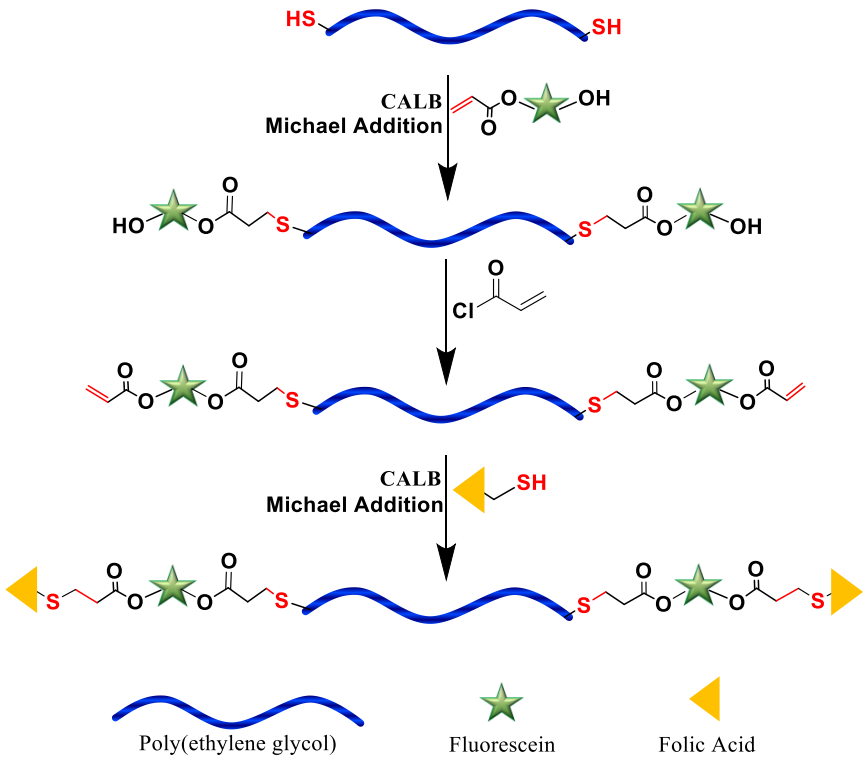

Figure 2.14 Strategy 2 for synthesizing folate-targeted PEG-based conjugate

for obtaining HS-PEG-SH by CALB-catalyzed transesterification of methyl 3-mercaptopropionate (MP-SH) with PEG. Kinetics of this transesterification of MP-SH with PEG of M_n = 1000 g/mol and M_n= 2050 g/mol is established to exclusively obtain monothiols with precise timing of the reaction. The third section in Chapter IV, Results and Discussion, discusses the CALB-catalyzed Michael addition of 2 equivalents of FA-SH to acrylated fluorescein-labeled PEGs synthesized using the second strategy to obtain FA-FL-PEG-FL-FA compounds.

In the third strategy presented in Figure 2.15, fluorescin (reduced form of fluorescein with free carboxylic acid group, FL-COOH) is lithiated using *n*-BuLi to obtain a lithiated fluorescin (FL-COOLi). Poly(ethylene glycol)(PEG)-dibromide (Br-PEG-Br) is then reacted with 2 equivalents of FL-COOLi with subsequent acrylation to obtain Ac-FL- PEG-FL-Ac. The Ac-FL-PEG-FL-Ac is then reacted with FA-SH through

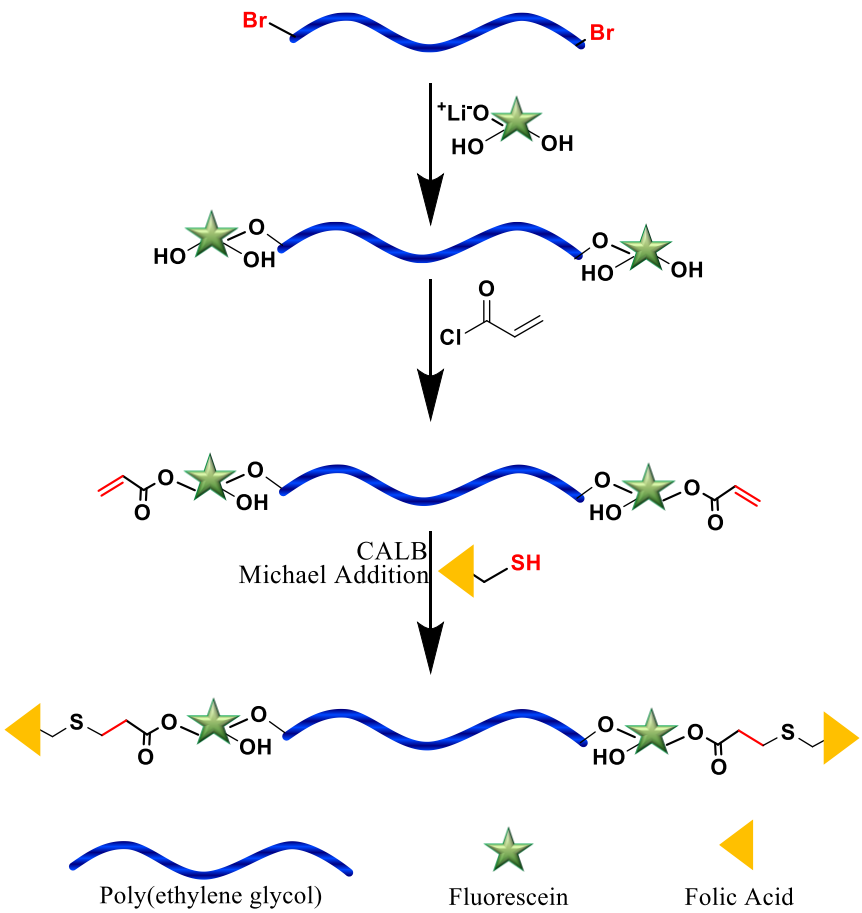

Figure 2.15 Strategy 3 for synthesizing folate-targeted PEG-based conjugate

CALB-catalyzed Michael addition for obtaining FA-FL-PEG-FL-FA. The fourth section in Chapter IV, Results and Discussion, discusses the synthesis of Br-PEG-Br via CALB-catalyzed transesterification of Ethyl 5-bromovalerate (EBV) with PEG.

In our strategies, we planned to use functionalized PEG molecules that are made by enzyme catalysis. Therefore, the background related to enzyme-catalyzed PEG functionalization through transesterification will be discussed next.

2.1.6. Polymer Functionalization by Enzyme Catalysis

Specific biochemical reactions occurring in the living systems are catalyzed by enzymes. Enzymes also have the ability to catalyze a number of organic chemical

reactions in organic media outside the naturally available aqueous systems.[42] Enzymes offer a wide variety of advantages over traditional chemical catalysts. They offer high efficiency and catalyst recyclability if immobilized on a solid carrier. They also work under milder conditions than traditional chemical catalysts due to which they are more environmentally friendly.[42] Enzymes are therefore a potential candidate for post-polymerization modifications; that is, they can serve as catalysts for functionalizing end-groups of a polymer.[7]

Dr Puskas' group was the pioneer in using enzymes for post-polymerization modifications.[7] They used *Candida antartica* Lipase B (CALB) enzyme to catalyze transesterification, esterification, and Michael addition reactions to quantitatively functionalize synthetic polymers in organic solvent and bulk conditions.[7-15] For example, they modified the hydroxyl functionalized end-group of PEG monomethyl ether to halogen functionality via CALB-catalyzed transesterification reaction under bulk conditions.[14] CALB-catalyzed transesterification of esters such as vinyl methacrylate, vinyl crotonate, and vinyl acrylate was also performed with PEGs under bulk conditions to achieve the respective methacrylate, crotonate, and acrylate functionalization of PEGs.[15]

Against this background, this dissertation will discuss the efficient synthesis of PEG-diamine, PEG-dithiols, and PEG-dibromides via CALB-catalyzed transesterifications. It will also discuss the three strategies we developed to synthesize the two-functional folate-polymer conjugates and my contribution to the synthesis of thiol-functionalized folic acid (FA-SH) which is the targeting precursor of these conjugates.

2.2 Synthesis of Multifunctional PEGs from Sucrose Ester of Soybean Oil

In this thesis I also explored the synthesis of multifunctional PEGs utilizing renewable resources. Sustainable development of materials demands the use of renewable resources. Carbohydrates and plant oils contain naturally occurring fatty acids; therefore, they are a sustainable and abundant renewable resource. "Sucrose, one such carbohydrate, is a disaccharide having eight hydroxyl groups and its esterification with fatty acids from vegetable oils yield sucrose esters of fatty acids (SEFA)."[43] Sefose, a sucrose ester of soybean oil, was developed by Proctor & Gamble (P&G) Chemicals. Sefose is a highly substituted molecule containing a mixture of sucrose hexaesters, heptaesters, and octaesters of fatty acids. Sefose is nearly 70% by weight octaester.[43] The structure of Sefose is shown in Figure 2.16. It can be observed from the figure that Sefose has a multivalent nature providing nearly 11 double bonds on its ~8 arms. These double bonds are highly desirable for a UV-mediated thiol-ene click reaction, where any moiety possessing a thiol end-group can be attached to this multivalent structure. Attaching FA-SH and a cancer drug to this structure will yield a multivalent folate-targeted cancer therapeutic agent which aligns with the objective of this research. However, since Sefose contains nearly 8 units of fatty acids, it is insoluble in water. Therefore, to make it water soluble, attaching of a hydrophilic polymer like PEG becomes imperative. Therefore, this dissertation will discuss the attachment of thiol functionalized TEGs and PEGs to the double bonds of Sefose via UV-mediated thiol-ene click reaction.

Thiol-ene click reaction is the addition of a thiol (nucleophile) with alkene (electrophile). The reaction is typically catalyzed using Lewis bases or free radical initiators that are activated through UV-light. Figure 2.17 describes the mechanism of a

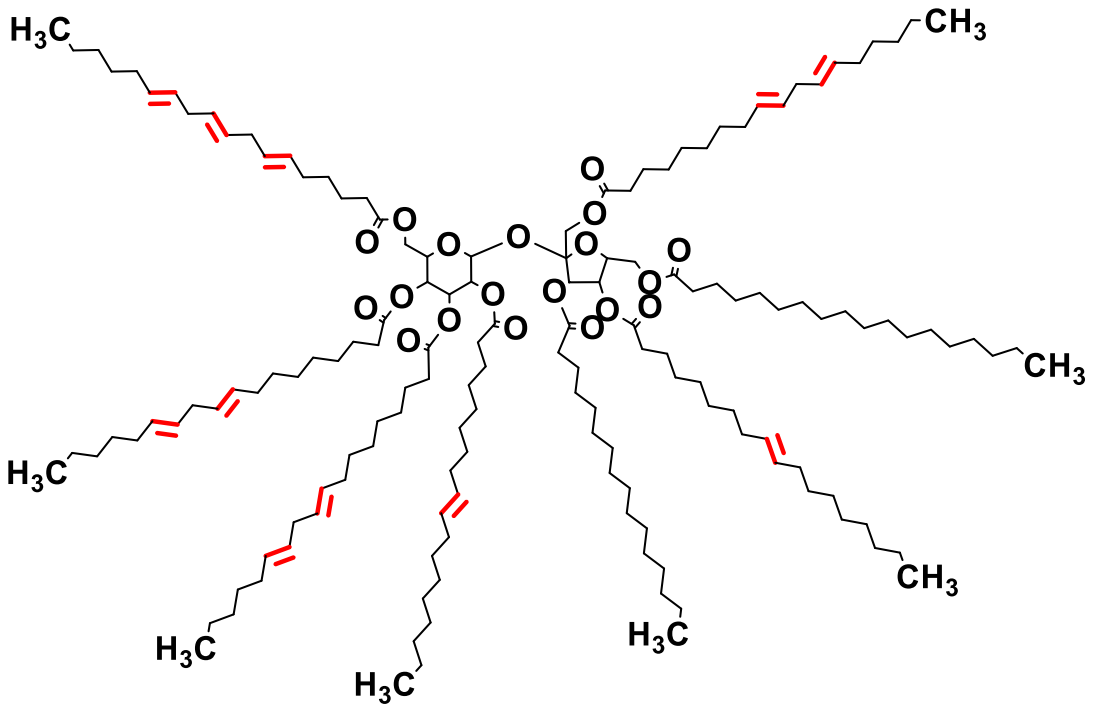

Figure 2.16. Molecular structure of Sefose 1618 U

thiol-ene 'Click' reaction. Initially, the thiol group scavenges the radical formed from the dissociation of the free radical initiator. The resulting thiol radical then couples with alkene group by the addition of two radicals, generating a 2° methyl radical. The 2° methyl radical later abstracts the proton from the unreacted thiol and forms the thiol-ene adduct (product). The thiol radical formed from the proton abstraction continues to participate in the next cycle of the addition reaction.[44]

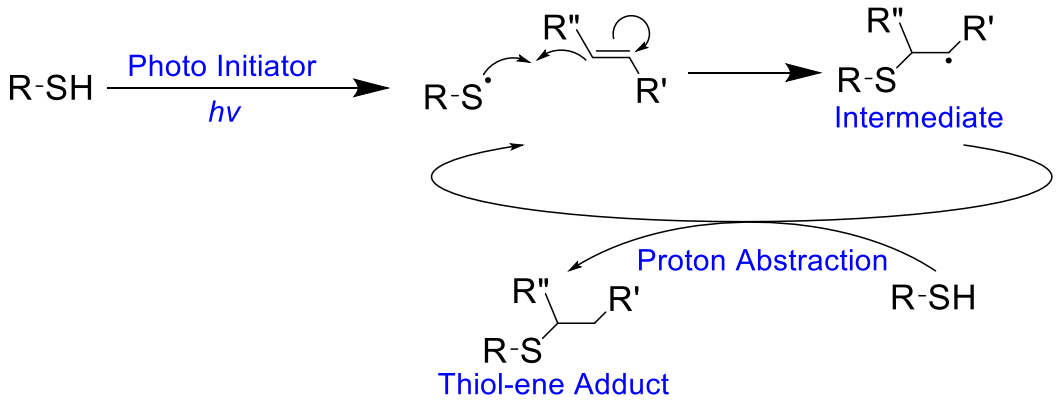

Figure 2.17. Schematic Representation of the Mechanism of the Free Radical-Initiated Thiol-ene 'Click' Reaction

2.3 Cyclic Polydisulfide Polymers

During my Ph. D., I volunteered to work on one of our group projects related to cyclic polydisulfides. This section will provide background on cyclic polymers and the synthetic routes reported in the literature to prepare them. A new method to synthesize cyclic polymers, Reversible Redox Ring polymerization (R3P), reported first by our group will also be discussed. Although this was not my main topic of doctoral research, I have reviewed the literature of cyclic polymers and contributed towards synthesis of cyclic poly(DODT).

CPs or ring polymers are polymers that do not have end-groups. These macrocycles have unique properties when compared to their linear equivalents. The properties that linear polymers (LP) exhibit, for example crystallinity, melt flow dynamics, and glass transition temperature that are attributed to the diffusion behavior of the end-groups.[45] Since there are no end groups present in CPs, they demonstrate different physical properties in bulk and dilute solutions than LPs. LPs diffuse in a polymer matrix due to their end-groups, however, CPs cannot diffuse in this manner, instead, they move with an amoeba-like motion.[46] CPs demonstrate greater intramolecular interactions due to their cyclic nature, that along with the amoeba-like motion result in lower melt viscosity,[47] higher density,[48] higher thermostability,[47] lesser chain entanglement, higher glass transition temperature,[49] higher refractive index[50] and higher rate of crystallization in bulk.[51] It was reported that CPs demonstrate lower radius of gyration (R_g) than LPs in dilute solutions.[52] CPs also exhibit lower hydrodynamic volume (R_v) and hydrodynamic radius (R_h) than their LP counterparts; the compact nature of CPs allows them to have a smaller hydrodynamic diameter, which can be characterized

by SEC.[53] This has also been reported by Bernal and Tirado[54] who conducted a series of simulation studies for CPs in general. They used rigid-body Monte-Carlo simulation and calculated the translational coefficients and intrinsic viscosities of LPs and CPs. They used two models: freely jointed and Gaussian. In the freely jointed model, for polymers with *number of repeating units* N = 10 to N = 80, the radius of gyration for CPs was calculated to be 0.55 times that of LPs. The intrinsic viscosity for CPs was calculated to be 0.6 times that of LPs. The Gaussian model also predicted identical results for CPs. Therefore, CPs exhibit nearly half radius of gyration and intrinsic viscosity values to that of LPs. Along with R_g and R_h, the scaling factors ν_g and ν_h (corresponding scaling law coefficients for $< R_g^2 > = (N-1)^{2\nu}$) are also lower in CPs compared to their LP counter parts. Linear polyethylenes are reported to have ν_g = 0.53 while the cyclic polyethylene has ν_g = 0.45.[55] Computer simulation studies have also shown that ν_g for a linear polymer is 0.5 and that for a cyclic polymer is 0.40.[56, 57]

Although CPs have shown attractive properties, efficient synthetic routes for preparing high-purity CPs remains a problem to be solved in the scientific community. An insightful understanding of the physical behavior of CPs is restricted mainly due to the lack of these synthetic routes. Also, these synthetic routes should be able to produce CPs on a large scale with predicted cyclic structure in order for CPs to have commercial applications. In addition, most methods yield materials with linear polymer impurities that will influence the validity of the physical measurements. CPs were first synthetically prepared by Jacobson *et al.* by ring-chain equilibrium polymerization of polyesters.[58] They synthesized cyclic poly(decamethylene adipate) (N = 81) by intramolecular transesterification in the polymer. They polymerized decamethylene glycol and adipic

acid using the catalyst *p*-toluenesulfonic acid (PTSA) as shown in Figure 2.18. Ring formation was obtained when the polymerization process was prolonged for > 100 hours with 10% volume concentration of the reaction mixture in the system. The ring formation within the polymers was asserted by observing lower melt viscosity (0.7 times that of linear counterparts) for the dilute polymer solutions. However, these early synthetic methods did not yield 100% cyclic structures.

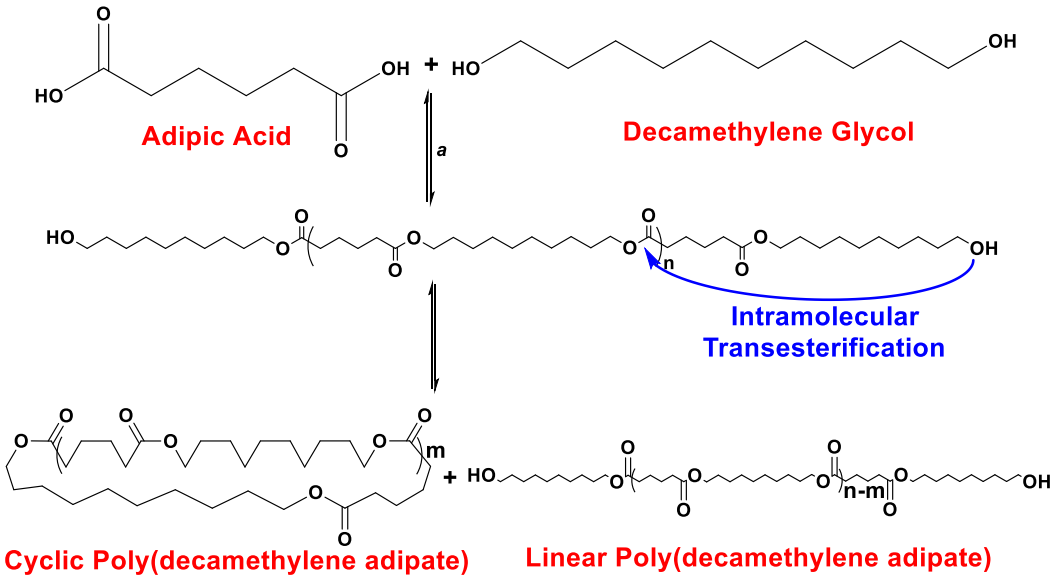

Figure 2.18 Synthesis of Poly(decamethylene adipate)[58]

The two main strategies developed till today to prepare CPs are ring closure reactions and ring expansion polymerizations (REP). In ring-closure reactions, the end-groups of a LP react to form a CP. In ring expansion polymerization, either the thiol end-groups of a LP are oxidized to form CPs or monomer units are inserted into a cyclic catalyst to expand the formed cyclic polymer.

2.3.1. Ring Closure Polymerization

The ring closure technique is of two types, ring closure of homo-di-functional polymers and ring closure of hetero-di-functional polymers. Previously, living di-anionic polymers were used for homo-di-functional ring closure technique owing to their synthetic feasibility. To favor intramolecular ring closure over intermolecular coupling, the ring closure technique requires high Ruggli–Ziegler dilution (1% vol/vol).[53] Geiser,[59] Hild,[60] and Vollmert[61] reported nearly at the same time methods for the preparation of CPs through ring closure technique. In these initial studies, cyclic polystyrene (*c*-PS) with M_n in the range of 3,000 g/mol - 60,000 g/mol was prepared with polydispersity indices (Đ) below 1.2. They prepared the *c*-PS by sodium naphthalene initiated anionic polymerization to create a bifunctional polymer. However, the yields of *c*-PS with this strategy were often low (< 50%). LPs and CPs were separated by fractionation; the mixture was reacted with a high molecular weight living polystyrene where all LPs with chlorine/bromine end-groups will react and precipitate from the solution.

The initial studies utilizing the hetero-difunctional ring closure technique were conducted by Schappacher and Deffieux.[62] They prepared extremely well defined LP precursors with Đ < 1.2 using the living characteristic of the cationic 2-chloroethyl vinyl ether (CEVE) polymerization. The cyclization was achieved by acid-catalyzed intramolecular coupling between a pendant hydroxyl functional end-group and a pendant vinyl ether functional end-group forming acetal links. It generated high amount of the CP (~70% yield) and low amount of an intermolecular condensation product (~20%, M_n = 1,000 g/mol to 3,000 g/mol). The hetero-difunctional ring-closure technique requires complimentary end-group moieties that are generated from near quantitative post-

polymerization end-group transformations making this process a synthetically demanding one. In addition, non-quantitative post-polymerization end-group transformations from linear precursors reduce the CP yield and form LP impurities.

2.3.2. Ring Expansion Polymerization (REP)

REP has a number of advantages over the ring closure approach. In REP, lactones are used as monomer units which are repeatedly inserted into a cyclic initiator or catalyst to form a macrocycle held together by labile bonds such as organometallic or electrostatic. Contrary to the ring-closure technique, REP does not require high dilution, which eliminates the requirement of high amounts of solvent. This approach is also less likely to form LP impurities. High molecular weight CPs can be favourably obtained using this technique.[63] The initial study on REP was performed by Kricheldorf and Lee using lactide monomers (β-butyrolactone and ε-caprolactone) and a cyclic SnO_2 catalyst.[63] They obtained the corresponding macrocycles ($M_n \cong 8000$ g/mol, Đ = 1.7, 3 days, 75 ^oC) by inserting the lactide monomer into the tin-oxygen bond of the catalyst. This cyclization was achieved under concentrated conditions (8.2×10^0 M) with a cyclization yield of 81%. The main disadvantages of REP are the lack of available options for compatible monomers, and limited chain termination control that leads to CPs having wide Đ (>1.3).

A special case of ring-expansion polymerizations is dithiol oxidation. Polymers with thiol end-groups are oxidized to achieve higher M_n with many disulfide bonds in the formed CP. Whittaker *et al*. prepared polystyrene (PS) with thiol end-groups by Reversible Addition Fragmentation chain Transfer polymerization (RAFT).[64] They then

oxidized the thiol end-groups of the PS (M_n = 3.7K g/mol) using iron chloride in DMF for 72 h at 60 °C to obtain an M_n of 14.5K g/mol. The formation of this CP was obtained using dilute conditions (2.5 x 10^{-4} M). This product contained 83% by weight monocyclic PS. You *et al.*[65] oxidized the thiol end-groups of their polymer precursors (M_n = 3.5K g/mol) using iodide in tetrahydrofuran for 36h at room temperature to form CPs with M_n = 35K g/mol. They used similar synthetic strategy for preparing cyclic polydisulfides from thiol-ended acrylic acid and 2-(dimethylamino)ethyl methacrylate as precursors. Tsarevsky and Matyjaszewski[66] prepared α,ω-bromine-ended polystyrene using Atom Transfer Radical Polymerization (ATRP) and substituted terminal Br atoms with thiol end-groups using thiodimethylformamide. The thiol end-groups of polystyrene (M_n = 16K g/mol) were then oxidized using ferric chloride in DMF for 22 h at 60 °C to obtain CPs having M_n = 39.5K g/mol.

2.3.3. Reversible Redox Ring Polymerization (R3P)

The Puskas group has recently invented an effective and "greener" synthetic route for the oxidative polymerization of 3,6-dioxa-1,8-octane-dithiol (DODT). This synthetic route yields poly(DODT) at room temperature, does not need protection of the thiol end-groups, and does not use chlorinated reagents or solvents.[67-69] Using pure oxygen pose an explosion and fire hazard which is eliminated in this route by using a dilute H_2O_2 (3% by weight). The triethylamine (TEA) catalyst used for R3P can be reused and recycled under industrial conditions.

Poly(DODT) was characterized using ^{1}H NMR, ^{13}C NMR, Fourier transform infrared (FTIR) spectroscopies, and matrix-assisted laser desorption/ionization with time-

of-flight (MALDI-ToF) mass spectrometry. These spectroscopic and spectrometric techniques confirmed the formation of poly(DODT) with monomer units connected via disulfide bonds. They also performed a degradation study of poly(DODT) using dithiothreitol that yielded the DODT monomer, which additionally confirmed that the monomer is indeed joined through only disulfide bonds. This polymerization method yields disulfide polymers with M_n = 250K g/mol and (Đ) under 1.5 in two hours. They reported that lower reaction temperatures reduce the Đ to 1.15 but still yielding a M_n = 113K g/mol in less than half an hour with nearly half the product being oligomers. MALDI-ToF mass spectrometry demonstrated that these oligomers were cyclic in nature (2–14-mers). Linear molecules were not observed in the spectrum (Figure 2.19).

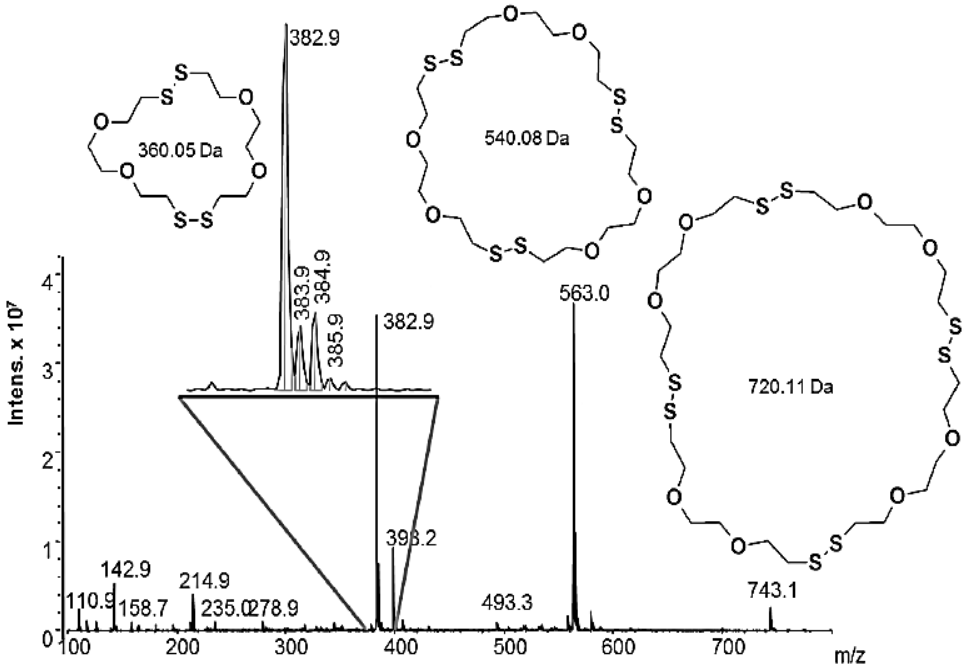

Figure 2.19 ESI Mass Spectrum of Poly(DODT). Reprinted with permission from *Molecules* **2015**, *20*(4), 6504-6519

The Puskas also reported the chain extension of poly(DODT) with ethylene-dithiol addition, that confirmed the living character of the reactivating the disulfide bonds obtained through R3P technique.[68] The chain extension produced a copolymer with M_n =

120K g/mol and Đ = 1.76 when a poly(DODT) of M_n = 20K g/mol and Đ = 1.79 was used. This polymerization produces conversions of over 90 % in mere two hours. Negligible amount of residual monomer is left behind that can be reused subsequent reactions.

Against this background, I performed a study to evaluate the effect of selected reaction parameters on the structure of the polymer. This dissertation presents a study conducted using a design of experiments to evaluate the effect of changing selected parameters on the molecular weight of the polymer.

CHAPTER III

EXPERIMENTAL

Parts of this chapter have been published:

- Adapted with permission from Puskas, J. E.; Castano, M.; Mulay, P.; Dudipala, V.; Wesdemiotis, C. Method for the Synthesis of γ-PEGylated Folic Acid and Its Fluorescein-Labeled Derivative. *Macromolecules* **2018**, *51(22)*, 9069-9077. Copyright © 2018 American Chemical Society.
- Adapted with permission from Mulay, P.; Shrikhande, G.; Puskas, J. E. Synthesis of Mono- and Dithiols of Tetraethylene Glycol and Poly(ethylene glycol)s via Enzyme Catalysis. *Catalysts* **2019**, *9(3)*, 228. Copyright © 2019 MDPI.

This chapter presents the details of the experimental approach used to accomplish the objectives of this investigation. This chapter provides the details of: the chemicals used for this research, the reaction procedures followed to obtain the desired products for this research, and the details of the instruments used and the sample preparation techniques employed for analysing the products.

3.1. Materials

L-Alanine (L-Al, 98+%, Aldrich), Di-tert butyl dicarbonate (*t*BOC, 99%, Aldrich), Triethyl amine (TEA, ≥99.5%, Sigma-Aldrich), Magnesium sulphate ($MgSO_4$,

anhydrous, EMD), Tetraethyleneglycol (TEG, 99%, Aldrich), *Candida antarctica* Lipase B (CALB, 33273 Da, 20 wt% immobilized on a macroporous acrylic resin Novozyme® 435), Poly(ethylene glycol) ($\overline{M_n}$ = 2050 g mol^{-1}, PEG_{2050}, Aldrich), Acetyl Chloride (AcCl, 98%, Sigma-Aldrich), β-Alanine (β-Al, 99+%, Aldrich). 2-Hydroxyethyl disulphide (2-HEDS, technical grade, 98%, Aldrich), Ethyl 4-bromobutyrate (EBB, 95%, Sigma-Aldrich), Folic Acid (FA, ≥ 97%, Sigma), *n*-butyllithium (*n*-BuLi, 1.6 M in cyclohexane, Sigma), Dithiothreitol (DTT, > 98%, TCI America), Fluorescein-*o*-acrylate (95%, FLA, Sigma-Aldrich), Methyl-3-mercaptopropionate (MP-SH, 98%, Alfa Aesar), Poly(ethylene glycol) ($\overline{M_n}$ = 1000 g mol^{-1}, PEG_{1000}, Aldrich), Poly(ethylene glycol) (Đ = 1, M.W. = 898 g mol^{-1}, $dPEG_{20}$, Quanta Biodesign^{TM}), Triethylene glycol monomethyl ether (M-TrEG-OH, Fluka), Poly(ethylene glycol) monomethyl ether ($\overline{M_n}$ = 750 g mol^{-1}, M-PEG_{750}-OH, Alfa Aesar), Poly(ethylene glycol) ($\overline{M_n}$ = 2000 g mol^{-1}, PEG_{2000}, Aldrich), Ethyl 5-bromovalerate (EBV, 99.2%, Chem-Impex Int'l Inc), Fluorescin (FL-COOH, 95%, TCI America), Sucrose ester of soybean oil (Sefose 1618 U, kindly provided by Dr. Dean Webster from North Dakota State University, USA), 2,2-Dimethoxy-2-phenylacetophenone (DMPA, 99%, Sigma-Aldrich), 2-[2-(2-sulfanylethoxy)ethoxy] ethanethiol (DODT, 95%, Aldrich), and Hydrogen Peroxide (H_2O_2, 3wt%, Sigma-Aldrich) were used without further purification.

Solvents: Methanol (MeOH, ≥99.8%, Fisher Scientific), Toluene (Tol, 99%, EMD Chemicals), Tetrahydrofuran (THF, 99%, Fisher Scientific), Hexanes (≥ 98.5%, Fisher Scientific), Ethyl Acetate (EtOAc, ≥ 99.5%, Fisher Scientific), Dimethyl sulfoxide (DMSO, anhydrous, ≥99.9%, Aldrich), Diethyl ether (DEE, ≥ 99.0%, Aldrich), N,N-Dimethylformamide (DMF, anhydrous, 99.8%, Aldrich) and acetone (≥ 99.8%, Sigma-

Aldrich), deuterated chloroform ($CDCl_3$, 99.8%, Cambridge Isotope Laboratories Inc.), and dimethyl sulfoxide–d6 (DMSO-*d6*, 99.9%, Cambridge Isotope Laboratories Inc.) were used without further purification.

3.2. Methods

3.2.1. Synthesis of PEG-diamines (H_2N-PEG-NH_2)

3.2.1.1. Esterification of L-Alanine with TEG

Protection of L -Alanine

L -Al (0.3030 g, 3.40 mmol, 1.0 eq.) and *t*BOC (1.1790 g, 5.40 mmol, 1.59 eq.) were dissolved in MeOH (5 mL). TEA (0.44476 g, 4.42 mmol, 1.30 eq.) was then added drop-wise to it and the contents were stirred for 60 minutes at RT (RT). The reactor contents were then refluxed for an additional 60 minutes. The MeOH was evaporated using a rotavap and the reaction mixture was then dried under vacuum at RT to recover the product (*t*BOC-L-Alanine).

Synthesis of tBOC-L-Al-TEG-L-Al-tBOC

TEG (0.7028 g, 3.62 mmol, 1.07 eq.) was dissolved in Tol (3 mL) at 50 °C. *t*BOC-L-Alanine (0.6371 g, 3.36 mmol, 1.0 eq.), CALB (0.1487 g resin @ 20 wt% enzyme, 8.93 x 10^{-4} mmol, 0.00026 eq.), and $MgSO_4$ (0.1 g) were then added to it and the pressure was then reduced to 240 mmHg. After 24 h, the reactor contents were diluted with 3 ml of THF and centrifuged for 30 minutes. The THF from the supernatant was evaporated using a rotavap and the product was dried under vacuum at RT for 12 hours.

3.2.1.2. Esterification of L-Alanine with PEG

Synthesis of tBOC-L-Al-PEG$_{2050}$-L-Al-tBOC

PEG$_{2050}$ (3.4766 g, 1.7 mmol, 0.5 eq.) was dried under vacuum at 65 ºC and 0.2 Torr for 16 hours. The dried PEG was dissolved in Tol (3 mL) and the temperature was reduced to 50 °C. *tBOC*-L-Alanine (0.6407 g, 3.38 mmol, 1.0 eq.), CALB (0.3072 g resin @ 20 wt% enzyme, 1.84 x 10^{-3} mmol, 0.00054 eq.), and $MgSO_4$ (0.1 g) were added to it and the pressure was reduced to 240 mmHg. After 24 hours, the reactor contents were diluted with 3 ml of THF and centrifuged for 30 minutes. The THF from the supernatant was evaporated using a rotavap and the product was dried under vacuum at RT for 12 hours.

De-protection of tBOC-L-Al-PEG$_{2050}$-L-Al-tBOC

*t*BOC-L-Al-PEG$_{2050}$-L-Al-*t*BOC (2.3246 g, 0.97 mmol, 1.0 eq.) was dissolved in EtOAc at RT and then MeOH (0.5 ml, 12.3 mmol, 12.72 eq.) was added to it. Acetyl chloride (0.5 ml, 7 mmol, 7.21 eq.) was added to it drop-wise and the reaction was continued for 15 hours. EtOAc and excess MeOH were evaporated from the reaction mixture using a rotavap. The remnants were then dissolved in 3 ml THF and the solution was precipitated in hexane to recover the product. The product was dried under vacuum at RT for 12 hours.

3.2.1.3. Esterification of β-Alanine with PEG

Protection of β-Alanine

β-Al (0.3093 g, 3.47 mmol, 1.0 eq.) and *t*BOC (1.1744 g, 5.38 mmol, 1.53 eq.) were dissolved in MeOH (5 mL). TEA (0.45 g, 4.45 mmol, 1.28 eq.) was then added drop-wise to it and the contents were stirred at RT for 60 minutes. The reactor contents were then refluxed for an additional 60 minutes. The MeOH was evaporated using a rotavap and the reaction mixture was then dried under vacuum at RT to recover the product (*t*BOC-β-Alanine).

Synthesis of tBOC-β-Al-PEG$_{2050}$-β-Al-tBOC

PEG$_{2050}$ (2.8745 g, 1.4 mmol, 0.4 eq.) was dried under vacuum at 65 ºC and 0.2 Torr for 16 hours. The dried PEG was dissolved in Tol (3 mL) and the temperature was reduced to 50 °C. *t*BOC-β-Alanine (0.6569 g, 3.47 mmol, 1.0 eq.), CALB (0.2963 g resin @ 20 wt% enzyme, 1.78 x 10^{-3} mmol, 0.00051 eq.), and $MgSO_4$ (0.1 g) were added to it and the pressure was reduced to 240 mmHg. After 24 hours, the reactor contents were diluted with 3 ml of THF and centrifuged for 30 minutes. The THF from the supernatant was evaporated using a rotavap and the product was dried under vacuum at RT for 12 hours.

De-protection of tBOC-Al-PEG$_{2050}$-Al-tBOC

*t*BOC-Al-PEG$_{2050}$-Al-*t*BOC (2.6662 g, 1.115 mmol, 1.0 eq.) was dissolved in EtOAc at RT and then MeOH (0.3 ml, 7.41 mmol, 6.65 eq.) was added to it. Acetyl chloride (0.5 ml, 7 mmol, 6.28 eq.) was added to it drop-wise and the reaction was

continued for 15 hours. EtOAc and excess MeOH were evaporated from the reaction mixture using a rotavap. The remnants were then dissolved in 3 ml THF and the solution was precipitated in hexane to recover the product. The product was dried under vacuum at RT for 12 hours.

3.2.2. Synthesis of FA-SH

3.2.2.1. Synthesis of FA-S-S-FA

CALB-Catalyzed Transesterification of EBB with 2-HEDS

2-HEDS (4.7388 g, 30.72 mmol, 1.0 eq.) was dried under vacuum (Schlenk line) at 65 ºC and 0.2 Torr until bubble formation stopped. Then EBB (25.8970 g, 132.7 mmol, 4.32 eq.) was added to the dried 2-HEDS. The temperature was reduced to 50 °C and CALB (1.0002 g resin @ 20 wt% enzyme, 0.0060 mmol, 0.00019 eq.) was added to it. The pressure was reduced to 0 mmHg. After 4h, the mixture was diluted with 3 ml of dried THF and was filtered over a Q5 filter paper. The filtrate was then precipitated in 100 ml hexane and the precipitate was dried under vacuum at RT for 12 hours. The molecular weight of Br-S-S-Br is 452.22 g/mol and the theoretical yield to be obtained is 13.89 g. The amount of product obtained was 10.6560 g, therefore, the experimental yield obtained is 76.71%.

γ-Lithiation of FA

FA (2.2039 g, 4.99 mmol, 1 eq.) was dissolved in 35 mL DMSO at 30 ^{o}C. The following morning, the round bottom flask was then introduced in a liquid nitrogen bath. After the contents were frozen, vacuum was applied to the flask for 3 minutes. The flask

was introduced in a warm water to thaw. Once it was thawed, the vacuum was then shut and nitrogen was passed through the flask for few minutes. The freeze-pump-thaw cycle was performed two more times. The assembly was taken in a dry box, n-BuLi. *n*-BuLi (3.2 ml, 5.12 mmol, 1.02 eq.) was then added drop-wise to the dissolved FA. An additional 8 ml anhydrous DMSO was added to it. The contents were stirred until a clear solution was obtained. Br-S-S-Br (1.1606 g, 2.56 mmol, 0.51 eq.) was then added drop-wise to it. After 24h, the reaction mixture was precipitated in 500 ml DEE and the precipitate was washed with 200 ml DEE. The product was dried under vacuum for 16 hours.

3.2.2.2. Reduction of FA-S-S-FA

FA-S-S-FA (0.5264 g, 0.490 mmol, 1 eq.) was dissolved in 10 mL DMF at 30 °C. DTT (0.074 g, 0.48 mmol, 0.98 eq.) was added to it under N_2. After 48 hours, the reactor contents were precipitated in 50 ml DEE and dried under vacuum for 16 hours.

3.2.3. Synthesis of Thiol-functionalized TEG and PEGs

3.2.3.1. Kinetics of CALB-catalyzed transesterification of MP-SH with TEG

TEG (1.9782 g, 10.2 mmol) was dried under vacuum (Schlenk line) at 65 ºC and 0.2 Torr until bubble formation ceased. It was then mixed with MP-SH (3.6204 g, 30.1 mmol) at 50 ºC and 420 Torr with CALB (0.2549 g resin @ 20 wt% enzyme, 0.0015 mmol). After 1 minute, the vacuum was removed, N_2 gas was passed through the system and an aliquot was collected. The vacuum was reinstated, and the procedure was repeated to collect aliquots at 3, 5, 10, 15, 30, 60, 120, 240, 300, 390, and 450 minutes.

Synthesis of HO-TEG-SH

TEG (3.8805 g, 20 mmol) was dried under vacuum (Schlenk line) at 65 ºC and 0.2 Torr until bubble formation ceased. It was then mixed with MP-SH (7.4007 g, 61.6 mmol) at 50 ºC and 420 Torr with CALB (0.4912 g resin @ 20 wt% enzyme, 0.0029 mmol). After 15 minutes, the reaction mixture was dissolved in 3 ml of dried THF, filtered on a Q5 filter paper and then dried under vacuum (Schlenk line) at 50 ºC for two hours. The product was dried under vacuum for 16 hours (4.1685 g, 93% reaction yield).

Synthesis of HS-TEG-SH

TEG (1.9782 g, 10.2 mmol) was dried under vacuum (Schlenk line) at 65 ºC and 0.2 Torr until bubble formation ceased. It was then mixed with MP-SH (3.6204 g, 30.1 mmol) at 50 ºC and 420 Torr with CALB (0.2549 g resin @ 20 wt% enzyme, 0.0015 mmol). After 450 minutes, the reaction mixture was dissolved in 3 ml of dried THF, filtered on a Q5 filter paper and then dried under vacuum (Schlenk line) at 50 ºC for two hours. The product was dried under vacuum oven for 16 hours (3.5327g, 88% reaction yield).

3.2.3.2. Kinetics of CALB-catalyzed transesterification of MP-SH with PEG_{1000}

PEG_{1000} (3.9893 g, 4.04 mmol) was dried under vacuum (Schlenk line) at 65 ºC and 0.2 Torr for 16 hours. It was then mixed with MP-SH (1.4563 g, 12.11 mmol) and reacted at 50 ºC and 420 Torr with CALB (0.0977 g resin @ 20 wt% enzyme, 0.00058 mmol). After 1 minute, the vacuum was removed and N_2 gas was passed through the system and an aliquot was collected. The vacuum was reinstated, and the procedure was

repeated to collect aliquots at 3, 5, 10, 15, 30, 60, 120, 240, 360, 480, 600, 720, 960, and 1440 minutes.

Synthesis of HO-PEG$_{1000}$-SH

PEG$_{1000}$ (6.0882 g, 6.16 mmol) was dried under vacuum (Schlenk line) at 65 ºC and 0.2 Torr for 16 hours. It was then mixed with MP-SH (2.1793 g, 18.13 mmol) and reacted at 50 ºC and 420 Torr and CALB (0.1501 g resin @ 20 wt% enzyme, 0.00090 mmol). After 24 hours, the reaction mixture was dissolved in 3 ml of dried THF, filtered on a Q5 filter paper and then dried under vacuum (Schlenk line) at 50 ºC for 16 hours. The product was dried under vacuum for 16 hours (6.0967 g, ~100% reaction yield).

Synthesis of HS-PEG$_{1000}$-SH

HO-PEG$_{1000}$-SH (2.1005 g, 1.95 mmol) was dried under vacuum (Schlenk line) at 65 ºC and 0.2 Torr for 16 hours. It was then mixed with MP-SH (3.1031 g, 25.8 mmol) at 50 ºC and 420 Torr and CALB (0.0940 g resin @ 20 wt% enzyme, 0.00056 mmol) for 24 hours. After 24 hours of reaction time, the reaction mixture was dissolved in 3 ml of dried THF, filtered on a Q5 filter paper and then dried under vacuum (Schlenk line) at 50 ºC for 16 hours. The product was dried under vacuum for 16 hours. (2.1461 g, 85% reaction yield).

3.2.3.3. Kinetics of CALB-catalyzed transesterification of MP-SH with PEG$_{2050}$

PEG$_{2050}$ (4.6117 g, 2.25 mmol) was dried under vacuum (Schlenk line) at 65 ºC and 0.2 Torr for 16 hours. It was then mixed with MP-SH (1.6550 g, 13.7 mmol) and

reacted at 50 ºC and 420 Torr and CALB (0.1134 g resin @ 20 wt% enzyme, 0.00068 mmol). After 1 minute, the vacuum was removed and N_2 gas was passed through the system and an aliquot was collected. The vacuum was reinstated, and the procedure was repeated to collect aliquots at 3, 5, 10, 15, 30, 60, 120, 240, 360, 480, 600, 720, 960, and 1440 minutes.

Synthesis of HO-PEG$_{2050}$-SH

PEG$_{2050}$ (4.6117 g, 2.25 mmol) was dried under vacuum at 65 ºC and 0.2 Torr for 16 hours. It was then mixed with MP-SH (1.6550 g, 13.7 mmol) and reacted at 50 ºC and 420 Torr and CALB (0.1134 g resin @ 20 wt% enzyme, 0.00068 mmol). After 24 hours, the reaction mixture was dissolved in 3 ml of dried THF, filtered on a Q5 filter paper, and precipitated in 100 mL DEE. The product was dried under vacuum oven for 16 hours (4.2034 g, ~100% reaction yield).

Synthesis of HS-PEG$_{2050}$-SH

HO-PEG$_{2050}$-SH (4.000 g, 1.87 mmol) was dried under vacuum (Schlenk line) at 65 ºC and 0.2 Torr for 16 hours. It was then mixed with MP-SH (2.7125 g, 22.5 mmol) at 50 ºC and 420 Torr and CALB (0.2274 g resin @ 20 wt% enzyme, 0.0013 mmol). After 24 hours, the reaction mixture was dissolved in 3 ml of dried THF, filtered on a Q5 filter paper and precipitated in 100 mL DEE. The product was dried under vacuum for 16 hours (3.7791 g, 94% reaction yield).

3.2.3.4. Synthesis of HS-dPEG$_{20}$-SH

dPEG$_{20}$ (0.4957 g, 0.55 mmol, 1.0 eq.) was dried under vacuum at 65 ºC and 0.2 Torr for 16 hours. MP-SH (0.6618 g, 5.50 mmol, 5 eq./OH) was then added to the dried dPEG$_{20}$ at 50 °C. CALB (0.1015 g resin @ 20 wt% enzyme, 0.00061 mmol) was then added to it and the pressure was reduced to 420 mmHg. After 24 hours, the mixture was dissolved in 3 ml of dried THF and was filtered on a Q5 filter paper. The filtrate was precipitated in DEE and the precipitate was redissolved in THF and again precipitated in DEE. This procedure was repeated three more times. The precipitate was dried under vacuum for 12 hours (0.5420 g, 91.41% conversion).

3.2.4. Michael Addition of FA-SH to Acrylate-functionalized TEG and PEGs

3.2.4.1. Michael Addition of FA-SH to Ac-FL-TEG-FL-Ac

FA-SH (0.2865 g, 0.48 mmol, 3.00 eq.) and Ac-FL-TEG-FL-Ac (0.1999 g, 0.16 mmol, 1 eq., provided by Gayatri Shrikhande) were dissolved in DMSO (2 mL) at 50 °C. CALB (0.0866 g resin @ 20 wt% enzyme, 0.00052 mmol) was then added to it. After 8 hours, the reactor contents were dissolved in 3 ml of DMSO and filtered on a Q5 filter paper. The filtrate was precipitated in hexane and dried under vacuum for 12 hours. The molecular weight of FA- FL-TEG-FL-FA is 2426.51 g/mol and the theoretical yield to be obtained is 0.3876 g. The amount of product obtained was 0.4793 g.

3.2.4.2. Michael Addition of FA-SH to Ac-FL-PEG$_{1000}$-FL-Ac

FA-SH (0.1333 g, 0.226 mmol, 3.14 eq.) and Ac-FL-PEG$_{1000}$-FL-Ac (0.1472 g, 0.072 mmol, 1 eq., provided by Gayatri Shrikhande) were dissolved in DMSO (2 mL) at

50 °C. CALB (0.098 g resin @ 20 wt% enzyme, 0.00059 mmol) was then added to it. After 8 hours, the reactor contents were dissolved in 3 ml of DMSO and filtered on a Q5 filter paper. The filtrate was precipitated in hexane and dried under vacuum for 12 hours. The molecular weight of FA-FL-PEG_{1000}-FL-FA is 3218.39 g/mol and the theoretical yield to be obtained is 0.2318 g. The amount of product obtained was 0.2082 g.

3.2.4.3. Michael Addition of FA-SH to Ac-FL-PEG_{2050}-FL-Ac

FA-SH (0.0645 g, 0.11 mmol, 3.6 eq.) and Ac-FL-PEG_{2050}-FL-Ac (0.0929 g, 0.030 mmol, 1 eq.) were dissolved in DMSO (2 mL) at 50 °C. CALB (0.0878 g resin @ 20 wt% enzyme, 0.00053 mmol) was then added to it. After 8 hours, the reactor contents were dissolved in 3 ml of DMSO and filtered on a Q5 filter paper. The filtrate was precipitated in hexane and the product was dried under vacuum oven at RT for 12 hours. The molecular weight of FA-FL-PEG_{2050}-FL-FA is 4218.22 g/mol and the theoretical yield to be obtained is 0.1287 g. The amount of product obtained was 0.1288 g.

3.2.4.4. Michael Addition of FA-SH to Ac-FL-$dPEG_{20}$-FL-Ac

FA-SH (0.2646 g, 0.45 mmol, 3.00 eq.) and Ac-FL-$dPEG_{20}$-FL-Ac (0.2934 g, 0.15 mmol, 1.0 eq.) were dissolved in DMSO (2 ml) at 50 °C. CALB (0.1232 g resin @ 20 wt% enzyme, 0.00074 mmol) was then added to it. After 8 hours, the reactor contents were dissolved in 3 ml of DMSO and filtered on a Q5 filter paper. The filtrate was precipitated in hexane and the product was dried under vacuum at RT for 12 hours. The molecular weight of FA-FL-$dPEG_{20}$-FL-FA is 3133.39 g/mol and the theoretical yield to be obtained is 0.4694 g. The amount of product obtained was 0.5528g.

3.2.5. Synthesis of Br-PEG-Br

PEG_{2000} (5.1652 g, 2.58 mmol) was dried under vacuum at 65 ºC and 0.2 Torr for 16 hours. EBV (5.2840 g, 25.2 mmol) and CALB (0.0935 g resin @ 20 wt% enzyme, 0.00056 mmol) were added to it and the pressure was reduced to 420 Torr. After 3 hours, the reactor contents were dissolved in 3 ml dried THF, filtered on a Q5 filter paper, and precipitated in 600 ml hexane. The product was dried under vacuum for 16 hours (4.3705 g, ~70% reaction yield).

3.2.6. Synthesis of FL-COO-PEG-OOC-FL

Br-PEG-Br (0.3526 g, 0.15 mmol) and Fluorescin (0.1011 g, 0.30 mmol) were dried at 65 ºC and 0.2 Torr for 16 hours in two separate two-necked round bottom flasks. Distilled DMSO (1 mL) was added to each flask under air-free Argon environment and the contents were stirred until a homogeneous solution was obtained. The Fluorescin solution was introduced in a liquid N_2 for degasification. After the contents were frozen, vacuum was applied to the flask for 3 minutes. The flask was introduced in warm water to thaw. Once the contents were thawed, the vacuum was then shut and argon was passed through the flask for few minutes. This freeze-pump-thaw cycle was performed two more times. The freeze-pump-thaw cycle was also performed with Br-PEG-Br solution for three times. The Fluorescin solution and Br-PEG-Br solutions were then taken in a dry box along with n-BuLi bottle. *n*-BuLi (0.19 ml, 0.30 mmol, 1.00 eq.) was then added drop-wise to the dissolved Fluorescin and stirred until the mixture was homogenized. An aliquot was obtained from it, precipitated in hexane, and dried under vacuum for 3 hours for ^{1}H-NMR analysis. Br-PEG-Br solution was withdrawn from its round bottom flask

and added dropwise to the lithiated Fluorescin solution. Aliquots were obtained at 1, 5, 10, 15, and 30 min reaction time. These aliquots were immediately precipitated in hexane and dried under vacuum for 3h for ^{1}H-NMR analysis.

3.2.7. Synthesis of Multifunctional PEGs from Sucrose Ester of Soybean Oil

3.2.7.1. Thiol-ene Click Reaction of M-TrEG-SH on Sefose

Synthesis of M-TrEG-SH

M-TrEG-OH (3.3083 g, 20.14 mmol) was dried under vacuum (Schlenk line) at 65 ºC and 0.2 Torr until bubble formation ceased. It was then mixed with MP-SH (4.2752 g, 35.57 mmol) at 50 ºC and 420 Torr in presence of CALB (0.4404 g resin @ 20 wt% enzyme, 0.0026 x 10^{-3} mmol). After 8h, the reaction mixture was diluted with 3 ml of dichloromethane, filtered over a Q5 filter paper and then dried under vacuum (Schlenk line) at 50 ºC for 5 hours. The product was then dried in a vacuum oven for further analysis (4.4336g, 87.2% reaction yield).

Synthesis of Sefose-(S-TrEG-M)$_{22}$

Sefose 1618 U (0.5108g, 0.23 mmol, 1 eq.), M-TrEG-SH(1.4622g, 5.8 mmol, 24.79 eq.) and 0.5 ml $CDCl_3$ were stirred at RT for 5 min to obtain a homogeneous mixture. DMPA (0.0374g, 1.86 wt%) was then added to it and stirred at RT until all the DMPA powder was dissolved. The reaction mixture was exposed to UV radiation for 15 min. A UV light strength of 162 mW was used and the distance maintained from the probe was 1.2 inch. After 15, 30, 45 and 60 minutes, an aliquot was obtained from the

reaction mixture. The NMR of the sample was obtained in $CDCl_3$. No work up was performed.

3.2.7.2. Thiol-ene Click Reaction of HO-TEG-SH on Sefose

Synthesis of Sefose-(S-TEG-OH)$_{22}$

Sefose 1618 U (0.5595g, 0.26 mmol, 1 eq.), HO-TEG-SH (1.727g, 6.1 mmol, 23.89 eq.) and 0.5 ml $CDCl_3$ were stirred at RT for 5 min to obtain a homogeneous mixture. DMPA (0.0334g, 1.44 wt%) was then added to it and stirred at RT until all the DMPA powder was dissolved. The reaction mixture was exposed to UV radiation for 15 min. A UV light strength of 162 mW was used and the distance maintained from the probe was 1.2 inch. After 15, 30, 45 and 60 minutes, an aliquot was obtained from the reaction mixture.

3.2.7.3. Thiol-ene Click Reaction of M-PEG$_{750}$-SH on Sefose

Synthesis of M-PEG-SH

M-PEG$_{750}$-OH (7.5157 g, 10.02 mmol) was dried under vacuum (Schlenk line) at 65 ºC and 0.2 Torr until bubble formation ceased. It was then mixed with MP-SH (3.6095 g, 30.03 mmol) at 50 ºC and 420 Torr in presence of CALB (0.4494 g resin @ 20 wt% enzyme, 0.0027 x 10^{-3} mmol). After 12h, the reaction mixture was diluted with 2 ml of THF, filtered over a Q5 filter paper and then dried under vacuum (Schlenk line) at 50 ºC for 2 hours. The product was then dried in a vacuum oven for further analysis.

Synthesis of Sefose-(S-PEG$_{750}$-OH)$_8$

Sefose 1618 U (0.4926g, 0.22 mmol, 1 eq.), M-PEG$_{750}$-SH (1.5948g, 1.83 mmol, 8.14 eq.) and 2 ml $CDCl_3$ were stirred at RT for 5 min to obtain a homogeneous mixture. DMPA (0.039g, 1.83 wt%) was then added to it and stirred at RT until all the DMPA powder was dissolved. The reaction mixture was exposed to UV radiation for 15 min. A UV light strength of 162 mW was used and the distance maintained from the probe was 1.2 inch. After 5, 10, and 15 minutes, an aliquot was obtained from the reaction mixture.

3.2.8. Synthesis of Poly(DODT) – Box-Behnken Design

Stock solutions of DODT in TEA namely A, B, and C were prepared where A had TEA/DODT molar ratio of 0.5, B had 2, and C had 3.5. For preparing stock solution A, DODT (10.9232 g, 59.9 mmol) was dissolved in TEA (3.0320 g, 30.0 mmol). For preparing stock solution B, DODT (10.9203 g, 59.9 mmol) was dissolved in TEA (12.1429 g, 120.0 mmol). For preparing stock solution C, DODT (10.9285 g, 59.9 mmol) was dissolved in TEA (21.2477 g, 210.0 mmol). The stock solutions were prepared in conical flasks and stirred for approximately 20 min at RT.

According to each experiment, a vial or glass beaker was filled with specific amount of hydrogen peroxide. To each vial or glass beaker, specific amount of stock solution (based on the experiment number, Table 3.1) was added in one shot under stirring. Each vial or glass beaker was reacted for a specific amount of time (based on the experiment number, Table 3.1) before the reaction was terminated by emptying the vial or beaker contents immediately into 30 ml methanol. Methanol was immediately decanted and then, the polymer was soaked in acetone for 24 hours. The acetone was

decanted and replenished every 24 hours for 72 hours. The contents were then dried under vacuum for 24 hours.

Table 3.1 Chemical Recipe for Synthesis of Poly(DODT) using Box-Behnken Experimental Design

Experiment No.	**Reaction Time (min)**	**DODT/TEA Stock Solution (mL)**	**H_2O_2 (mL)**
1	1	1.30 (A)	12.68
2	1	3.90 (B)	13.57
3	9	1.30 (A)	12.68
4	9	3.90 (B	13.57
5	1	2.60 (B)	3.33
6	1	2.60 (B)	23.33
7	9	2.60 (B)	3.33
8	9	2.60 (B)	23.33
9	5	1.30 (A)	3.17
10	5	1.30 (A)	22.18
11	5	3.90 (C)	3.39
12	5	3.90 (C)	7.92
13	5	2.60 (B)	13.33

3.3. Characterization

Nuclear magnetic resonance (NMR) spectroscopy, matrix assisted laser desorption/ionization mass spectrometry (MALDI MS), and Electrospray Ionization Mass Spectrometry (ESI-MS) were used to analyse the products synthesized for this investigation. MALDI MS and ESI MS was performed at Dr Chrys Wesdemiotis' lab at the University of Akron and at the Mass Spectrometry and Proteomics Facility at The Ohio State University.

3.3.1. Nuclear Magnetic Resonance (NMR) Spectroscopy

Proton (^{1}H) and carbon (^{13}C) NMR spectra were obtained on Varian Mercury 300 MHz and/or Varian NMRS 500 MHz spectrometer at the University of Akron. $CDCl_3$

and DMSO-*d*6 were used as NMR solvents. The signals corresponding to the protons present in the non-deuterated chloroform and non-deuterated dimethylsulfoxide appear at δ=7.27 ppm and δ=2.5 ppm respectively in the ^{1}H NMR spectrum. The signals corresponding to the carbon atoms present in $CDCl_3$ and DMSO-*d6* appear at δ=77.23 ppm and δ=39.51 ppm respectively in the ^{13}C NMR spectrum. These signals were used as internal references. The samples for ^{1}H NMR spectroscopy characterization were prepared with 10-15mg of product dissolved in 0.6 ml of NMR solvent in NMR tubes with 5 mm diameter. The spectra were obtained with 32-128 transients and a relaxation delay of 1-10 sec. Samples for ^{13}C NMR spectroscopy characterization were prepared similarly with 50-60 mg of the product dissolved in 0.6 ml of NMR solvent. The spectra were obtained with 5000-20000 transients and a relaxation delay of 1-5 sec.

CHAPTER IV

RESULTS AND DISCUSSION

Parts of this chapter have been published:

- Reprinted with permission from Puskas, J. E.; Castano, M.; Mulay, P.; Dudipala, V.; Wesdemiotis, C. Method for the Synthesis of γ-PEGylated Folic Acid and Its Fluorescein-Labeled Derivative. *Macromolecules* **2018**, *51(22)*, 9069-9077. Copyright © 2018 American Chemical Society.
- Reprinted with permission from Mulay, P.; Shrikhande, G.; Puskas, J. E. Synthesis of Mono- and Dithiols of Tetraethylene Glycol and Poly(ethylene glycol)s via Enzyme Catalysis. *Catalysts* **2019**, *9(3)*, 228. Copyright © 2019 MDPI.

The objective of this research was to synthesize two-functional folate-targeted fluorescein-labeled poly(ethylene-glycol)(PEG)-based diagnostic agents (FA-FL-PEG-FL-FA) that have potential applications in TNBC diagnosis. For this purpose, three synthetic strategies were investigated. These strategies, along with their synthesis and characterization will be discussed in detail in this chapter. Strategy 1 uses PEG-diamines and thiol-functionalized (FA-SH) as the one of the starting materials. This strategy along with the novel enzyme-catalyzed methods to synthesize PEG-diamine and FA-SH will be discussed in Section 4.1. Strategy 2 uses PEG-dithiols. The novel enzyme-catalyzed methods to synthesize PEG-dithiols will be discussed in Section 4.2. The Michael addition of FA-SH on two-functional folate-targeted PEG will be presented in Section 4.3. Strategy 3 using lithium technology for

PEGylation of fluorescin will be discussed in Section 4.4. This investigation also explored the possibility of using sucrose esters of soybean oil as a multivalent carrier for PEG-based cancer diagnostic agents and the same will be presented in Section 4.5. The synthesis and characterization of cyclic polydisulfide polymers from DODT monomer will be discussed in Section 4.6.

4.1 Syntheses of H_2N-PEG-NH_2 and FA-SH

FA-FL-PEG-FL-FA was initially synthesized as shown in Figure 2.7 for the Cleveland Clinic *in vitro* trials using commercial FLDA and H_2N-PEG-NH_2 (Section 2.1.5). First poly(ethylene glycol)(PEG)-diamine (H_2N-PEG-NH_2) was reacted with 2 equivalents of Fluorescein-*o,o'*-diacrylate (FLDA) via an enzyme (*Candida antartica* Lipase B, CALB)-catalyzed Michael addition to obtain an acrylated fluorescein-labeled PEG (Ac-FL-PEG-FL-Ac). The Ac-FL-PEG-FL-Ac was then reacted with 2 equivalents of a thiol-functionalized Folic Acid (FA-SH) through CALB-catalyzed Michael addition for obtaining a FA functionalized fluorescein-labeled PEG (FA-FL-PEG-FL-FA). Because of the concern about possible side products by chain-chain coupling in the reaction of FLDA with H_2N-PEG-NH_2, we developed Strategy 1, presented in Figure 2.13. In Strategy 1, first H_2N-PEG-NH_2 is reacted with 2 equivalents of Fluorescein-*o*-acrylate (FLA) through CALB-catalyzed Michael addition for obtaining a fluorescein-labeled PEG (FL-PEG-FL). The FL-PEG-FL is then reacted with 2 equivalents of acryloyl chloride (AcCl) in presence of trimethylamine (TEA) to obtain an acrylated fluorescein-labeled PEG (Ac-FL-PEG-FL-Ac). The Ac-FL-PEG-FL-Ac is then reacted with FA-SH through CALB-catalyzed Michael addition for obtaining FA-FL-PEG-FL-FA.

Strategy 1 uses PEG-diamine and FA-SH. I developed a new synthesis method for PEG-diamine and modified the synthesis method for FA-SH that was developed earlier. The syntheses will be discussed in the next two sections.

4.1.1 Synthesis of H_2N-PEG-NH_2

The ^{1}H-NMR spectrum of commercial H_2N-PEG-NH_2 (M_n = 2000 g/mol, ~45 monomer units) from Sigma is shown in Figure 4.1. The -CH_2- protons (b) besides the amine end-groups appearing at δ = 2.87 ppm are set to an integral value of 4. The internal -CH_2- protons (c) appear at δ = 3.52 and show an integral value of 4.34. In addition, the theoretical integral value of the -CH_2- protons (d) from the PEG backbone should be approximately 43 x 4 = 172 and the obtained value is 245, suggesting a presence of more than one product in the H_2N-PEG-NH_2 sample.

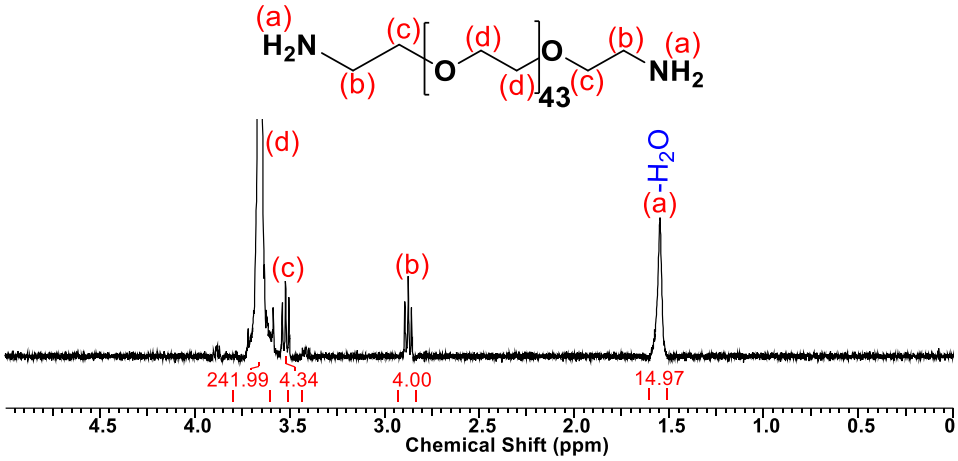

Figure 4.1 ^{1}H-NMR spectrum of commercial H_2N-PEG-NH_2 from Sigma

Commercial H_2N-PEG-NH_2 from Sigma was analysed using MALDI mass spectrometry. A mass spectrum of H_2N-PEG-NH_2 is shown in Figure 4.2. There are two distributions of signals, each separated by 44 *m/z* units. The smaller distribution belongs to the H_2N-PEG-NH_2. The signal at *m/z* 2218.077 (inset) belongs to the hydrogen complex of 48-mer unit of H_2N-PEG-NH_2 [2218.077 ≅ 48 x 44.02 (C_2H_4O repeat unit) + 44.08 ($H_2NC_2H_4$- end group) + 60.08 ($H_2NC_2H_4O$- end group) + 1.01

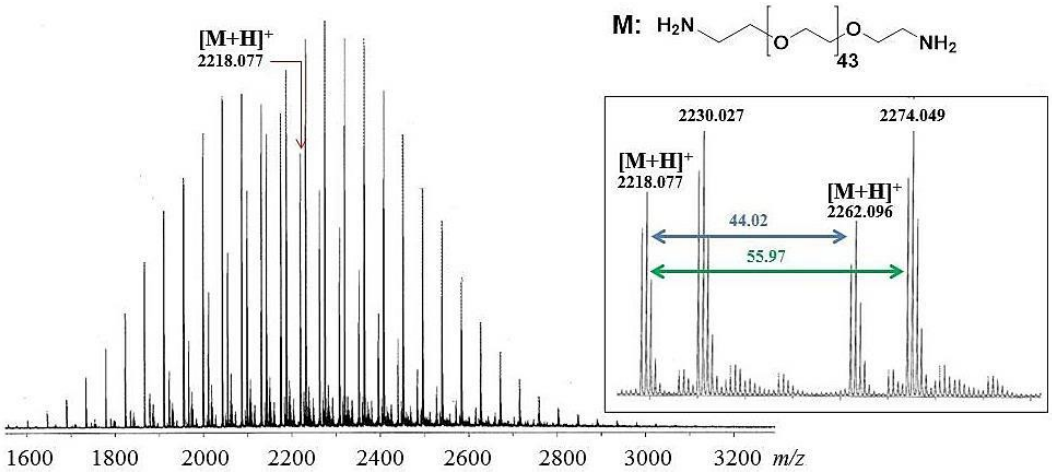

Figure 4.2 MALDI mass spectrum of commercial H_2N-PEG-NH_2 (M_n = 2000 g/mol) from Sigma. Inset: spectrum of 48- and 49-mer fractions, 44 *m/z* = PEG repeat unit

(H+)]. The major distribution is unknown and it appears at a difference of 56 *m/z* from the product distribution. The signal at *m/z* 2274.049 (inset) belongs to the hydrogen complex of 48-mer unit of this unknown product. In conclusion, the commercially available H_2N-PEG-NH_2 contains a significant amount of impurity. Therefore, I decided to synthesize PEG-diamines.

PEG-diamines are reportedly prepared by reacting PEG with tosyl chloride in basic medium followed by reaction with ammonia/hydrazine hydrate (Gabriel Synthesis) which provides 90% yield.[70-75] PEG-diamines are also synthesized by reacting dibromoethyl-PEG and ammonia under pressure (Hoffman reaction)[76] or by reacting PEG with imidazoles followed by reduction with piperazines.[77] Another reported method to obtain PEG-diamines is by reacting PEG with chlorine, followed by nitrilation, and later reduction with H_2 and Ni/carbon catalysis under pressure.[78-80] An improved method involved chlorination of PEG and then "nucleophilic displacement of the chlorine groups with phthalimide and hydrazinolysis of the phthalimide".[81, 82] PEG-diamines were also obtained by reacting PEG with pthalimide in a Mitsunobu type reaction followed by hydrozinolysis.[83, 84] In another method, PEG was first reacted with bis(4-nitrophenyl)biscarbonate, followed by reaction with 1-*N*-

t-butyloxycarbonyl-ethylenediamine, and deprotection with trifluoroacetic acid, producing PEG-diamines.[85] Recently, butyloxycarbonyl (BOC)-protected amino acids were reacted with PEG using catalysts DCC/EDC/DMAP, yielding di-BOC functionalized PEG that on de-protection produces PEG-diamines.[86-88]

I developed a new synthetic strategy for the synthesis of H_2N-PEG-NH_2, shown in Figure 4.3. First, the carboxylic acid end-group of a *tert*-butyloxycarbonyl protected L-Alanine (*t*BOC-L-Al) is reacted with the hydroxyl end-group of the PEG using CALB- catalyzed esterification to obtain a protected alanine-functionalized PEG (*t*BOC-L-Al-PEG-L-Al-*t*BOC). The *t*BOC group is later de-protected using HCl formed *in situ* with acetyl chloride that yields a diamine-functionalized PEG (H_2N-PEG-NH_2). First a model reaction with tetraethylene glycol (TEG) was carried out.

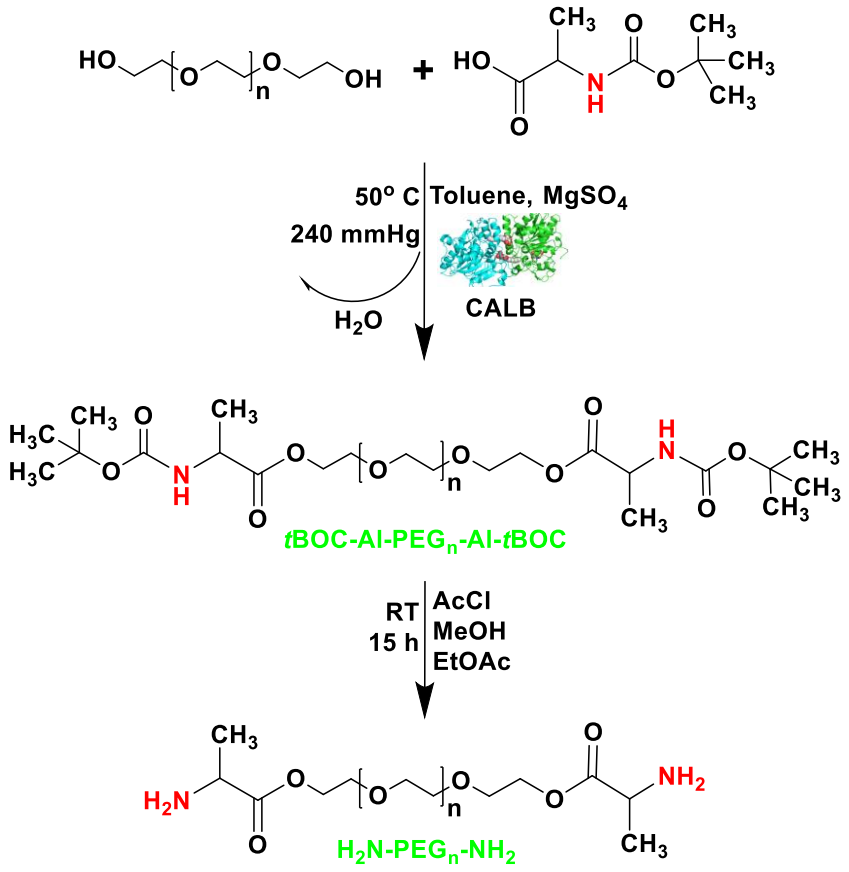

Figure 4.3 Reaction scheme for enzymatic synthesis of H_2N-PEG-NH_2

4.1.1.1 Esterification of L-Alanine with TEG

Alanines are aliphatic amino acids with amine and carboxylic acid as end-groups with two carbon units in between. There are two types of alanine present in nature, α and β, in which the amino group is situated at either the α or β position, respectively, from the carboxylate group. α-Alanine has two stereoisomers, L and D, whereas β-Alanine has none. L-Alanine (NH_2CHCH_3COOH) is a branched chain amino acid with one methyl group between the amino and the carboxylic acid end-groups.[89] Alanine is chosen to amine-functionalize the TEG because it is a small molecule with an amine group as the functional moiety on one end and a carboxylic acid end-group to react with the hydroxyl group of the TEG on the other end. L-Alanine was chosen instead of D-Alanine because D-Alanine is toxic to the living systems.[90] In order to prevent side reactions with the amine group, *t*BOC protected L-alanine was prepared. Figure 4.4 shows the reaction to synthesize *t*BOC protected L-alanine. The amine of the L-Alanine is protected with a *tert*-butyloxycarbonyl group (*t*BOC) by refluxing the L-Alanine with di-*tert*-butyl dicarbonate in methanol to obtain a *t*BOC protected alanine (*t*BOC-L-Al).

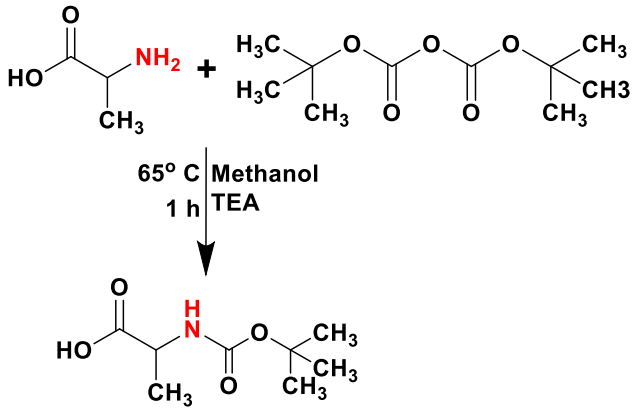

Figure 4.4 Reaction scheme for protection of L-Alanine

Figure 4.5 shows the ^{1}H-NMR spectrum of L-Alanine. The signal for the methyl protons (g) appear at δ = 1.47 ppm and the signal for the methine proton (f) appear at δ = 3.77 ppm.

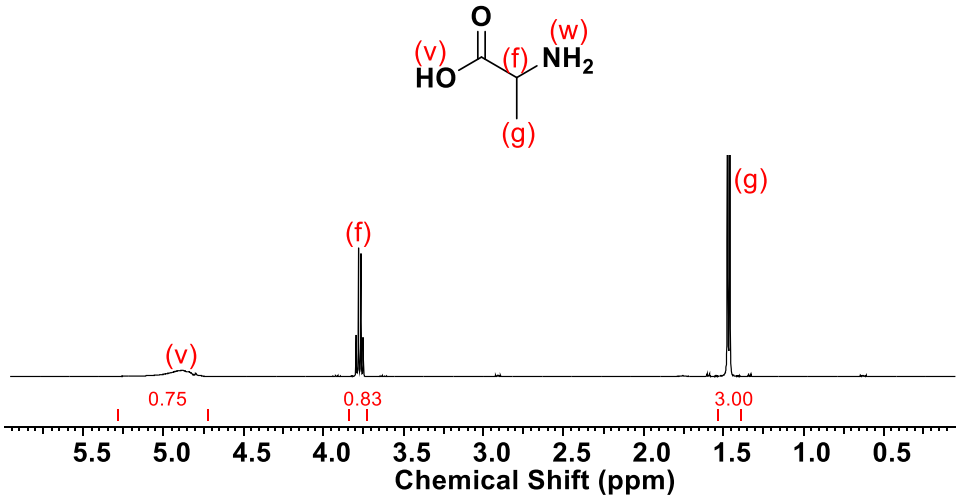

Figure 4.5 ^{1}H-NMR spectrum of L-alanine

Figure 4.6 shows the ^{1}H-NMR spectrum of the *t*BOC-L-Al. The signal belonging to the methine proton (f) from L-Alanine moved downfield to (f') at δ = 4.05 ppm after protection of the amine group. The relative integrals of (j): (f'): (g) are in the ratio of 9.00 : 0.83 : 3.02, demonstrating the completion of the reaction (~100% conversion) by NMR spectroscopy analysis. Figure 4.6 also indicates the presence of the residual TEA with signals corresponding to it appearing at δ = 3.00 ppm (-CH_2- protons of TEA) and δ = 1.40 ppm (methyl protons of TEA).

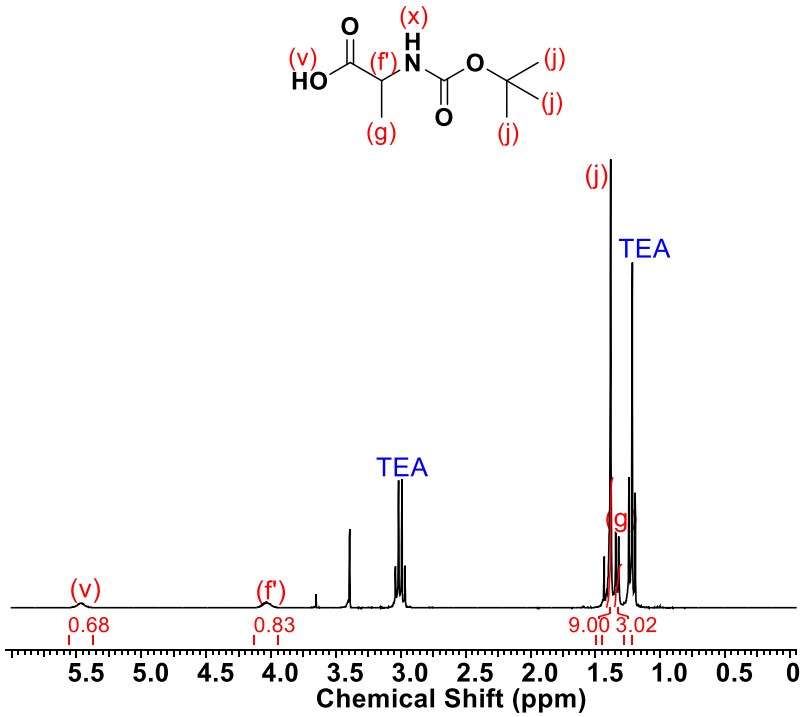

Figure 4.6 ^{1}H-NMR spectrum of L-alanine after *t*BOC protection

TEG was then reacted with the –COOH end group of *t*BOC-L-Al to obtain *t*BOC-L-Al functionalized TEG (*t*BOC-L-Al-TEG-L-Al-*t*BOC). Since esterification is a reversible reaction, the removal of the by-product (water in this case) becomes necessary to push the reaction in the forward direction. The removal of water was achieved by pulling a mild vacuum of 240 mmHg and by adding anhydrous magnesium sulphate to absorb water. Figure 4.7 shows the ^{1}H-NMR spectrum of TEG. The signal for the -CH_2- protons (b) besides the hydroxyl end-group appear at δ = 3.53 ppm and the signal for the TEG backbone -CH_2- protons (d) appear at δ = 3.60 ppm. The integral value of (d) is set to 8 that correspond to the 8 protons in the TEG backbone. The integral values obtained for (b) and (c) are 4.09 and 4.24 that correspond to the 4 protons each from the end-group.

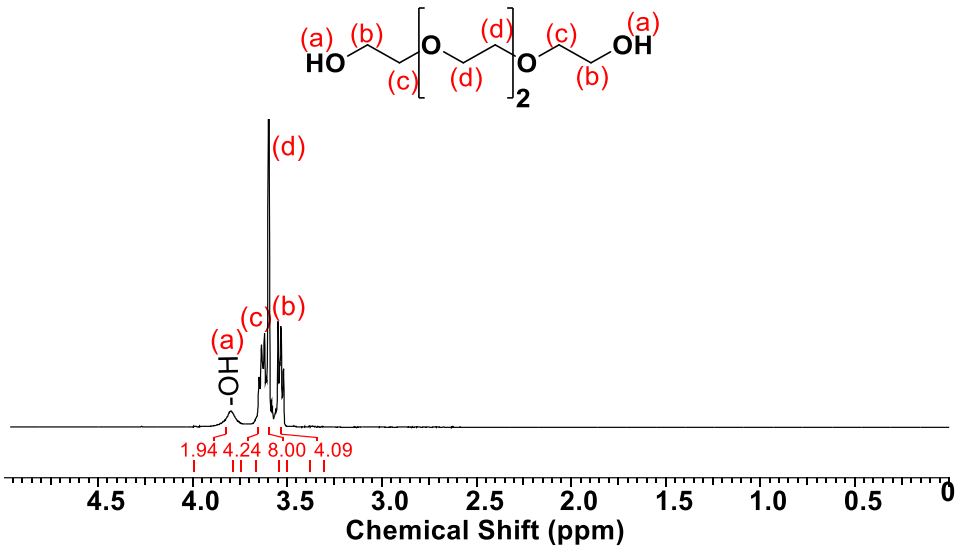

Figure 4.7 ^{1}H-NMR spectrum of TEG

Figure 4.8 shows the ^{1}H-NMR spectrum of *t*BOC-L-Al-TEG-L-Al-*t*BOC. The signal corresponding to the methine proton (f') from *t*BOC-L-Al moved downfield to (f") δ = 4.30 ppm after protection of the amine group. A new peak appeared at δ = 4.30 ppm (b') overlapping with signal (f"), which belongs to the -CH_2- proton besides the newly formed ester group. The signal corresponding to (b) at δ = 3.53 ppm has completely disappeared. The relative integrals of (b') + (f"): (j) are in the ratio 6.04:

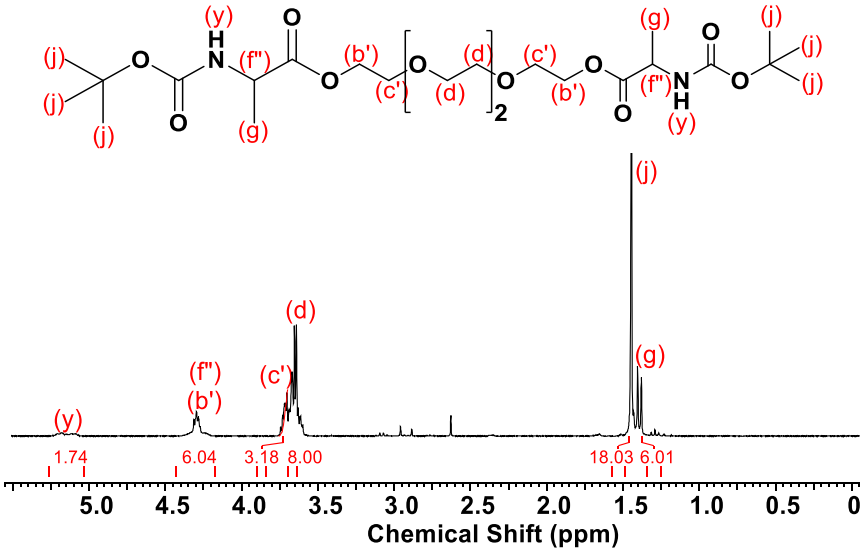

Figure 4.8 ^{1}H-NMR spectrum of *t*BOC-L-Al-TEG-L-Al-*t*BOC

18.03, demonstrating ~100% conversion. The (d) signal belongs to the -CH_2- protons present in the TEG backbone. Figure 4.8 does not show the presence of TEA. The signals corresponding to TEA appearing at δ = 3.00 ppm (-CH_2- protons of TEA) and δ = 1.40 ppm (methyl protons of TEA) have disappeared, suggesting its complete removal from the system in the precipitation process.

For the selective removal of the *t*BOC protective group to get back the amine functionality, Nudelman *et. al.* showed that hydrogen chloride is a useful reagent at room temperature, which can be quantitatively formed *in situ* by addition of AcCl to MeOH.[91] This allows the de-protection reaction to be performed without the use of expensive trifluoroacetic acid. The mechanism of de-protection of *t*BOC is shown in Figure 4.9. The reaction happens in two main steps – generation of the *in situ* hydrogen chloride gas (HCl) and then consecutive de-protection of the *t*BOC group by the HCl. The generation of HCl occurs in two steps, an addition step then an elimination stage. In the addition step, the nucleophilic lone pair on the oxygen atom of the methanol molecule attacks the fairly positive carbonyl atom of the acetyl chloride. In the elimination step, the C=O bond is reformed and a Cl^- is pushed off. Then a hydrogen ion is removed by Cl^- to form methyl acetate and hydrogen chloride.

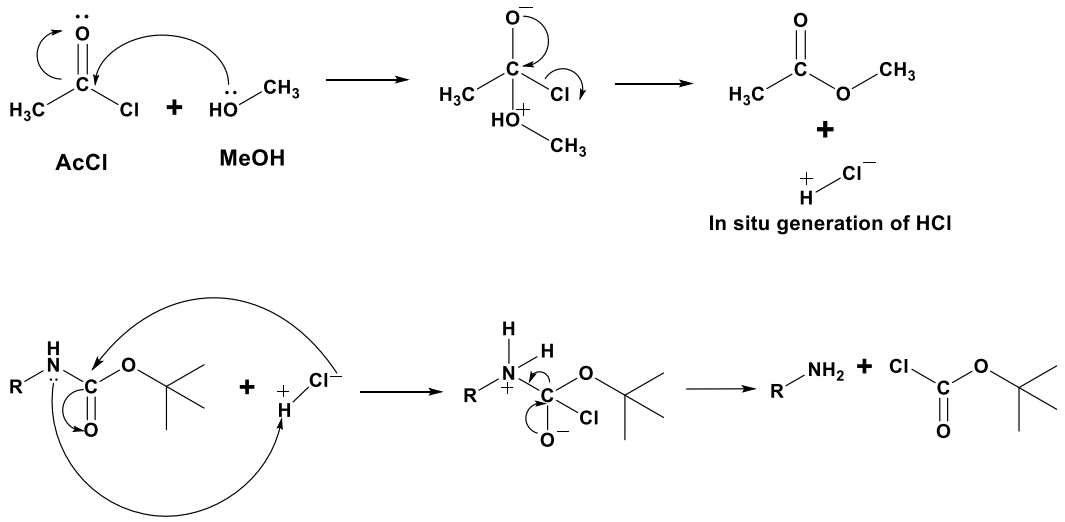

Figure 4.9 Mechanism of *t*BOC protective group removal

For the de-protection of *t*BOC group, first, the nucleophilic lone pair on the amine attacks the proton from the HCl and the nucleophilic chlorine atom from the HCl attacks the carbonyl carbon of the *t*BOC group. Then, the C=O bond is reformed breaking the carbon-nitrogen bond to give a free amine and *tert*-butoxycarbonyl chloride. Therefore, I chose to use this method for the removal of the *t*BOC protective group, by reacting the *t*BOC-protected product with acetyl chloride and methanol (MeOH) at room temperature in ethyl acetate (EtOAc). I did not attempt to de-protect the *t*BOC-L-Al-TEG-L-Al-*t*BOC, but I de-protected *t*BOC-L-Al-PEG-L-Al-*t*BOC using this method.

4.1.1.2 Esterification of L-Alanine with PEG

*t*BOC-protected L-Alanine was esterified with PEG_{2050} via CALB-catalyzed esterification reaction using the same reaction conditions that were used for TEG to obtain *t*BOC-L-Al functionalized PEG_{2050} (*t*BOC-L-Al-PEG_{2050}-L-Al-*t*BOC). Figure 4.10 shows the ^{1}H-NMR spectrum of PEG_{2050}. The signal for the -CH_2- protons (b) besides the –OH end-group appear at δ = 3.59 ppm. The signal for the -CH_2- protons from the PEG backbone (c) and (d) appear at δ = 3.63 ppm. It was difficult to

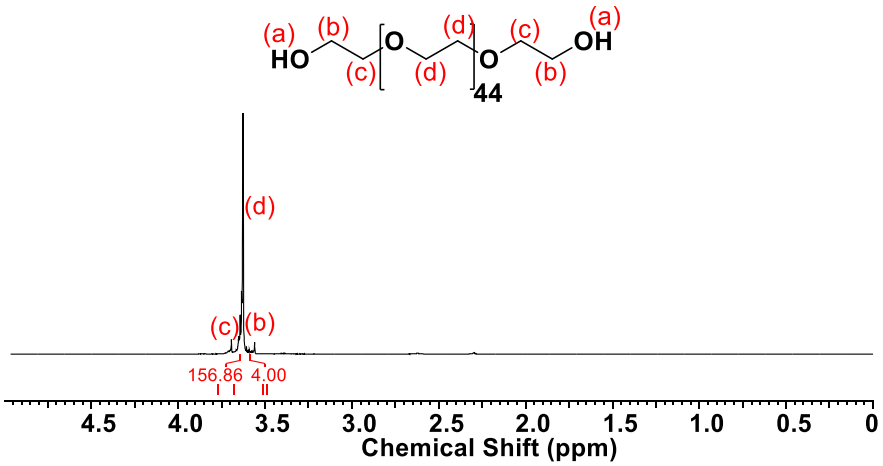

Figure 4.10 ^{1}H-NMR spectrum of PEG_{2050}

exclusively integrate the signal (b) due to its proximity to the PEG backbone -CH_2- protons. The integral of signal (b) was set to 4 corresponding to the 4 -CH_2- protons. No signals appear beyond δ = 5 ppm.

Figure 4.11 shows the ^{1}H-NMR spectrum of *t*BOC-L-Al-PEG_{2050}-L-Al-*t*BOC. The signal corresponding to the methine proton (f') from *t*BOC-L-Alanine moved downfield to (f") δ = 4.25 ppm after protection of the amine group. A new signal appeared at δ = 4.20 ppm (b') overlapping with signal (f"), which belongs to the -CH_2- proton besides the newly formed ester group. The signal for the -CH_2- protons (c) besides the –OH end-group in PEG_{2050} also shift after formation of the ester, however, its shift is difficult to observe in the ^{1}H-NMR spectrum due to its proximity

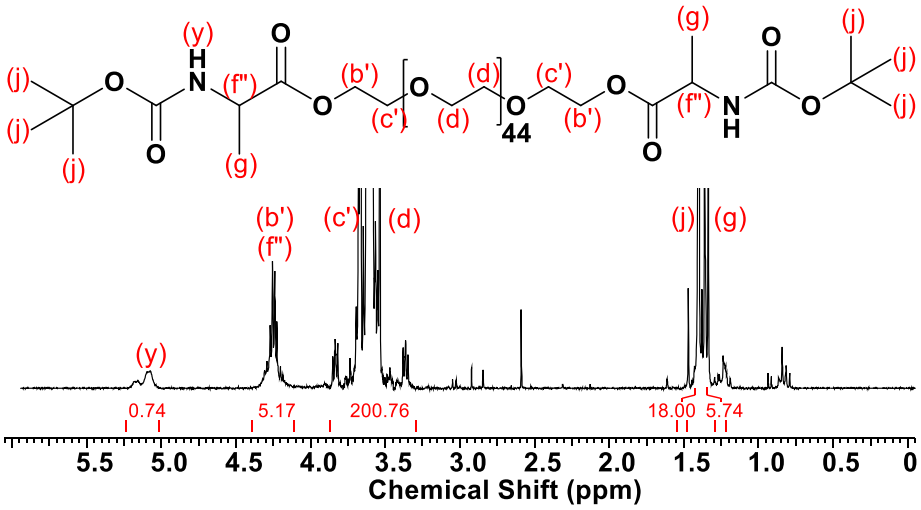

Figure 4.11 ^{1}H-NMR spectrum of *t*BOC-L-Al-PEG_{2050}-L-Al-*t*BOC

to the peak of the PEG backbone protons (d). The $-CH_3$ protons from the *t*BOC appearing at δ = 1.46 ppm are set to the integral value of 18 corresponding to the 18 protons on the *t*BOC-L-Al-PEG_{2050}-L-Al-*t*BOC. The relative integrals of (b') + (f''): (g) protons are in the ratio 5.17: 5.74 demonstrating ~100% conversion of reaction. The (c') and (d) peaks belong to the $-CH_2-$ protons present in the PEG_{2050} backbone and they appear at δ = 3.60 ppm. Figure 4.11 does not show the presence of TEA, the signals corresponding to TEA appearing at δ = 3.00 ppm ($-CH_2-$ protons of TEA) and δ = 1.40 ppm (methyl protons of TEA) have disappeared, suggesting its complete removal from the system in the precipitation process.

The *t*BOC protective group from *t*BOC-L-Al-PEG_{2050}-L-Al-*t*BOC was removed by reacting it with acetyl chloride and methanol (MeOH) at room temperature in ethyl acetate (EtOAc) to obtain diamine functionalized PEG_{2050} (H_2N-L-Al-PEG_{2050}-L-Al-NH_2). Figure 4.12 shows the ^{1}H-NMR spectrum of H_2N-L-Al-PEG_{2050}-L-Al-NH_2. The signal corresponding to the methine proton (f') from *t*BOC-L-Alanine moved upfield to (f''') at δ = 2.90 ppm after de-protection of the amine group. A new signal corresponding to the amino proton (z) appears at δ = 7.80 ppm which indicates the formation of product. The relative integrals of (f'): (z) are in the ratio 4.05: 4.13 demonstrating the successful de-protection.

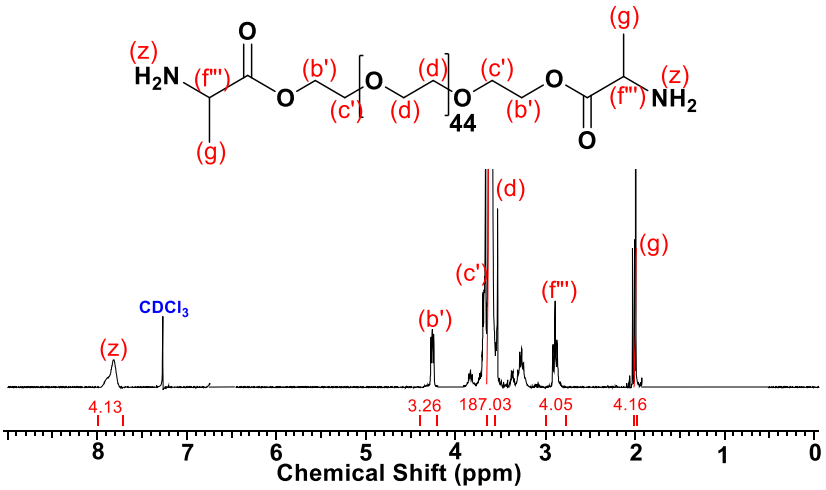

Figure 4.12 ^{1}H-NMR spectrum of H_2N-L-Al-PEG_{2050}-L-Al-NH_2

A mass spectrum of H_2N-L-Al-PEG_{2050}-L-Al-NH_2 is shown in Figure 4.13. There are two distributions of signals, each separated by 44 *m/z* units. The major distribution belongs to the H_2N-L-Al-PEG_{2050}-L-Al-NH_2. The signal at *m/z* 2142.614 (inset) belongs to the hydrogen complex of 43-mer unit of H_2N-L-Al-PEG_{2050}-L-Al-NH_2 [2142.614 ≅ 43 x 44.03 (C_2H_4O repeat unit) + 116.14 ($H_2NCHCH_3COOC_2H_4$- end group) + 132.14 ($H_2NCHCH_3COOC_2H_4O$ - end group) + 1.01 (H+)]. The smaller distribution belongs to the mono-substituted PEG, i.e. H_2N-L-Al-PEG_{2050}-OH. The signal at *m/z* 2114.652 (inset) belongs to the hydrogen complex of 44-mer unit of H_2N-L-Al-PEG_{2050}-OH [2114.652 ≅ 44 x 44.03 (C_2H_4O repeat unit) + 116.14 ($H_2NCHCH_3COOC_2H_4$- end group) + 61.06 (HOC_2H_4O - end group) + 1.01 (H+)]. Since the NMR spectrum in Figure 4.12 demonstrated the formation of the diamine, it is possible that the second distribution is formed during the MALDI mass spectrum measurement.

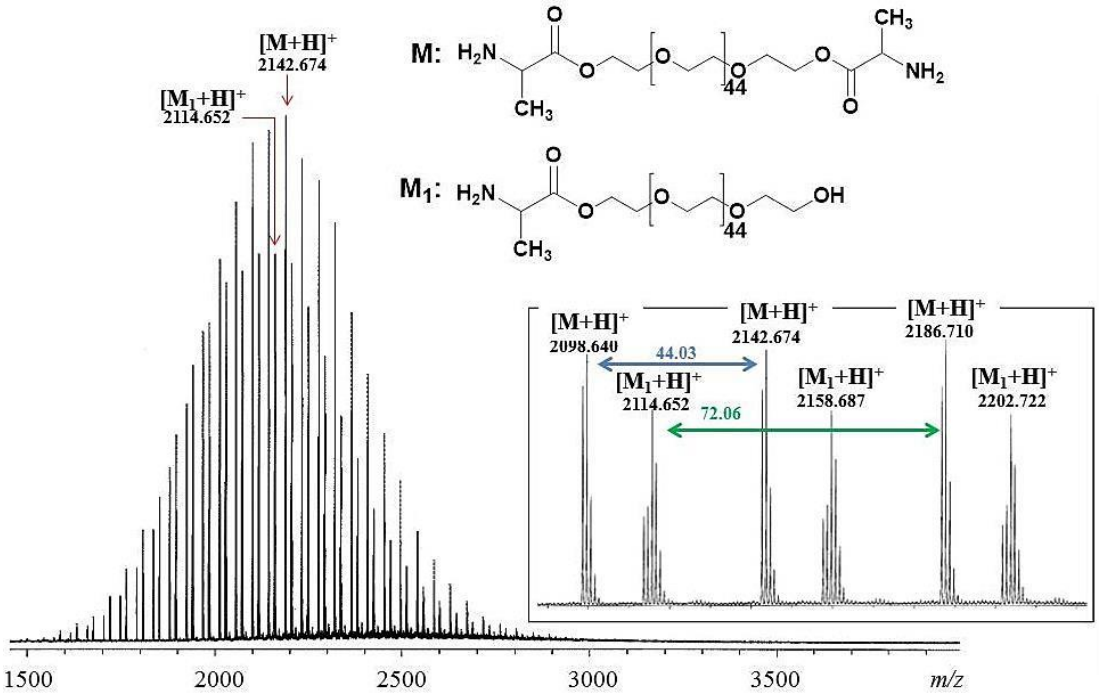

Figure 4.13 MALDI mass spectrum of H_2N-L-Al-PEG_{2050}-L-Al-NH_2. Inset: spectrum 42- to 44-mer fractions, 44 *m/z* = PEG repeat unit

4.1.1.3 Esterification of β-Alanine with PEG

Next, I tried using β-Alanine ($NH_2CH_2CH_2COOH$), a straight chain amino acid with two -CH_2- groups between the amino and the carboxylic acid groups, for amine functionalization of PEG_{2050}. Unlike L-Alanine, β-Alanine does not have a pendant methyl group that can cause steric hindrance during further derivatization. First, the amine of the β-Alanine is protected with a *t*BOC by refluxing the β-Alanine with di-*tert*-butyl dicarbonate under methanol to obtain a *t*BOC protected alanine (*t*BOC-β-Al).

Figure 4.14 shows the ^{1}H-NMR spectrum of β-Alanine. The signal for the -CH_2- protons (f) and (g) appear at δ = 2.54 ppm and 3.16 ppm.

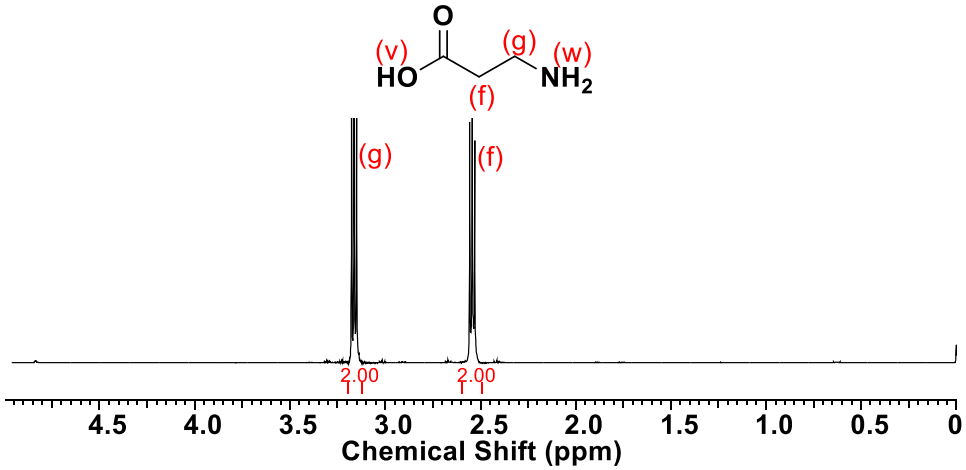

Figure 4.14 ^{1}H-NMR spectrum of β-alanine

Figure 4.15 shows the ^{1}H-NMR spectrum of *t*BOC-β-Al. The -CH_2- protons (g) from β-alanine moved downfield from δ = 3.16 ppm to δ = 3.35 ppm after protection. Similarly, the -CH_2- protons (f) from β-alanine moved upfield from δ = 2.54 ppm to δ = 2.40 ppm. The relative integrals of (j): (g'): (f') are in the ratio 8.9: 2.08: 2.0 demonstrating the completion of reaction (~100% conversion). Figure 4.15 also indicates the presence of the residual TEA.

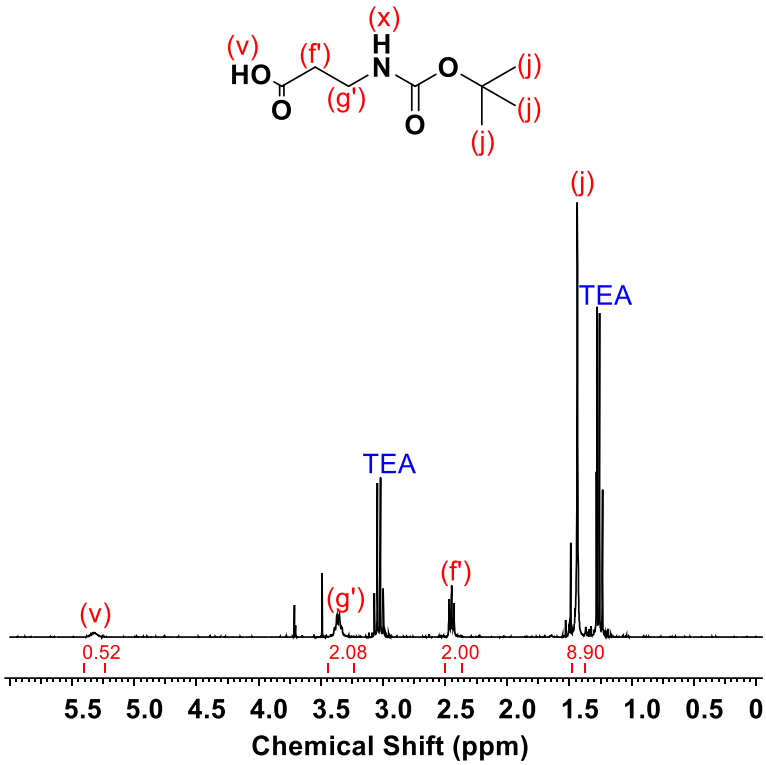

Figure 4.15 ^{1}H-NMR spectrum of *t*BOC-β-Alanine

*t*BOC-protected β-Alanine was esterified with PEG_{2050} via CALB-catalyzed esterification reaction using the same reaction conditions that were used for TEG to obtain *t*BOC-β-Al functionalized PEG_{2050} (*t*BOC-β-Al-PEG_{2050}-β-Al-*t*BOC). Figure 4.16 shows the ^{1}H-NMR spectrum of *t*BOC-β-Al-PEG_{2050}-β-Al-*t*BOC. The -CH_2- protons (f') from *t*BOC-β-Alanine moved downfield from δ = 2.40 ppm to δ = 2.55 ppm after esterification. A new peak appeared at δ = 4.20 ppm (b'), which belongs to

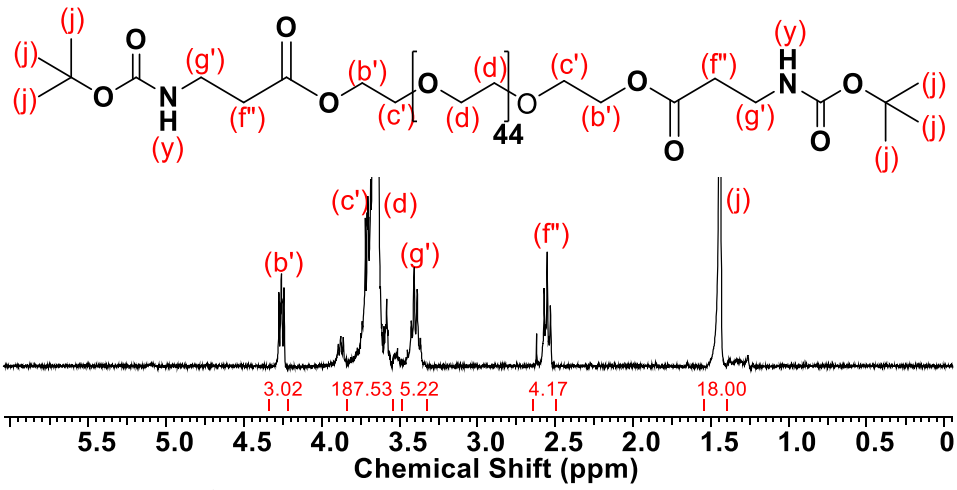

Figure 4.16 ^{1}H-NMR spectrum of *t*BOC-β-Al-PEG_{2050}-β-Al-*t*BOC

the -CH_2- protons besides the newly formed ester group. The relative integrals of (b): (j) are in the ratio 3.02: 18.00. The antenna signals of PEG_{2050} backbone signal (d) overlap with the signal for -CH_2- protons (g'), and that is why, the integral value of signal (g') is 5.22, which is higher than the expected value of 4. In Figure 4.16, the signals corresponding to TEA appearing at δ = 3.00 ppm (-CH_2- protons of TEA) and δ = 1.40 ppm (methyl protons of TEA) have disappeared, suggesting its complete removal from the system in the precipitation process.

MALDI mass spectrometry was used for further verification of the di-substituted PEG_{2050}. Figure 4.17 shows the MALDI mass spectrum of *t*BOC-β-Al-PEG_{2050}-β-Al-*t*BOC. It shows a single distribution indicating the formation of the di-substituted PEG_{2050} with no traces of the mono-substituted or unreacted PEG_{2050}, therefore, 100% conversion of the PEG_{2050} to *t*BOC-β-Al-PEG_{2050}-β-Al-*t*BOC was confirmed by MALDI mass spectrometry analysis. The signal at *m/z* 2144.332 g belongs to the Na complex of 38-mer unit of *t*BOC-β-Al-PEG_{2050}-β-Al-*t*BOC. The theoretical *m/z* for this signal is = 2144.332 [38 x 44.03 (C_2H_4O repeat unit) + 216.26

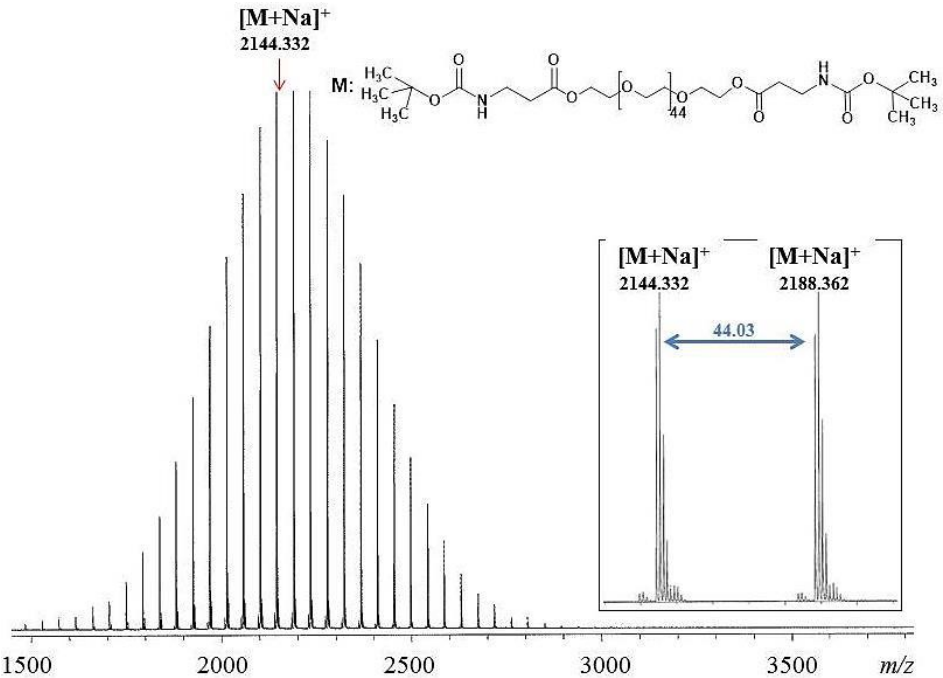

Figure 4.17 MALDI mass spectrum of *t*BOC-β-Al-PEG_{2050}-β-Al-tBOC. Inset: spectrum of 38- to 39-mer fractions, 44 *m/z* = PEG repeat unit

($((CH_3)_3CHOCONHC_2H_4COOC_2H_4$ end-group) + 232.26 ($(CH_3)_3CHOCONHC_2H_4COOC_2H_4O$ end-group) + 22.99 (Na^+)]. The signals were at a distance of 44 Da from each other that correspond to one monomer unit. This confirms that each oligomer in the *t*BOC-β-Al-PEG_{2050}-β-Al-*t*BOC carries the *t*BOC-β-Alanine end group.

The *t*BOC-β-Al-PEG_{2050}-β-Al-*t*BOC was then de-protected with hydrogen chloride formed *in situ* by reaction of AcCl and MeOH to obtain diamine functionalized PEG_{2050} (H_2N-β-Al-PEG_{2050}-β-Al-NH_2). Figure 4.18 shows the ^{1}H-NMR spectrum of H_2N-β-Al-PEG_{2050}-β-Al-NH_2. The disappearance of the peak (j) at δ = 1.49 ppm indicates the formation of product. The conjugation is indicated by the shift in signal (g') from δ = 4.30 ppm to δ = 2.95 ppm. The relative integrals of (b'): (d) are in the ratio 3.61: 180 demonstrating the successful de-protection by NMR spectroscopy analysis. The ^{1}H-NMR spectrum also shows the presence of residual ethyl acetate (EtOAc) in the product with the signals corresponding to it appearing at δ = 4.12 ppm, 2.05 ppm, and 1.26 ppm.

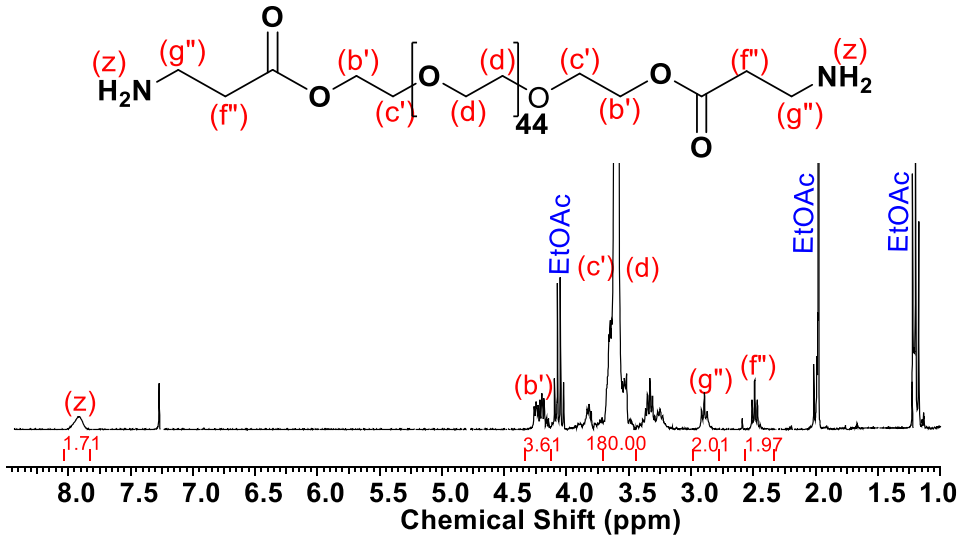

Figure 4.18 ^{1}H-NMR spectrum of H_2N-β-Al-PEG_{2050}-β-Al-NH_2

Figure 4.19 shows the ^{13}C-NMR spectrum of H_2N-β-Al-PEG_{2050}-β-Al-NH_2. It suggests the formation of the product by appearance of a peak belonging to the -CH_2-proton (B') at δ = 64.89 ppm. The signal corresponding to the carbonyl carbon

appears at δ = 169.92 ppm and the -CH_2- carbons (G") and (F") appear at δ = 49.08 ppm. The signal for the carbon atoms from the PEG backbone appear between δ = 68.44 ppm – 70.53 ppm. The signals from the carbon atoms from ethyl acetate also show up at δ = 170.34 ppm, 61.50 ppm, 20.83 ppm, and 16.06 ppm. The signal appearing at δ = 63.49 ppm and 72.41 ppm may correspond to the carbon atoms besides the –OH end-group (B) and (C) suggesting the presence of mono-substituted and unsubstituted PEG_{2050}.

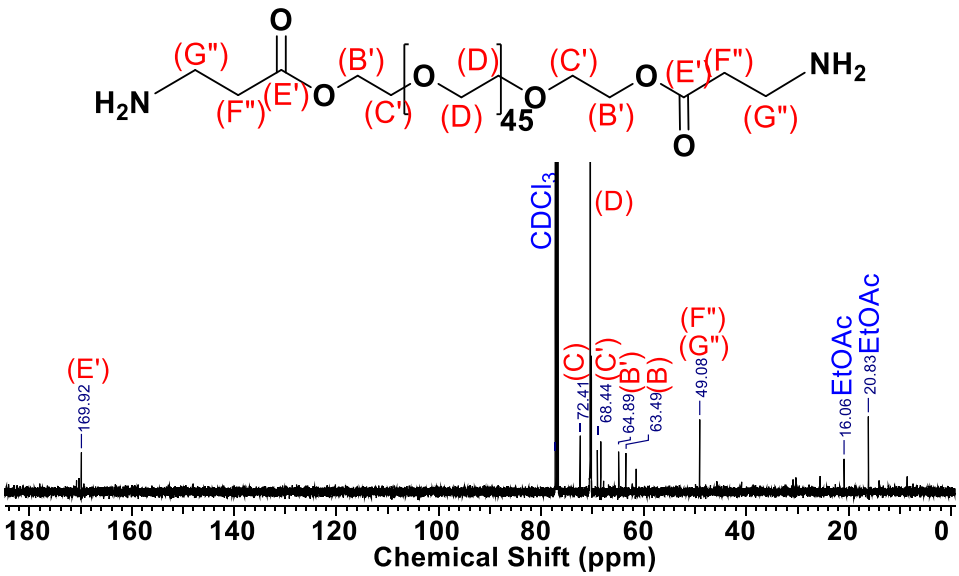

Figure 4.19 ^{13}C-NMR spectrum of H_2N-β-Al-PEG_{2050}-β-Al-NH_2

Figure 4.20 shows the MALDI mass spectrum of the product. It shows three distributions: the major distribution belongs to H_2N-β-Al-PEG_{2050}-β-Al-NH_2, and the two minor distributions belong to mono-substituted PEG_{2050} (H_2N-β-Al-PEG_{2050}-OH) and un-substituted PEG_{2050}, each separated by 44 *m/z* units. The signal at *m/z* 2142.681 (inset) belongs to the hydrogen complex of the 43-mer unit of H_2N-β-Al-PEG_{2050}-β-Al-NH_2 [2142.681 ≅ 43 x 44.03 (C_2H_4O repeat unit) + 116.14 ($H_2NC_2H_4COOC_2H_4$- end group) + 132.14 ($H_2NC_2H_4COOC_2H_4O$ - end group) + 1.01 (H+)]. The signal at *m/z* 2164.683 (inset) belongs to the Na complex of the 43-mer unit of H_2N-β-Al-PEG_{2050}-β-Al-NH_2 [2164.683 ≅ 43 x 44.03 (C_2H_4O repeat unit) +

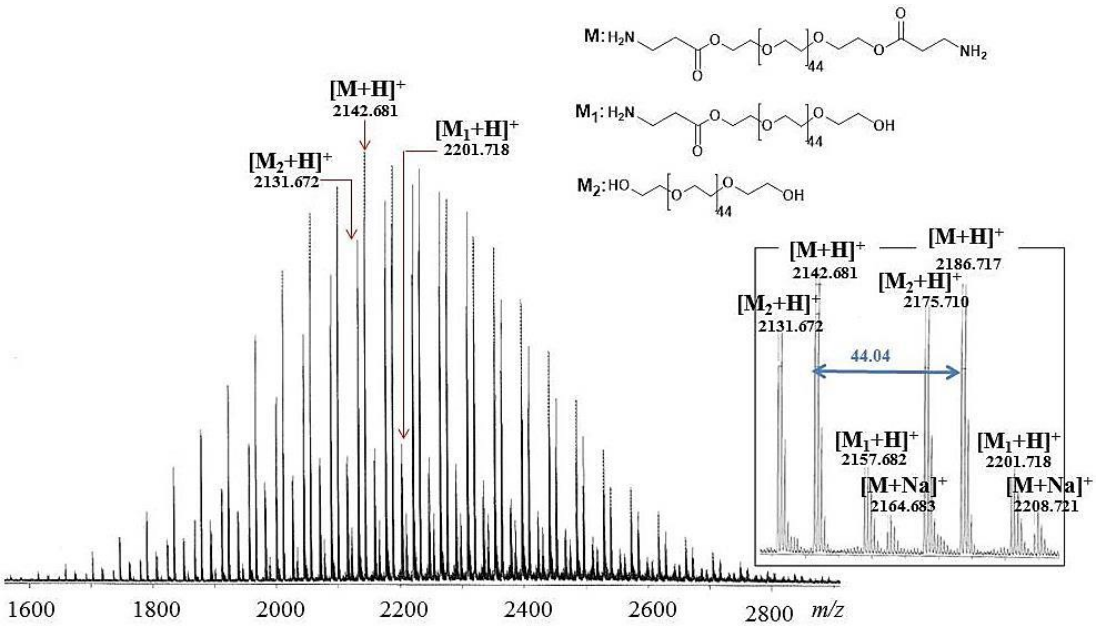

Figure 4.20 MALDI mass spectrum of H_2N-β-Al-PEG_{2050}-β-Al-NH_2. Inset: spectrum of 45- and 46-mer fractions, 44 *m/z* = PEG repeat unit

116.14 ($H_2NC_2H_4COOC_2H_4$- end group) + 132.14 ($H_2NC_2H_4COOC_2H_4O$ - end group) + 22.99 (Na+)]. One of the smaller distributions belongs to the mono-substituted PEG, i.e. H_2N-β-Al-PEG_{2050}-OH. The signal at *m/z* 2157.682 (inset) belongs to the hydrogen complex of the 45-mer unit of H_2N-β-Al-PEG_{2050}-OH [2157.682 ≅ 45 x 44.03 (C_2H_4O repeat unit) + 116.14 ($H_2NC_2H_4COOC_2H_4$- end group) + 61.06 (HOC_2H_4O - end group) + 1.01 (H+)]. The other smaller distribution belongs to the un-substituted PEG, i.e. HO-PEG_{2050}-OH. The signal at *m/z* 2131.672 (inset) belongs to the hydrogen complex of the 46-mer unit of HO-PEG_{2050}-OH [2131.672 ≅ 46 x 44.03 (C_2H_4O repeat unit) + 45.06 (HOC_2H_4 - end group) + 61.06 (HOC_2H_4O- end group) + 1.01 (H+)].

The intermediate product (*t*BOC-β-Al-PEG_{2050}-β-Al-*t*BOC) showed a single distribution as observed in Figure 4.17. Therefore, it can be concluded that MALDI-mass spectrometry analysis confirmed the complete conversion of PEG_{2050} to the di-functionalized PEG without any side product and the three products are generated during the de-protection reaction or during MALDI. It can be theorized that the

nucleophilic chlorine atom from the HCl attacks the carbonyl carbon of the β-alanine group instead of the *t*BOC group. The C=O bond is then reformed breaking the carbon-oxygen bond to give a free hydroxyl end-group on the PEG. These reactions would lead to a mixture of di-, mono-, and un-substituted PEG_{2050}. These side reactions can be avoided in the future with shorter reaction time.

In summary, these new methods can be utilized to synthesize PEG-diamines.

4.1.2. Synthesis of FA-SH

The synthesis of thiol functionalized folic acid (FA-SH) was developed by former group members. It involves first the lithiation of the γ-carboxyl group of the glutamic acid moiety in FA using 1 molar equivalent of *n*-butyllithium. Subsequently the γ-lithiated FA was then reacted with 1 equivalent of a bis(2-ethyl 4-bromovalerate) disulfide compound that was able to react with the lithium salt effectively to form FA-γ-bis(2-ethyl 4-bromovalerate) disulfide (FA-S-S-FA). The FA-S-S-FA was then cleaved with dithiothreitol (DTT) to obtain a thiol-functionalized folic acid compound (FA-SH).[92]

I synthesized FA-SH using the strategy developed in our group to use it as the starting material for preparing two-functional folate-targeted fluorescein-labeled TEG and PEGs. However, I chose to prepare bis(2-ethyl 4-bromobutyrate) disulfide (Br-S-S-Br) instead of bis(2-ethyl 4-bromovalerate) disulfide as the starting material for FA-S-S-FA. The starting material for preparing bis(2-ethyl 4-bromobutyrate) disulfide is ethyl 4-bromobutyrate (EBB) and the starting material for preparing bis(2-ethyl 4-bromovalerate) disulfide is ethyl 5-bromovalerate (EBV). EBB is chosen instead of EBV because EBB is approximately 8 times less expensive than EBV.

The detailed reaction scheme for the Br-S-S-Br compound and the scheme for preparing FA-S-S-FA is presented in Section 4.1.2.1. The reaction scheme for the cleavage reaction is shown in Figure 4.21 and discussed in Section 4.1.2.2.

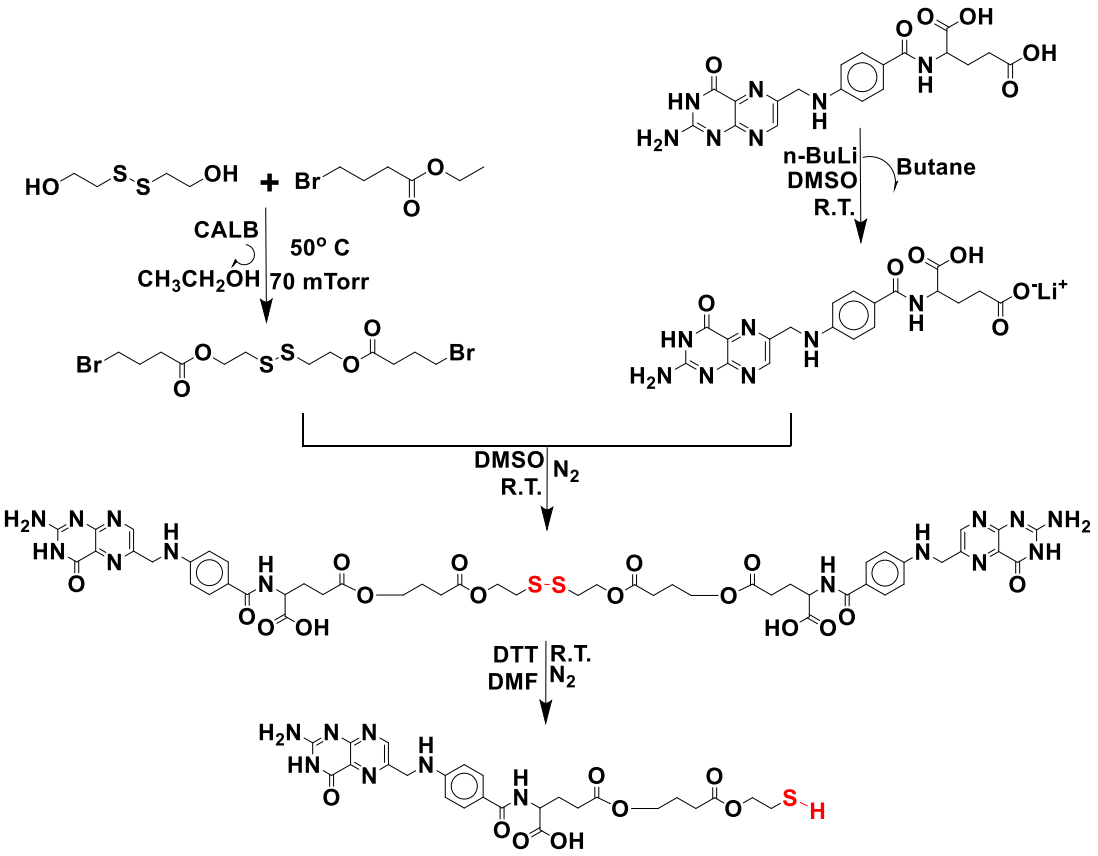

Figure 4.21 Synthetic strategy for FA-γ-SH

4.1.2.1. Synthesis of FA-S-S-FA

CALB-Catalyzed Transesterification of EBB with 2-HEDS

Halo functionalization of PEGs was previously reported by our group.[14] A similar strategy was used to synthesize a dibromine disulphide compound (bis(2-ethyl 5-bromobutanoate) disulfide, Br-S-S-Br) by CALB catalyzed transesterification of 4-ethylbromobutyrate (EBB) with 2-hydroethyl disulphide (2-HEDS). This synthetic strategy has been previously reported by our group using Ethyl 5-bromovalerate (EBV). EBB was used in this scheme instead of EBV due to its lower cost. The reaction scheme for the synthesis of Br-S-S-Br is presented in Figure 4.22.

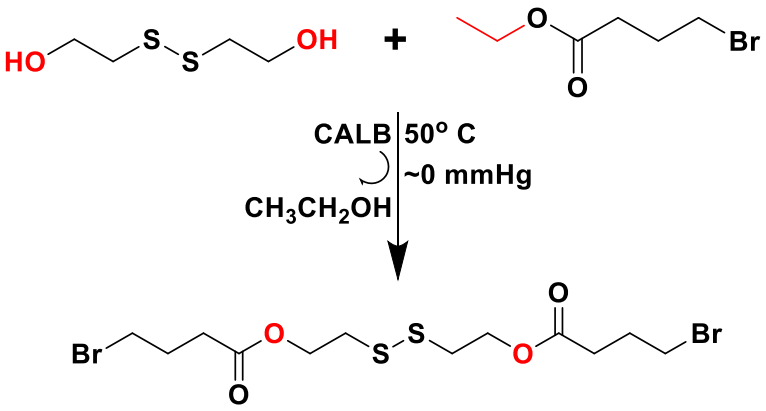

Figure 4.22 Reaction scheme for synthesis of Br-S-S-Br

Figure 4.23 shows the ^{1}H-NMR spectrum of EBB. The signal for the -CH_2- protons in the butyrate moiety (a – besides bromine), (b), and (c – besides the carbonyl carbon) appear at δ = 3.40 ppm, δ = 2.10 ppm, and δ = 2.45 ppm. The peak for the -CH_2- protons from the ethyl moiety (y) appear at δ = 4.10 ppm and the signal for the methyl protons from the ethyl moiety (z) appear at δ = 1.20 ppm. No signals appear beyond δ = 5 ppm.

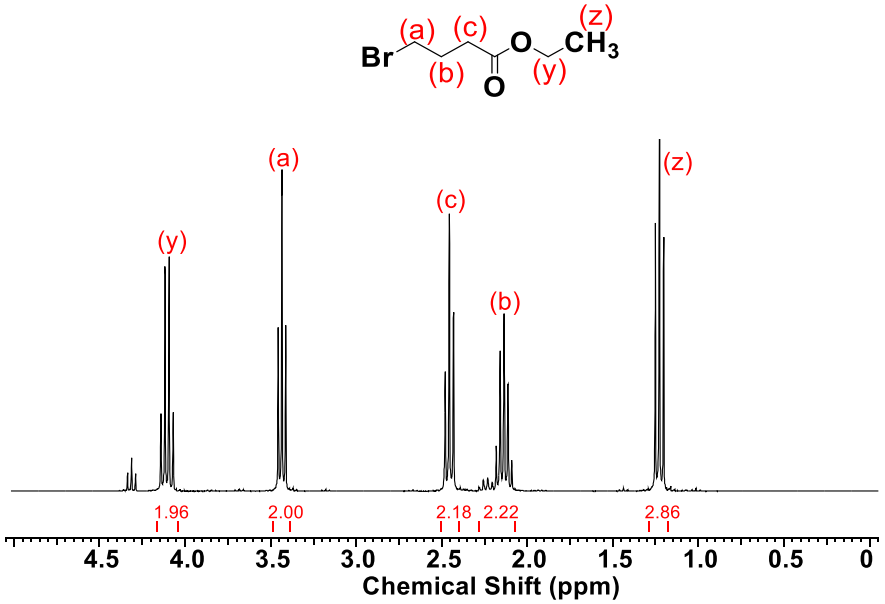

Figure 4.23 ^{1}H-NMR spectrum of Ethyl 4-bromobutyrate

Figure 4.24 shows the ^{1}H-NMR spectrum of 2-HEDS. The signal for the methylene protons besides the –OH (e) appears at δ = 3.90 ppm and the signal for the

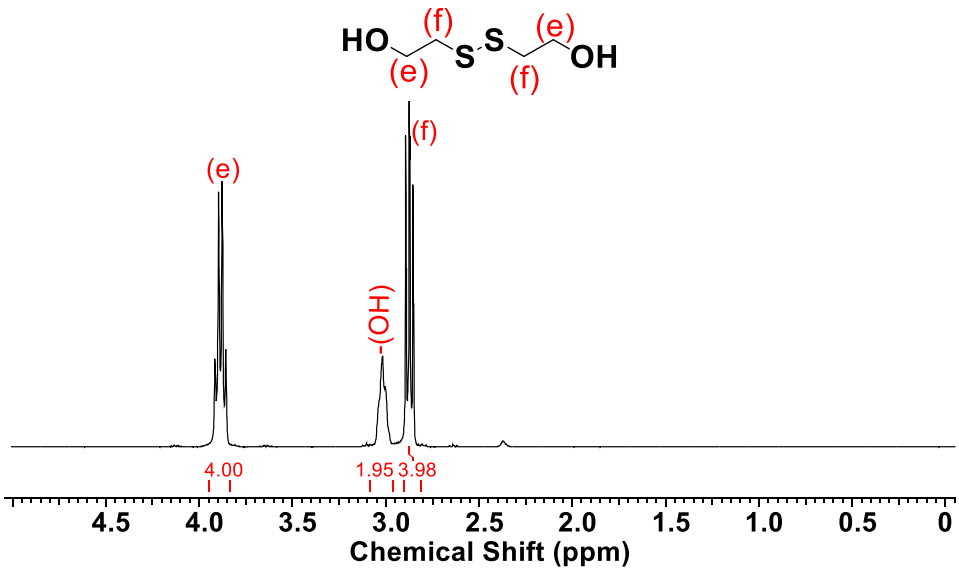

Figure 4.24 ^{1}H-NMR spectrum of 2-HEDS

-CH_2- protons besides the disulfide bond (f) appears at δ = 2.85 ppm. The signal for the –OH protons appears at δ = 3.00 ppm. No signals appear beyond δ = 5 ppm.

In the ^{1}H-NMR spectrum of Br-S-S-Br shown in Figure 4.25, it can be observed that the signals corresponding to the -CH_2- (y) and methyl protons (z) from EBB appearing at δ = 4.10 ppm and δ = 1.20 ppm have disappeared. The signal corresponding to the -CH_2- protons (e) from 2-HEDS appearing at δ = 3.85 ppm

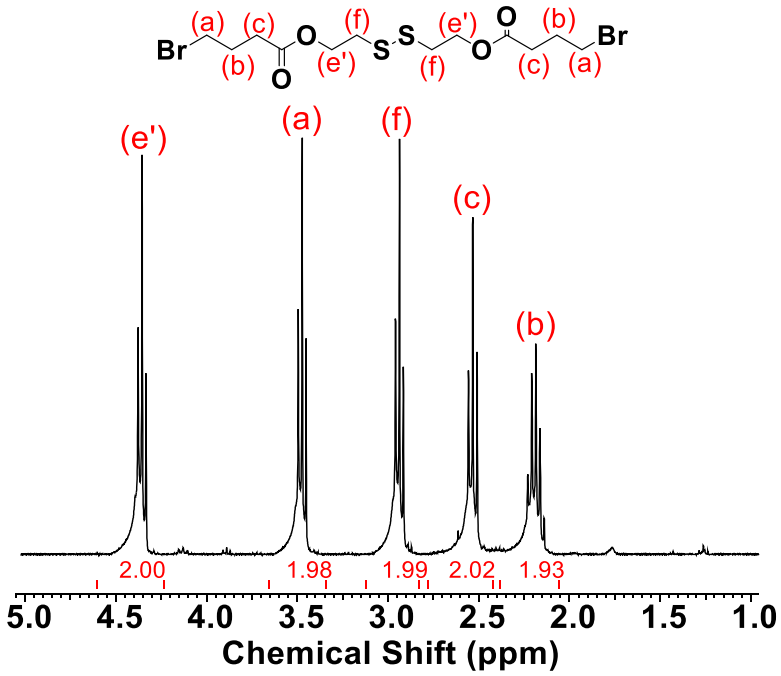

Figure 4.25 ^{1}H-NMR spectrum of Br-S-S-Br

moved downfield to δ = 4.35 ppm indicating the formation of the new ester bond. The relative integrals of (e'): (a) are in the ratio 2.00: 1.98 demonstrating the completion of reaction with 100% conversion. No signals appear beyond δ = 5 ppm.

Figure 4.26 shows the ^{13}C-NMR spectrum of Br-S-S-Br. It indicates the formation of product by appearance for a signal corresponding to the -CH_2- proton (E') at δ = 62.35 ppm. No signals corresponding to the starting materials are observed.

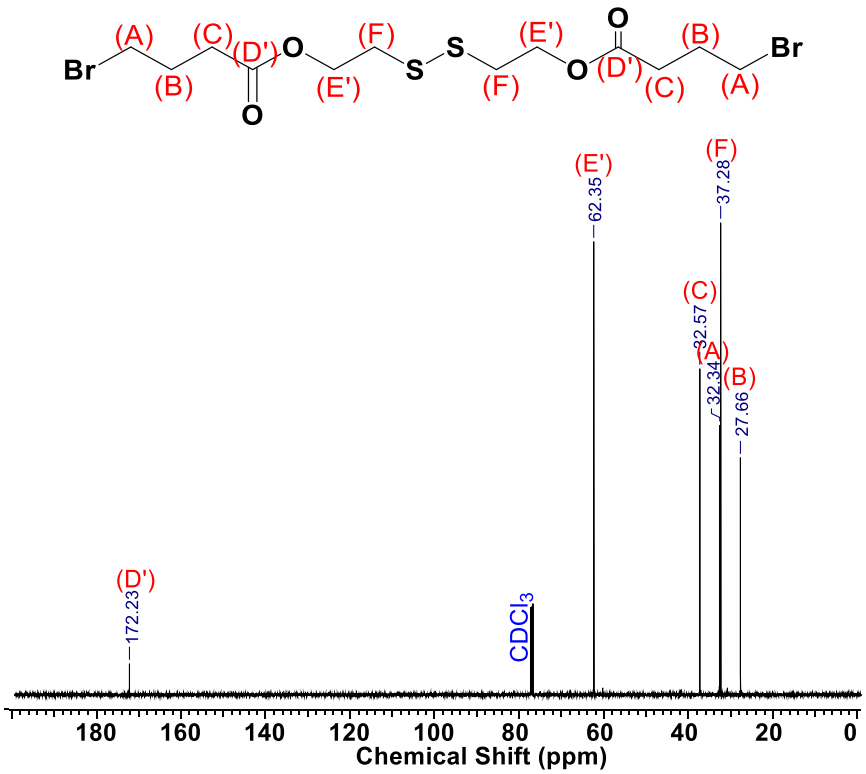

Figure 4.26 ^{13}C-NMR spectrum of Br-S-S-Br

Figure 4.27 shows the ESI mass spectrum of Br-S-S-Br. The calculated monoisotopic mass for the sodium-complex of Br-S-S-Br is 475.21 Da [≅ 452.22 ($C_{12}H_{20}Br_2O_4S_2$) + 22.99 (Na)]. A signal at *m/z* 475.0 Da confirms the formation of the Br-S-S-Br. A potassium salt of Br-S-S-Br is also observed at 491.0 Da [≅ 452.22 ($C_{12}H_{20}Br_2O_4S_2$) + 39.10 (K)]. An adduct of 3-butenoic acid with sodium-complex of Br-S-S-Br is also observed at *m/z* 561.1 Da [≅452.22 ($C_{12}H_{20}Br_2O_4S_2$) + 86.09 ($C_4H_6O_2$) + 22.99 (Na)]. This adduct is generated in the instrument by HBr removal

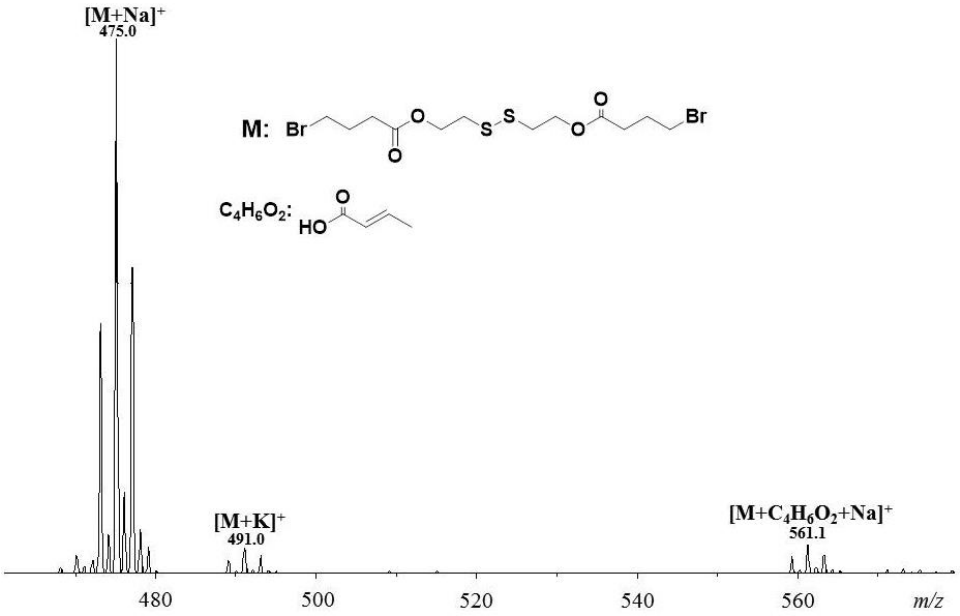

Figure 4.27 ESI mass spectrum of Br-S-S-Br

from 4-bromobutanoic acid. The starting material EBB may contain 4-bromobutanoic acid as an impurity.

γ-lithiation of FA

Folic Acid functionalization to obtain FA-conjugates has been reported in the literature by the so-called "activated ester" method using condensing agents such as *N,N'*-dicyclohexylcarbodiimide (DCC)[93-95] and 1-ethyl-3-(3-dimethylaminopropyl) carbodiimide (EDC)[96-98], with or without activators such as *N*-hydroxy succinimide (NHS) and hydroxybenzotriazole (HOBt). However, the characterization of the FA-conjugates is often cursory. Some studies assumed that the γ-carboxylic acid site reacts preferentially because the α-carboxylic acid is more sterically hindered, and proceeded with the use of the mixed conjugated product. Others used HPLC to separate the γ-substituted product. Some studies reported that the NMR signals of the FA were lost in the baseline of the FA-conjugate spectrum. Since a good ^{1}H NMR data was not found in the literature for the FA-conjugate synthesized by the activated ester method, a reaction between FA and CH_3O-PEG-NH_2 was performed by Dr Seo

from our group using (benzotriazol-1-yloxy)tripyrrolidinophosphonium hexafluorophosphate (PyBOP) as an activator based on a recipe provided by the University of Michigan. He reported that a mixture of γ, α, and difunctional (γ and α) products were obtained in the reaction, with about 40% FA-γ-PEGM.[99] The magnified region of the ^{1}H NMR spectrum of the product, as shown in Figure 4.28, shows two sharp singlet proton signals (13', 13) at 8.63 and 8.65 ppm. Dr Seo reported that the signals appear as doublets because of *J*-coupling. However, based on discussion with Dr. Dudipala regarding the appearance of a doublet, it was concluded that the signal at

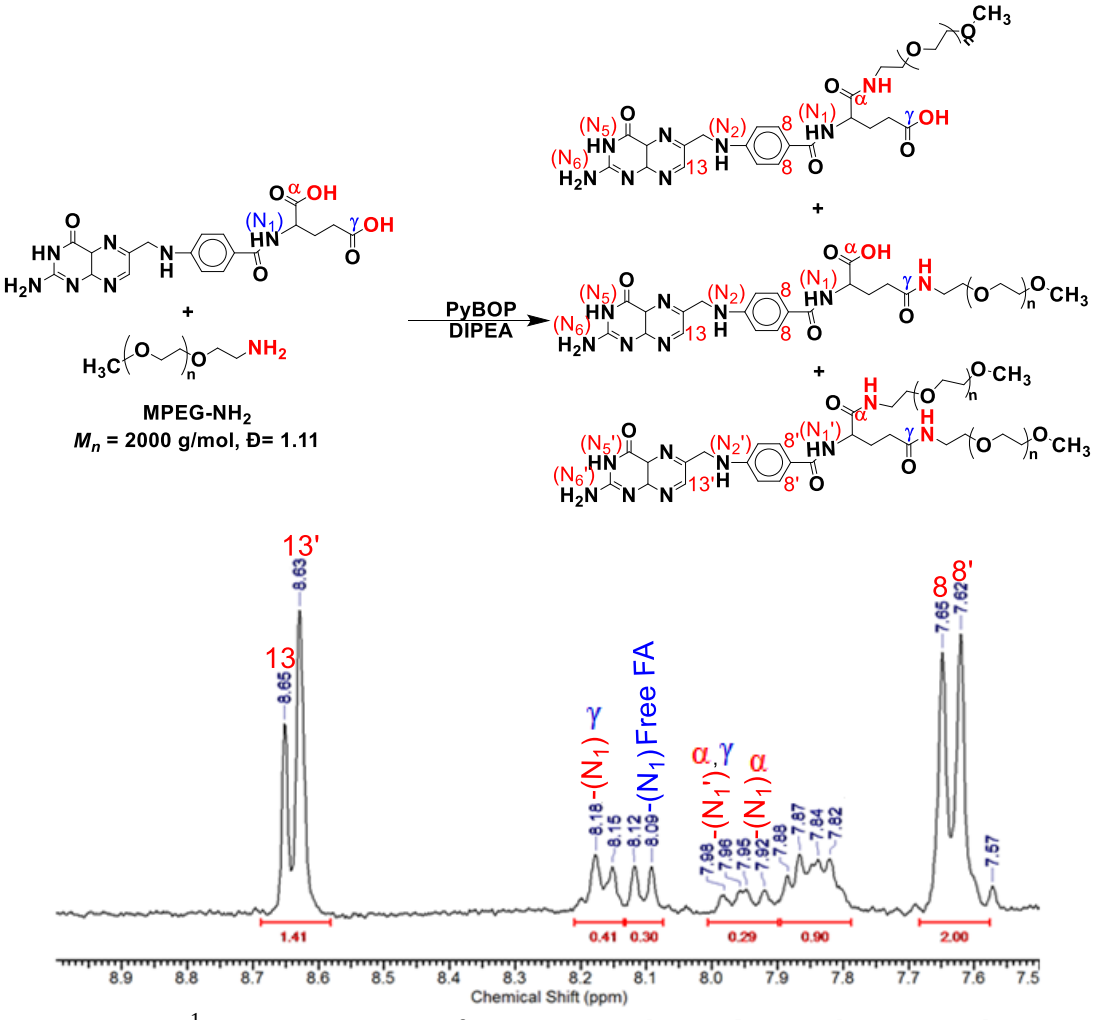

Figure 4.28 ^{1}H NMR spectrum of PEG-FA synthesized using the activated ester method – magnified region from 7.5 – 8.9 ppm. δ - 8.65 (13) – α or γ monosubstituted FA, 8.63 (13') - α,γ-disubstituted FA, 8.18, 8.15 (N_1 – γ-monosubstituted FA), 8.12, 8.09 (N_1 – unsubstituted FA), 7.98, 7.96 (N_1' – α,γ-disubstituted FA), 7.95, 7.92 (N_1 – α-monosubstituted FA), 7.65 (8) – α or γ monosubstituted FA, 7.62 (8') - α,γ-disubstituted FA. Reprinted with permission from *Macromolecules* **2018**, *51(22)*, 9069-9077. Copyright © 2018 American Chemical Society

8.65 ppm belongs to the proton of the pteorate ring of monosubstituted FA (either γ or α), which is in agreement with the literature, and the signal at 8.63 ppm was assigned to di-substituted (γ and α) FA. The di-substituted FA has twice the molecular weight of the mono-substituted products, causing a slightly different bending of the molecule that in turn leads to a separate resonance signal. Similarly, two signals appear at 7.65 and 7.62 ppm for the protons of the aromatic ring (8, 8') for the mono- and di-substituted FA. The exchangeable secondary amine proton (N_1) signals are weak but can be distinguished clearly: δ = 8.15 and 8.18 ppm for the γ-substituted FA, δ = 7.92 and 7.95 ppm for the α-substituted FA, and δ=7.96 and 7.98 ppm for the di-substituted (α and γ) FA. This explanation was a crucial contribution since the existence of double-substituted PEG can be excluded based on proton NMR spectroscopy. This was not presented in the literature until our paper was published.[92] The signals δ = 8.09 and 8.12 ppm are assigned to the residual unsubstituted FA. The data suggests that regioselectivity is quite poor, contrary to the earlier claims.

Dr. Puskas theorized that the γ-carboxylic acid of FA will react preferentially with *n*-BuLi because the γ-carboxyl position is more acidic. The pK_a values (where K_a is an acid dissociation constant) of γ-carboxyl acid = 4.5, 4.8, and 4.25 and α-carboxyl acid = 2.5, 3.5, and 2.19 were reported.[100] Other organometallic compounds (K, Na, Ce) could also be used but *n*-BuLi was preferred because the progress of the reaction could be conveniently monitored by the evolution of *n*-butane gas that bubbles out of the reaction. The synthetic strategy I used for the synthesis of FA-S-S-FA based on this lithiation strategy is presented in Figure 4.29.

The carboxylic acid groups of FA at α and γ positions are in a similar chemical environment, which is best demonstrated by the ^{13}C NMR signals of the carbonyl groups of FA at δ = 173.97 (α) and δ = 173.77 (γ) ppm. Mindt *et al.* synthesized

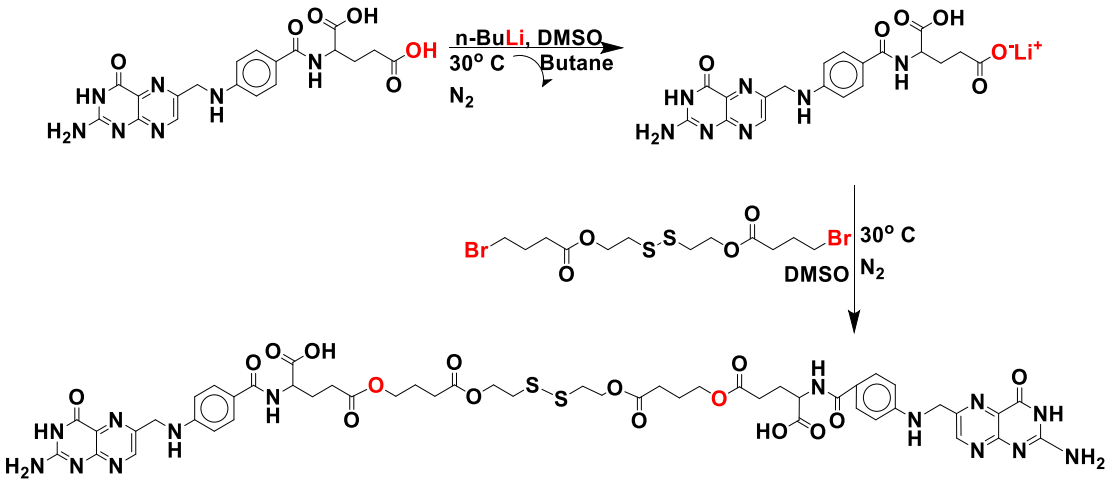

Figure 4.29 Synthetic strategy for FA-S-S-FA

various amide-substituted FA compounds and showed that the substituted carbonyl carbon signals are better distinguishable and appear at δ = 172.76 (α) ppm and δ = 171.50 (γ) ppm.[101]

The lithiation method yielded excellent regioselectivity, but the original interpretation of the ^{13}C NMR was erroneous (Figure 4.30).[99] I repeated the experiments and clarified the assignments.[92] The expanded region of ^{13}C NMR spectrum of FA-γ-Li is shown in Figure 4.31. Upon lithiation, the signal of the γ-carbon moved downfield to δ = 174.72 ppm while the signal of the α carbon remained almost unchanged at δ = 173.93 ppm. The distance between them also increased to 0.79 ppm as shown in Figure 4.31 (bottom). Therefore, it can be concluded that the γ-

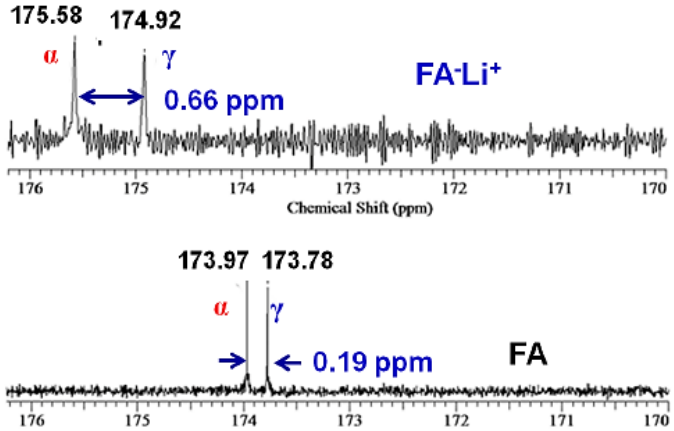

Figure 4.30 Expanded region of ^{13}C NMR spectra of FA (top) and its lithiated intermediate (bottom) reported by Dr. Seo[99]

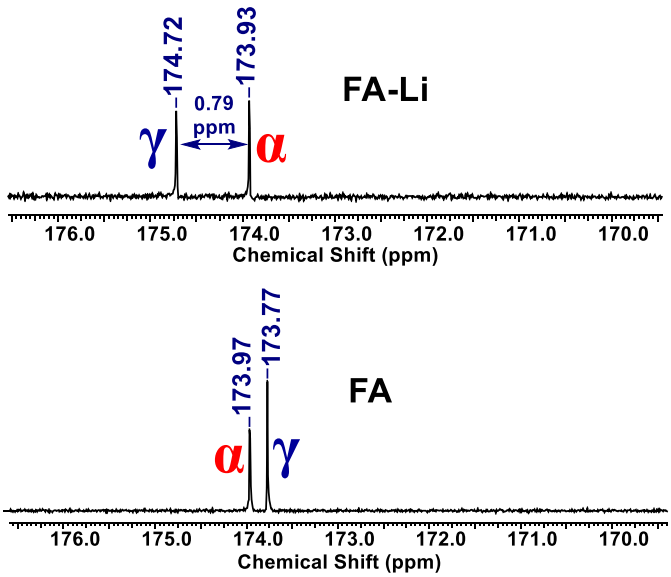

Figure 4.31 Expanded region of ^{13}C NMR spectra of FA (top) and its lithiated intermediate (bottom). Adapted with permission from *Macromolecules* **2018**, *51(22)*, 9069-9077. Copyright © 2018 American Chemical Society

carboxyl group was lithiated exclusively, while the α-carboxylic acid remained unaffected during lithiation.

The lithiated FA was then reacted with Br-S-S-Br. Figure 4.32 shows the ^{1}H-NMR spectrum of FA. The signal corresponding to the aromatic proton (13) appearing at δ = 8.65 ppm is set to an integral value of 1.00. The NH proton signal (N_1) appear at δ = 8.05 ppm for FA.

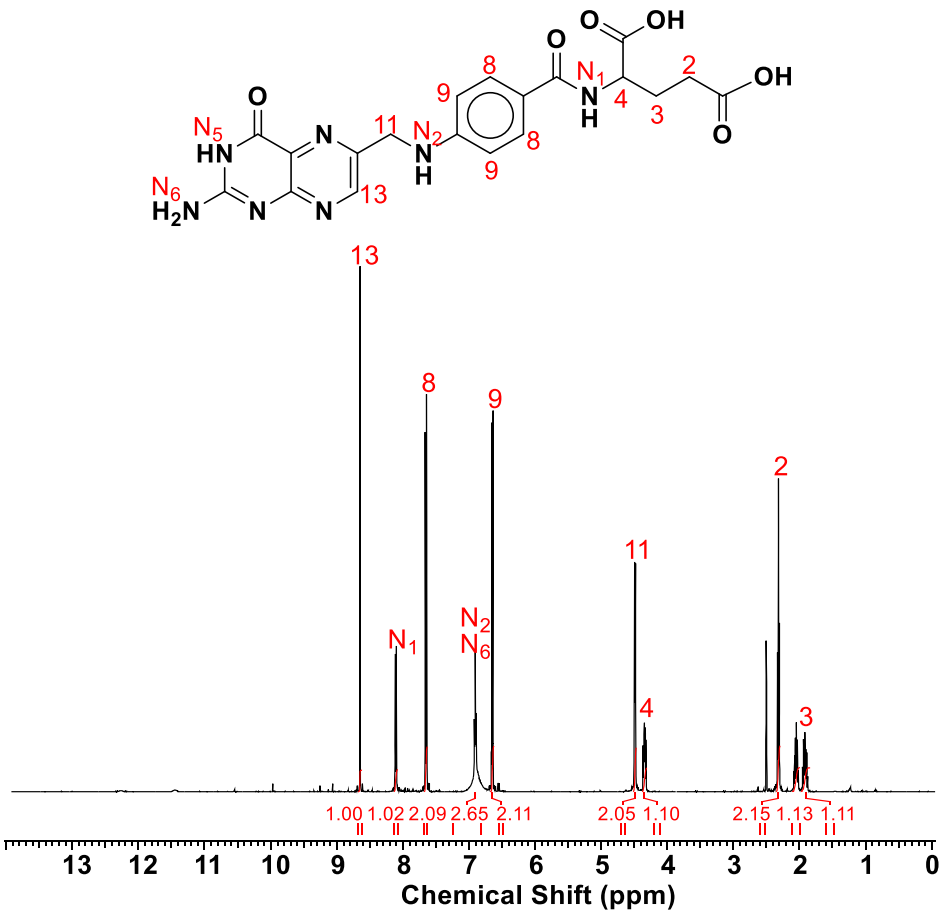

Figure 4.32 ^{1}H-NMR spectrum of Folic Acid

Figure 4.33 shows the ^{1}H-NMR spectrum of FA-S-S-FA. The signal corresponding to the -CH_2- proton (a) shifts downfield from δ = 3.50 ppm to proton (a') at δ = 4.10 ppm suggesting the successful conjugation of Br-S-S-Br to FA. Figure 4.33 demonstrates the absence of the α-folate and mixed product signals between 7.8 and 8.0 ppm, but shows the γ –substituted NH proton signal (N_1') at 8.2 ppm. The NH proton peak (N_1) at 8.05-8.06 ppm shows the presence of residual free folic acid. The ratio of (N_1) to (13) is 0.26/1 that suggests a 26 mol% free folic acid in the mixture. The ratio of (N_1') to (13) is 0.72/1 indicating 72% conversion.

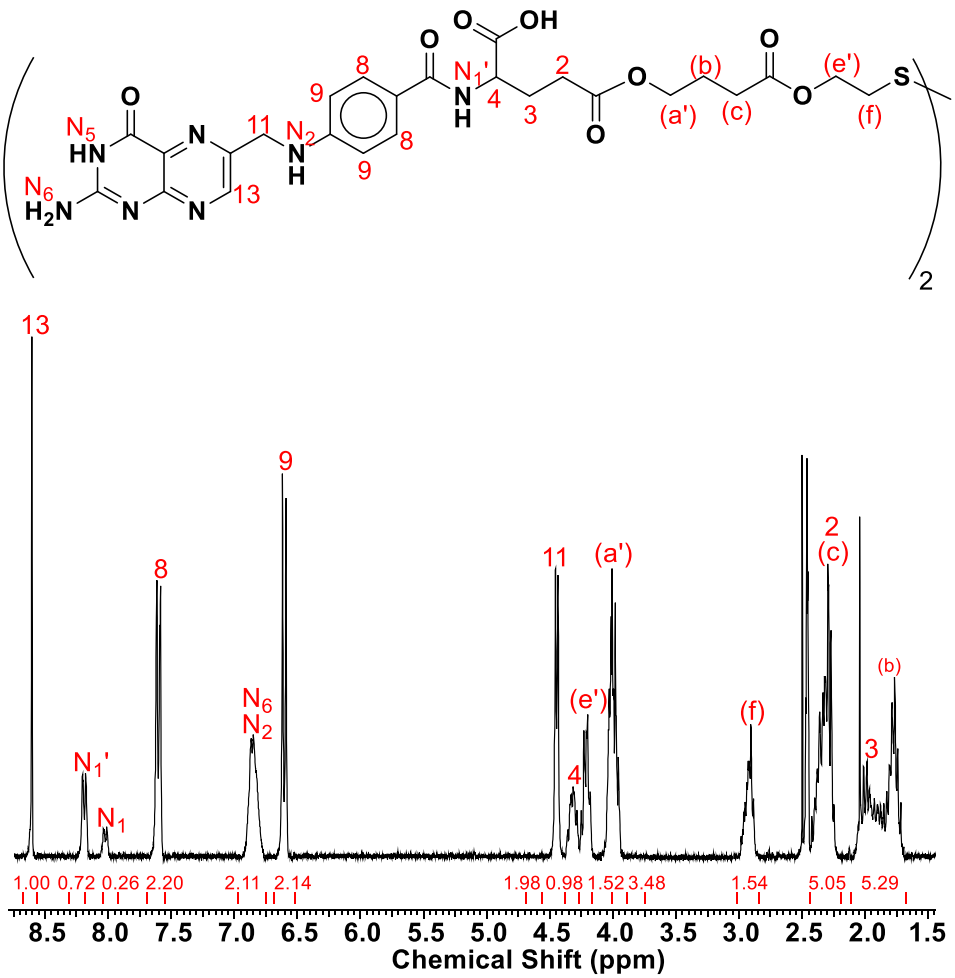

Figure 4.33 ^{1}H-NMR spectrum of FA-S-S-FA

The ^{13}C NMR spectrum of the product is shown in Figure 4.34, the peaks corresponding to the two carboxyl groups in the glutamic moiety of the conjugated FA appeared at δ = 174.59 ppm (5) and δ = 172.45 ppm (1). The ester signal from the butyrate group appears at δ = 171.99 ppm (D'). Therefore, the ^{13}C NMR spectrum of FA-S-S-FA also confirmed its structure.

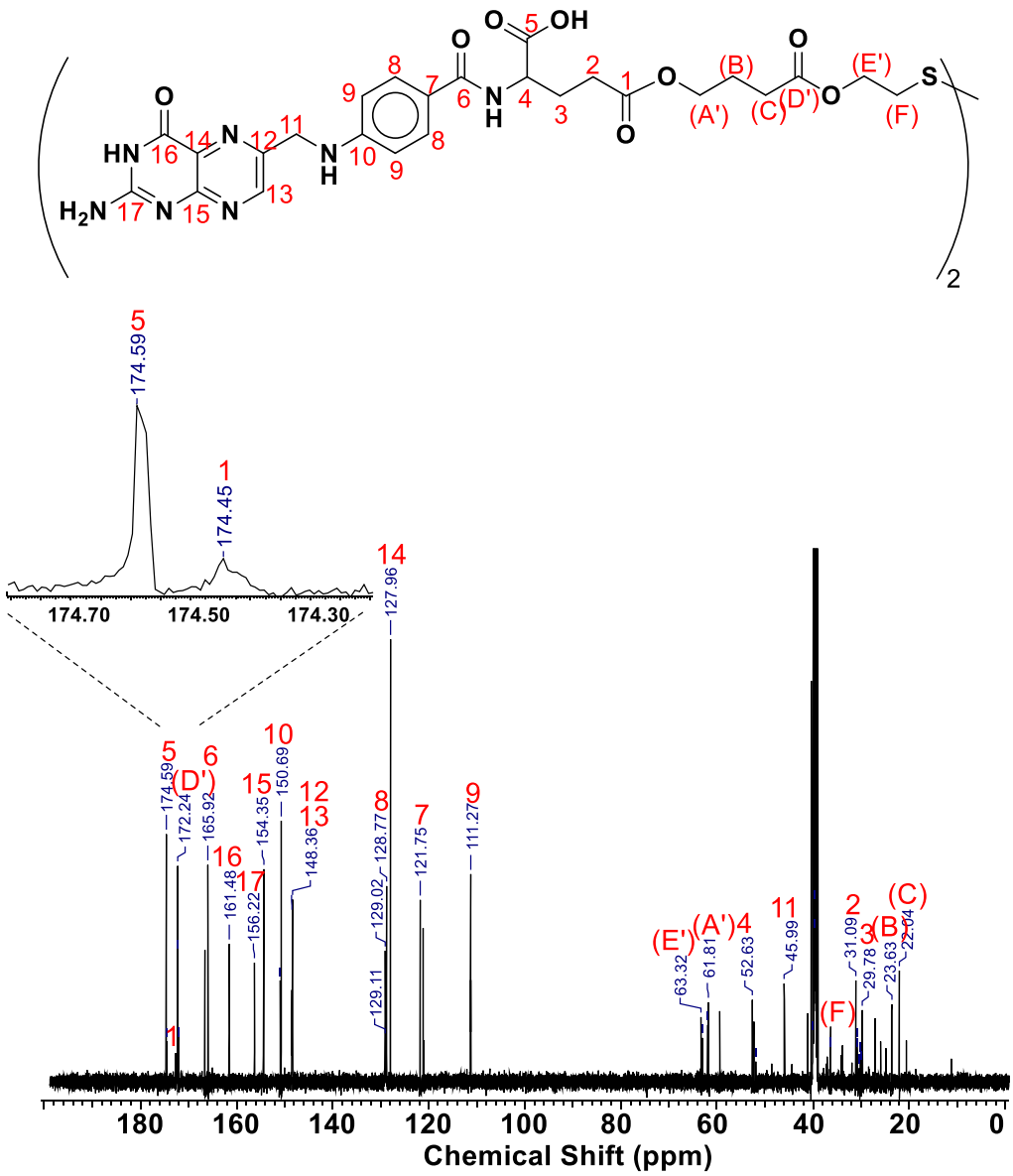

Figure 4.34 ^{13}C-NMR spectrum of FA-S-S-FA

MALDI mass spectrometry (MS) was used for further verification of the structure. Figure 4.35 shows the MALDI mass spectrum of FA-S-S-FA. The signal at *m/z* 1195.2 Da belongs to the sodiated FA-S-S-FA (denoted as "M" in the spectrum) [1173.20 (M) + 22.99 (Na)]. Its potassium salt is also observed at *m/z* 1211.2 Da. Therefore, MALDI mass spectrometry confirms the formation of the product. The spectrum also indicates the formation of the FA-S-S-Br (denoted as "M_1" in the spectrum), which is formed when one equivalent of Br-S-S-Br reacts with one equivalent of FA instead of two equivalent of FA, or one FA is lost during MALDI.

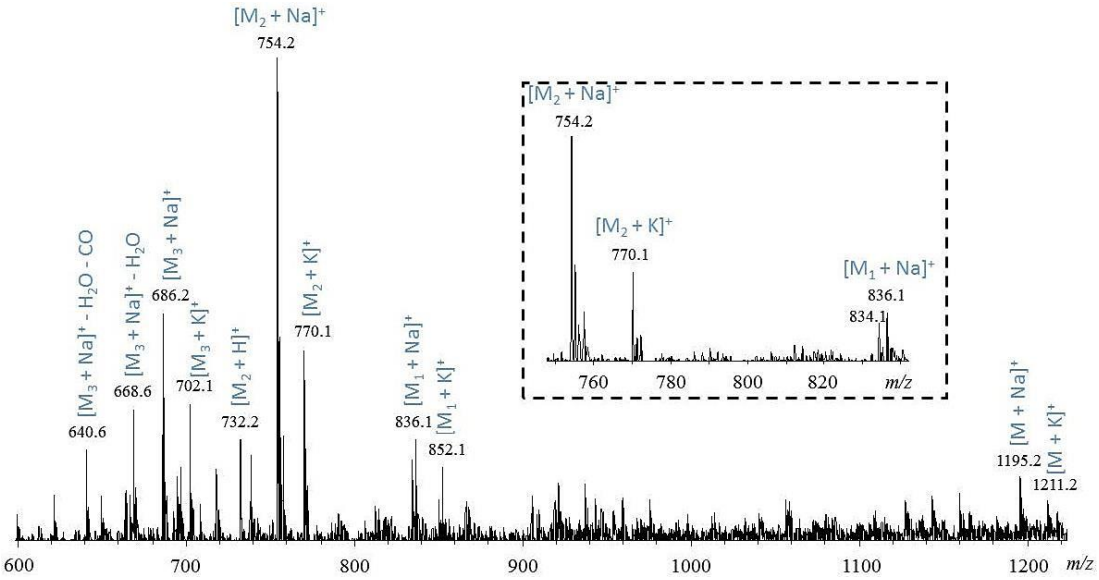

Figure 4.35 MALDI mass spectrum of FA-S-S-FA. Inset: spectrum of *m/z* 750 to 840

The signal at *m/z* 836.1 Da belongs to the sodium salt of FA-S-S-Br [812.71 (M_1) + 22.99 (Na)]. Its potassium salt is also observed at *m/z* 852.1 Da. Two unknown major signals were observed at *m/z* 754.2 Da and 686.2 Da denoted as M_2 and M_3 in the spectrum. A Tandem mass spectrometry was performed on the product signal at *m/z* 1195.2 Da to observe the fragments formed from it during ionization. The mass spectrum obtained from the Tandem MS is shown in Figure 4.36. The signal at *m/z* 754.1 Da can be observed in Figure 4.36 which is formed when the R_4 moiety (seen in the Figure 4.35) is fragmented from the sodiated product during ionization (M_2 + Na = M + Na – R_4). Therefore, we can conclude that this signal appears in Figure 4.35 due to the fragmentation of the product signal in the instrument. Its potassium salt is also observed at *m/z* 770.1 Da. Figure 4.35 also shows the presence of the signal at *m/z* 686.2 Da which forms when the R_5 moiety (Figure 4.36) is fragmented from the sodiated product (M_3 + Na = M + Na – R_5). Its potassium salt is also observed at *m/z* 702.1 Da. All the possible structures observed in the mass spectrum contain at least one FA moiety and one disulphide bond. Therefore, cleaving the disulphide bond will yield all FA moieties containing thiol functionalities.

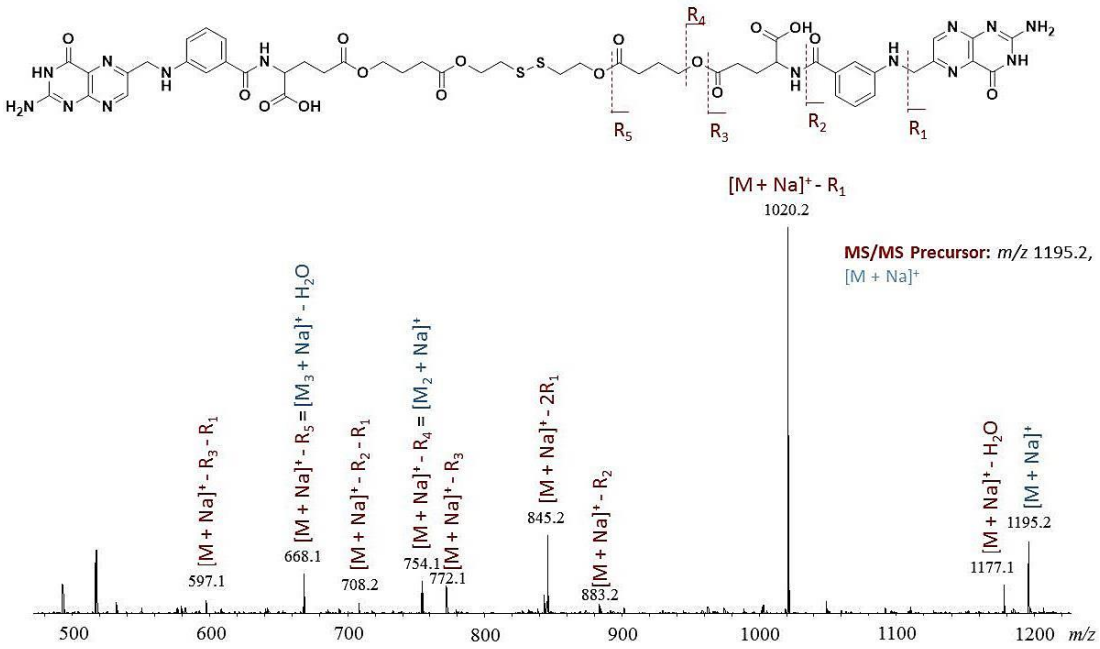

Figure 4.36 Tandem mass spectrum of the product signal at *m/z* 1195.2 Da

Figure 4.33 showed the presence of free FA in the FA-S-S-FA product. This free FA was removed by salting out with sodium ions. As discussed previously, the pK_a value of α-carboxyl acid is 2.5 and that of γ-carboxyl acid is 4.5. The FA-S-S-FA is conjugated via the γ-carboxyl whereas, the γ-carboxyl of the folic acid is free for forming salt with sodium.

The α-carboxyl is free for forming salt with sodium in free FA as well as FA-S-S-FA. Therefore, to exclusively salt out the FA via the free γ-carboxyl acid group, using a sodium ion solution of pH 9.5 – 11.5 is desirable. A calculated amount of pH 10 solution was prepared to salt out free FA from 100 mg of FA-S-S-FA sample. The sodium salt of free folic acid was soluble in the pH 10 solution whereas the FA-S-S-FA precipitated out. The ^{1}H-NMR of the dried precipitate is shown in Figure 4.37. It can be observed from the figure that the signal corresponding to the –NH proton from free FA appearing at δ = 8.05 ppm has disappeared confirming the complete elimination of free FA from the FA-S-S-FA.

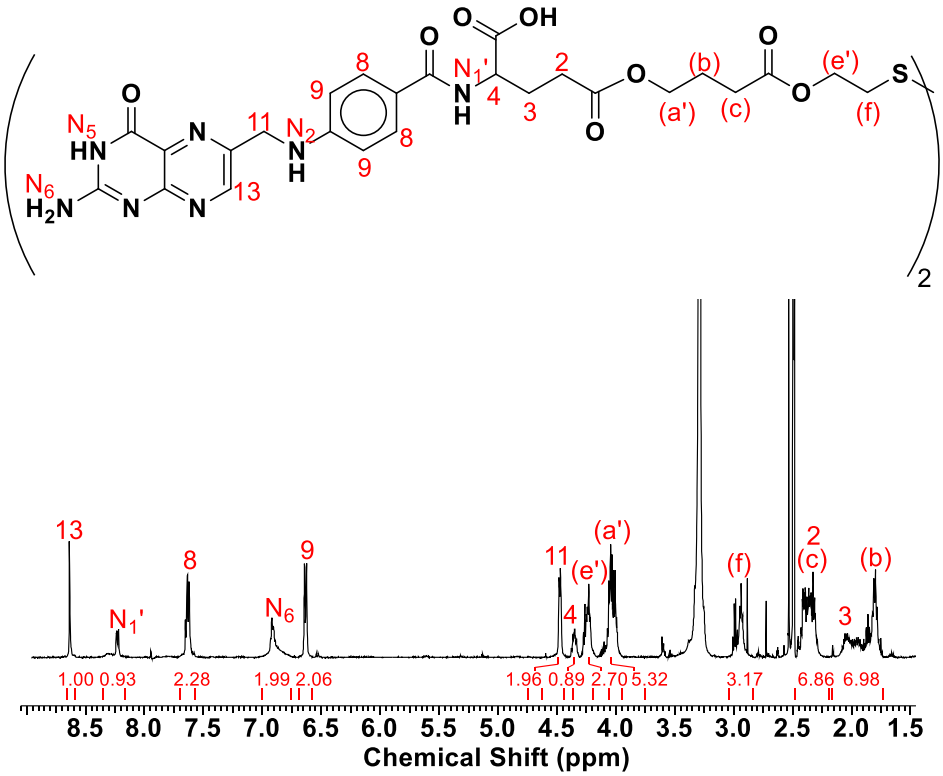

Figure 4.37 ^{1}H-NMR spectrum of FA-S-S-FA after salting out Free FA

4.1.2.2. Reduction of FA-S-S-FA

FA-SH was prepared as shown in Figure 4.38. The disulphide bond in FA-S-S-FA was cleaved using dithiothreitol (DTT) under nitrogen and at room temperature using Dimethylformamide (DMF) as the solvent. The free thiol from the FA-SH is prone to oxidation when exposed to air, therefore, FA-SH was prepared freshly for each Michael addition reaction required in each of the three strategies.

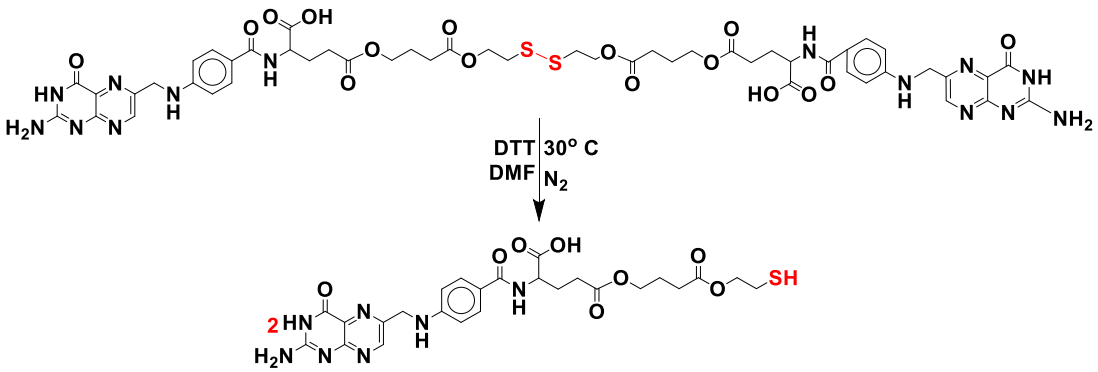

Figure 4.38 Reaction scheme for preparing FA-SH

Figure 4.39 displays the ^{1}H-NMR spectrum of FA-SH. The ^{1}H NMR spectrum shows signals of FA at δ=7.59 ppm (8), δ=6.61 ppm (9) and δ=8.58ppm (13) appeared at the expected positions. A new peak at δ=2.69 ppm that belongs to the -CH_2- (f') attached to the SH group appeared.

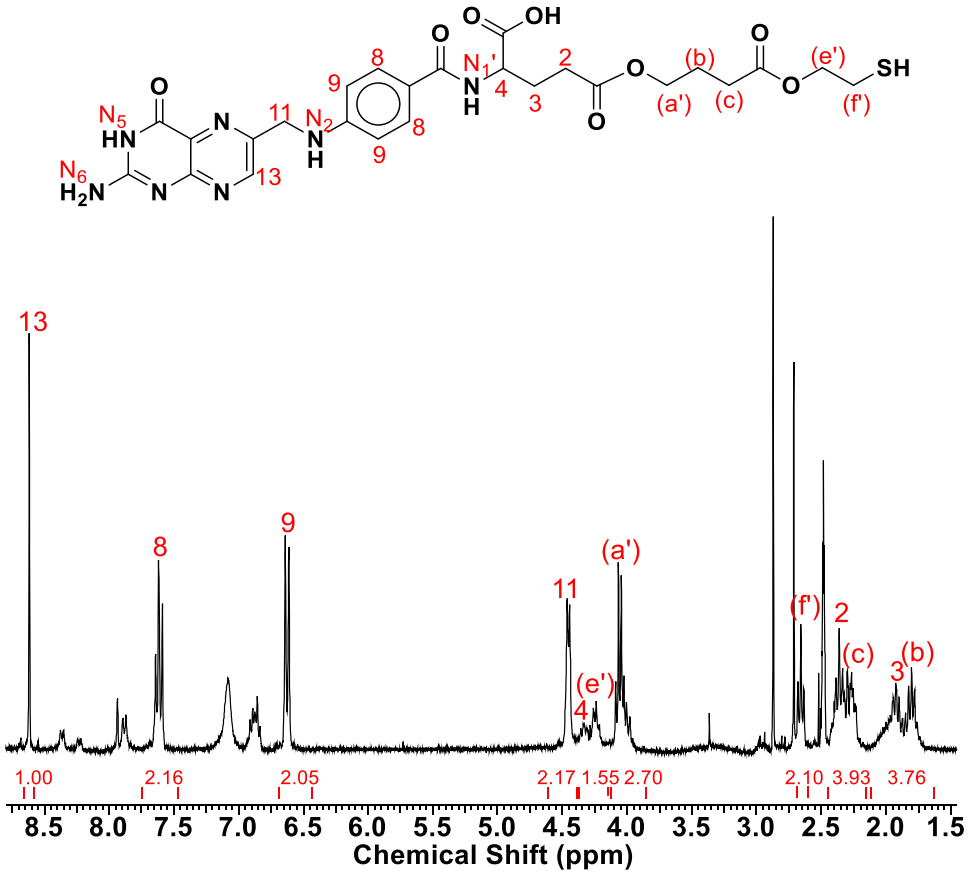

Figure 4.39 ^{1}H-NMR spectrum of FA-SH

Figure 4.40 displays the ^{13}C-NMR spectrum of FA-SH. The ^{13}C NMR spectrum confirmed the conjugation. Most of the carbon signals match the expected structure of FA-SH and the carbon signal associated with the butyrate carbons did not change after the reaction. The carbons attributed to the two carboxyl groups in the glutamic moiety of the conjugated FA appeared at δ = 173.94 ppm (α) and δ = 172.03 ppm (γ). The -CH_2- carbon besides the disulphide bond (F) appearing at δ = 36 ppm moved upfield to δ = 24 ppm (F') after cleavage of the disulphide bond. Therefore, the ^{13}C NMR spectrum of FA-SH confirmed the structure.

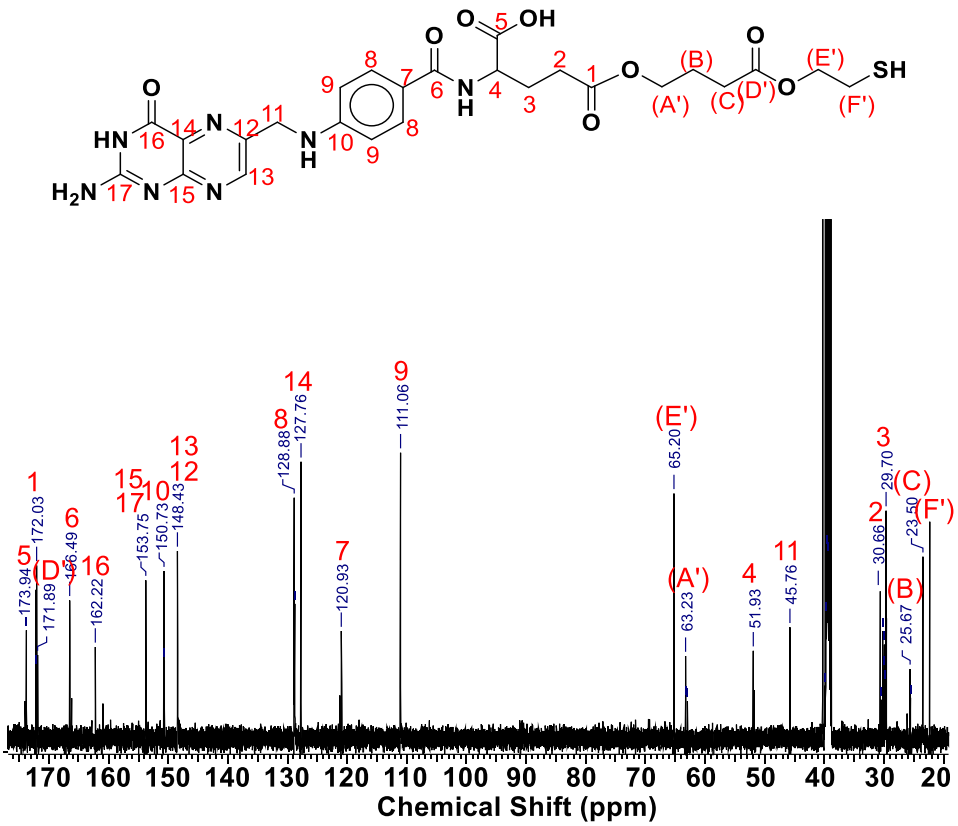

Figure 4.40 ^{13}C-NMR spectrum of FA-SH

4.2. Synthesis of Thiol-functionalized TEG and PEGs

We obtained a mixture of products with H_2N-PEG-NH_2 as discussed in Section 4.1.1.3. Therefore, to overcome this problem, we developed Strategy 2, presented in Figure 2.14. In Strategy 2, first poly(ethylene glycol)(PEG)-dithiol (HS-PEG-SH) is reacted with 2 equivalents of Fluorescein-*o*-acrylate (FLA) via *Candida antartica* Lipase B (CALB)-catalyzed Michael addition to obtain a fluorescein-labeled PEG (FL-PEG-FL). The FL-PEG-FL is then reacted with 2 equivalents of acryloyl chloride (AcCl) in presence of trimethylamine (TEA) to obtain an acrylated fluorescein-labeled PEG (Ac-FL-PEG-FL-Ac). The Ac-FL-PEG-FL-Ac is then reacted with 2 equivalents of a thiol-functionalized Folic Acid (FA-SH) via CALB-catalyzed Michael addition to obtain FA functionalized fluorescein-labeled PEG (FA-FL-PEG-FL-FA).

Strategy 2 uses PEG-dithiol (HS-PEG-SH) as the PEG linker. I developed a new synthesis method for HS-PEG-SH. The HS-PEG-SH is synthesized by CALB-catalyzed transesterification of methyl 3-mercaptopropionate (MP-SH) with PEG. The kinetics of this transesterification of MP-SH with TEG and PEGs of M_n = 1000 g/mol and M_n= 2050 g/mol was investigated in detail and will be presented in this section.

The fluorescein attachment to the HS-PEG-SH and its subsequent acrylation to obtain Ac-FL-PEG-FL-Ac is performed by Gayatri Shrikhande. Section 4.3 discusses the FA-SH attachment to the Ac-FL-PEG-FL-Ac via enzyme catalyzed Michael addition reaction in order to obtain the proposed bivalent folate-targeted fluorescein-labeled PEG (FA-FL-PEG-FL-FA).

The synthetic strategy for obtaining PEG-thiols has been previously reported in the literature. Mahou *et al.*[102] reported the single synthetic strategy to obtain PEG-monothiol. They tosylated one hydroxyl end-group of the PEG-diol using *p*-toluenesulfonyl chloride with silver oxide and potassium iodide as catalysts and toluene as the solvent. The tosylated PEG was then reduced with sodium hydrosulfide at 60 °C to yield PEG-monothiol with 84% yield. PEG-dithiols have been synthesized by various methods. In one method, the hydroxyl end groups were reacted with allyl bromide at 120 °C, followed by a radical-mediated addition of thioacetic acid and subsequent reduction to thiol using sodium hydroxide/sodium thiomethoxide, with 56% yield.[103-105] Another route reported tosylation of the hydroxyl end groups, followed by reaction with a xanthate and de-protection with an alkyl amine that gave 98% yield.[106-108] The simplest method used esterification of mercapto-acids in toluene at 120 °C using p-toluenesulfonic acid or sulfuric acid as catalysts: an example is shown in Figure 4.41.[109-116]

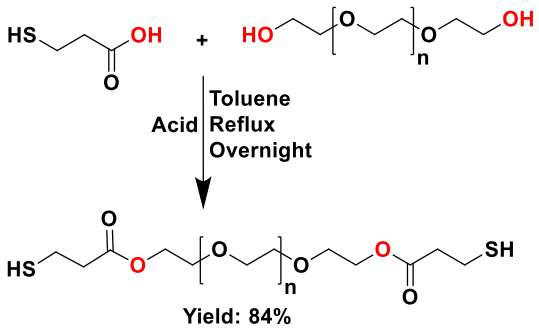

Figure 4.41 Synthesis of PEG-dithiol[109]

These methods employ acid catalysts; and hence are not "green". Against this background, the synthesis of thiol-functionalized tetraethylene glycol (TEG) and PEGs by transesterification of methyl 3-mercaptopropionate (MP-SH) under solventless conditions using CALB was investigated. Precise thiol-functionalization of TEG and PEGs by enzyme catalysis has not been reported previously in the literature. This section presents the first examples of precision synthesis of TEG and PEG monothiols and dithiols.

4.2.1. Kinetics of CALB-catalyzed transesterification of MP-SH with TEG

First a model kinetic reaction with tetraethylene glycol (TEG) was carried out. The ^{1}H-NMR spectrum of TEG is presented in Figure 4.7 in Section 4.1.1.1. The progress of the reaction was monitored by ^{1}H-NMR spectroscopy as shown in Figure 4.42. At time 0, the protons from MP-SH (thiol proton triplet at 1.60 ppm (i), -CH_2- protons - quartet at δ = 2.73 ppm (h) and triplet at δ = 2.61 ppm (g)) can be seen together with the proton signals of TEG (CH_2 protons besides the -OH end group at δ = 3.57 ppm (b) and at δ = 3.64 ppm (c) and the internal CH_2 protons of TEG at δ = 3.63 ppm (d)). It can be observed from Figure 4.42 that the intensity of the signal at δ = 3.57 ppm (b) gradually decreases as the reaction time increases. The formation of the ester bond is demonstrated by the appearance of a new signal at δ = 4.23 ppm, corresponding to the -CH_2- protons besides the carbonyl group in the product (b',

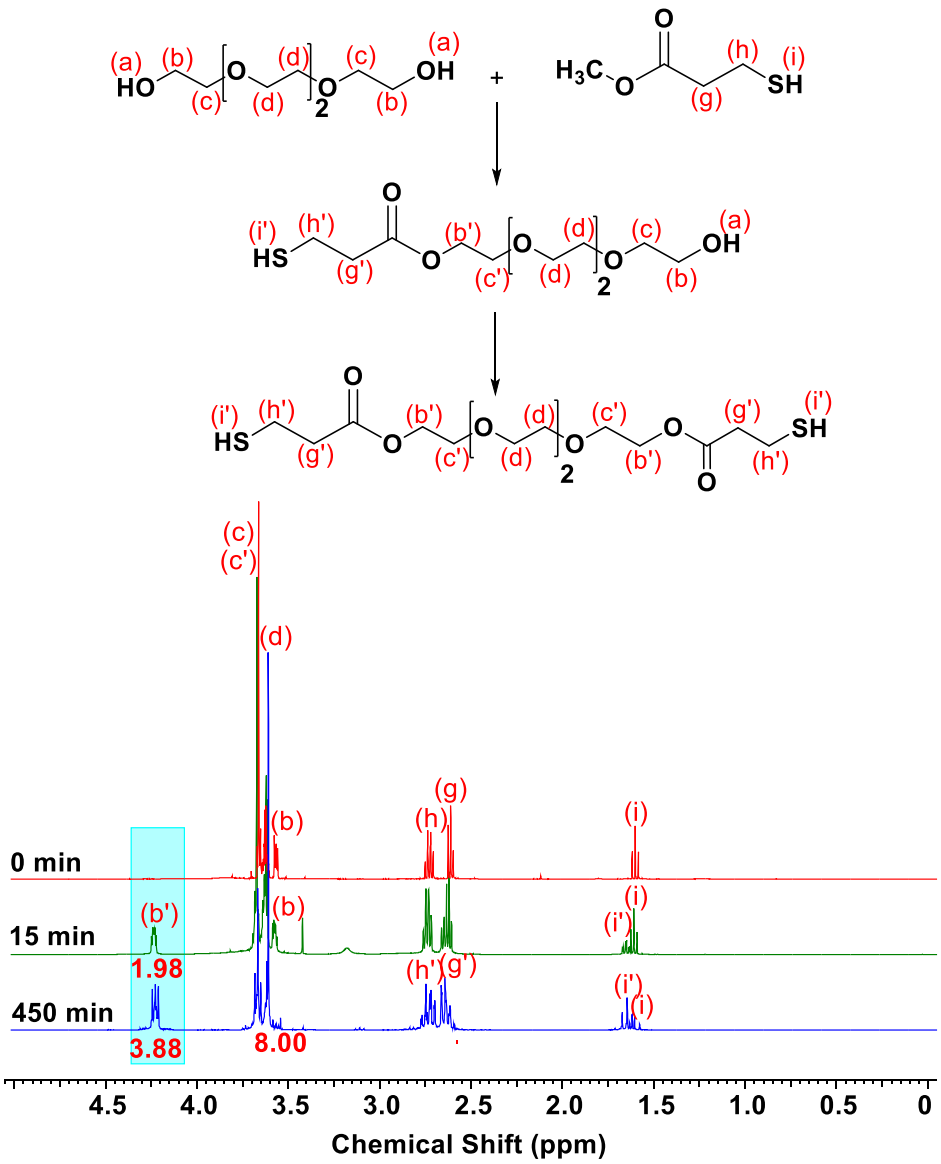

Figure 4.42 ^{1}H-NMR spectroscopy monitoring of the kinetics of the transesterification of MP-SH with TEG. Reprinted with permission from *Catalysts* **2019**, *9(3)*, 228. Copyright © 2019 MDPI

Figure 4.42). The proton signals h and g slightly shift to 2.75 ppm (h') and δ = 2.64 ppm (g'). After 15 minutes reaction time, the ratio of the internal CH_2 protons of TEG at δ = 3.61 ppm (d) to (b') in the product was 8:1.98, indicating the formation of TEG-monothiol. After the formation of TEG-monothiol, the reaction slowed down considerably. Complete conversion to dithiol took 450 minutes, and the relative integrals of (d): (b') at 8:3.88 indicated the formation of TEG-dithiol (Figure 4.42).

Figure 4.43 illustrates our rendition of the mechanism of CALB-catalyzed transesterification of MP-SH with TEG inspired by our group's previous publication.[9]

The catalytic triad of this enzyme consists of aspartate (Asp187), histidine (His224), and serine (Ser105).[117] The top dark shaded portion of the enzyme is the "carbonyl pocket" and the bottom lighter shaded portion is the "hydroxyl pocket". First, the lone pair of electrons on the hydroxyl group from Ser105 in the free enzyme attacks the carbonyl group of the MP-SH, which forms the first tetrahedral intermediate (THI_1). This THI_1 is stabilized by the three H bonds present in the carbonyl pocket: two from threonine (Thr40) and one from glutamine (Gln106).[117] Then the ester bond in THI_1 is cleaved forming an acyl-enzyme complex (AEC) releasing the corresponding alcohol

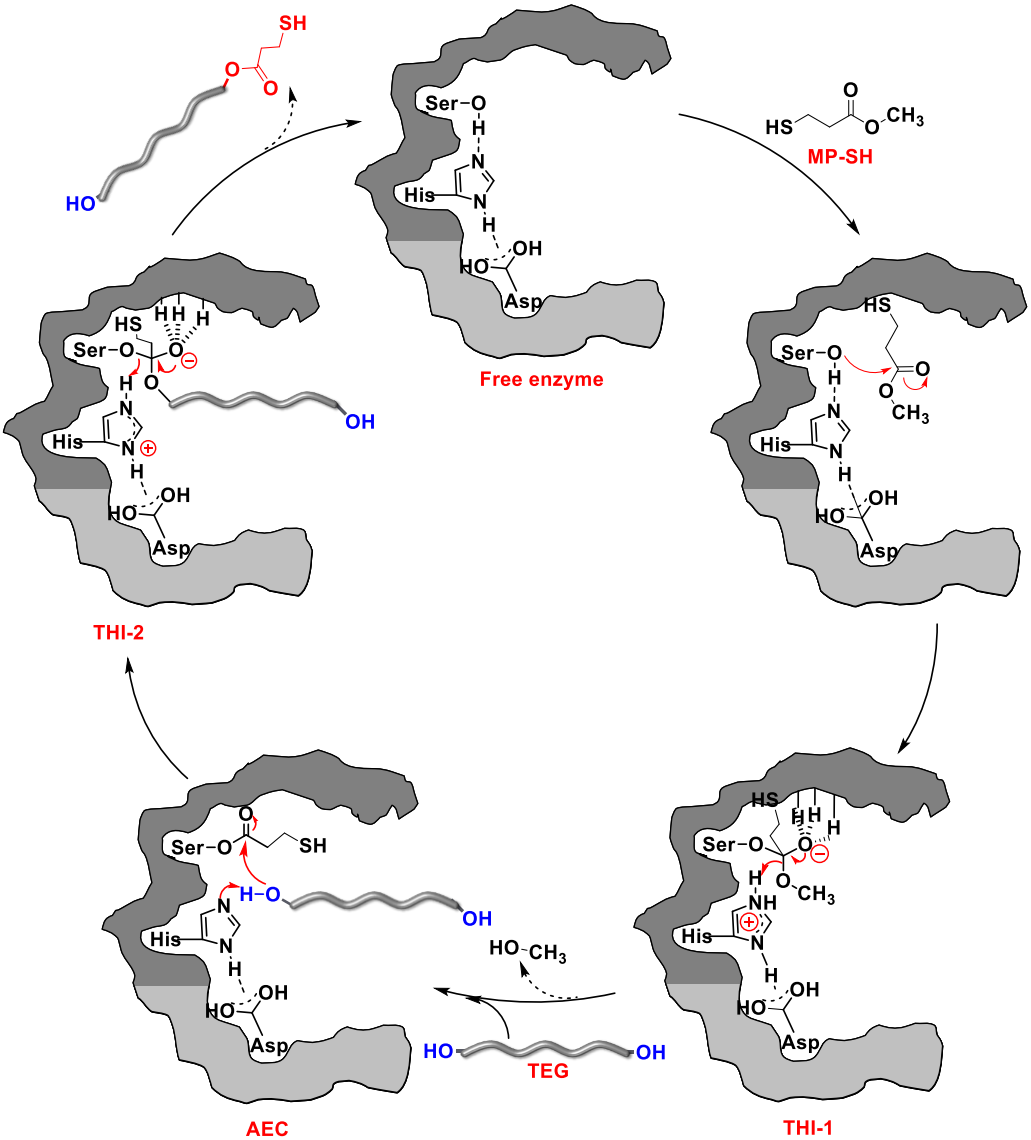

Figure 4.43 Reaction mechanism of CALB-catalyzed transesterification of MP-SH with TEG – first cycle. Reprinted with permission from *Catalysts* **2019**, *9(3)*, 228. Copyright © 2019 MDPI

from the thioester, methanol in this case, which is removed due to the applied vacuum (420 Torr), which makes the process irreversible. Then the lone pair on the hydroxyl end-group of the diol positioned in the hydroxyl pocket attacks the carbonyl of the AEC, which forms the second tetrahedral intermediate (THI_2) that is also stabilized by the three H bonds in the carbonyl pocket. Lastly, the enzyme releases the acyl product from THI_2, TEG-monothiol in this case, and gets regenerated.

The second -OH group of the TEG-monothiol will then be converted to thiol in a second cycle in a similar manner as the first cycle as shown in Figure 4.44. In principle, the first and second cycle may proceed simultaneously in a competitive reaction between the hydroxyl groups of unreacted TEG and TEG-monothiol. However, our data show that the first step is completed quickly to yield monothiol,

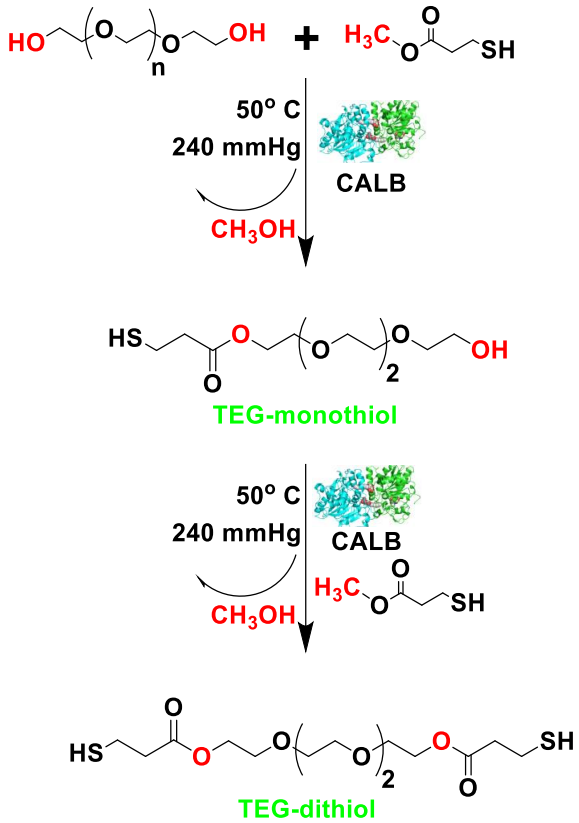

Figure 4.44 CALB-catalyzed transesterification of MP-SH with TEG. Reprinted with permission from *Catalysts* **2019**, *9(3)*, 228. Copyright © 2019 MDPI

and the reaction slows down before yielding the dithiol. Therefore with precise timing we were able to synthesize TEG-monothiol.

TEG-monothiol (HO-TEG-SH) was obtained by precise timing of the transesterification reaction of MP-SH with TEG based on the data from the kinetic study presented above. Figure 4.45 shows the ^{1}H-NMR spectrum of TEG-monothiol synthesized with a reaction time of 15 minutes after filtering the enzyme and removing the excess thioester but without further purification (93% yield because some material is lost with the enzyme). The ratio of the integral of the -CH_2- protons besides the -SH group in the product at 2.75 ppm (h') and δ = 2.64 ppm (g') to the integral of the -CH_2- protons besides the carbonyl group at δ = 4.23 ppm (b') is 4.00:2.00, indicating the formation of TEG-monothiol with 100% conversion.

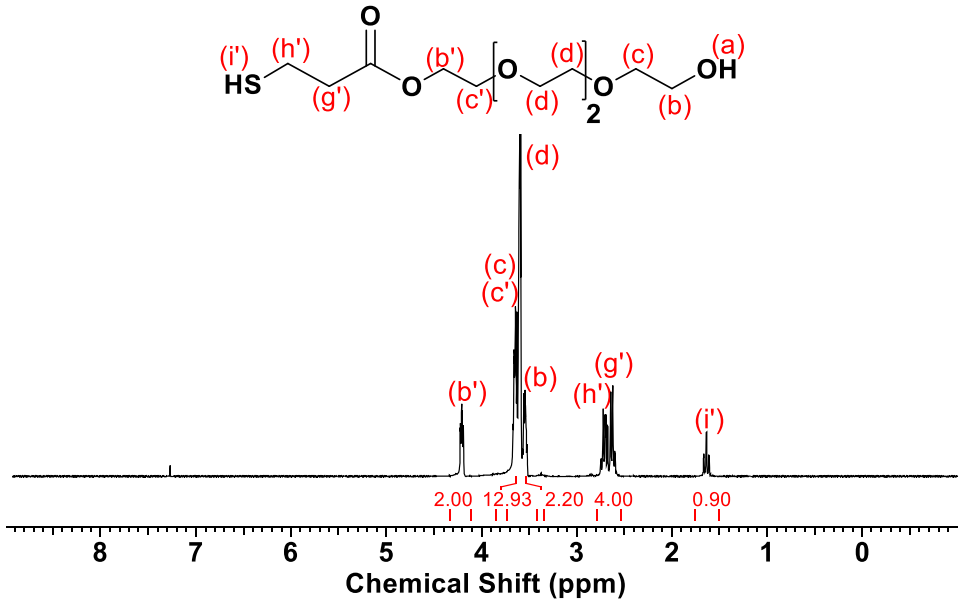

Figure 4.45 ^{1}H-NMR spectrum of TEG-monothiol. Reprinted with permission from *Catalysts* **2019**, *9(3)*, 228. Copyright © 2019 MDPI

Figure 4.46 shows the ^{13}C-NMR spectrum of TEG-monothiol. The signals corresponding to the carbons in the thiol end group (H', G', F') appear at δ = 19.2 ppm, δ = 37.9 ppm, and 171.0 ppm respectively. The signals corresponding to the carbons in the TEG end-group that underwent transesterification (B' and C') appear at δ = 63.2 ppm and δ = 68.5 ppm. The carbons besides the -OH end group (B and C)

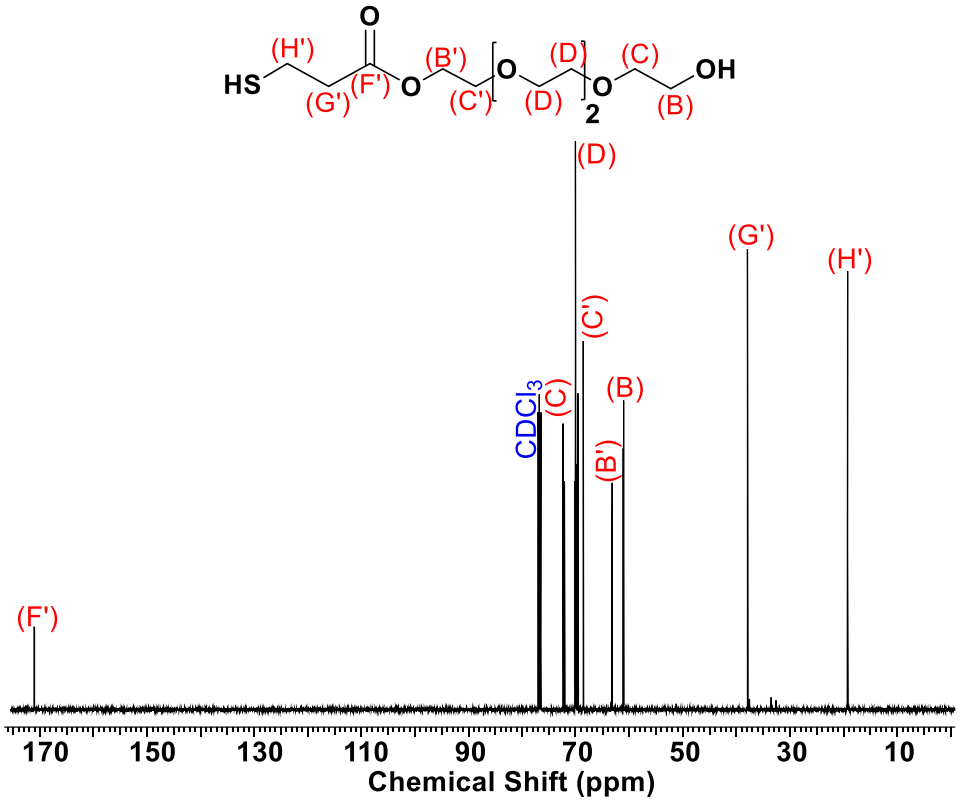

Figure 4.46 ^{13}C-NMR spectrum of TEG-monothiol. Reprinted with permission from *Catalysts* **2019**, *9(3)*, 228. Copyright © 2019 MDPI

that did not undergo transesterification appear distinctly at δ = 61.16 ppm and δ = 72.38 ppm. ^{13}C-NMR spectroscopy confirmed the formation of TEG-monothiol.

TEG-dithiol (HS-TEG-SH) was obtained by precise timing of the transesterification reaction of MP-SH with TEG based on the data from the kinetic study presented above. HS-TEG-SH was used in the synthesis of FA-functionalized fluorescein-labeled TEG (FA-FL-TEG-FL-FA) presented in section 4.3.1. Figure 4.47 shows the ^{1}H-NMR spectrum of TEG-dithiol that was synthesized with a reaction time of 7.5 hours (88% yield). The ratio of the integral values of signals (h') + (g') to (b') are 8.00:3.88, indicating the formation of TEG-dithiol.

The ^{13}C-NMR spectrum of TEG-dithiol is shown in Figure 4.48. It shows only the signals corresponding to carbons in the thiol end-groups (H' and G'), with only traces of signals corresponding to the carbons besides the -OH (B and C) at δ = 72.38

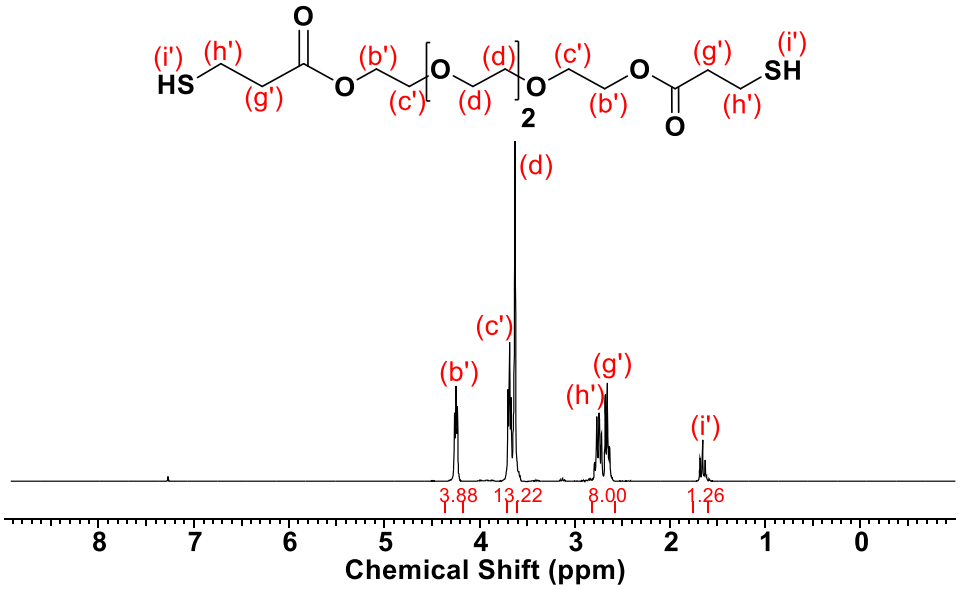

Figure 4.47 ^{1}H-NMR spectrum of TEG-dithiol. Reprinted with permission from *Catalysts* **2019**, *9(3)*, 228. Copyright © 2019 MDPI

ppm and δ = 61.16 ppm, possibly from traces of residual TEG-monothiol, indicating 100% conversion of the -OH groups to thiols.

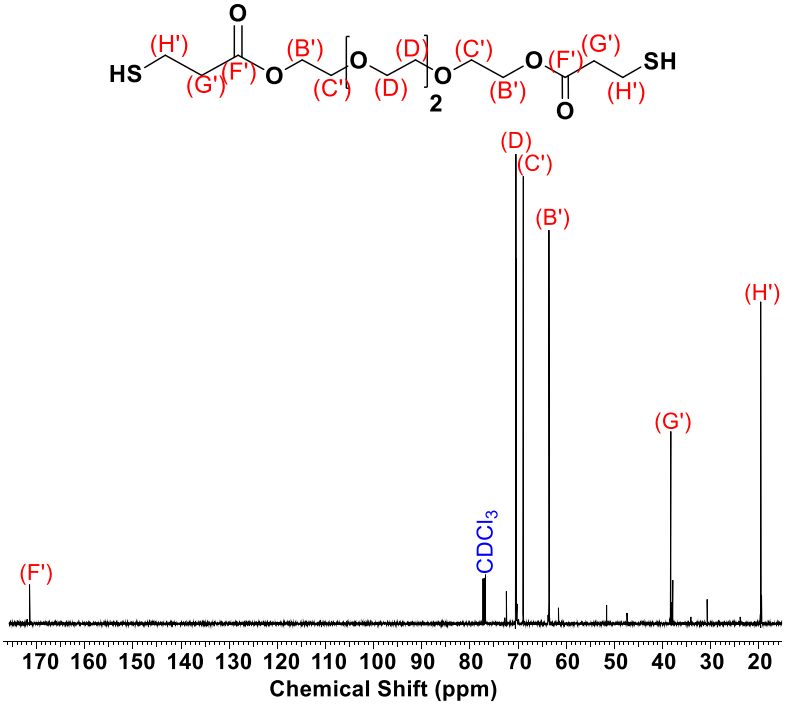

Figure 4.48 ^{13}C-NMR spectrum of TEG-dithiol. Reprinted with permission from *Catalysts* **2019**, *9(3)*, 228. Copyright © 2019 MDPI

4.2.2. Kinetics of CALB-catalyzed transesterification of MP-SH with PEGs

MP-SH was reacted with PEG_{1000} using enzyme catalysis, and the reaction was monitored over 24 hours with ^{1}H-NMR spectroscopy as shown in Figure 4.49. Because low molecular weight PEGs (< 3000 g/mol) are liquid at the reaction temperature and are miscible with MP-SH, no solvent was necessary as a medium for the reaction. The main chain protons (d) and the -CH_2- protons besides the –OH (b and c) and the thioester (c') appear at δ = 3.61 ppm. For PEG_{1000}-monothiol, the new -CH_2- protons besides the carbonyl group (b') appear at δ = 4.23 ppm, which makes the integral value of internal protons of PEG_{1000} (d, b, c, and c'): 88 - 2 = 86.

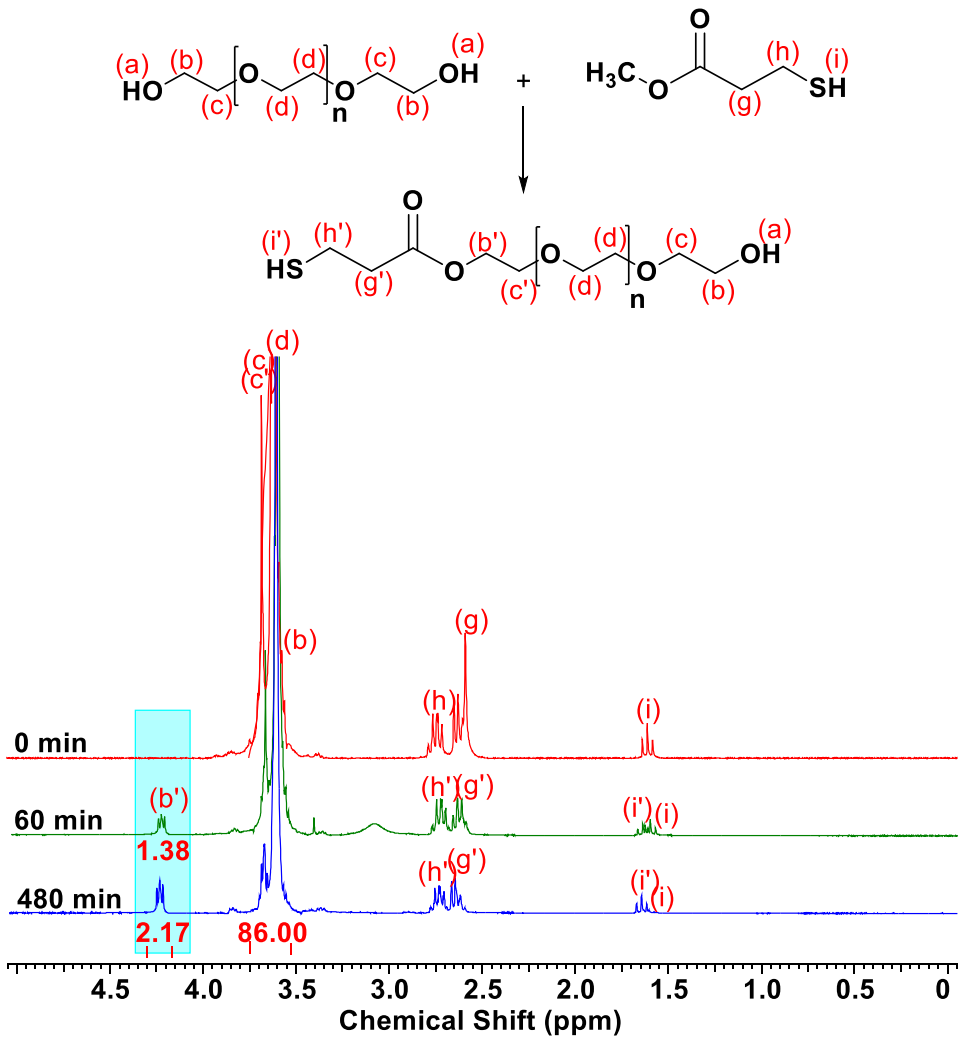

Figure 4.49 ^{1}H-NMR spectroscopy monitoring of the kinetics of transesterification of MP-SH with PEG_{1000}. Reprinted with permission from *Catalysts* **2019**, *9(3)*, 228. Copyright © 2019 MDPI

Therefore, the integral value of the internal protons was set to 86 for calculating the extent of reaction. Based on the integral ratio of (d, b, c, and c'): (b'), about 60% of the PEG_{1000} was converted to PEG_{1000}-monothiol in 60 minutes (Figure 4.49). Then the reaction slowed down, and it took 8 hours to convert all PEG_{1000} into monothiol. Dithiol was not detected even after 24 hours. The mechanism presented in Figure 4.43 for TEG also applies for PEG. Thus, we theorize that in the second cycle the carbonyl group of the free MP-SH competes with the carbonyl group of the PEG-monothiol for complexation in the carbonyl pocket of CALB, thereby slowing down the second cycle of the reaction. In addition, the CALB may be deactivated by the methanol released in the reactions that is not completely removed by vacuum.

PEG_{1000}-monothiol (HO- PEG_{1000}-SH) was obtained by precise timing of the transesterification reaction of MP-SH with PEG_{1000} based on the data from the kinetic study presented above. Figure 4.50 shows the ^{1}H-NMR spectrum of PEG_{1000}-monothiol synthesized with a reaction time of 8 h after filtering the enzyme and removing the excess thioester but without further purification. The integral ratio of (h') + (g') to the -CH_2- protons in the new ester bond at δ = 4.23 ppm (b') is 4:00:1.86, indicating the formation of PEG_{1000}-monothiol.

Figure 4.51 shows the ^{13}C-NMR spectrum of PEG_{1000}-monothiol. Signals corresponding to the carbons besides the thioester (B', δ = 63.8 ppm and C' = 69.1 ppm) and –OH end groups (B, δ = 61.7 ppm and C, δ = 72.66 ppm) appear simultaneously, indicating the formation of monothiol.

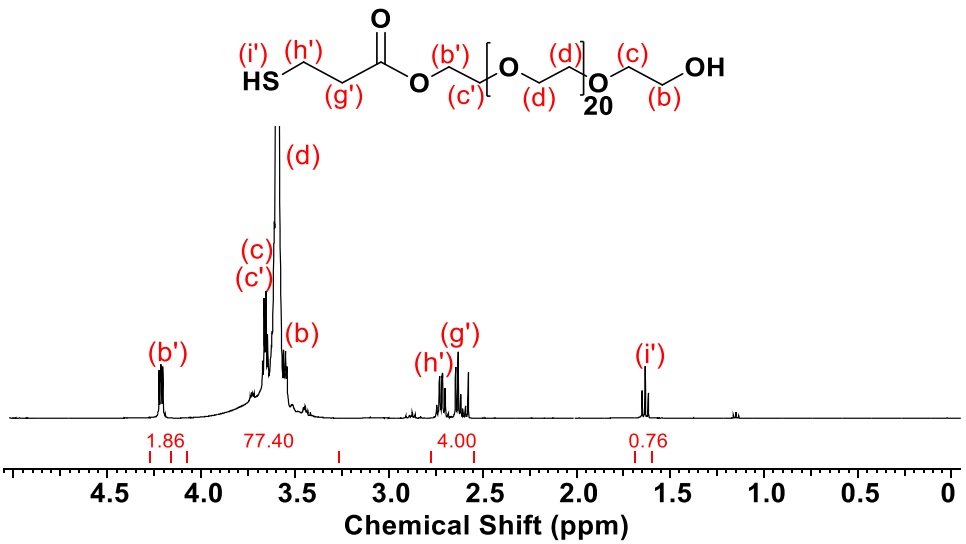

Figure 4.50 ^{1}H-NMR spectrum of PEG_{1000}-monothiol. Reprinted with permission from *Catalysts* **2019**, *9(3)*, 228. Copyright © 2019 MDPI

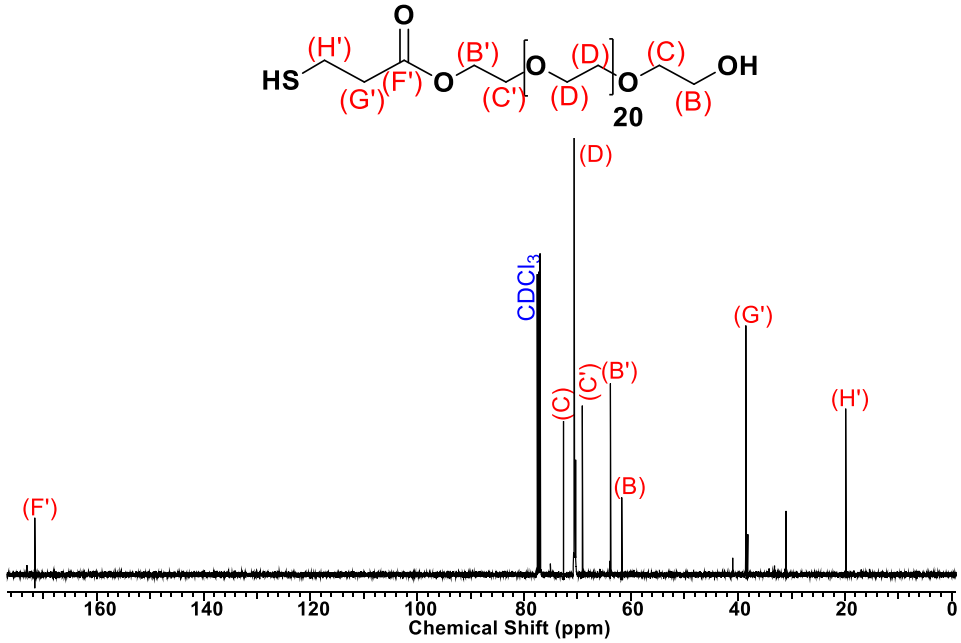

Figure 4.51 ^{13}C-NMR spectrum of PEG_{1000}-monothiol. Reprinted with permission from *Catalysts* **2019**, *9(3)*, 228. Copyright © 2019 MDPI

The product was further analysed by MALDI mass spectrometry and Figure 4.52 shows the spectrum. There are two major distributions of signals, each separated by 44 m/z units (inset). The signal at *m/z* 1097.63 belongs to the Na complex of the 22-mer fraction of PEG_{1000} monothiol [1097.63 = 22 x 44.03 (C_2H_4O repeat unit) + 89.14 (HSC_2H_4CO- end group) + 17 (HO- end group) + 22.99 (Na^+)]. The signal at *m/z* 560.31 belongs to the doubly charged Na complex of the 22-mer fraction of

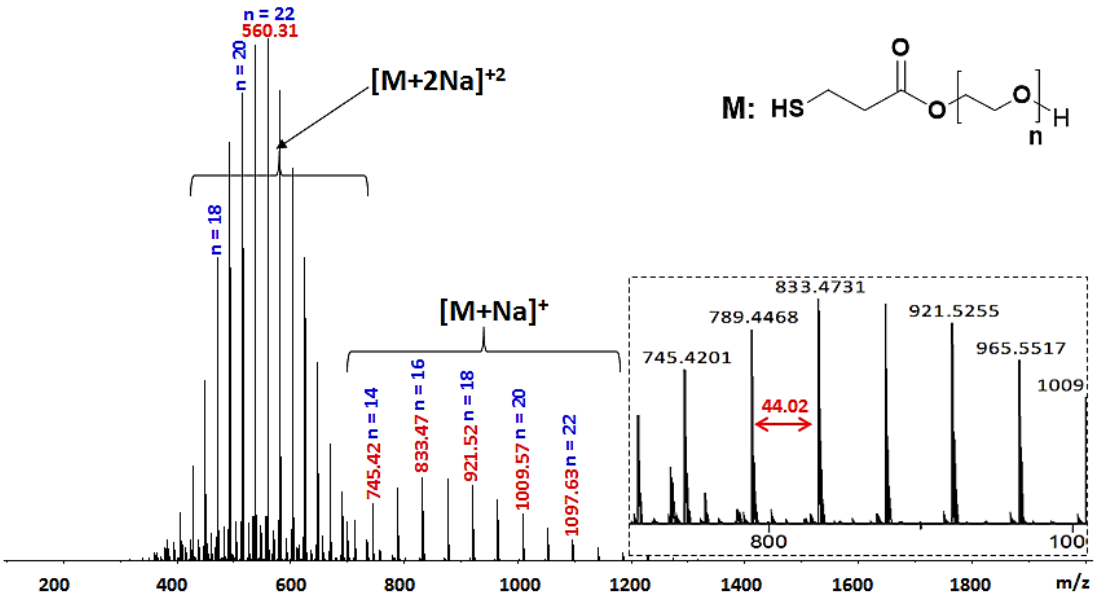

Figure 4.52 MALDI mass spectrum of PEG_{1000} monothiol. Inset: spectrum of 14- to 20- mer fractions, 44 m/z = PEG repeat unit. Reprinted with permission from *Catalysts* **2019**, *9(3)*, 228. Copyright © 2019 MDPI

PEG_{1000}-monothiol [560.31 = [(1097.63 ($[M + Na]^+$) + 22.99 (Na^+)]/2]. The small distribution of signals appearing under the doubly charged Na complex distribution belongs to traces of unreacted PEG_{1000} from the reaction mixture (< 5%) that could not be detected by NMR. Thus based on the MALDI data, over 95% conversion of one of the OH groups to thiol was achieved in 24 hours. No traces of PEG-dithiol were found. Therefore, it can be concluded that the product was exclusively PEG_{1000}-monothiol with no traces of dithiol, with 100% yield.

PEG_{1000}-dithiol (HS-PEG_{1000}-SH) was obtained by reacting PEG_{1000}-monothiol with fresh MP-SH and CALB for 24 hours under solventless conditions. HS-PEG_{1000}-SH was used to obtain FL-PEG_{1000}-FL and subsequently FA-FL-PEG_{1000}-FL-FA discussed in section 4.3.2. Figure 4.53 shows the ^{13}CNMR spectrum of the PEG_{1000}-dithiol. The disappearance of the signals (B and C) at δ = 72.66 ppm and δ = 61.72 ppm, corresponding to the -CH_2- protons besides the hydroxyl end-groups from the PEG_{1000}-monothiol indicates full conversion to PEG_{1000}-dithiol in 24 hours with 85% reaction yield.

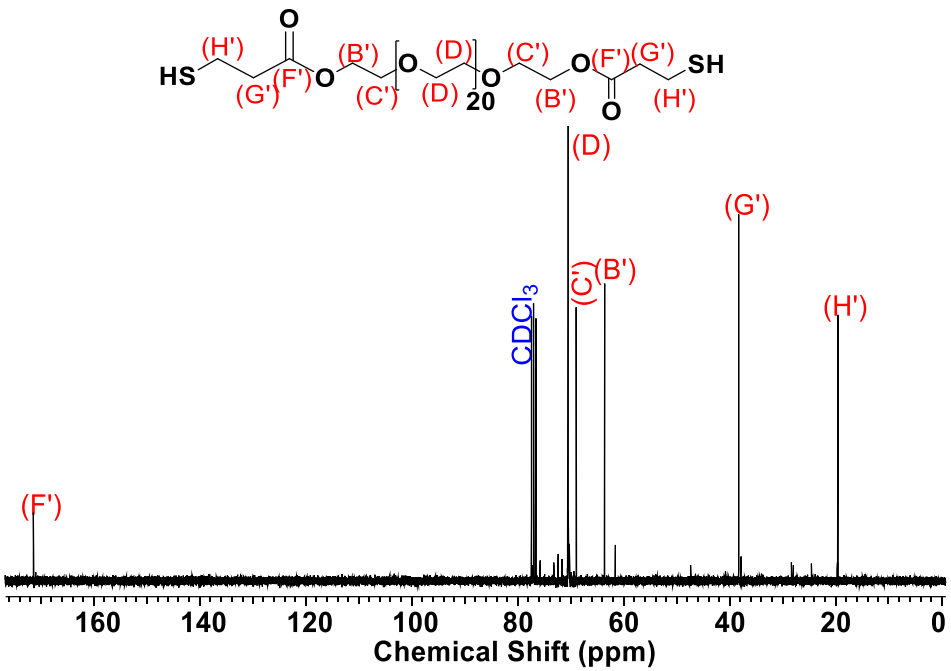

Figure 4.53 ^{13}C-NMR spectrum of PEG_{1000} dithiol. Reprinted with permission from *Catalysts* **2019**, *9(3)*, 228. Copyright © 2019 MDPI

Similar to PEG_{1000}, MP-SH was also transesterified with PEG_{2050} and the reaction was monitored over 24 hours by ^{1}H-NMR spectroscopy as shown in Figure 4.54. Similar to the PEG_{1000}, only monothiol was obtained. The main chain protons (d) and the -CH_2- protons besides the –OH (b and c) and the thioester (c') appear at δ = 3.61 ppm. For PEG_{2050}-monothiol, the new -CH_2- protons besides the carbonyl group (b') appear at δ = 4.23 ppm, which makes the integral value of internal protons of PEG_{2050} (d, b, c, and c'): 184 - 2 = 182. Therefore, the integral value of the internal protons was set to 182 for calculating the extent of reaction. Based on the integral ratio of (d, b, c, and c'): (b'), about 40% of the PEG_{2050} was converted to PEG_{2050}-monothiol in 60 minutes (Figure 4.54). Then the reaction slowed down, and it took 16 hours to convert all PEG_{2050} into monothiol. Dithiol was not detected even after 24 hours. Complete conversion to monothiol was achieved in 16 hours, which suggests higher molecular weight required longer reaction time.

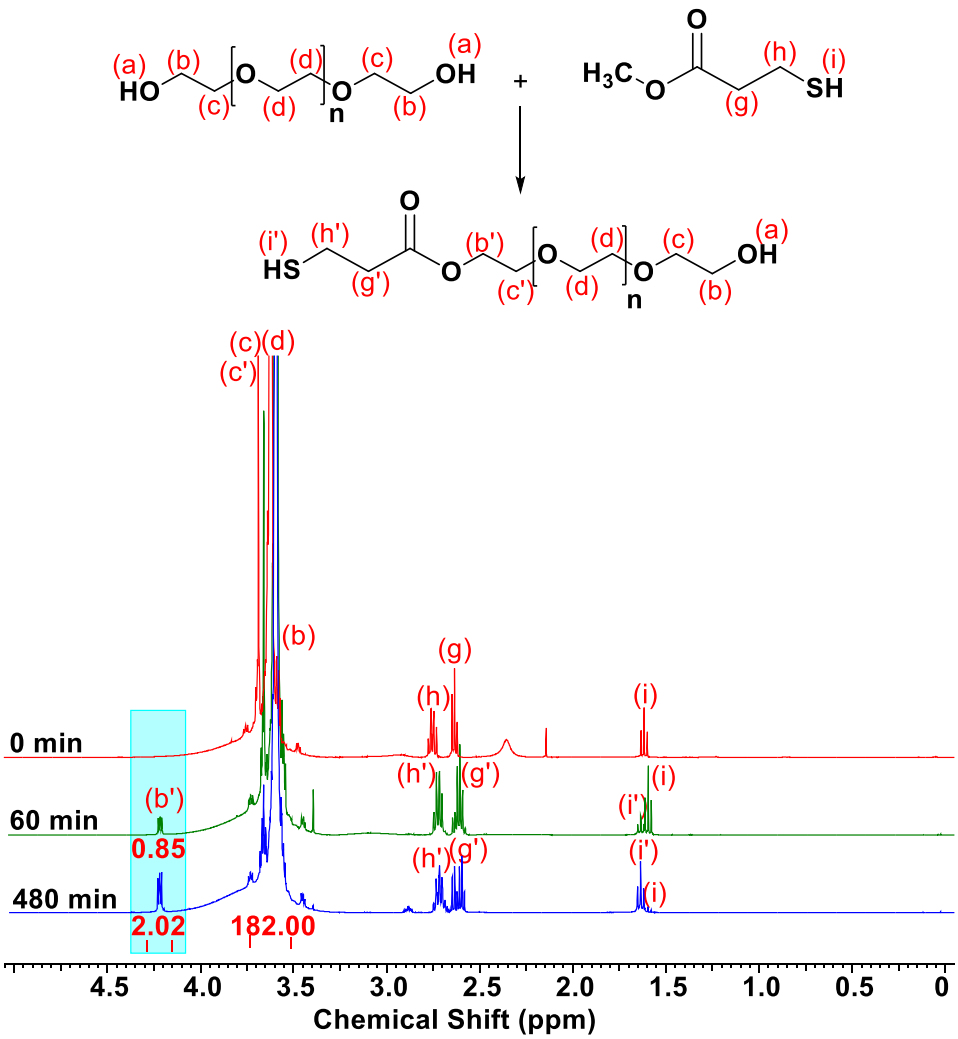

Figure 4.54 ^{1}H-NMR spectroscopy monitoring of the kinetics of transesterification of MP-SH with PEG_{2050}

PEG_{2050}-monothiol (HO- PEG_{2050}-SH) was obtained by precise timing of the transesterification reaction of MP-SH with PEG_{2050} based on the data from the kinetic study presented above. Figure 4.55 shows the ^{1}H-NMR spectrum of PEG_{2050}-monothiol synthesized with a reaction time of 16 h after filtering the enzyme and removing the excess thioester but without further purification. The integral ratio of (h') to the -CH_2- protons in the new ester bond (b') at δ = 4.23 ppm is 2:39:2.28, indicating the formation of PEG_{2050}-monothiol.

PEG_{2050}-dithiol was obtained by reacting PEG_{2050}-monothiol with fresh MP-SH and CALB for 24 hours under solventless conditions. HS-PEG_{2050}-SH was used to obtain FL-PEG_{2050}-FL and subsequently FA-FL-PEG_{2050}-FL-FA discussed in section

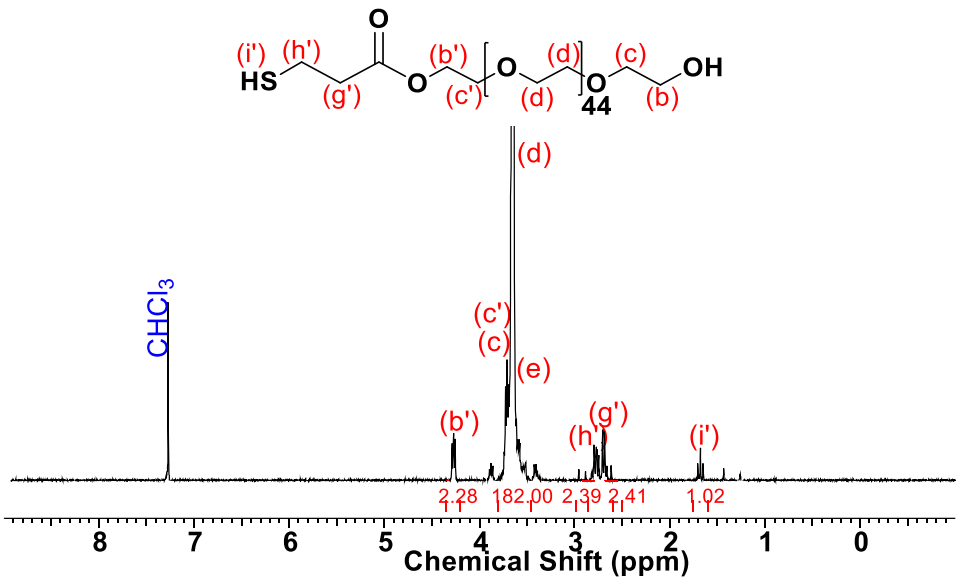

Figure 4.55 ^{1}H-NMR spectrum of PEG_{2050}-monothiol. Reprinted with permission from *Catalysts* **2019**, *9(3)*, 228. Copyright © 2019 MDPI

4.3.3. Figure 4.56 shows the ^{1}H-NMR spectrum of PEG_{2050}-monothiol synthesized with a reaction time of 24 h after filtering the enzyme and removing the excess thioester but without further purification. The integral ratio of the PEG backbone protons (c', d) to the -CH_2- protons in the new ester bond (b') at δ = 4.23 ppm is 180:2.28, indicating the formation of PEG_{2050}-dithiol with 94% reaction yield.

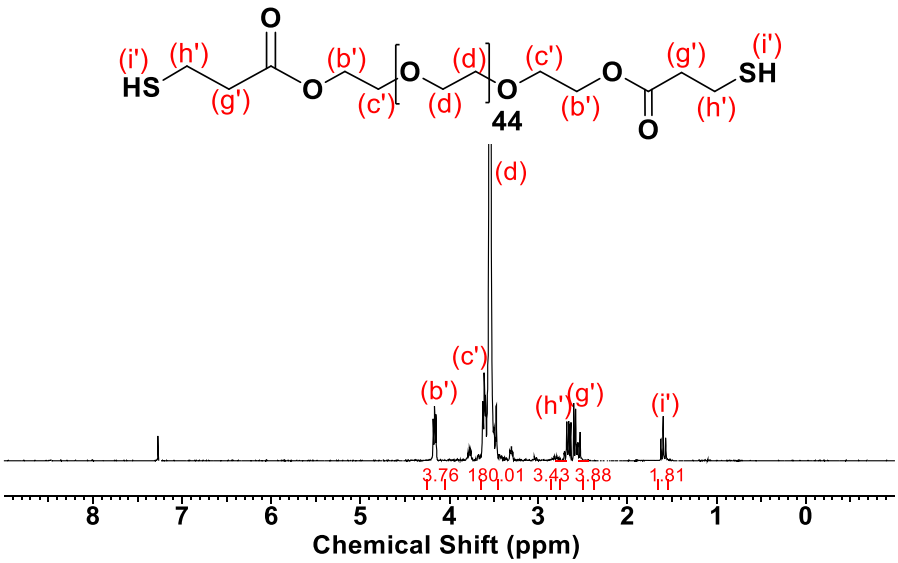

Figure 4.56 ^{1}H-NMR spectrum of PEG_{2050}-dithiol. Reprinted with permission from *Catalysts* **2019**, *9(3)*, 228. Copyright © 2019 MDPI

Similar to PEG_{1000} and PEG_{2050}, MP-SH was also transesterified with $dPEG_{20}$ for 24 hours to obtain HS-$dPEG_{20}$-SH. $dPEG_{20}$ is a monodispersed PEG (Đ = 1) with

twenty ethylene glycol monomer units. $dPEG_{20}$-dithiol (HS-$dPEG_{20}$-SH) was obtained by reacting $dPEG_{20}$ with fresh MP-SH and CALB for 24 hours under solventless conditions. HS-$dPEG_{20}$-SH was used to obtain FL-$dPEG_{20}$-FL and subsequently FA-FL-$dPEG_{20}$-FL-FA discussed in section 4.3.4. This conjugate was prepared to study the effect of dispersity of the polymer on the multivalent binding to the folate receptor. Figure 4.57 shows the ^{1}H-NMR spectrum of HS-$dPEG_{20}$-SH. A new signal corresponding to the -CH_2- proton (b') appears at δ = 4.25 ppm indicates the formation of product. The signal corresponding to the mercapto proton (i') is a triplet and appears at δ = 1.65 ppm. The relative integrals of (b'): (i') are in the ratio 4.00: 1.78 demonstrating the completion of reaction with ~100% conversion.

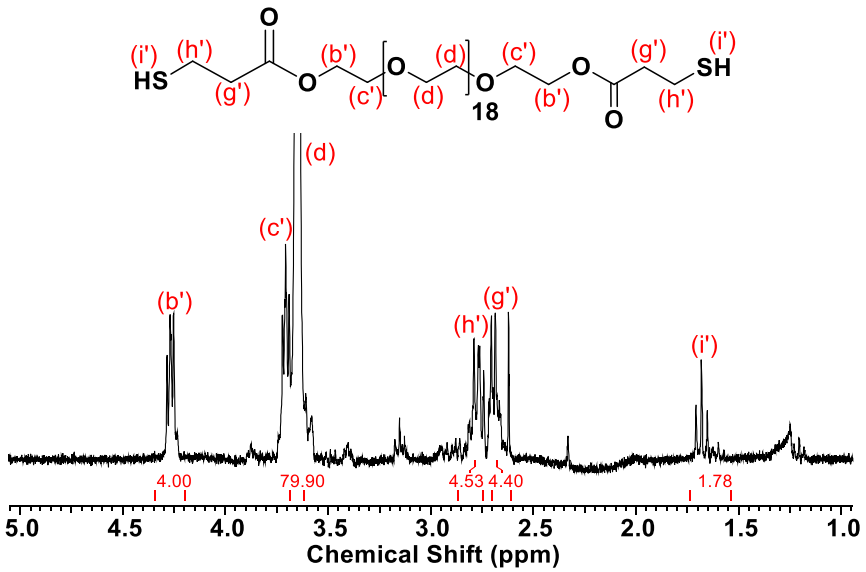

Figure 4.57 ^{1}H-NMR spectrum of HS-$dPEG_{20}$-SH

Figure 4.58 shows the ^{13}C-NMR spectrum of HS-$dPEG_{20}$-SH. It indicates the formation of product by appearance for a signal corresponding to the -CH_2- proton (B') at δ = 21 ppm. The absence of starting material, i.e. MP-SH is confirmed by the absence of signals corresponding to its methyl carbon in the range δ = 46 - 57 ppm. Therefore, NMR analysis confirmed that the conversion of $dPEG_{20}$ was quantitative in 24 hours.

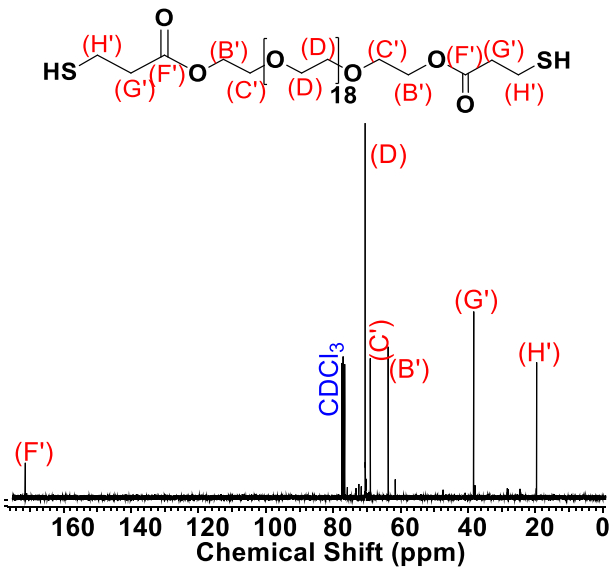

Figure 4.58 ^{13}C-NMR spectrum of HS-dPEG$_{20}$-SH

4.3. Michael Addition of FA-SH to Acrylate-functionalized TEG and PEGs

This section discusses the final step in Strategy 2, i.e. the Michael addition of FA-SH to two-functional fluorescein-labeled TEG and PEGs, to obtain the two-functional folate-targeted fluorescein-labeled molecules. Michael addition of HS-TEG-SH and HS-PEG-SH molecules to FLA and their subsequent acrylation was carried out by Gayatri Shrikhande. HS-TEG-SH and HS-PEG-SH molecules were provided by me, which were synthesized by strategies discussed in Section 4.2.1 and 4.2.2.

4.3.1. Michael Addition of FA-SH to Ac-FL-TEG-FL-Ac

FA-SH was added onto the acrylate groups of the two-functional fluorescein-labeled TEG (Ac-FL-TEG-FL-Ac) via CALB-catalyzed Michael addition to obtain two-functional folate-targeted fluorescein-labeled TEG (FA-FL-TEG-FL-FA). The synthetic strategy is presented in Figure 4.59.

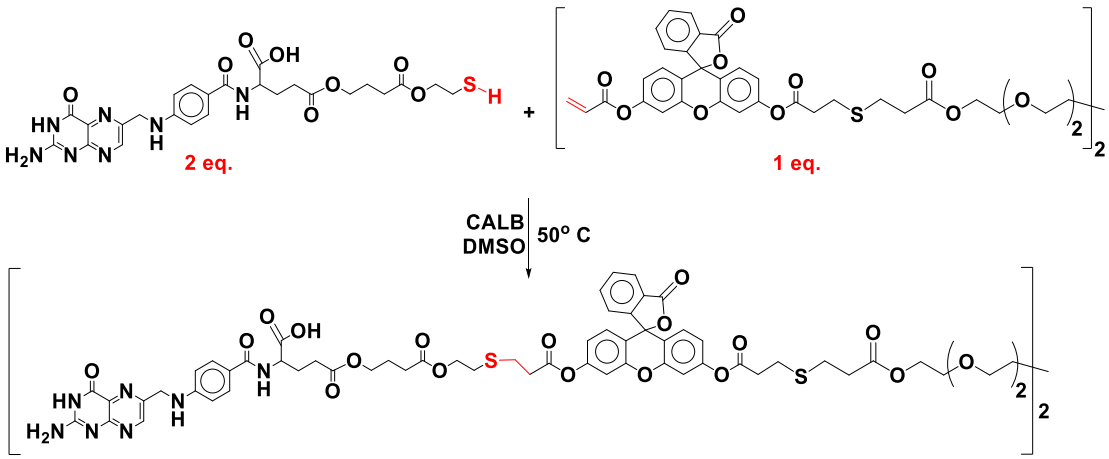

Figure 4.59 Reaction scheme for synthesis of FA-S-FL-S-TEG-S-FL-S-FA [FA-SH] = 2.43 x 10^{-1} mol/L; [Ac-FL-S-TEG-S-FL-Ac] = 7.98 x 10^{-2} mol/L; [CALB] = 2.60 x 10^{-4} mol/L; V = 2 mL; 8h.

Figure 4.60 shows the ^{1}H-NMR spectrum of FA-FL-TEG-FL-FA. It can be observed from the spectrum that the acrylate signals from the starting compound Ac-FL-TEG-FL-Ac appearing between δ = 6 ppm to δ = 6.5 ppm have disappeared. New signal corresponding to the -CH_2- protons (f") and (18") formed after conjugation with FA-SH appear at δ = 2.65 ppm and δ = 2.85 ppm indicate the formation of product. The relative integrals of (13): (f") + (18") + (19') are in the ratio 1: 7.41 demonstrating a ~100% conversion of the product.

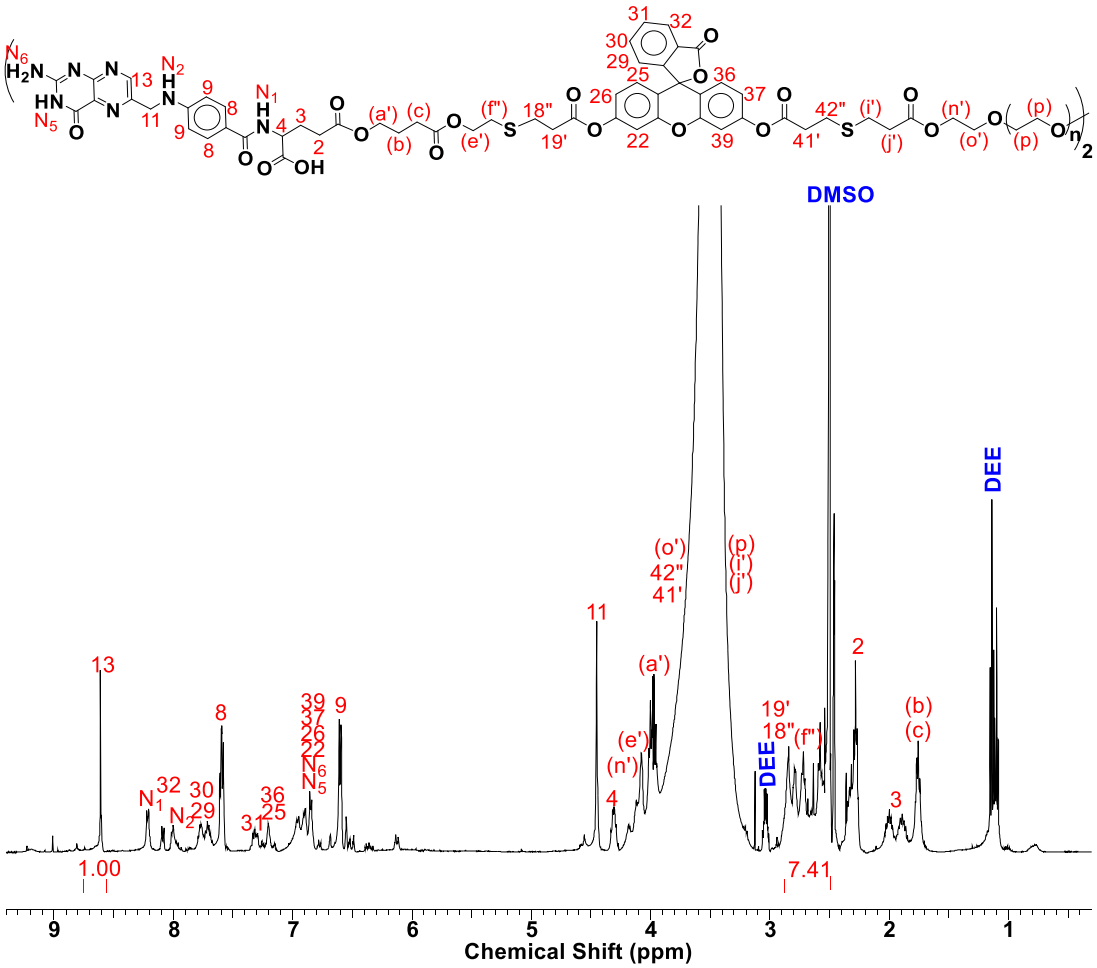

Figure 4.60 ^{1}H-NMR spectrum of FA-FL-TEG-FL-FA

4.3.2. Michael Addition of FA-SH to Ac-FL-PEG$_{1000}$-FL-Ac

FA-SH was added onto the acrylate groups of the two-functional fluorescein-labeled PEG$_{1000}$ (Ac-FL-PEG$_{1000}$-FL-Ac) via CALB catalyzed Michael addition to obtain two-functional folate-targeted fluorescein-labeled PEG$_{1000}$ (FA-FL-PEG$_{1000}$-FL-FA). The synthetic strategy is similar to the one presented in Figure 4.59 with 8h reaction time. Figure 4.61 shows the ^{1}H-NMR spectrum of FA-FL-PEG$_{1000}$-FL-FA. It can be observed from the spectrum that the acrylate signals from Ac-FL-PEG$_{1000}$-FL-Ac appearing between δ = 6 ppm to δ = 6.5 ppm have disappeared although not completely. New signal corresponding to the -CH$_2$- protons (f") and (18") formed after conjugation with FA-SH appear at δ = 2.65 ppm and δ = 2.85 ppm indicate the

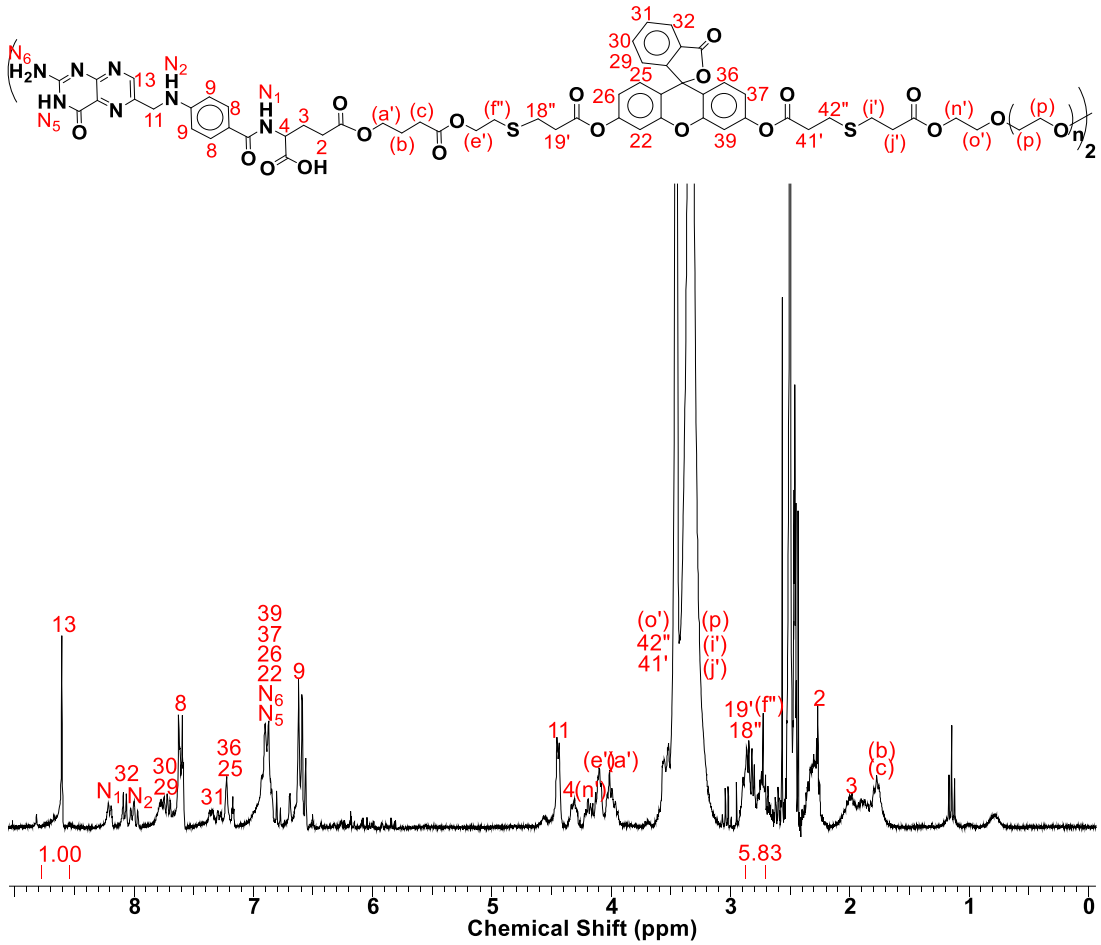

Figure 4.61 ^{1}H-NMR spectrum of FA-FL-PEG$_{1000}$-FL-FA

formation of product. The relative integrals of (13): (f") + (18") + (19') are in the ratio 1: 5.83 demonstrating a ~100% conversion of the product.

4.3.3. Michael Addition of FA-SH to Ac-FL-PEG$_{2050}$-FL-Ac

FA-SH was added onto the acrylate groups of the two-functional fluorescein-labeled PEG$_{2050}$ (Ac-FL-PEG$_{2050}$-FL-Ac) via CALB catalyzed Michael addition to obtain two-functional folate-targeted fluorescein-labeled PEG$_{1000}$ (FA-FL-PEG$_{2050}$-FL-FA). The synthetic strategy is similar to the one presented in Figure 4.59 with 8h reaction time. Figure 4.62 shows the ^{1}H-NMR spectrum of FA-FL-PEG$_{2050}$-FL-FA. It can be observed from the spectrum that the acrylate signals from Ac-FL-PEG$_{2050}$-FL-Ac appearing between δ = 6 ppm to δ = 6.5 ppm have disappeared although not

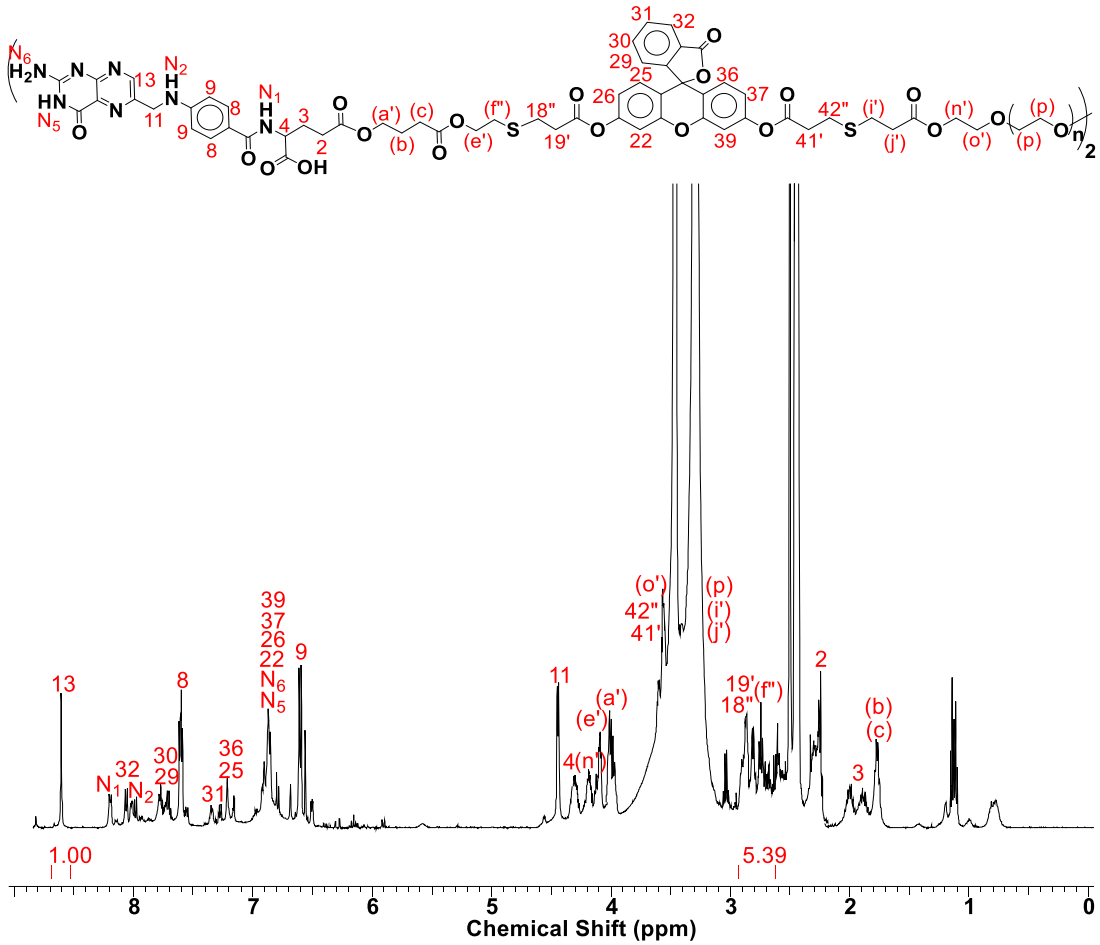

Figure 4.62 ^{1}H-NMR spectrum of FA-FL-PEG$_{2050}$-FL-FA

completely. New signal corresponding to the -CH_2- protons (f") and (18") formed after conjugation with FA-SH appear at δ = 2.65 ppm and δ = 2.85 ppm indicate the formation of product. The relative integrals of (13): (f") + (18") + (19') are in the ratio 1: 5.39 demonstrating a ~100% conversion of the product.

4.3.4. Michael Addition of FA-SH to Ac-FL-dPEG$_{20}$-FL-Ac

FA-SH was added onto the acrylate groups of the two-functional fluorescein-labeled dPEG$_{20}$ (Ac-FL-dPEG$_{20}$-FL-Ac) via CALB-catalyzed Michael addition to obtain two-functional folate-targeted fluorescein-labeled dPEG$_{20}$ (FA-FL-dPEG$_{20}$-FL-FA). The synthetic strategy is similar to the one presented in Figure 4.59 with 8h reaction time. Figure 4.63 shows the ^{1}H-NMR spectrum of FA-FL-dPEG$_{20}$-FL-FA. It

can be observed from the spectrum that the acrylate signals from Ac-FL-dPEG$_{20}$-FL-Ac appearing between δ = 6 ppm to δ = 6.5 ppm have disappeared. New signal corresponding to the -CH$_2$- protons (f") and (18") formed after conjugation with FA-SH appear at δ = 2.65 ppm and δ = 2.85 ppm indicate the formation of product. The relative integrals of (13): (f") + (18") + (19') are in the ratio 1: 7.09 demonstrating a ~100% conversion of the product.

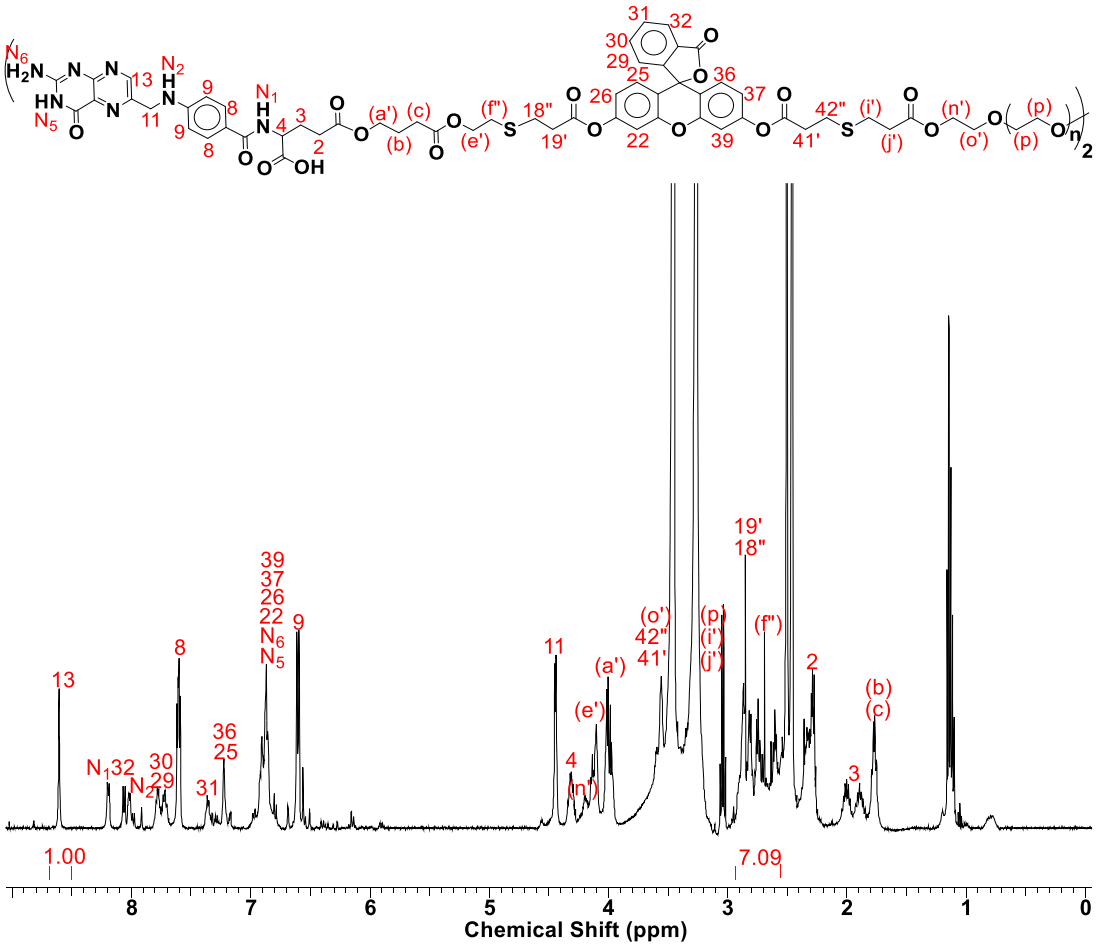

Figure 4.63 ^{1}H-NMR spectrum of FA-FL-dPEG$_{20}$-FL-FA

These compounds were given to the Cleveland Clinic to qualitatively evaluate their cellular uptake on Triple Negative Breast Cancer (TNBC) cell lines MDA_MB_231 (epithelial cells_HTB-132_adenocarcinoma_patient ethnicity Caucasian) and MDA_MB_468 (epithelial cells_HTB-26_adenocarcinoma_patient

ethnicity African American) using immunocytochemistry. The quantitative evaluation will be performed using flow cytometry by Cleveland Clinic.

4.4. Strategy 3: PEGylation of Fl via Lithium Technology

Strategy 3 is presented in Figure 2.15. In Strategy 3, first fluorescin (reduced form of fluorescein with free carboxylic acid group, FL-COOH) is lithiated using *n*-butyllithium (*n*-BuLi) to obtain a lithiated fluorescin (FL-COOLi). Poly(ethylene glycol)(PEG)-dibromide (Br-PEG-Br) is then reacted with 2 equivalents of FL-COOLi to obtain a fluorescin-labeled PEG (FL-COO-PEG-OOC-FL). The FL-COO-PEG-OOC-FL is then reacted with 2 equivalents of acryloyl chloride in the presence of triethyl amine (TEA) to obtain an acrylated fluorescin-labeled PEG (Ac-FL-COO-PEG-OOC-FL-Ac). The Ac-FL-COO-PEG-OOC-FL-Ac is then reacted with a thiol functionalized Folic Acid (FA-SH) via CALB)-catalyzed Michael addition to obtain FA-FL-COO-PEG-OOC-FL-FA.

Strategy 3 uses Br-PEG-Br and FL-COOLi. I synthesized PEG-dibromide (Br-PEG-Br) and FL-COO-PEG-OOC-FL. The syntheses will be discussed in the next two sections.

4.4.1. Synthesis of Br-PEG-Br

Based on the method previously reported by our group for synthesizing PEG monomethyl ether monobromide (MPEG-Br) via CALB-catalyzed transesterification of halo-esters with MPEG,[14] I synthesized PEG-dibromide (Br-PEG-Br) as shown in Figure 4.64. Ethyl 5-bromovalerate (EtBrVa) is reacted with PEG_{2000} (M_n = 2000 g/mol) via CALB-catalyzed transesterification reaction under solventless conditions for 3h at 50 °C to obtain Br-PEG_{2000}-Br.

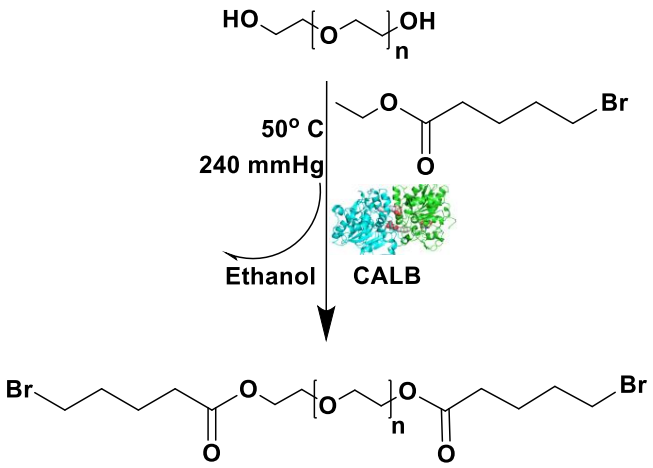

Figure 4.64 Synthetic strategy for Br-PEG-Br

Figure 4.65 shows the ^{1}H-NMR spectrum of PEG_{2000}. The signal for the -CH_2- protons (b) besides the –OH end-group appear at δ = 3.60 ppm. The signal for the -CH_2- protons from the PEG backbone (c) and (d) appear at δ = 3.64 ppm. It was difficult to exclusively integrate the signal (b) due to its proximity to the PEG backbone -CH_2- protons. The integral of signal (b) was set to 4 corresponding to the 4 -CH_2- protons. No signals appear beyond δ = 5 ppm.

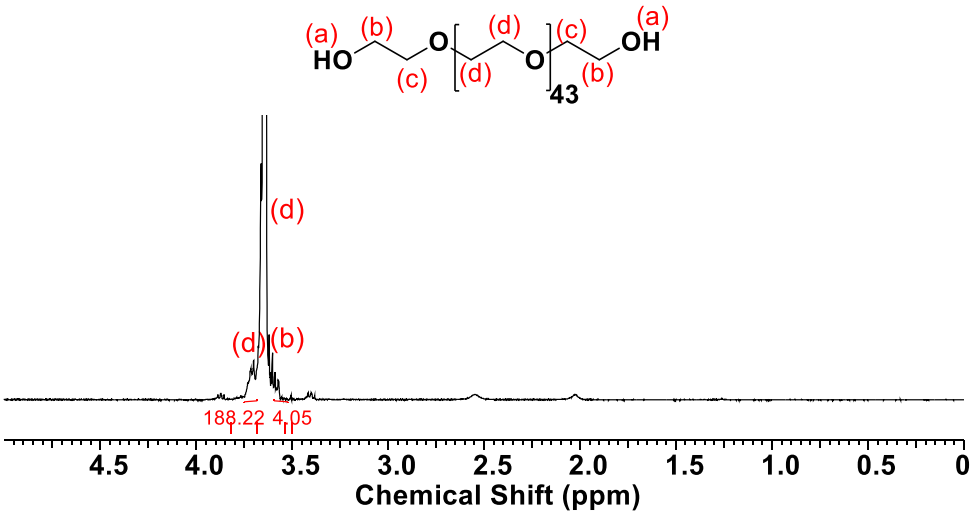

Figure 4.65 ^{1}H-NMR spectrum of PEG_{2000}

Figure 4.66 shows the ^{1}H-NMR spectrum of EBV. The signal for the -CH_2- protons (j) from the ester group appear at δ = 3.60 ppm. The signal for the methyl protons (k) from the ester group appear at δ = 4.14 ppm. The signal for the -CH_2- protons (h) besides the C=O of the ester group appear at δ = 2.33 ppm and is set to an

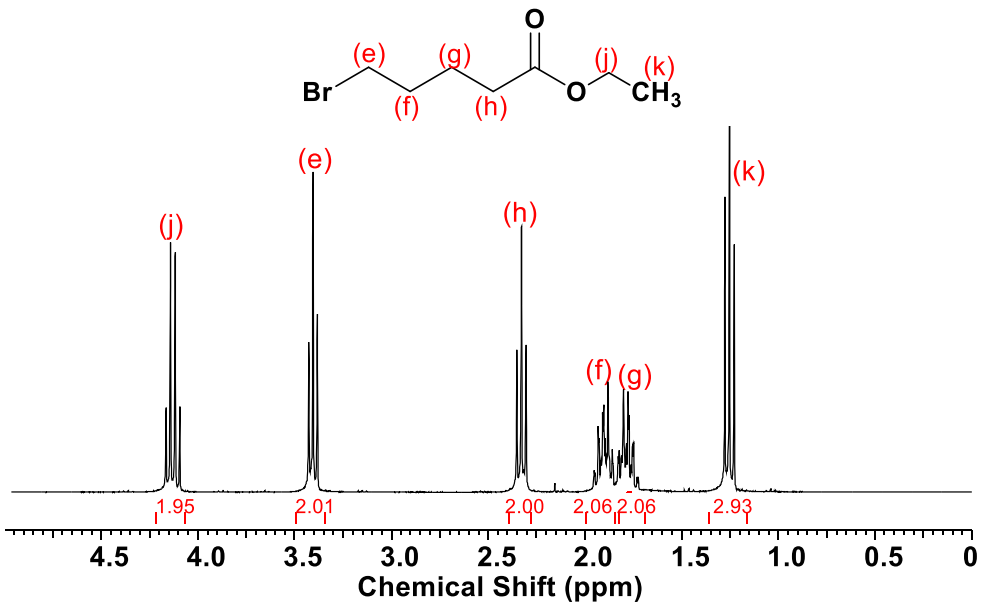

Figure 4.66 ^{1}H-NMR spectrum of EBV

integral value of 2 corresponding to the 2 -CH_2- protons (h). No signals appear beyond δ = 5 ppm.

Figure 4.67 shows the ^{1}H-NMR spectrum of Br-PEG_{2000}-Br. The signals of the -CH_2- protons from EBV (e), (f), (g), and (h) did not shift. A new signal appeared at δ = 4.24 ppm (b'), which belongs to the -CH_2- proton besides the newly formed ester group. The relative integrals of (b'): (h) protons are in the ratio 3.71: 4.01 demonstrating ~95% conversion of reaction. The signal (e) overlaps with the satellite signal of PEG backbone -CH_2- protons, therefore, its integral value is higher than the expected value of 4. The signal (f) and (g) overlap with the signal for water (impurity from the deuterated solvent), therefore, their combined integral value is higher than the expected value of 8. Figure 4.67 does not show the presence of residual EBV, the signals corresponding to EBV appearing at δ = 4.14 ppm (j) and δ = 1.26 ppm (k) have disappeared, suggesting its removal from the system in the precipitation process. No signals appear beyond δ = 5 ppm.

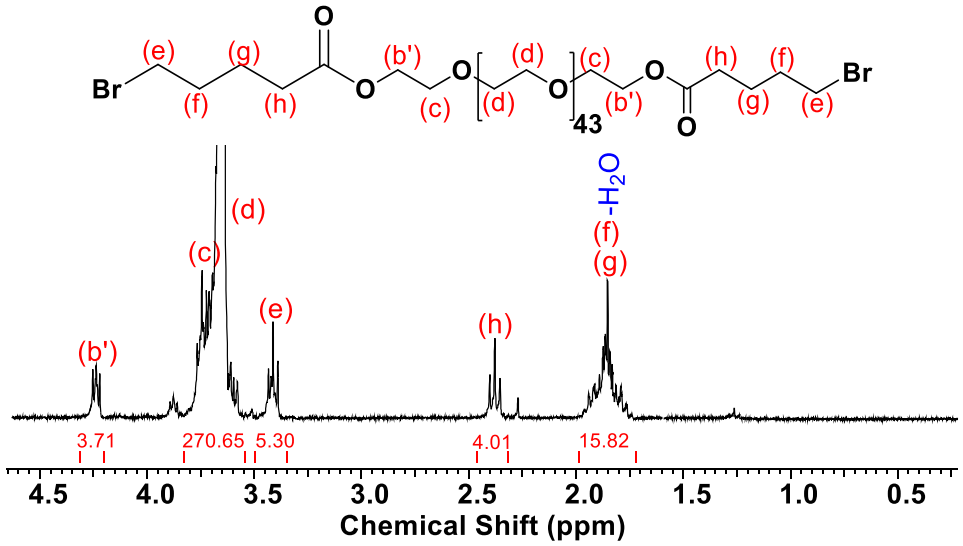

Figure 4.67 ^{1}H-NMR spectrum of Br-PEG$_{2000}$-Br

4.4.2. Synthesis of FL-COO-PEG-OOC-FL

Fluorescin labeled PEG was synthesized using a novel lithiation technology discussed in Section 4.1.2. The reaction scheme for the synthesis of FL-COO-PEG-OOC-FL is shown in Figure 4.68.

First, the carboxylic acid group on the fluorescin is lithiated using *n*-butyllithium (*n*-BuLi) under air-free N_2 conditions at room temperature to obtain a lithiated fluorescin (FL-COOLi). The progress of the reaction was monitored by observing the evolution of butane gas. An immediate color change in the reaction mixture was observed from orange to dark red on addition of *n*-BuLi (Figure 4.69). Lumps were formed in the reaction mixture suggesting the insolubility of FL-COOLi salt in DMSO solvent.

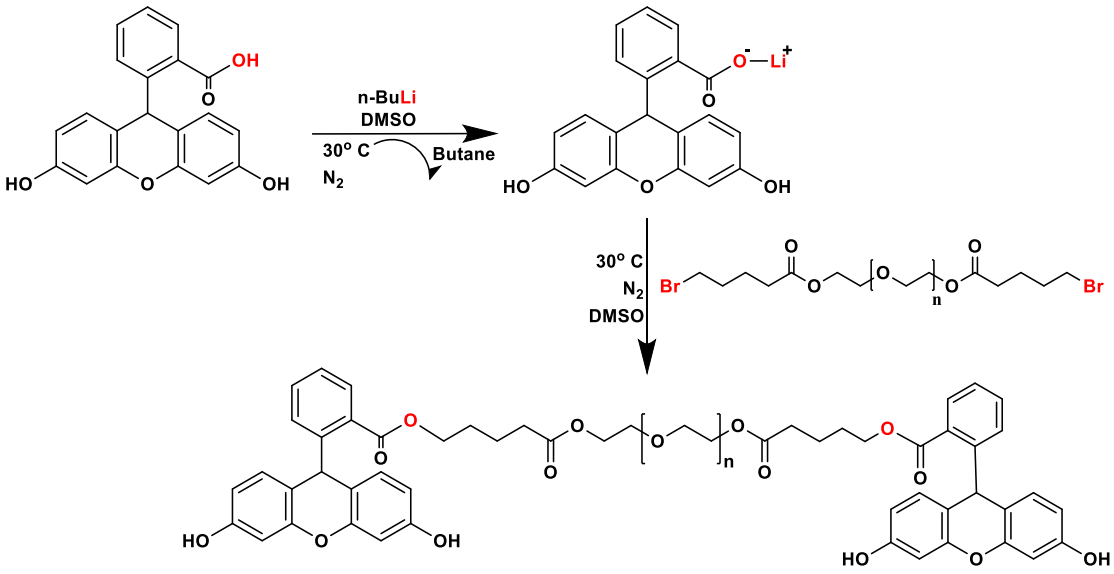

Figure 4.68 Synthetic strategy for FL-COO-PEG-OOC-FL

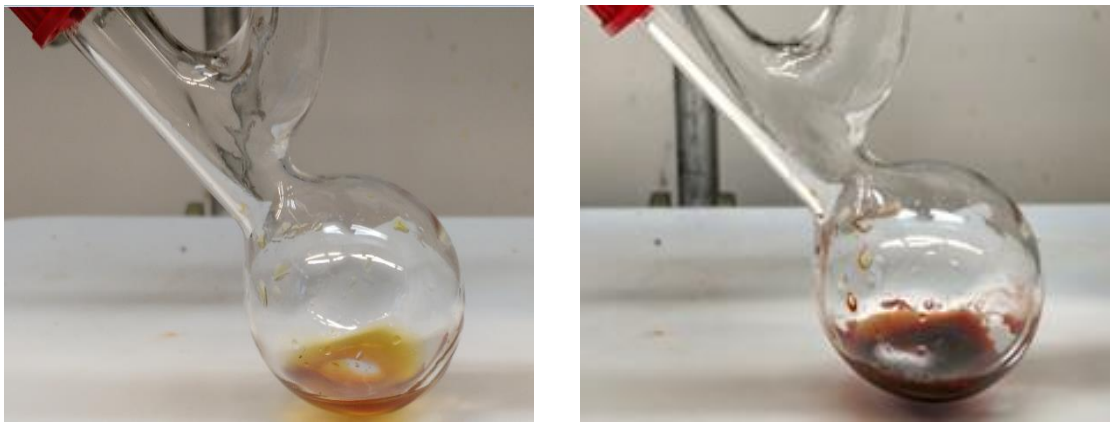

Figure 4.69 Left: Fluorescin dissolved in DMSO. Right: After addition of *n*-BuLi

Figure 4.70 shows the ^{1}H-NMR spectrum of fluorescin (FL-COOH). All the signals corresponding to the aromatic protons appear between δ= 6.00 ppm to δ =8.00 ppm. The integration value of the doublet signal at δ = 7.72 ppm is set to 1 corresponding to the aromatic proton (l). No signals appear between δ = 5 ppm and 10 ppm besides moisture.

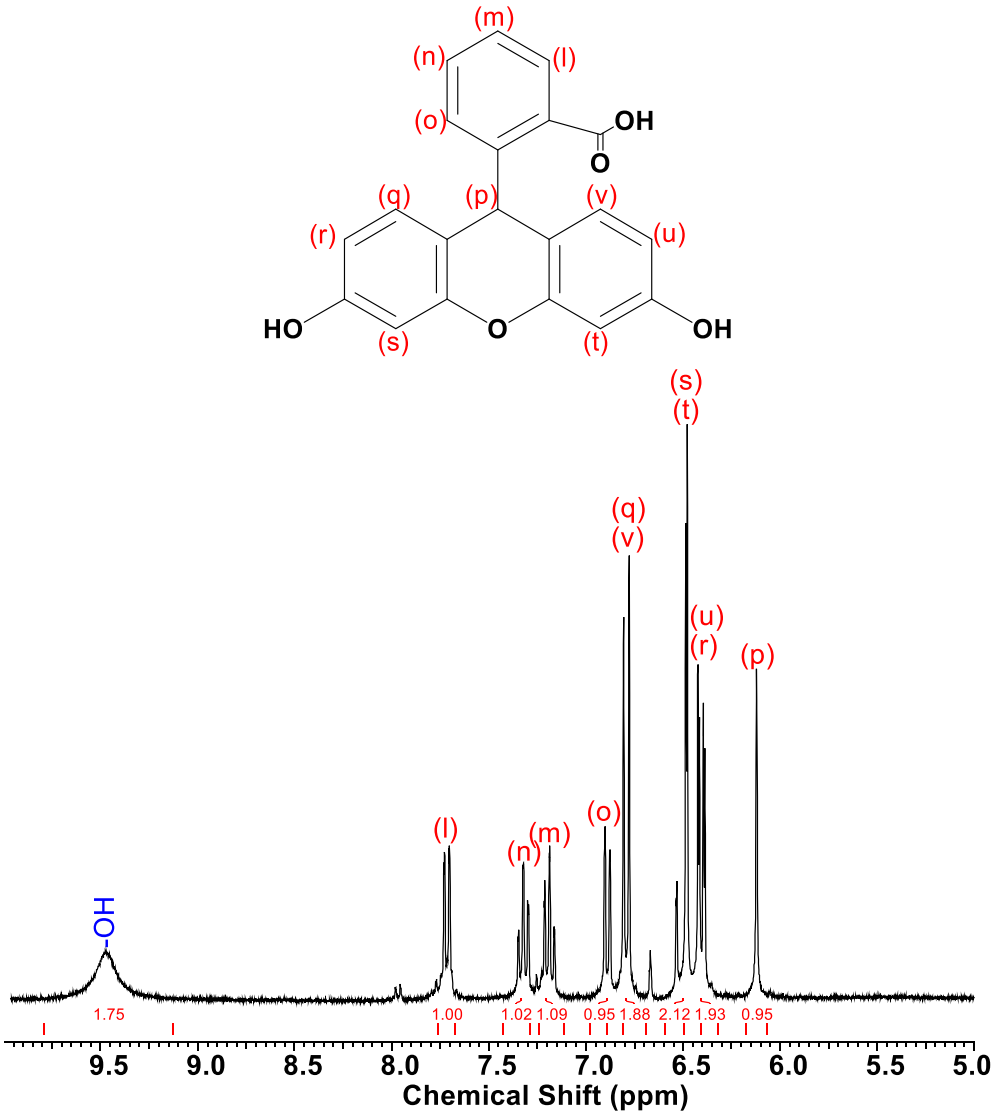

Figure 4.70 ^{1}H-NMR spectrum of Fluorescin

Figure 4.71 shows the ^{1}H-NMR spectrum of fluorescin after lithiation (FL-COOLi). The aromatic protons (l), (m), (n), (o), (r), (s), (t), and (u) moved upfield by a shift of δ = 0.30 ppm. The aromatic protons (q) and (v) and the methine proton (p) moved downfield by a shift of δ = 0.20 ppm after lithiation. No signals appear between δ = 5 ppm and 10 ppm besides moisture.

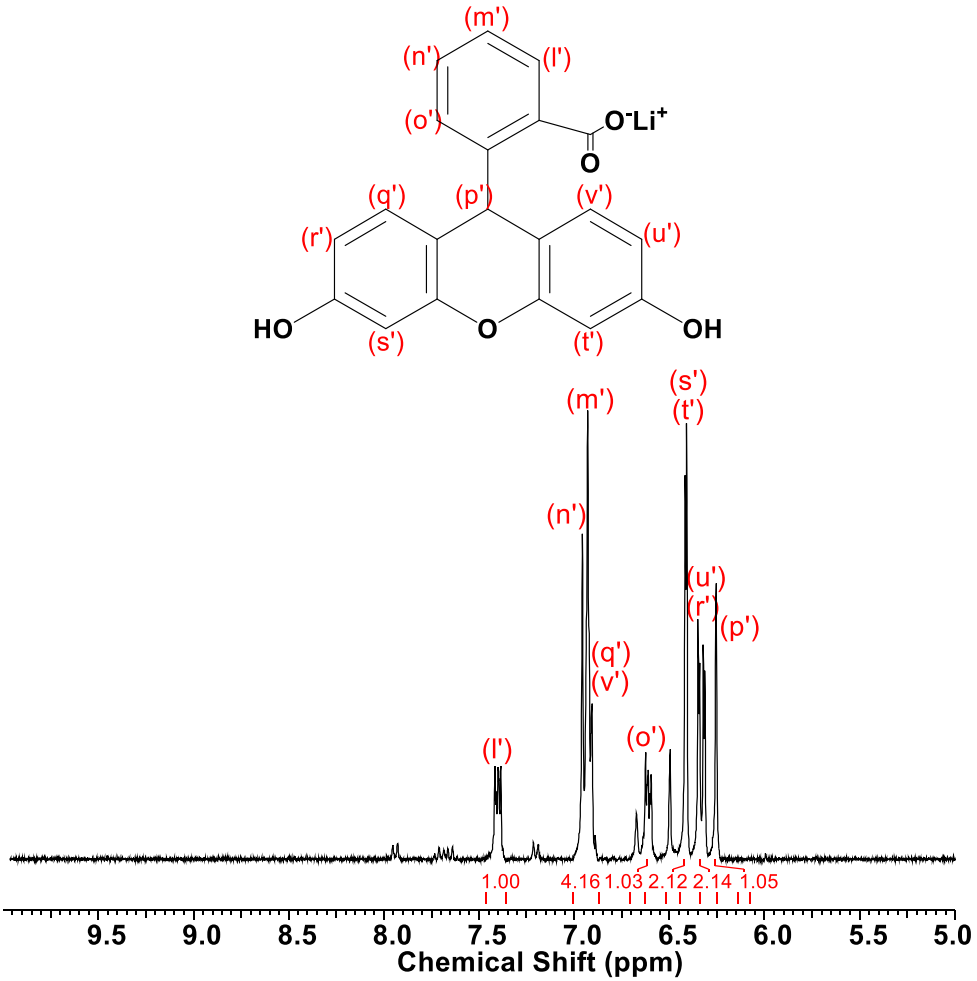

Figure 4.71 ^{1}H-NMR spectrum of lithiated Fluorescin

Br-PEG$_{2000}$-Br is then reacted with 2 equivalents of FL-COOLi to obtain a fluorescin-labeled PEG (FL-COO-PEG-OOC-FL). The reaction was monitored for 1, 5, 10, 15, and 30 minutes. Figure 4.72 shows the progress of the reaction monitored by ^{1}H-NMR spectroscopy. Aromatic protons of the fluorescin that had moved upfield during lithiation, moved downfield after conjugation with Br-PEG$_{2000}$-Br with a shift of δ = 0.25 ppm. The methine proton (p) from the fluorescin that had moved downfield during lithiation, moved upfield to δ = 5.91 ppm after conjugation. The signal (e) from the Br-PEG$_{2000}$-Br should reduce as the reaction progresses, however, the signal overlaps with the PEG backbone -CH_2- protons, therefore, it is difficult to evaluate the reduction in its integral value. The signal (b') from the Br-PEG$_{2000}$-Br shifts upfield after conjugation appearing at δ = 4.08 ppm and its integral value was

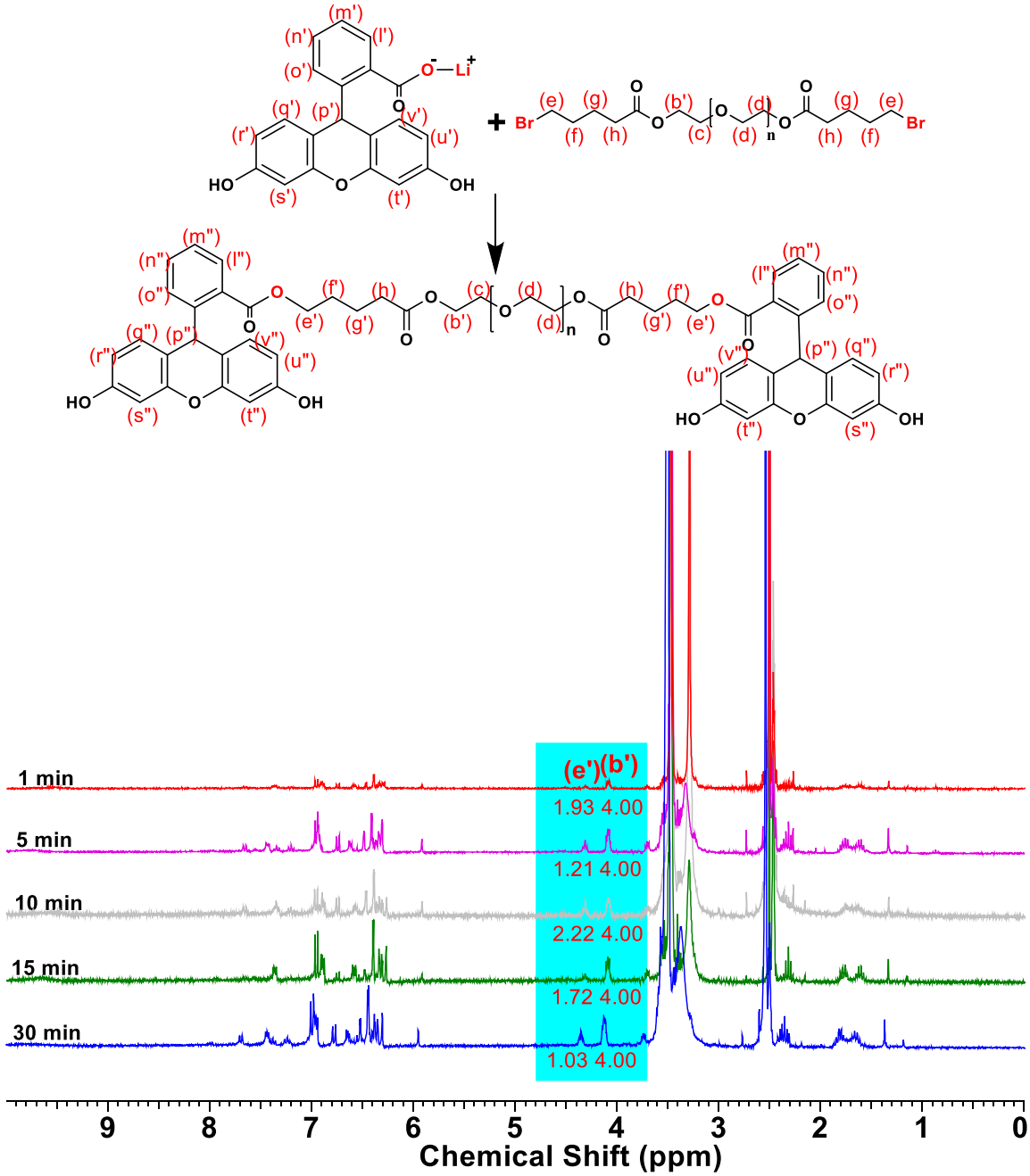

Figure 4.72 ^{1}H-NMR spectroscopy monitoring of the kinetics of the reaction of Br-PEG$_{2000}$-Br with FL-COOLi

set to 4 corresponding to the 4 -CH_2- protons. A new signal appeared at δ = 4.31 ppm (e'), which belongs to the -CH_2- proton besides the newly formed ester group. The integral value of the signal (e') was evaluated for determining the progress of the reaction. The ratio of (e') to (b') increased from 1.93:4.00 to 2.22:4.00 for 1 minute reaction time to 10 minutes reaction time. After 10 minutes reaction time, the ratio of (e') to (b') started to decreased and reached a value of 1.03:4.00 at 30 minutes

reaction time. Therefore, it can be concluded that the maximum conversion obtained from this reaction is at 10 minutes. At 10 minutes reaction time, the ratio of (e') to (b') is 2.22:4.00 suggesting that nearly half the Br-PEG_{2000}-Br has reacted with the FL-COOLi, that is, only one Br end-group has reacted with the FL-COOLi to yield a mono-substituted product, i.e. FL-COO-PEG_{2000}-Br.

The sample obtained at 10 minutes reaction time was analyzed using MALDI mass spectrometry. Figure 4.73 shows the MALDI mass spectrum of the sample obtained at 10 minutes reaction time. The spectrum shows multiple distributions, each separated by 44 *m/z* units. However, no distribution corresponding to the di-fluorescin-labeled PEG (FL-COO-PEG_{2000}-OOC-FL) was observed. One distribution was identified and it belongs to the mono-substituted PEG, i.e. FL-COO-PEG_{2000}-OH. The signal at *m/z* 1337.771 (inset) belongs to the Na complex of the 20-mer fraction of FL-COO-PEG_{2000}-OH [1337.771 ≅ 20 x 44.02 (C_2H_4O repeat unit) + 433.44 (FLC_4H_8COO- end group) + 1.01 (H - end group) + 22.99 (Na^+)]. Since we could not obtain a di-fluorescin-labeled PEG (FL-COO-PEG_{2000}-OOC-FL), we did not go ahead with this strategy.

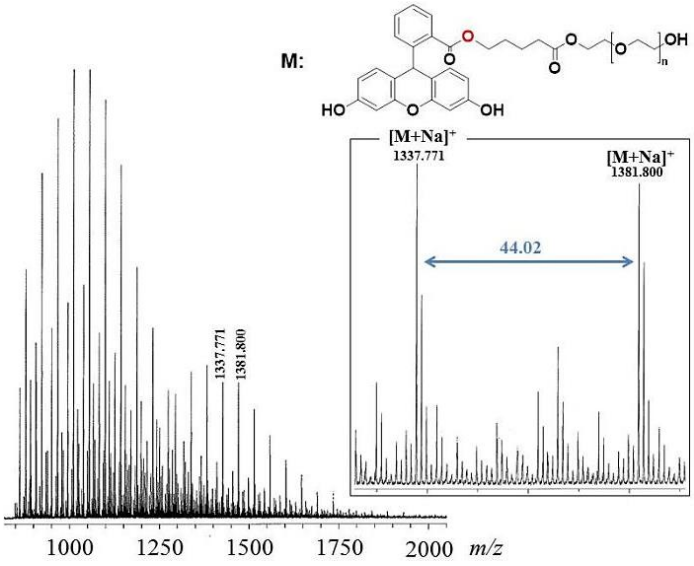

Figure 4.73 MALDI mass spectrum of reaction sample of FLCOOLi and Br-PEG_{2000}-Br at 10 minutes reaction time. Inset: spectrum of 20- and 21- mer fractions, 44 *m/z* = PEG repeat unit

Discussion

TNBC is associated with high mortality and the treatment is an obvious challenge exacerbated by the lack of exclusive targeted therapies. Chemotherapy has low targeting efficiency and administering high doses of non-targeted drugs or imaging molecules affects the surrounding healthy cells increasing the systemic toxicity.[16] Therefore, development of effective targeted diagnostics and therapies that target TNBC cells and minimize damage to the healthy cells is an immediate requirement.

FRs, that metabolize FA nutrient in cells, are over-expressed in nearly 86% of the TNBC cases, which qualifies them to be potential biomarkers for targeted diagnostics of TNBC.[18] This over-expression of FRs causes the TNBC cells to compete for FA with the healthy cells making FA an attractive targeting precursor.[19]

Leamon and Low were the pioneers in demonstrating the targeting ability of FA by binding 1-10 FA molecules per protein molecule. Folate-conjugated proteins bound and internalized readily to the cancer cell via folate-mediated endocytosis whereas non-conjugated proteins did not show any binding or internalization. They also reported a key finding that the internalized proteins retained their activity in the tumor cells establishing folate-targeting as an attractive method to administer imaging molecules or drugs to tumor cells via folate-mediated endocytosis.[20] Although the efficacy of binding multiple FA molecules to one macromolecule was demonstrated nearly 30 years ago by Low, only small molecule diagnostic and therapeutic conjugates with a single FA targeting group made it to the human clinical trials.[2]

While these monovalent folate-targeted small molecule conjugates could not deliver the promised efficiency in clinical trials,[28] multivalent polymer-based folate-targeting has become an attractive strategy to develop novel diagnostics and

therapeutics for cancer applications with reduced systemic toxicity and increased efficacy.[38, 39] Baker *et al.* synthesized multivalent folate-targeted generation 5 PAMAM dendrimer that had an average of five folic acid molecules that demonstrated nearly 71,400 fold better binding than free FA molecules.[4] Attaching only two FA molecules to the dendrimer is desirable, since the binding did not increase significantly after attaching more than an average of 2.6 FA per dendrimer.[4]

These folate-targeted dendrimer showed great promise for selectively targeting tumor cells both *in vitro* and *in vivo.*[38, 39] However, FA was conjugated to the dendrimer randomly; therefore, every dendrimer molecule did not have a precise number of FAs leading to a broad distribution of FA molecules present per dendrimer. To overcome this challenge, a two-functional folate-targeted polymeric conjugate (FA-FL-PEG-FL-FA) was synthesized using chemo-enzymatic methods in our group to evaluate its targeting efficacy *in vitro* in MDA_MB_231 and MDA_MB_468 TNBC cell lines. It demonstrated higher specificity towards the FRs (90% cellular uptake) and higher water solubility at three times lower concentration than non-polymer conjugated agents (unpublished data). It was also able to selectively target the FR over-expressing liver cancer tissue in a rat model efficiently without causing toxicity to the surrounding healthy cells.[41]

This two-functional folate-targeted polymeric conjugate showed great promise for selectively targeting tumor cells both *in vitro* and *in vivo*, however, the synthetic strategy (Figure 2.7) used to synthesize the FA-FL-PEG-FL-FA raised the concern about formation of possible side products by chain-chain coupling in the reaction of FLDA with H_2N-PEG-NH_2. In addition, mass spectrometry analysis confirmed that the commercially available H_2N-PEG-NH_2 contained a significant amount of impurity.

Therefore, to overcome this problem, based on this strategy, we developed three strategies to more effectively synthesize two-functional folate-receptor targeted fluorescein-labeled PEG-based conjugates and evaluated them for their synthetic convenience and feasibility. These three strategies had PEG-diamines, PEG-dithiols, and PEG-dibromides as their precursors.

In the first strategy (Chapter IV, Section 4.1), fluorescein-*o*-acrylate (FLA) that has only one acrylate functionality, was used in order to avoid formation of possible side products by chain-chain coupling in the reaction of FLDA with H_2N-PEG-NH_2. In addition, PEG-diamines were synthesized, instead of using commercially available ones, through a novel CALB-catalyzed esterification of *t*BOC-protected amino acids (Alanines) with PEG (M_n = 2050 g/mol) under solventless conditions with subsequent de-protection (Chapter IV, Section 4.1.1). This three-step synthesis procedure was performed to avoid the use of the impure commercially available PEGs that lead to the formation of a mixture of products.

CALB-catalyzed functionalization of PEGs was reported by our group to yield quantitative results without requiring further purification.[12-15] Other methods reported in the literature employ multiple purification steps and use acid catalysts; therefore, these methods are not environmentally friendly as opposed to CALB-catalyzed reactions.[70-88] The esterification of *t*BOC protected L-Alanine and β-Alanine with PEG_{2050} gave quantitative yield of pure products as demonstrated by ^{1}H-NMR spectroscopy and MALDI mass spectrometry (Chapter IV, Section 4.1.1). However, this synthetic strategy had two drawbacks. First, de-protection of *t*BOC in L-Alanine conjugated PEG lead to the formation of PEG-diamines as the major product and PEG-monoamines as the minor product as confirmed through MALDI mass spectrometry. These PEG-diamines were used as precursors for CALB-catalyzed

Michael addition with FLA to obtain FL-PEG-FL. However, this Michael addition was not quantitative possibly due to the steric hindrance caused by the pendant -CH_3 group on L-Alanine that prevents the reaction from progressing. Second, the de-protected β-Alanine conjugated PEG contained a mixture products as confirmed by MALDI mass spectrometry. This mixture was formed possibly because of long de-protection reaction time during which the HCl generated by AcCl cleaves the ester bonds on the β-Alanine rather than the ones on *t*BOC. Therefore, a pure PEG-diamine was not obtained. Due to these drawbacks, Strategy 1 to synthesize FA-FL-PEG-FL-FA was abandoned.

To address the problems faced in the first strategy, PEG with stronger nucleophilic end-groups than primary amines were used as the precursors for FA-FL-PEG-FL-FA. The second strategy is similar to the first strategy; however, PEG-dithiols were used instead of PEG-diamines. PEG-dithiols were synthesized using a novel one-step CALB-catalyzed transesterification of MP-SH with PEGs (M_n = 1000 g/mol and M_n = 2050 g/mol) and dPEG (MW = 898 g/mol with Đ = 1) under solventless conditions and without further purification (Chapter IV, Section 4.2). This one-step process with a straight chain thioester is an improvement over the three-step process required for synthesizing PEG-diamines. Other methods reported in the literature employ multiple purification steps and use acid catalysts; therefore, these methods are not environmentally friendly as opposed to CALB-catalyzed reactions.[102-116] The kinetics of this reaction was performed and it was observed that the reactions proceeded in a step-wise manner, first producing monothiols. The synthesis of dithiols required additional fresh CALB and MP-SH. PEG-dithiols with varying chain lengths were quantitatively prepared in order to possibly examine the

effect of PEG chain length and dispersity on the *in vitro* performance of the corresponding FA-FL-PEG-FL-FAs.

A thiol-functionalized FA (FA-SH) was also synthesized as the targeting precursor for preparing the FA-FL-PEG-FL-FAs. FA has two sites available for conjugation, α-carboxyl and γ-carboxyl, however, FR binding is only observed when FA is conjugated via its γ-carboxyl group.[25] γ- conjugation of FA is a challenge that has often been met with low yield and poor binding efficacy.[93-98] To overcome this challenge, a new synthetic route was developed to synthesize γ-substituted FA with very high efficiency (Chapter IV, Section 4.1.2).[92] FA-SH was synthesized by exclusively lithiating FA at the γ-carboxyl position with 1 molar equivalent of *n*-BuLi and subsequently reacting it with 1 equivalent of Br-S-S-Br to form FA-S-S-FA. The carboxylic acid at γ-position of FA reacted with *n*-BuLi instead of the α-carboxyl because of the higher acidity of the γ-carboxyl position.[23] This exclusive reaction was confirmed by the shift observed in the γ-carboxyl carbon in the ^{13}C-NMR spectrum of the lithiated FA. The unreacted free FA was removed from FA-S-S-FA by exclusively salting it out with sodium ions at pH 10. The disulfide bond in the FA-S-S-FA was then cleaved with dithiothreitol (DTT) to quantitatively yield FA-SH.

Using the quantitatively synthesized precursor, HS-PEG-SH, PEG was fluorescein-labeled with FLA and subsequently acrylated with acryloyl chloride by fellow lab member Gayatri Shrikhande to obtain Ac-FL-PEG-FL-Ac. The novel CALB-catalyzed attachment of FA-SH to the Ac-FL-PEG-FL-Ac is discussed in this dissertation (Chapter IV, Section 4.3). ^{1}H-NMR spectroscopy of the final product, FA-FL-PEG-FL-FA, provided spectral evidences of presence of exactly two molecules of FA, two molecules of FL, and one molecule of PEG. Therefore, strategy 2 was successful in providing the quantitative synthesis of a two-functional folate-

targeted PEG-based conjugate. These conjugates would be tested for their *in vitro* performance at Dr McLennan's lab at the Cleveland Clinic.

After the successful demonstration of Strategy 2 in yielding the two-functional folate-targeted PEG-based conjugate, a third strategy was evaluated wherein the fluorescein-labelling of PEG was achieved through lithiation technology instead of the CALB-catalyzed Michael addition. FL-COOH was lithiated similarly to FA as discussed in Section 4.1.2 to obtain FL-COOLi, which was subsequently reacted with Br-PEG-Br to form FL-PEG-FL. Br-PEG-Br was quantitatively synthesized using CALB-catalyzed transesterification of EBV with PEG, this method was based on a previously reported method by our group for preparing M-PEG-Br.[14] The kinetics of the reaction of FL-COOLi with Br-PEG-Br was performed and a mono-substituted product (FL-PEG-OH) was achieved instead of FL-PEG-FL at 10 minutes of reaction time, after which formation of side-products was observed. MALDI mass spectrometry analysis of the product formed at 10 minutes confirmed that the reaction yielded a mono-substituted product (FL-PEG-OH) and did not proceed to di-substitution of Fluorescin on PEG. Therefore, this strategy was not investigated further. The goal of synthesizing a two-functional folate-targeted PEG-based conjugate was hence, achieved through implementing Strategy 2.

This dissertation reports the first two-functional folate-targeted polymeric diagnostic conjugates. The folate-targeted polymeric diagnostic conjugates reported in literature are either monovalent in nature,[31-34] or the FA is conjugated randomly to a multivalent carrier giving an unprecise broad distribution of FA.[40] This dissertation discussed the precise synthesis and characterization of a two-functional folate-targeted polymeric agent for potential application in TNBC diagnosis.

In summary, folate-targeted cancer diagnostics has been extensively researched. The chemo-enzymatic synthesis of two-functional folate-targeted polymeric conjugate reported in this dissertation ensured attachment of FA in all the conjugates. The specificity of these conjugates for the FRs has a potential to selectively target the TNBC cells, causing reduced toxicity and negligible side effects in cancer patients. If these conjugates yield desirable results in human TNBC cell lines and animal models, they can be then also tested in any cancer subtype that over-expresses FRs. In addition, it is possible to deliver these agents locally (intra-arterially) and in close vicinity of the tumor cells that will guarantee improved uptake and reduced toxicity.[41] Multivalent folate-targeted polymer-based diagnosis, therefore, have the potential to provide enhanced diagnosis efficacy and improved outcomes for cancer detection.

4.5 Synthesis of Multifunctional PEGs from Sucrose Ester of Soybean Oil

This section discusses the attachment of thiol-functionalized PEGs to Sefose via UV-mediated thiol-ene Click reaction. As model reactions, thiol-functionalized methoxy-triethylene glycol and hydroxyl-tetraethylene glycol were attached to the Sefose molecule before proceeding to attach larger molecules like PEG.

The exact molecular structure of Sefose is not reported in literature. However, an attempt was made to estimate the structure based on the information provided in the literature. Sefose is a sucrose ester of soybean oil with average degree of substitution 7.7 (Available sites for substitution = 8) and iodine value 117. The soybean oil composition is presented in Table 4.1.[118]

Table 4.1. Soybean Oil Composition

Component	Weight Percent	Molecular Weight (g/mol)	Carbon Atoms: Number of Double Bonds
Palmitic Acid	12	256.42	16:0
Stearic Acid	5	284.48	18:0
Oleic Acid	25	282.46	18:1
Linoleic Acid	52	280.45	18:2
Linolenic Acid	6	278.43	18:3

The calculation for estimating the number of double bonds present is demonstrated as follows:

Average Molecular Weight of Fatty Acid in Soybean Oil

= (0.12*256.42) + (0.05*284.48) + (0.25*282.46) + (0.52*280.45) + (0.06*278.43)

= 278.1492 g/mol

Therefore, average molecular weight of Sefose 1618 U

= molecular weight of sucrose + (7.7 * average molecular weight of soybean oil) – (7.7 * molecular weight of water)

= 342.30 + (7.7 * 278.1492) – (7.7 * 18.01528)

= 2345.33 g/mol

Average number of double bonds present in Sefose 1618 U[119]

$$= \frac{Iodine\ Value\ of\ Sefose * Average\ Molecular\ Weight\ of\ Sefose}{254g\ I_2 * 100g\ Sefose}$$

$$= \frac{117 * 2345.33}{254 * 100}$$

= 10.8

Therefore, the average number of allyl protons present in Sefose 1618 U = 10.8 * 2 = 21.6 ≅ 22

The molecular weights of the fatty acids are nearly the same. Linoleic acid contributes towards nearly 50% of the soybean oil composition; therefore, it can be

assumed that out of the 8 arms possessed by the Sefose, linoleic acid forms 3 arms (3 x 2 = 6 double bonds). With similar deductions, we can safely conclude that oleic acid forms 2 arms (2 x 1 = 2 double bonds) and the other acids form 1 arm each (3 double bonds from linolenic acid and 0 double bonds from palmitic acid and stearic acid each). With this deduction, number of double bonds is 6 + 2 + 3 + 0 + 0 = 11 that matches with the experimental number of double bonds estimated from the iodine value.

The ^{1}H-NMR spectrum of Sefose is presented in Figure 4.74. The signal for the protons (a), (b), (g), and (j) from sucrose moiety in Sefose appear distinctly from δ = 4.35 ppm to δ = 4.00 ppm. Their integral value is set to 7 corresponding to their 7 protons. The signal for the allylic protons from Sefose appear at δ = 5.35 ppm along with the signal for the 4 protons from sucrose moiety in Sefose ((c), (e), (f), (k)). The obtained integration value of the signal at δ = 5.35 ppm is 25, in which 4 protons are from sucrose moiety in the Sefose molecule. Therefore, there are 25 – 4 = 21 allylic protons present in the Sefose molecule. The signal for the methyl protons from the fatty acid end-groups appear distinctly at δ = 0.85 ppm with 21.71 integral value.

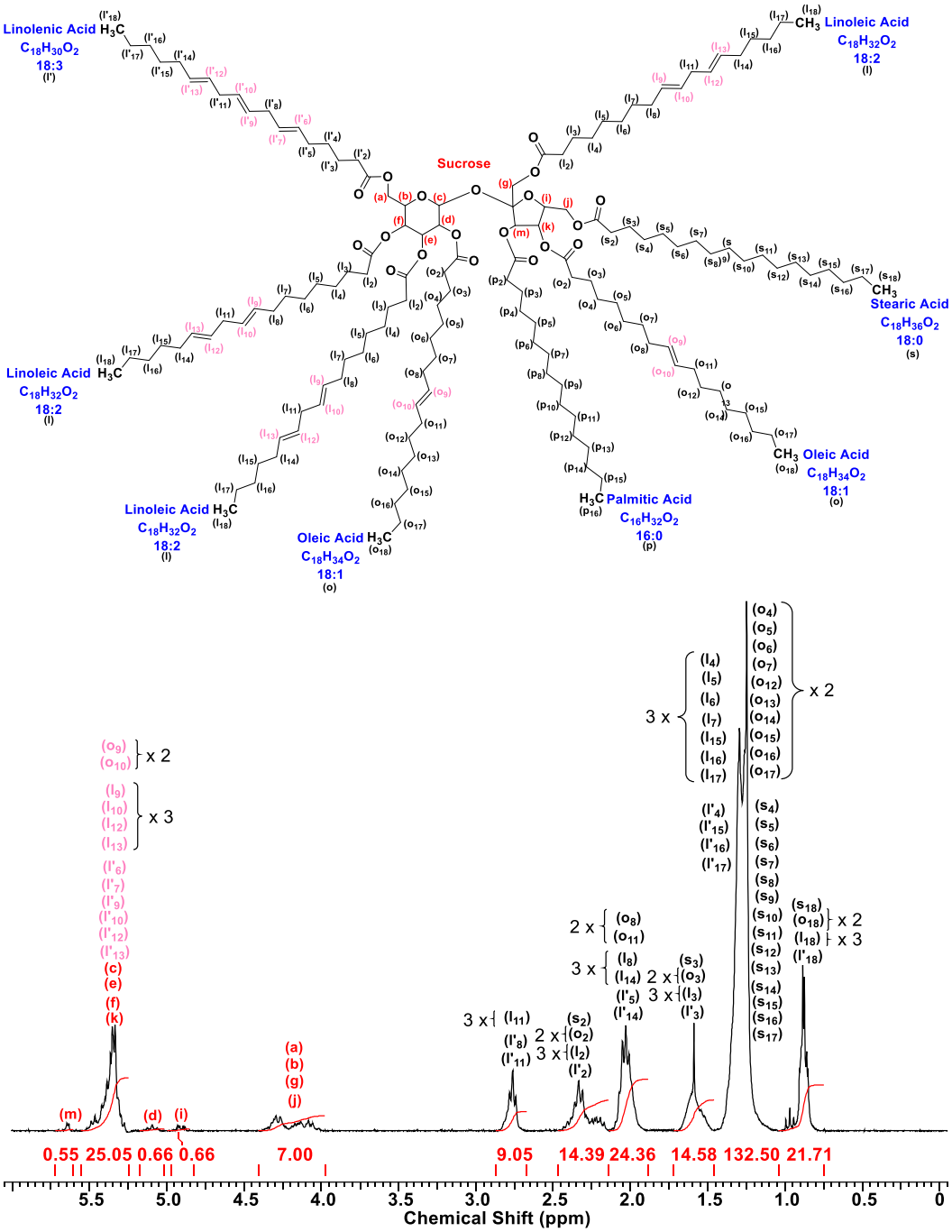

Figure 4.74 ^{1}H-NMR spectrum of Sefose 1618 U

4.5.1 Thiol-ene Click Reaction of M-TrEG-SH on Sefose

M-TrEG-SH was attempted to be clicked onto the double bonds present on Sefose 1618 U using Thiol-ene UV click strategy and the photoinitiator 2,2-dimethoxy-2-phenylacetophenone (DMPA) to produce Sefose-(S-TrEG-M)$_{22}$. Since Sefose 1618 U contains nearly 22 allylic hydrogens, 25 molar equivalent of M-TrEG-

SH was reacted with 1 molar equivalent of Sefose 1618 U. The reaction scheme for UV-mediated thiol-ene click reaction on Sefose 1618 U is presented in Figure 4.75.

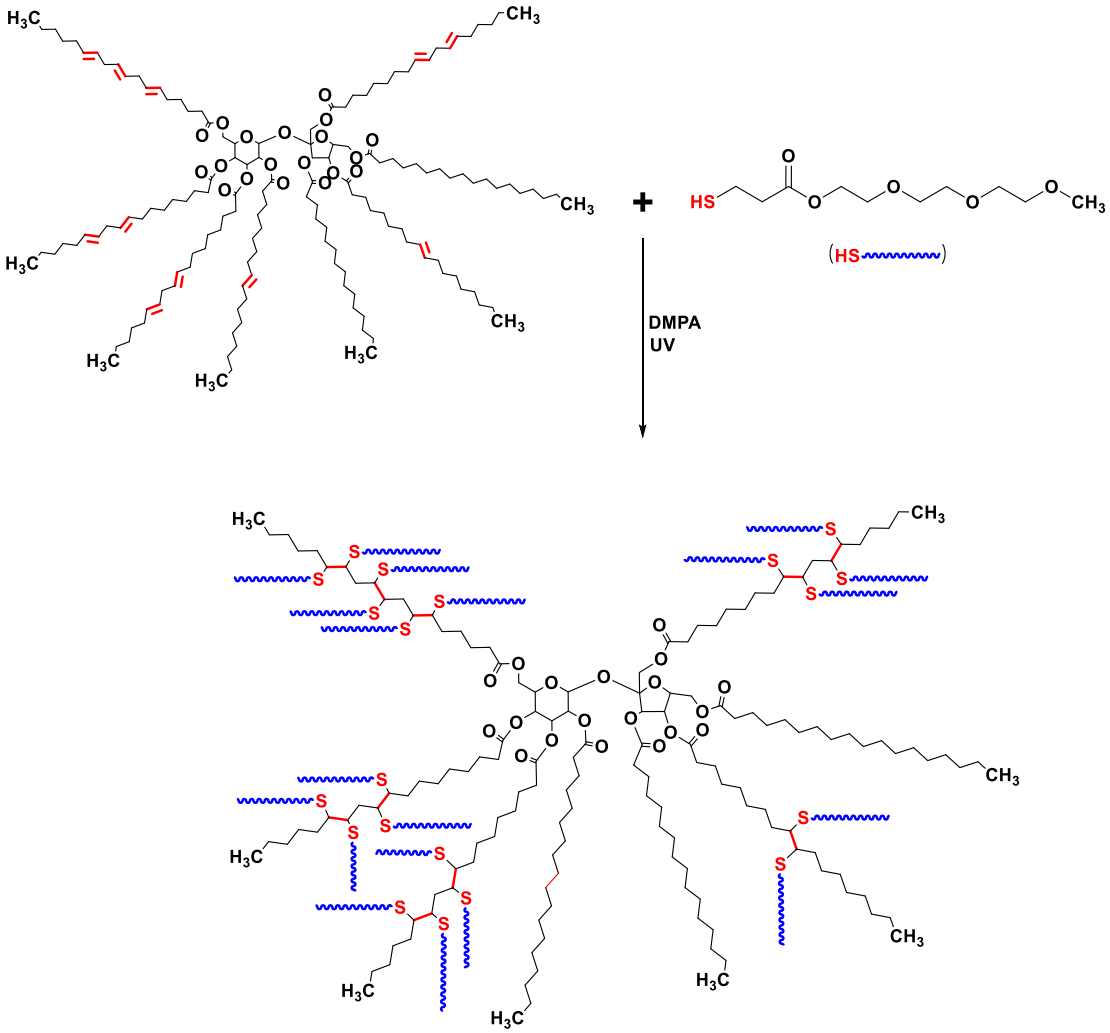

Figure 4.75 Reaction scheme for UV-mediated thiol-ene click reaction on Sefose 1618 U

Figure 4.76 shows the ^{1}H-NMR of M-TrEG-SH. The –CH_2- protons (t) besides the -OH group in M-TrEG-OH appearing at δ = 3.51 ppm move downfield to δ = 4.20 ppm (t') after transesterification reaction. The integral value of the –CH_2- protons besides the newly formed ester (t') with the methyl protons (n, δ = 3.30 ppm) from the starting material is in the ratio 2:3 indicating the quantitative transesterification of MP-SH with M-TrEG-OH.

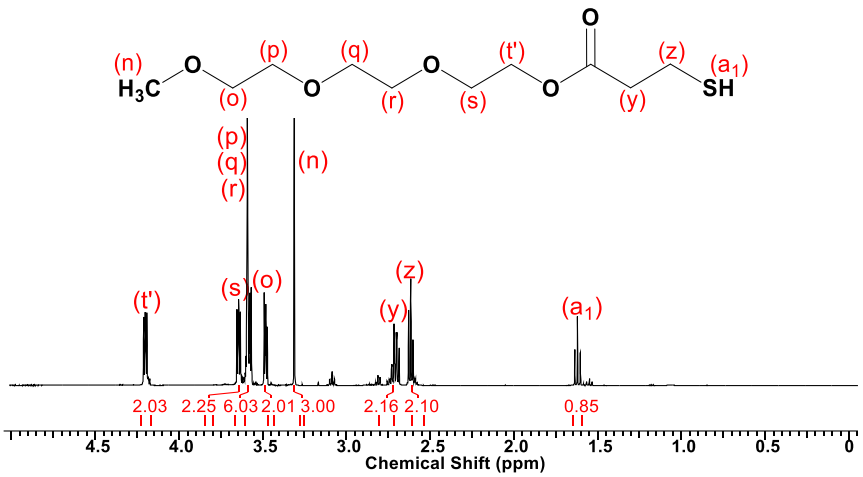

Figure 4.76 ^{1}H-NMR spectrum of M-TrEG-SH

Figure 4.77 shows the ^{1}H-NMR spectroscopy monitoring of the kinetics of the click reaction of M-TrEG-SH with Sefose 1618 U. The disappearance of allylic hydrogens appearing at δ = 5.35 ppm was monitored over time. After a complete UV-Click Reaction (100% conversion of limiting reagent Sefose 1618 U), if the integration of signal corresponding to the methyl protons, δ = 0.75 to δ = 1.05, is set to 21.71, the integration of signals corresponding to the alkene protons, δ = 5.25 to δ = 5.55, should reduce to 4.00. The integral value 4 belongs to the 4 protons of sucrose ((c), (e), (f), (k)). The disappearance of the signal corresponding to the alkene protons belongs to the complete reaction. Therefore, Actual Integral Value of Alkene Protons = 25.05 – 4 = 21.05. Table 4.2 presents the calculation of the conversion of the Sefose to Sefose-(S-TrEG-M)$_{22}$.

Therefore, 91.87% of the double bonds of Sefose 1618U were added onto by TrEG-SH within 60 minutes by UV-mediated Thiol-ene Click Reaction.

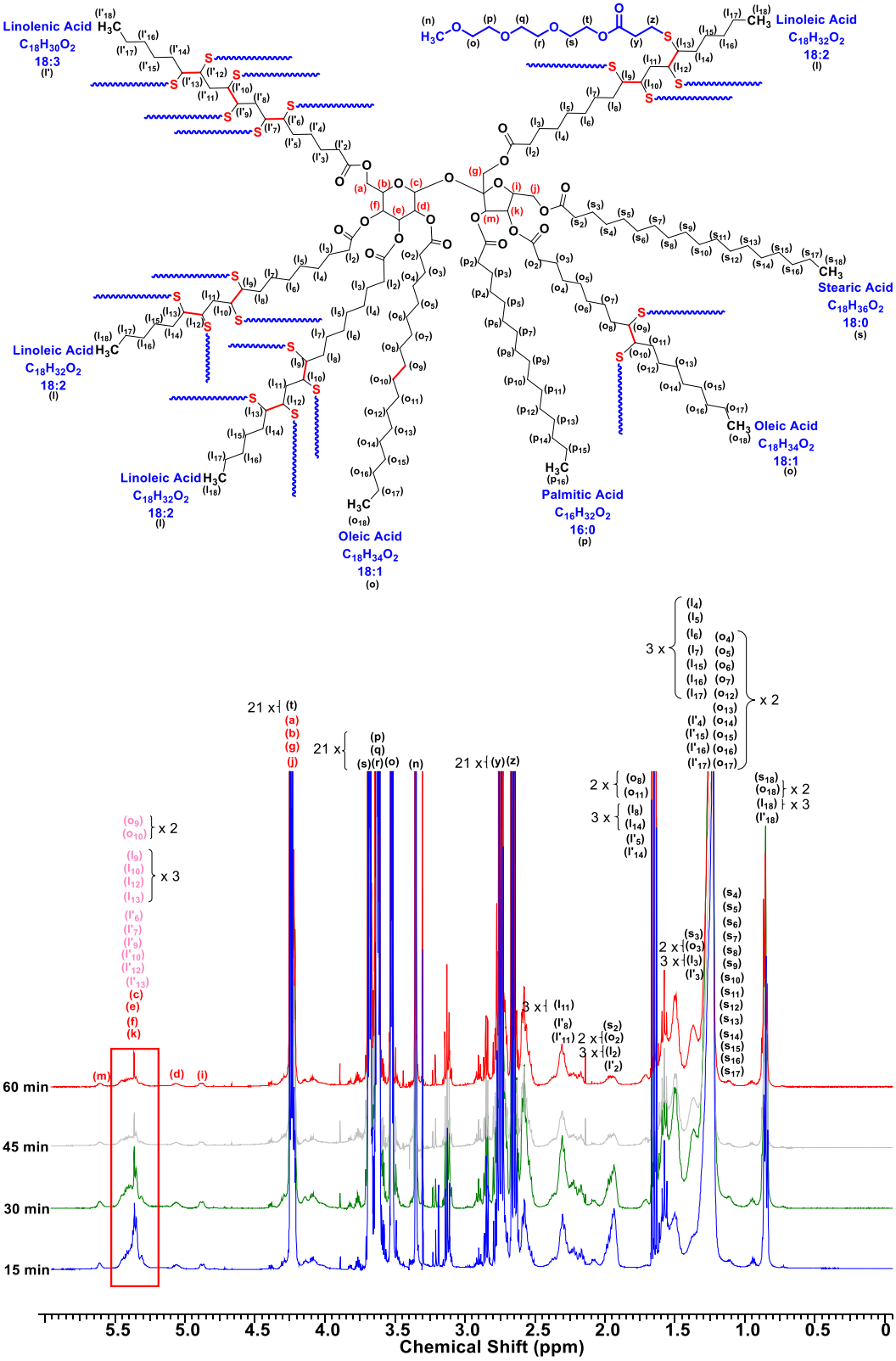

Figure 4.77 ^{1}H-NMR spectroscopy monitoring of the kinetics of the click reaction of M-TrEG-SH with Sefose 1618 U

Table 4.2 Time vs. Conversion of Sefose to Sefose-(S-TrEG-M)$_{22}$

Time (min)	**Integral Value of Alkene Proton Peak**	**Actual Integral Value of Alkene Proton Peak (A = X - 4)**	**Conversion (B = 21.05 – A)**	**Conversion (%) (B*100/21.05)**
0	25.05	21.05	0	0
15	13.08	9.08	11.97	56.86
30	9.37	5.37	15.68	74.48
45	9.46	5.46	15.54	74.06
60	5.71	1.71	19.34	91.87

4.5.2 Thiol-ene Click Reaction of HO-TEG-SH to Sefose

HO-TEG-SH was attempted to be clicked onto the double bonds present on Sefose 1618 U using the same synthetic strategy presented in Section 4.5.1. In the previous section, a methoxy-ended ethylene glycol molecule was used for the click reaction. In this section, a hydroxyl-ended ethylene glycol was used for the click reaction. Hydroxyl group being a reactive group unlike a methoxy might affect the kinetics of thid click reaction. In this section, the effect of the hydroxyl group on the kinetics of the click reaction was studied.

Figure 4.78 shows the ^{1}H-NMR spectroscopy monitoring of the kinetics of the click reaction of HO-TEG-SH with Sefose 1618 U. The conversion was calculated similarly to the calculation presented in Section 4.5.1. Table 4.3 presents the calculation of the conversion of the Sefose to Sefose-(S-TEG-OH)$_{22}$.

Therefore, 50.97% of the double bonds of Sefose 1618U were added onto by HO-TEG-SH within 60 minutes by UV- Thiol-ene Click Reaction. It can be deducted that nearly 11 allylic protons were reduced in the Sefose structure to obtain Sefose-(S-TEG-OH)$_{11}$ in one hour. The conversion obtained is nearly half compared to when the hydroxyl group is absent. Therefore, it can be concluded that the presence of the reactive -OH group present of the TEG molecule affects the kinetics of the reaction.

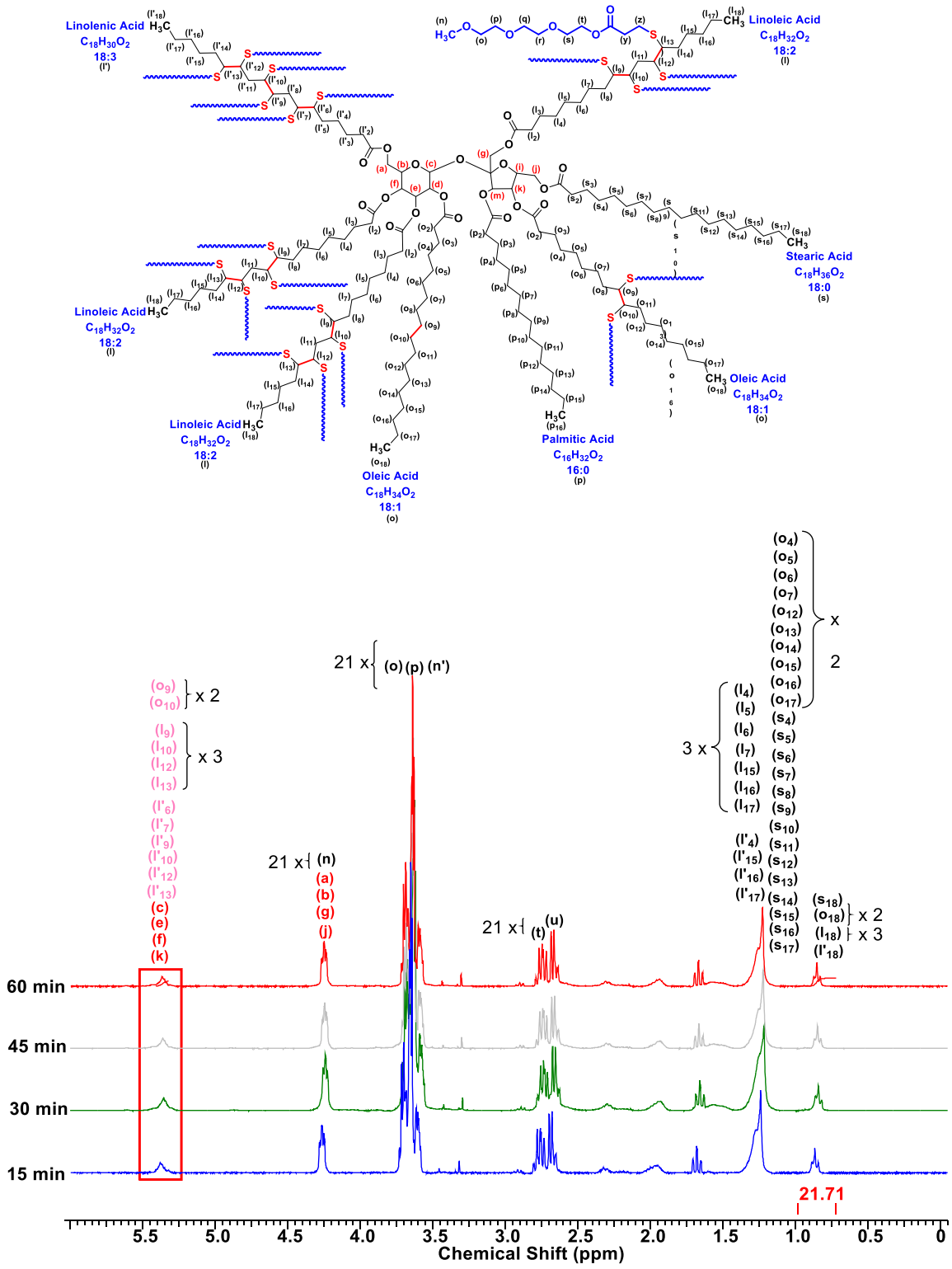

Figure 4.78 ^{1}H-NMR spectroscopy monitoring of the kinetics of the click reaction of HO-TEG-SH with Sefose 1618 U

Table 4.3 Time vs. Conversion of Sefose to Sefose-(S-TEG-OH)$_{22}$

Time (min)	**Integral Value of Alkene Proton Peak**	**Actual Integral Value of Alkene Proton Peak (A = X - 4)**	**Conversion (B = 21.05 – A)**	**Conversion (%) (B*100/21.05)**
0	25.05	21.05	0	0
15	16.84	12.84	8.21	39.00
30	16.30	12.30	8.75	41.56
45	15.20	11.20	9.85	46.79
60	14.32	10.32	10.73	50.97

4.5.3 Thiol-ene Click Reaction of M-PEG$_{750}$-SH on Sefose

M-PEG$_{750}$-SH was attempted to be clicked onto the double bonds present on Sefose 1618 U using the same synthetic strategy presented in Section 4.5.1. The objective of this study is to attach PEG to the Sefose molecule to make the Sefose water soluble. In the previous sections, short chain ethylene glycol molecules were used for the click reaction. In this section, poly(ethylene glycol) with a M_n of 750 g/mol (~17 ethylene glycol units) was used for the click reaction. Sefose molecule has 8-arms each of 16-18 carbon length attached to a sucrose molecule. PEG chains are longer in length than TrEG and TEG chains, therefore, attaching them will affect the kinetics of the reaction. In this section, the effect of the length of the polymer on the kinetics of the click reaction was studied.

The reaction mixture turned viscous at 15 minutes and it formed a gel-like substance at 30 minutes of reaction time. The stir bar was not able to rotate freely due to the gel-like substance formation. Therefore, ^{1}H-NMR spectroscopy was performed only on the 15 minute sample. The other samples did not dissolve in $CDCl_3$.

Figure 4.79 shows the ^{1}H-NMR spectrum of M-PEG$_{750}$-SH. The –CH_2- protons (t) besides the -OH group in M-PEG$_{750}$-OH appearing at δ = 3.51 ppm move downfield to δ = 4.25 ppm (t') after transesterification reaction. The integral value

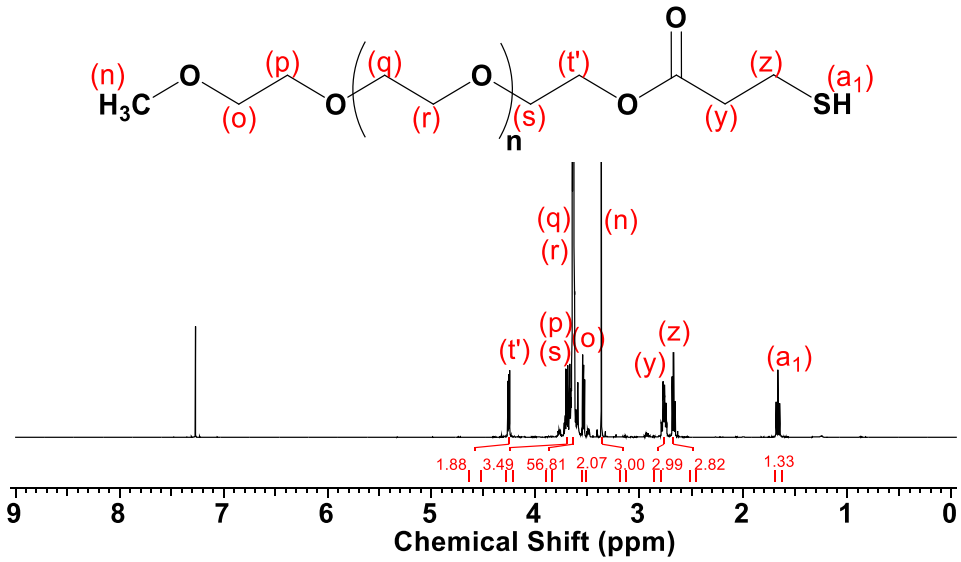

Figure 4.79 ^{1}H-NMR spectrum of M-PEG$_{750}$-SH

of the –CH_2- protons besides the newly formed ester (t') with the methyl protons (o, δ = 3.35 ppm) from the starting material is in the ratio 1.88:3 indicating the quantitative transesterification of MP-SH with M-PEG$_{750}$-OH.

Figure 4.80 shows the ^{1}H-NMR spectrum of the click reaction of HO-TEG-SH with Sefose 1618 U at 15 minutes. The conversion was calculated similarly to the calculation presented in Section 4.5.1. 47.98% conversion of Sefose 1618U was obtained within 15 minutes by UV- Thiol-ene Click Reaction after which the reaction mixture turned viscous and eventually formed a gel-like substance.

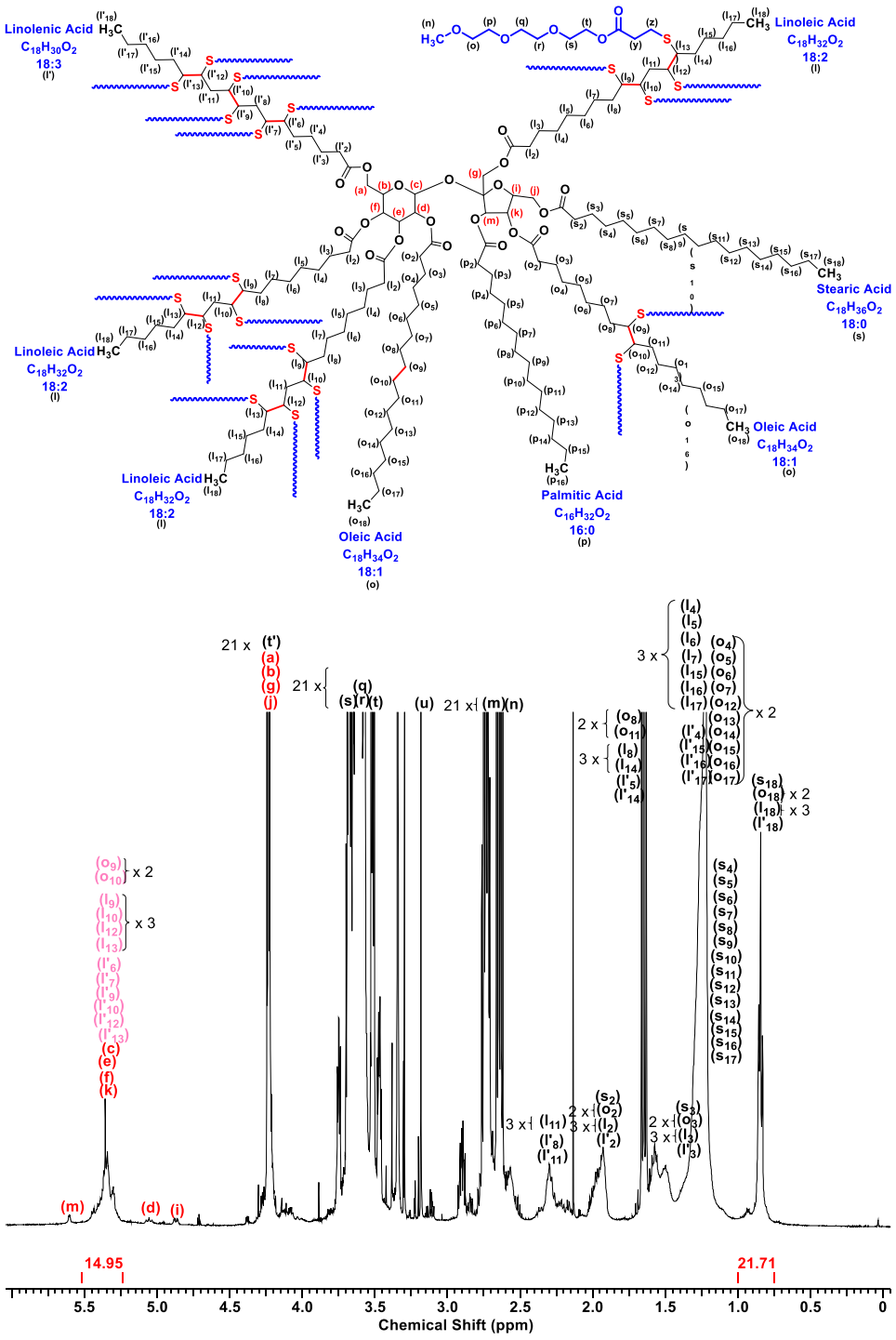

Figure 4.80 ^{1}H-NMR spectrum of the click reaction of M-PEG$_{750}$-SH with Sefose 1618 U at 15 minutes

The gel-like substance was attempted to solubilize in THF in order to perform SEC on it. Therefore, 19.6 mg of this gel was added to 3.1964 g of dry THF. The mixture was vigorously stirred over a vortex mixer for 5 minutes. 1 ml of this mixture was filtered over a 0.45µm PTFE filter and SEC was performed on this filtrate. The

filtration was not a smooth process since the gel did not completely dissolve in the THF. The SEC trace is presented in Figure 4.81.

The light scattering signal appearing at 40 min elution does not have a dRI signal. Therefore, it is present in an extremely low concentration, which may correspond to the negligible amount of the gel-like substance that did dissolve in the THF. The signal appearing at 50 minutes of elution time may correspond to the reacted or unreacted Sefose. And the signals appearing at 55 minutes of elution time correspond to the unreacted M-PEG$_{750}$-SH.

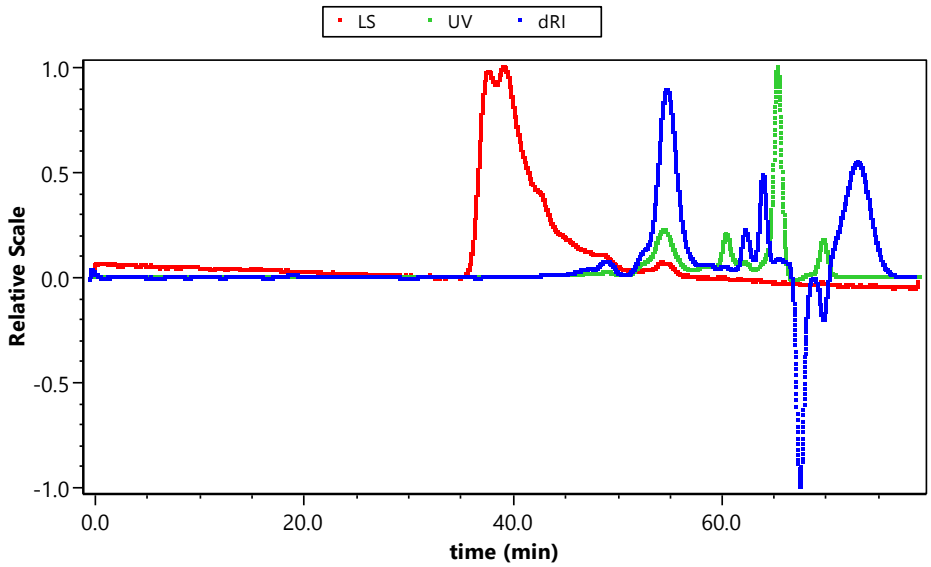

Figure 4.81 SEC trace of Sefose-S-PEG-M Gel

In the previous experiment, 25 molar equivalents of M-PEG$_{750}$-SH was attempted to be clicked onto the 22 double bonds present on 1 molar equivalent of Sefose 1618 U. Therefore, a new experiment was conducted in an objective to obtain one PEG-attachment per arm of Sefose 1618 U by using 8 molar equivalents of M-PEG$_{750}$-SH for 1 molar equivalent of Sefose 1618 U. The reaction mixture again turned viscous at 15 minutes and it formed a gel-like substance when reaction was continued until 30 minutes. The stir bar was not able to rotate freely due to the gel-

like substance formation. Therefore, the reaction was repeated by monitoring kinetics at 5, 10, and 15 minutes.

Figure 4.82 shows the ^{1}H-NMR spectroscopy monitoring of the kinetics of the click reaction of M-PEG$_{750}$-SH with Sefose 1618 U. The conversion was calculated similarly to the calculation presented in Section 4.5.1. Table 4.4 presents the calculation of the conversion of the Sefose to Sefose-(S-PEG$_{750}$-OH)$_{8}$.

Therefore, 67.70% of the double bonds of Sefose 1618U were added onto by M-PEG$_{750}$-SH within 15 minutes by UV- Thiol-ene Click Reaction implying approximately 5 PEG-arm attachments per molecule of Sefose 1618 U.

A gel-like substance was obtained within 15 minutes of reaction time when 25 molar equivalents of M-PEG$_{750}$-SH was attempted to be clicked onto the 22 double bonds present on 1 molar equivalent of Sefose 1618 U. Approximately 5 PEG-arm attachments per molecule of Sefose 1618 U was obtained within 15 minutes of reaction time when 8 molar equivalents of M-PEG$_{750}$-SH was attempted to be clicked onto 1 molar equivalent of Sefose 1618 U. The reaction mixture formed a gel-like substance when reaction was continued until 30 minutes. Therefore, for obtaining one PEG-attachment per arm of Sefose 1618 U, reaction mixture should be analysed at 20 and 25 minutes of reaction time, that is before the formation of gel-like substance. In addition, the solubility of the reaction products should be investigated in order for Sefose 1618 U to be used in biomedical applications demanding aqueous medium solubilization.

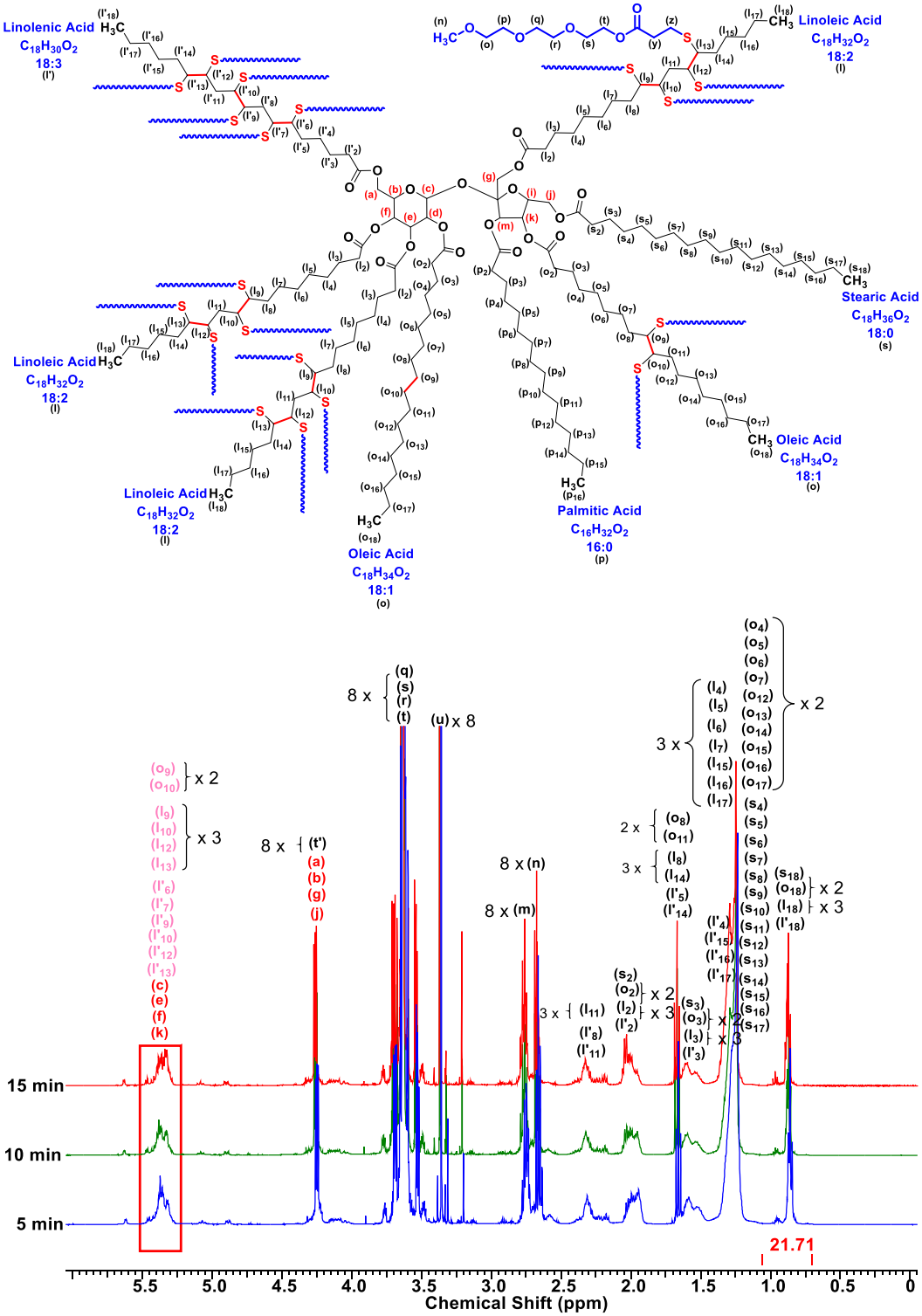

Figure 4.82 ^{1}H-NMR spectroscopy monitoring of the kinetics of the click reaction of M-PEG$_{750}$-SH with Sefose 1618 U

Table 4.4 Time vs. Conversion of Sefose to Sefose-(S-PEG_{750}-OH)$_8$

Time (min)	Integral Value of Alkene Proton Peak (X)	Actual Integral Value of Alkene Proton Peak (A = X – 17.05)	Conversion (B = 8 – A)	Conversion (%) (B*100/8)
0		8.05	0	0
5	22.23	5.23	2.82	35.03
10	21.21	4.21	3.84	47.70
15	19.60	2.6	5.45	67.70

4.6. Synthesis of Cyclic Polydisulfide Polymers from DODT

Polydisulphide polymers were made from 3,6-dioxa-1,8-octane-dithiol (DODT), referred to as poly(DODT), using an effective and "greener" route for the living oxidative polymerization called Reversible Redox Ring Polymerization (R3P) as reported in the literature.[67-69] The reaction scheme of the polymerization of DODT using R3P technique is shown in Figure 4.83. This polymerization uses Triethyl Amine (TEA) as the base to abstract the proton from the thiol group of DODT monomer and Hydrogen Peroxide (H_2O_2) as the oxidizing agent.

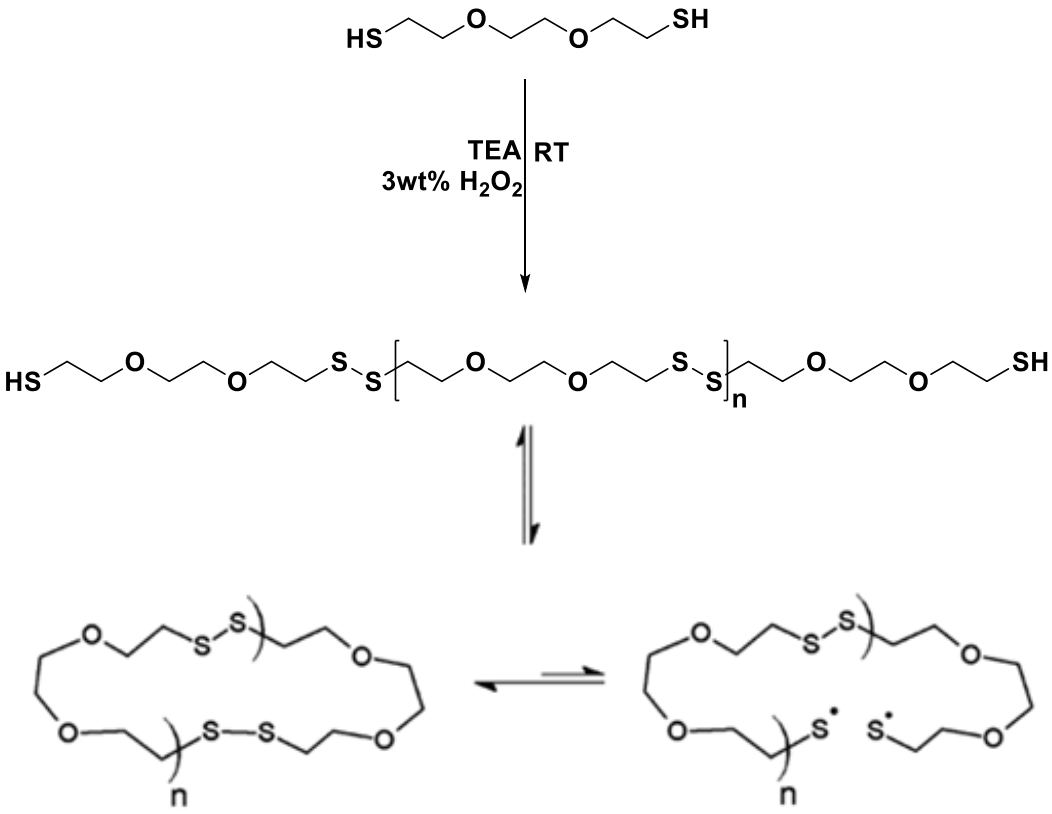

Figure 4.83 Synthesis of Disulphide Polymers by R3P

The goal of this research was to study the structure of the polymer obtained when the reaction parameters were varied. The following three reaction parameters were varied: 1) reaction time, 2) TEA/DODT molar ratio, and 3) H_2O_2/DODT molar ratio. Therefore, an experimental design was set up with varying levels of parameters as shown in Table 4.5. Table 4.5 also shows the representation of the levels. There are 3 factors (reaction parameters) with 3 levels (values) to be considered to design the experiments. If a full factorial design is applied, the number of experiments to be performed will be 3^3, that is, 27 experiments. However, a Box-Behnken (BB) design, which reduced the number of experiments to 13, was chosen. The limiting factor of this design is that the levels for the chosen parameters should be equidistant. The experimental design matrix along with its represented values is shown in Table 4.6.

Table 4.5 Corresponding Levels of Reaction Parameters for Poly(DODT) BB Experimental Design

Factors	**Represented Levels**		
Time (min)	-1	0	1
TEA/DODT Molar Ratio	-1	0	1
H_2O_2/DODT Molar Ratio	-1	0	1

Factors	**Actual Levels**		
Time (min)	1	5	9
TEA/DODT Molar Ratio	0.5	2	3.5
H_2O_2/DODT Molar Ratio	0.5	2	3.5

Table 4.6 Experimental Design Matrix with Represented and Actual Values

Exp. No.	Represented Levels			Actual Levels		
	Time (min)	**TEA/DODT Molar Ratio**	**H_2O_2/DODT Molar Ratio**	**Time (min)**	**TEA/DODT Molar Ratio**	**H_2O_2/DODT Molar Ratio**
1	-1	-1	0	1	0.5	2
2	-1	1	0	1	3.5	2
3	1	-1	0	9	0.5	2
4	1	1	0	9	3.5	2
5	-1	0	-1	1	2	0.5
6	-1	0	1	1	2	3.5
7	1	0	-1	9	2	0.5
8	1	0	1	9	2	3.5
9	0	-1	-1	5	0.5	0.5
10	0	-1	1	5	0.5	3.5
11	0	1	-1	5	3.5	0.5
12	0	1	1	5	3.5	3.5
13	0	0	0	5	2	2

The reaction parameters used, along with a visual description of the reaction product, molecular weight, and molecular weight distribution, are shown in Table 4.7. The molecular weight and molecular weight distribution was measured by Dr Carin Helfer using size exclusion chromatography.

It can be observed from Table 4.7 that when the TEA/DODT molar ratio is lower than the stoichiometric ratio of 2 as seen in Experiment 1, 3, and 10, an emulsion is formed even though the molar ratio of H_2O_2/DODT is higher than 2. The polymer is difficult to separate out immediately from such emulsions, therefore, an accurate measurement on the SEC was not obtained for Experiment 1, 3, and 10. It can be concluded that the minimum TEA/DODT molar ratio of 2 is required for polymer formation. When the H_2O_2/DODT molar ratio is lower than the stoichiometric ratio of 2, as seen in Experiment 5, 7, 9, and 11, a liquid polymer sample was obtained. These liquid

Table 4.7 Preliminary Observations from Poly(DODT) BB Experiments

Exp. No.	Time (min)	TEA/DODT Molar Ratio	H_2O_2/DODT Molar Ratio	Observation	M_n (g/mol)	Mw/M_n
1	1	0.5	2	Emulsion		
2	1	3.5	2	Solid Precipitate (Polymer)	165,400	1.88
3	9	0.5	2	Emulsion		
4	9	3.5	2	Solid Precipitate (Polymer)	121,500	1.684
5	1	2	0.5	Translucent Liquid	**	**
6	1	2	3.5	Solid Precipitate (Polymer)	179,600	1.567
7	9	2	0.5	Translucent Liquid	**	**
8	9	2	3.5	Solid Precipitate (Polymer)	196,100	1.467
9	5	0.5	0.5	Translucent Liquid	**	**
10	5	0.5	3.5	Emulsion		
11	5	3.5	0.5	Translucent Liquid	**	**
12	5	3.5	3.5	Solid Precipitate (Polymer)	234,000	1.207
13	5	2	2	Solid Precipitate (Polymer)	268,100	1.638

polymer samples when characterized on the SEC showed low molecular weights that were out of the calibration range. Therefore, it can be concluded that when the H_2O_2/DODT molar ratio is lower than the stoichiometric ratio of 2, low molecular weight polymer or oligomers are obtained. In addition to SEC, polymer samples from Experiment 2, 5, 7, 9, and 11 were further analyzed using ^{1}H NMR spectroscopy and

MALDI mass spectroscopy (MS). Figure 4.84 shows the ^{1}H NMR spectrum for the monomer DODT. According to work by Rosenthal and co- workers,[68] a triplet signal near 1.58 ppm was attributed to the terminal thiol protons, indicating the presence of thiol end groups.

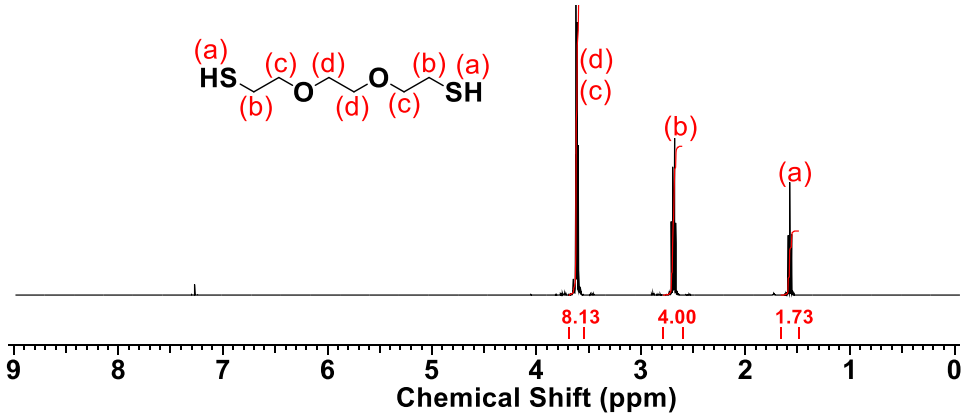

Figure 4.84 ^{1}H-NMR spectrum of the DODT Monomer (purchased from Sigma-Aldrich)

Figure 4.85 shows the ^{1}H NMR spectrum for the product obtained from Experiment 2. The signals (b) and (c) shifted from their position from the monomer DODT on account of the disulfide bond formation. There is a small signal at 1.60 ppm, that may indicate thiol end groups (although it is not a triplet). The ratio of the integrals of (a)/(b') yields 7 units in the chain, corresponding to M_n ~ 1300 g/mol. However, SEC gave M_n = 167,000 g/mol. Thus this signal is likely due to unreacted monomer residues.

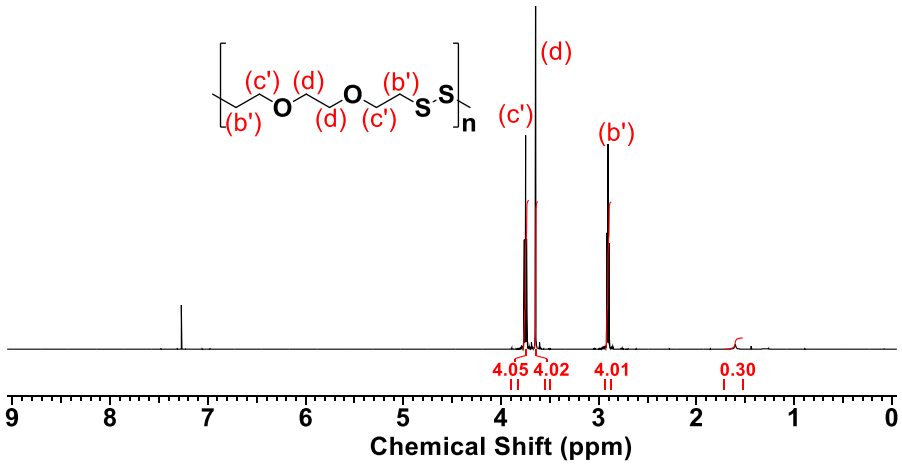

Figure 4.85 ^{1}H-NMR spectrum of product from Experiment 2

Figure 4.86 shows the MALDI mass spectrum of product obtained from Experiment 2. There is a single distribution of signals separated by *m/z* = 180 corressponding to the DODT repeating unit. The *m/z* = 1103.173 belongs to the Na complex of a hexamer, with no thiol end groups (cyclic structure). The zoomed image of the signal at *m/z* = 1103.173 is shown in the inlet. The zoomed image shows a signal at *m/z* = 1105.164. This signal belongs to the sodium complex of the hexamer containing the isotope of sulfur having atomic weight 34 g/mol (^{34}S) which has a relative abundance of 4.21%. However, if the product contains thiol-end-groups, that is if the structure is linear (2 additional H atoms), its sodium complex will also appear at *m/z* = 1105. Therefore, the signal at *m/z* = 1105 may belong to both, the linear polymer and the ^{34}S isotope containing cyclic polymer. To determine the linear content of the hexamer of the product from Experiment 2, we generated a theoretical isotopic pattern of the cyclic hexamer and manually measured the ratio of the expected height of the signals at *m/z* = 1103 and 1105.

Then we manually measured the height of the experimental signal at *m/z* = 1103.73, and calculated the expected height for the signal at *m/z* = 1105.164 from the previously calculated ratio. If the calculated height is more than the expected height, the product contains linear fractions. In this case, a linear content of 3.85% was calculated for the hexamer fraction of the poly(DODT) from Experiment 2 using above method. Therefore, it can be concluded that using TEA/DODT molar ratio 3.5 and H_2O_2/DODT ratio 2, we predominantly obtain cyclic sructure in the hexamer fraction of poly(DODT). This method can be applied to determine the linear content in other fractions of this product.

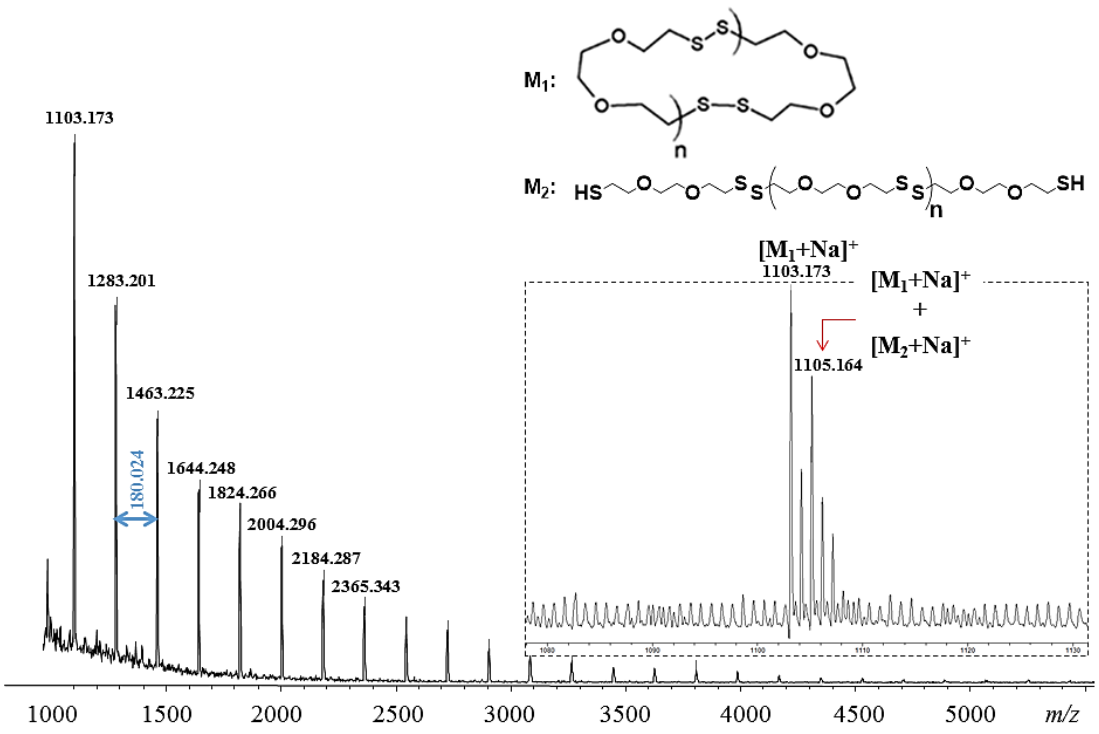

Figure 4.86 MALDI mass spectrum of product from Experiment 2, 180 *m/z* = DODT repeat unit. Inset: spectrum of the hexamer fraction

Figure 4.87 shows the ^{1}H NMR spectrum for the product of Experiment 11. The ^{1}H NMR spectrum shows a small peak observed at 1.60 ppm, which may indicate thiol end groups. In addition to the polymer signals (b', c' and d), other signals appear that may correspond to monomer or oligomers.

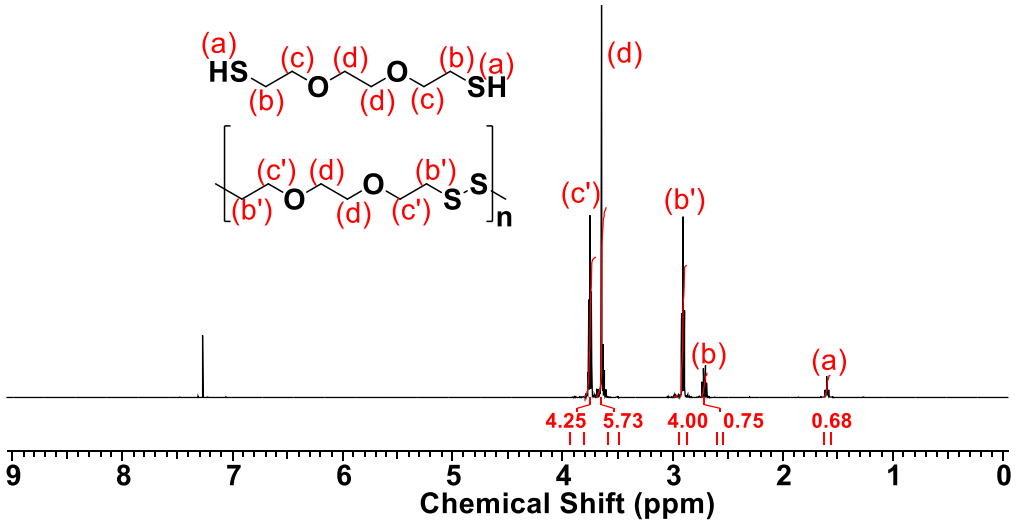

Figure 4.87 ^{1}H-NMR spectrum of product from Experiment 11

Figure 4.88 shows the MALDI of product obtained from Experiment 11. The main distribution belongs to sodium complex of the linear chains with thiol end groups – *m/z* = 1105.064 (hexamer). The signal at *m/z* = 1103.027 in the inlet of the Figure 4.96 belongs to the sodium complex of a hexamer, with no thiol end groups (cyclic structure). Thus the polymer from Experiment 11 contains mostly linear chains with some cyclic polymer chains. A linear content of 81.8% was calculated for the hexamer fraction of the poly(DODT) from Experiment 11 using the method used for calculating the linear content in the hexamer fraction of the polymer from Experiment 2. Therefore, it can be concluded that using TEA/DODT molar ratio 3.5 and H_2O_2/DODT ratio 0.5 (< stoichoimetric ratio), we predominantly obtain linear sructure in the hexamer fraction of poly(DODT).

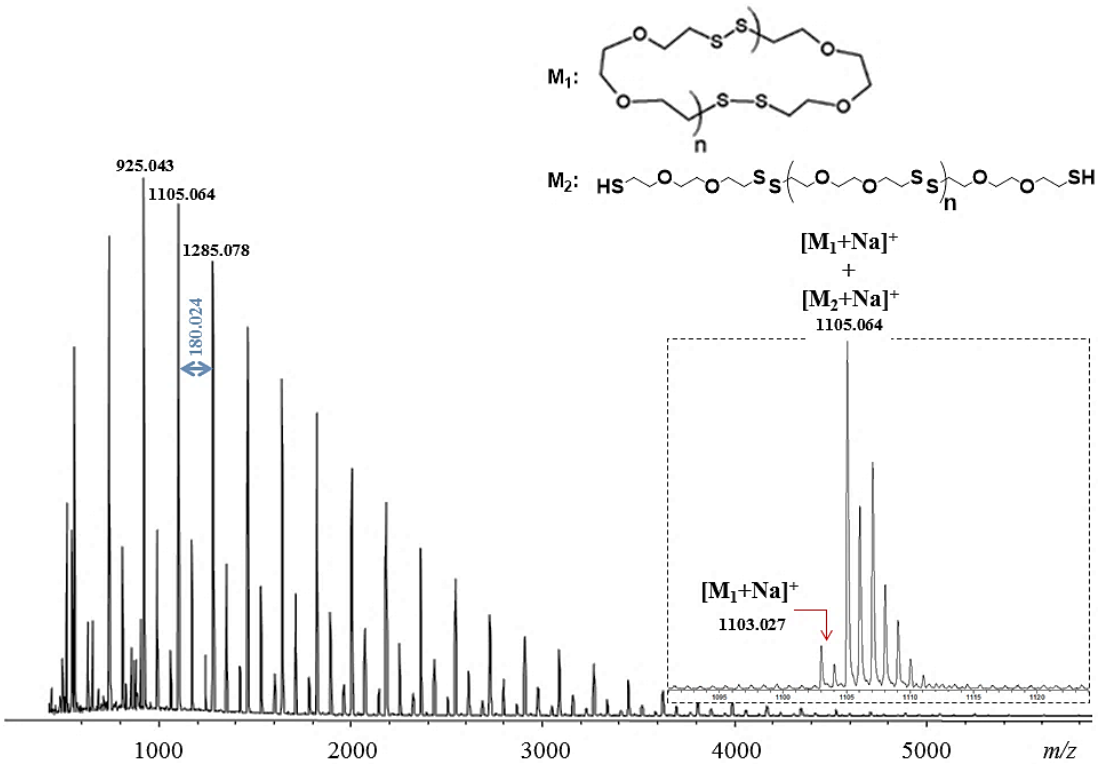

Figure 4.88 MALDI mass spectrum of product from Experiment 11, 180 *m/z* = DODT repeat unit. Inset: spectrum of the hexamer fraction

The ^{1}H NMR and MALDI spectra of the product from Experiment 5, 7, and 9 are very similar to that of Experiment 11. Therefore, it can be concluded that when TEA/DODT molar ratio is ≥ 2 (the stoichoimetric ratio) and H_2O_2/DODT molar ratio is < 2 (the stoichoimetric ratio), we predominantly obtain linear polymers of DODT. Therefore, in order to predominantly obtain cyclic polymers, the TEA/DODT and H_2O_2/DODT molar ratios must be maintained above their stoichoimetric value.

CONCLUSIONS

This dissertation primarily investigated the synthesis of two-functional folate-targeted PEG-based conjugates for potential applications in breast cancer diagnosis. The enzyme-catalyzed synthesis of the precursors, functionalized PEGs and thiol-functionalized folic acid, was also investigated. Three strategies were proposed to synthesize these conjugates that demanded the use of PEG-diamines, PEG-dithiols, PEG-dibromides and thiol-functionalized folic acid.

As discussed in Section 4.1.1., I prepared PEG-diamines via CALB-catalyzed esterification of *tert*-butyloxycarbonyl protected Alanines with PEG having M_n = 2050 g/mol. The amino acids L-Alanine and β-Alanine were protected with a *t*BOC-group and were used to functionalize the end-groups of the PEG with amine moieties. Enzyme-catalysis provided quantitative esterification under mild conditions without generating any side products. The quantitative esterification was confirmed by the single distribution of product obtained from MALDI mass spectrometry. The *t*BOC group was removed using HCl formed *in situ* by AcCl to yield amine functionalized PEGs. However, due to longer reaction times used, the newly formed ester bond from esterification was broken down after the de-protection of the amine group by HCl that yielded multiple side products. This was confirmed by the multiple distributions obtained from MALDI mass spectrometry.

In Section 4.1.2, thiol-functionalized Folic Acid (FA-SH) was successfully prepared to be used as the targeting moiety in the 2-funtional folate-targeted PEG-based conjugate for potential applications in TNBC diagnosis.

FA-SH and its intermediate products were thoroughly characterized using ^{1}H-NMR and ^{13}C-NMR spectroscopy, and MALDI mass spectrometry. FA-SH was synthesized by exclusively lithiating FA at the γ-carboxyl position with 1 molar equivalent of *n*-butyllithium (*n*-BuLi) and subsequently reacting it with 1 equivalent of a bis(2-ethyl 4-bromobutanoate) disulfide (Br-S-S-Br) compound to form FA-γ-bis(2-ethyl bromobutanoate) disulfide (FA-S-S-FA). The carboxylic acid at γ-position of FA reacted with *n*-BuLi instead of the α-carboxyl because of the higher acidity of the γ-carboxyl position. This exclusive reaction was confirmed by the shift observed in the γ-carboxyl carbon in the ^{13}C-NMR spectrum of the lithiated FA. Br-S-S-Br was quantitatively prepared using CALB-catalyzed transesterification of EBB with 2-HEDS under mild solventless conditions. The unreacted free FA was removed from FA-S-S-FA by exclusively salting it out with sodium ions at pH 10. The disulfide bond in the FA-S-S-FA was then cleaved with dithiothreitol (DTT) to yield FA-SH.

In Section 4.2, I successfully demonstrated synthesis of thiol-functionalized TEGs and PEGs via enzyme catalyzed transesterification of MP-SH with TEG, and PEGs having M_n = 1000, and 2050 g/mol. These reactions were performed without using solvents (in bulk) and using CALB as an enzyme catalyst. The transesterification was found to be a step-wise consecutive reaction. TEG-monothiol was exclusively formed in 15 minutes, followed by a slower second cycle yielding TEG-dithiol in 7.5 hours. PEG_{1000}-monothiol was obtained within 8 hours; however, dithiol formation was not observed even after 24 hours of reaction. PEG_{1000}-dithiol was obtained by reacting PEG_{1000}-monothiol with fresh CALB and MP-SH for 24 hours. PEG_{2050}-monothiol was formed in 16 hours, and dithiol formation demanded more CALB and MP-SH. CALB-catalyzed transesterification of MP-SH was also

performed with $dPEG_{20}$ to yield quantitative thiol functionalization of the hydroxyl end-groups under solventless mild conditions.

In Section 4.3, two-functional folate-targeted PEG-based conjugates (FA-FL-PEG-FL-FA) for potential applications in breast cancer diagnosis were successfully synthesized via CALB-catalyzed Michael addition of 2 equivalents of thiol functionalized folic acid to 2-functional fluorescein-labeled TEG and PEGs (Ac-FL-PEG-FL-Ac). The Michael addition reaction was quantitative within 8 hours. These compounds were given to our collaborator, Dr McLennan's lab, at the Cleveland Clinic to qualitatively evaluate their cellular uptake on TNBC cell lines MDA_MB_231 (epithelial cells_HTB-132_adenocarcinoma_patient ethnicity Caucasian) and MDA_MB_468 (epithelial cells_HTB-26_adenocarcinoma_patient ethnicity African American) using immunocytochemistry. The quantitative evaluation will be performed using flow cytometry at Dr McLennan's lab.

In Section 4.4, a new strategy was proposed to synthesize two-functional fluorescein-labeled PEG (FL-PEG-FL) using lithium technology. Fluorescin (reduced form of fluorescein) was lithiated using *n*-BuLi to obtain a lithiated fluorescin (FL-COOLi) which was subsequently reacted with PEG-dibromide (Br-PEG-Br) to obtain a FL-PEG-FL. Br-PEG-Br was quantitatively synthesized via CALB-catalyzed transesterification of EBV with PEG. However, we did not proceed with this strategy because the reaction yielded a mono-substituted product (FL-PEG-OH) and did not proceed to di-substitution of Fluorescin on PEG.

Therefore, in conclusion, two-functional folate-targeted PEG-based conjugates with varying chain length were successfully synthesized using combinatorial strategies of enzyme catalysis and lithium chemistry. These conjugates are expected to have potential applications in diagnosis of TNBC.

REFERENCES

[1] American Cancer Society. Breast Cancer Facts and Figures 2017-2018. Atlanta: American Cancer Society, Inc. [Online] 2017.

[2] Low, P. S.; Kularatne, S. A. Folate-Targeted Therapeutic and Imaging Agents for Cancer. *Current Opinion in Chemical Biology* **2009**, *13(3)*, 256-262.

[3] Garcia-Bennett, A.; Nees, M.; Fadeel, B. In Search of the Holy Grail: Folate-Targeted Nanoparticles for Cancer Therapy. *Biochemical Pharmacology* **2011**, *81(8)*, 976-984.

[4] Hong, S.; Leroueil, P. R.; Majoros, I. J.; Orr, B. G.; Baker, J. R.; Holl, M. M. B. The Binding Avidity of a Nanoparticle-Based Multivalent Targeted Drug Delivery Platform. *Chemistry & Biology* **2007**, *14(1)*, 107-115.

[5] Castano Gil, Y. Green Polymer Chemistry: The Role of Candida antartica Lipase B in Polymer Functionalization. Ph.D. Dissertation, The University of Akron, Akron, OH, 2014.

[6] Klonis, N.; Sawyer, W. H. Spectral Properties of the Prototropic Forms of Fluorescein in Aqueous Solution. *Journal of Fluorescence* **1996**, *6(3)*, 147-157.

[7] Puskas, J. E.; Sen, M. Y. Process of Preparing Functionalized Polymers via Enzyme Catalysis. US8710156B2, 2014.

[8] Sen, S.; Puskas, J. E. Green Polymer Chemistry: Enzyme Catalysis for Polymer Functionalization. *Molecules* **2015**, *20(5)*, 9358-9379.

[9] Puskas, J. E.; Sen, M. Y.; Seo, K. S. Green Polymer Chemistry Using Nature's Catalysts, Enzymes. *Journal of Polymer Science Part A: Polymer Chemistry* **2009**, *47(12)*, 2959-2976.

[10] Sen, M. Y.; Puskas, J. E.; Ummadisetty, S.; Kennedy, J. P. Green Polymer Chemistry: II. Enzymatic Synthesis of Methacrylate-Terminated Polyisobutylenes. *Macromolecular Rapid Communications* **2008**, *29(19)*, 1598-1602.

[11] Castano, M.; Seo, K. S.; Guo, K.; Becker, M. L.; Wesdemiotis, C.; Puskas, J. E. Green Polymer Chemistry: Synthesis of Symmetric and Asymmetric Telechelic Ethylene Glycol Oligomers. *Polymer Chemistry* **2015**, *6(7)*, 1137-1142.

[12] Puskas, J. E.; Sen, M. Y.; Kasper, J. R. Green Polymer Chemistry: Telechelic Poly(Ethylene Glycol)s via Enzymatic Catalysis. *Journal of Polymer Science Part A: Polymer Chemistry* **2008**, *46(9)*, 3024-3028.

[13] Puskas, J. E.; Seo, K. S.; Sen, M. Y. Green Polymer Chemistry: Precision Synthesis of Novel Multifunctional Poly(Ethylene Glycol)s Using Enzymatic Catalysis. *European Polymer Journal 47(4)*, 524-534.

[14] Castano, M.; Seo, K. S.; Kim, E. H.; Becker, M. L.; Puskas, J. E. Green Polymer Chemistry VIII: Synthesis of Halo-ester-Functionalized Poly(Ethylene Glycol)s via Enzymatic Catalysis. *Macromolecular Rapid Communications* **2013**, *34(17)*, 1375-1380.

[15] Puskas, J. E.; Seo, K. S.; Castano, M.; Casiano, M., Wesdemiotis, C. Green Polymer Chemistry: Enzymatic Functionalization of Poly(ethylene glycol)s under solventless conditions. In *Green Polymer Chemistry: Biocatalysis and Materials II*; Cheng, H.N., Gross, R.A., Smith, P.B., Eds.; ACS Symposium Series, American Chemical Society: Washington D.C., USA, 2013; Vol. 1144, ISBN 978-0-8412-2895-5.

[16] Aleskandarany M.A.; Ellis I.O.; Rakha E.A. Molecular Classification of Breast Cancer. In *Precision Molecular Pathology of Breast Cancer*; Khan A., Ellis I., Hanby A., Cosar E., Rakha E., Kandil D. Eds.; Springer: New York, NY, 2015; Vol. 10.

[17] Russell-Jones, G.; McTavish, K.; McEwan, J.; Rice, J.; Nowotnik, D. Vitamin-Mediated Targeting as a Potential Mechanism to Increase Drug Uptake by Tumours. *Journal of Inorganic Biochemistry* **2004**, *98(10)*, 1625-1633.

[18] O'Shannessy, D. J.; Somers, E. B.; Maltzman, J.; Smale, R.; Fu, Y. S. Folate Receptor Alpha (FRA) Expression in Breast Cancer: Identification of a New Molecular Subtype and Association with Triple Negative Disease. *SpringerPlus* **2012**, *1(1)*, 22.

[19] Toffoli, G.; Russo, A.; Gallo, A.; Cernigoi, C.; Miotti, S.; Sorio, R.; Tumolo, S.; Boiocchi, M. Expression of Folate Binding Protein as a Prognostic Factor for Response to Platinum-Containing Chemotherapy and Survival in Human Ovarian Cancer. *International Journal of Cancer* **1998**, *79*, 121–126.

[20] Leamon, C. P.; Low, P. S. Delivery of Macromolecules into Living Cells: A Method that Exploits Folate Receptor Endocytosis. *Proceedings of the National Academy of Sciences* **1991**, *88(13)*, 5572-5576.

[21] Lee, R. J.; Low, P. S. Delivery of Liposomes into Cultured KB Cells via Folate Receptor-Mediated Endocytosis. *Journal of Biological Chemistry* **1994**, *269(5)*, 3198-3204.

[22] Reddy, J.A.; Low, P. S. Folate-Mediated Targeting of Therapeutic and Imaging Agents to Cancers. *Critical Reviews in Therapeutic Drug Carrier Systems* **1998**, *15* 587–627.

[23] Poe, M. Acidic Dissociation Constants of Folic Acid, Dihydrofolic Acid, and Methotrexate. *Journal of Biological Chemistry* **1977**, *252(11)*, 3724-3728.

[24] Wang, S.; Low, P. S. Folate-Mediated Targeting of Antineoplastic Drugs, Imaging Agents, and Nucleic Acids to Cancer Cells. *Journal of Controlled Release* **1998**, *53(1)*, 39-48.

[25] Wang, S.; Lee, R. J.; Mathias, C. J.; Green, M. A.; Low, P. S. Synthesis, Purification, and Tumor Cell Uptake of ^{67}Ga-Deferoxamine−Folate, A Potential Radiopharmaceutical for Tumor Imaging. *Bioconjugate Chemistry* **1996**, *7(1)*, 56-62.

[26] Wong, P. T.; Choi, S. K. Mechanisms of Drug Release in Nanotherapeutic Delivery Systems. *Chemical Reviews* **2015**, *115(9)*, 3388-3432.

[27] Lu, Y.; Low, P.S. Folate-mediated Delivery of Macromolecular Anticancer Therapeutic Agents. *Advanced Drug Delivery Reviews* **2012**, *64*, 342-352.

[28] Hernot, S.; van Manen, L.; Debie, P.; Mieog, J. S. D.; Vahrmeijer, A. L. Latest Developments in Molecular Tracers for Fluorescence Image-Guided Cancer Surgery. *The Lancet Oncology* **2019**, *20(7)*, 354-367.

[29] Siegel, B. A.; Dehdashti, F.; Mutch, D. G.; Podoloff, D. A.; Wendt, R.; Sutton, G. P.; Burt, R.W.; Ellis, P.R.; Mathias, C.J.; Green, M.A.; Gershenson, D. M. Evaluation of ^{111}In-DTPA-Folate as a Receptor-Targeted Diagnostic Agent for Ovarian Cancer: Initial Clinical Results. *Journal of Nuclear Medicine* **2003**, *44(5)*, 700-707.

[30] Morris, R. T.; Joyrich, R. N.; Naumann, R. W.; Shah, N. P.; Maurer, A. H.; Strauss, H. W.; Uszler, J.M.; Symanowski, J.T.; Ellis, P.R.; Harb, W. A. Phase II Study of Treatment of Advanced Ovarian Cancer with Folate-Receptor-Targeted Therapeutic (Vintafolide) and Companion SPECT-based Imaging Agent (^{99m}Tc-Etarfolatide). *Annals of Oncology* **2014**, *25(4)*, 852-858.

[31] Aronov, O.; Horowitz, A. T.; Gabizon, A.; Gibson, D. Folate-Targeted PEG as a Potential Carrier for Carboplatin Analogs. Synthesis and *in vitro* Studies. *Bioconjugate Chemistry* **2003**, *14(3)*, 563-574.

[32] Viola-Villegas, N.; Rabideau, A. E.; Cesnavicious, J.; Zubieta, J.; Doyle, R. P. Targeting the Folate Receptor (FR): Imaging and Cytotoxicity of Re^{I} Conjugates in FR-Overexpressing Cancer Cells. *ChemMedChem* **2008**, *3(9)*, 1387-1394.

[33] Viola-Villegas, N.; Vortherms, A.; Doyle, R. P. Targeting Gallium to Cancer Cells Through the Folate Receptor. *Drug Target Insights* **2008**, *3*, 13.

[34] Ak, G.; Yurt Lambrecht, F.; Sanlier, S. H. Radiolabeling of Folate Targeted Multifunctional Conjugate with Technetium-99m and Biodistribution Studies in Rats. *Journal of Drug Targeting* **2012**, *20(6)*, 509-514.

[35] Majoros, I. J.; Thomas, T. P.; Mehta, C. B.; Baker, J. R. Poly (amidoamine) dendrimer-based multifunctional engineered nanodevice for cancer therapy. *Journal of Medicinal Chemistry* **2005**, *48(19)*, 5892-5899.

[36] Majoros, I. J.; Myc, A.; Thomas, T. P.; Mehta, C. B.; Baker, J. R. PAMAM Dendrimer-Based Multifunctional Conjugate for Cancer Therapy: Synthesis, Characterization, and Functionality. *Biomacromolecules* **2006**, *7(2)*, 572-579.

[37] Patri, A. K.; Majoros, I. J.; Baker Jr, J. R. Dendritic polymer macromolecular carriers for drug delivery. *Current Opinion in Chemical Biology* **2002**, *6(4)*, 466-471.

[38] Baker, J. R. Dendrimer-Based Nanoparticles for Cancer Therapy. *American Society of Hematology Education Program Book* **2009**, *2009(1)*, 708-719.

[39] Thomas, T. P.; Majoros, I. J.; Kotlyar, A.; Kukowska-Latallo, J. F.; Bielinska, A.; Myc, A.; Baker, J. R. Targeting and Inhibition of Cell Growth by An Engineered Dendritic Nanodevice. *Journal of Medicinal Chemistry* **2005**, *48(11)*, 3729-3735.

[40] Islam, M. T.; Majoros, I. J.; Baker Jr, J. R. HPLC Analysis of PAMAM Dendrimer based Multifunctional Devices. *Journal of Chromatography B* **2005**, *822(1-2)*, 21-26.

[41] Koirala, N.; Das, D.; Fayazzadeh, E.; Sen, S.; McClain, A.; Puskas, J. E.; Drazba, J. A.; McLennan, G. Folic Acid Conjugated Polymeric Drug Delivery Vehicle for Targeted Cancer Detection in Hepatocellular Carcinoma. *Journal of Biomedical Materials Research Part A* **2019**, *107(11)*, 2522-2535.

[42] Koeller, K. M.; Wong, C. H. Enzymes for Chemical Synthesis. *Nature* **2001**, *409*, 232-240.

[43] Pan, X.; Sengupta, P.; Webster, D. C. Novel Biobased Epoxy Compounds: Epoxidized Sucrose Esters of Fatty Acids. *Green Chemistry* **2011**, *13*(4), 965-975.

[44] Hoyle, C. E.; Bowman, C. N. Thiol–ene Click Chemistry. *Angewandte Chemie International Edition* **2010**, *49*(9), 1540-1573.

[45] Patrick, J.C. US Patent 1,890,191. 1932.

[46] Obukhov, S. P.; Rubinstein, M.; Duke, T. Dynamics of A Ring Polymer in A Gel *Physical Review Letters* **1994**, *73*, 1263-1266.

[47] Kricheldorf, H. R. Cyclic Polymers: Synthetic Strategies and Physical Properties. *Journal of Polymer Science Part A-Polymer Chemistry* **2010**, *48*, 251-284.

[48] Orrah, D. J.; Semlyen, J. A.; Rossmurphy, S. B. Studies of Cyclic and Linear Poly(Dimethylsiloxanes) 28. Viscosities and Densities of Ring and Chain Poly(Dimethylsiloxane) Blends. *Polymer* **1988**, *29*, 1455-1458.

[49] Clarson, S. J.; Semlyen, J. A. Cyclic Polysiloxanes. 1. Preparation and Characterization of Poly(Phenylmethylsiloxane) *Polymer* **1986**, *27*, 1633-1636.

[50] Bannister, D. J.; Semlyen, J. A. Studies of Cyclic and Linear Poly(Dimethyl siloxanes). 6. Effect of Heat. *Polymer* **1981**, *22*, 377-381.

[51] Shin, E. J.; Jeong, W.; Brown, H. A.; Koo, B. J.; Hedrick, J. L.; Waymouth, R. M. Crystallization of Cyclic Polymers: Synthesis and Crystallization Behavior of High Molecular Weight Cyclic Poly(ε-Caprolactone)s. *Macromolecules* **2011**, *44*, 2773-2779.

[52] Roovers, J. Dilute-Solution Properties of Ring Polystyrenes. *Journal of Polymer Science Part B-Polymer Physics* **1985**, *23*, 1117-1126.

[53] Lonsdale, D. E.; Bell, C. A.; Monteiro, M. J. Strategy for Rapid and High-Purity Monocyclic Polymers by CuAAC "Click" Reactions. *Macromolecules* **2010**, *43*, 3331-3339.

[54] Bernal, J. M. G.; Tirado, M. M.; Freire, J. J.; Delatorre, J. G. Monte-Carlo Calculation of Hydrodynamic Properties of Linear and Cyclic Polymers in Good Solvents. *Macromolecules* **1991**, *24*, 593-598.

[55] Jang, S. S.; Cagin, T.; Goddard, W. A. Effect of Cyclic Chain Architecture on Properties of Dilute Solutions of Polyethylene from Molecular Dynamics Simulations. *The Journal of Chemical Physics* **2003**, *119*, 1843-1854.

[56] Muller, M.; Wittmer, J. P.; Cates, M. E. Topological Effects in Ring Polymers: A Computer Simulation Study. *Physical Review E* **1996**, *53*, 5063-5074.

[57] Brown, S.; Szamel, G. Computer Simulation Study of the Structure and Dynamics of Ring Polymers. *The Journal of Chemical Physics* **1998**, *109*, 6184-6192.

[58] Jacobson, H.; Beckmann, C. O.; Stockmayer, W. H. Intramolecular Reaction in Polycondensations. II. Ring-Chain Equilibrium in Polydecamethylene Adipate. *The Journal of Chemical Physics* **1950**, *18*, 1607-1612.

[59] Geiser, D.; Höcker, H. Synthesis and Investigation of Macrocyclic Polystyrene. *Macromolecules* **1980**, *13*, 653.

[60] Hild, G.; Kohler, A.; Rempp, P. Synthesis of Ring-Shaped Macromolecules. *European Polymer Journal* **1980**, *16*, 525.

[61] Vollmert, B.; Huang, J. Coil Properties of Ring-Shaped Polymer Chains. Theoretical Calculation and Experimental Determination of $[\eta]_{ring}/[\eta]_{open}$. *Macromolecular Rapid Communications* **1980**, *1*, 333.

[62] Schappacher, M.; Deffieux, A. Synthesis of Macrocyclic Poly (2-Chloroethyl Vinyl Ether)s. *Macromolecular Rapid Communications* **1991**, *12*, 447.

[63] Kricheldorf, H. R.; Lee, S. R. Polylactones. 35. Macrocyclic and Stereoselective Polymerization of. β-D,L-Butyrolactone with Cyclic Dibutyltin Initiators. *Macromolecules* **1995**, *28*(20), 6718-6725.

[64] Whittaker, M. R.; Goh, Y. K.; Gemici, H.; Legge, T. M.; Perrier, S.; Monteiro, M. J. Synthesis of Monocyclic and Linear Polystyrene Using the Reversible Coupling/Cleavage of Thiol/Disulfide Groups. *Macromolecules* **2006**, *39*, 9028-9034.

[65] You, Y. Z.; Manickam, D. S.; Zhou, Q. H.; Oupický, D. A Versatile Approach to Reducible Vinyl Polymers via Oxidation of Telechelic Polymers Prepared by Reversible Addition Fragmentation Chain Transfer Polymerization. *Biomacromolecules* **2007**, *8*(6), 2038-2044.

[66] Tsarevsky, N. V.; Matyjaszewski, K. Reversible Redox Cleavage/Coupling of Polystyrene with Disulfide or Thiol Groups Prepared by Atom Transfer Radical Polymerization. *Macromolecules* **2002**, *35(24)*, 9009-9014.

[67] Puskas, J.E.; Rosenthal, E.Q. New Method for the Synthesis of Polydisulfide Polymers. US 8,552,143, 2013.

[68] Rosenthal-Kim, E. Q.; Puskas, J. E. Green Polymer Chemistry: Living Oxidative Polymerization of Dithiols. *Pure and Applied Chemistry* **2012**, *84*, 2121-2133.

[69] Rosenthal, E. Q.; Puskas, J. E.; Wesdemiotis, C. Green Polymer Chemistry: Living Dithiol Polymerization via Cyclic Intermediates. *Biomacromolecules* **2012**, *13*, 154-164.

[70] Liang, Y.; Gao, W.; Peng, X.; Deng, X.; Sun, C.; Wu, H.; He, B. Near Infrared Light Responsive Hybrid Nanoparticles for Synergistic Therapy. *Biomaterials* **2016**, *100*, 6-90.

[71] Neal, J.C.; Stolnik, S.; Schacht, E.; Kenawy, E.R.; Garnett, M.C.; Davis, S.S.; Illum, L. *In vitro* Displacement by Rat Serum of Adsorbed Radiolabeled Poloxamer and Poloxamine Copolymers from Model and Biodegradable Nanospheres. *Journal of Pharmaceutical Sciences* **1998**, *87*, 1242-1248.

[72] Furukawa, S.; Katayama, N.; Iizuka, T.; Urabe, I.; Okada, H. Preparation of Polyethylene Glycol-bound NAD and its Application in a Model Enzyme Reactor. *FEBS Letters* **1980**, *121*, 239-242.

[73] Shi, C.; Guo, X.; Qu, Q.; Tang, Z. Wang, Y.; Zhou, S. Actively Targeted Delivery of Anticancer Drug to Tumor Cells by Redox-Responsive Star-Shaped Micelles. *Biomaterials* **2014**, *35*, 8711-8722.

[74] Renil, M.; Ferreras, M.; Delaisse, J.M.; Foged, N.T.; Meldal, M. PEGA Supports for Combinatorial Peptide Synthesis and Solid-Phase Enzymatic Library Assays. *Journal of Peptide Science* **1998**, *4*, 195.

[75] Mutter, M. Soluble Polymers in Organic Synthesis: I. Preparation of Polymer Reagents using Polyethylene Glycol with Terminal Amino Groups as Polymeric Component. *Tetrahedron Letters* **1978**, *19*, 2839-2842.

[76] Jankoa, K.; Kops, J.: ^{1}H-NMR Investigation of Quantitative Functionalization of Poly (ethylene glycol) s. *Journal of Applied Polymer Science* **1994**, *54*, 1027-1032.

[77] Ranucci, E.; Ferruti, P. A New Synthetic Method for Amino-Terminated Poly (Ethyleneglycol) Derivatives. *Synthetic Communications* **1990**, *20*, 2951-2957.

[78] Singh, P.; Gupta, U.; Asthana, A.; Jain, N.K. Folate and Folate−PEG−PAMAM Dendrimers: Synthesis, Characterization, and Targeted Anticancer Drug Delivery Potential in Tumor Bearing Mice. *Bioconjugate Chemistry* **2008**, *19*, 2239-2252.

[79] Liu, M.; Xie, C.; Xu, W.; Lu, W. Separation of Polyethylene Glycols and their Amino-Substituted Derivatives by High-Performance Gel Filtration Chromatography at Low Ionic Strength with Refractive Index Detection. *Journal of Chromatography A* **2004**, *1046*, 121-126.

[80] Sakai, T.; Matsunaga, T.; Yamamoto, Y.; Ito, C.; Yoshida, R.; Suzuki, S.; Sasaki, N.; Shibayama, M.; Chung U.I. Design and Fabrication of a High-Strength Hydrogel with Ideally Homogeneous Network Structure from Tetrahedron-like Macromonomers. *Macromolecules* **2008**, *41*, 5379-5384.

[81] Wang, L.; Wang S. Synthesis and Characterization of Macroinitiator-Amino Terminated PEG and Poly (γ-Benzyl-L-Glutamate)-PEO-Poly (γ-Benzyl-L-Glutamate) Triblock Copolymer. *Polymers for Advanced Technologies* **2004**, *15*, 617-621.

[82] Geckeler K. Functionalization of Soluble Polymers. *Polymer Bulletin* **1979**, *1*, 427-431.

[83] Wiss, K.T.; Kessler, D.; Wendorff, T.J.; Theato, P. Versatile Responsive Surfaces via Hybrid Polymers Containing Acetal Side Groups. *Macromolecular Chemistry and Physics* **2009**, *210*, 1201-1209.

[84] Mongondry, P.; Bonnans-Plaisance, C.; Jean, M.; Tassin, J.F. Mild Synthesis of Amino-Poly (Ethylene Glycol)s. Application to Steric Stabilization of Clays. *Macromolecular Rapid Communications* **2003**, *24*, 681-685.

[85] Fu, Y.; Nitecki, D.E.; Maltby, D.; Simon, G.H.; Berejnoi, K.; Raatschen, H.J.; Yeh, B.M.; Shames, D.M.; Brasch, R.C. Dendritic Iodinated Contrast Agents with PEG-Cores for CT Imaging: Synthesis and Preliminary Characterization. *Bioconjugate Chemistry* **2006**, *17*, 1043-1056.

[86] Pawar, G.M.; Koenigs, M.; Fahimi, Z.; Cox, M.; Voets, I.K.; Wyss, H.M.; Sijbesma, R.P. Injectable Hydrogels from Segmented PEG-Bisurea Copolymers. *Biomacromolecules* **2012**, *13*, 3966-3976.

[87] Fu, X.; Shen, Y.; Ma, Y.; Fu, W.; Li, Z. Tunable Supramolecular Hydrogels from Polypeptide-PEG-Polypeptide Triblock Copolymers. *Science China Chemistry* **2015**, *58*, 1005-1012.

[88] Zalipsky, S.; Chang, J.L.; Albericio, F.; Barany, G. Preparation and Applications of Polyethylene Glycol-Polystyrene Graft Resin Supports for Solid-Phase Peptide Synthesis. *Reactive Polymers* **1994**, *22*, 243-258.

[89] Lehninger, A. L.; Nelson, D. L.; Cox, M. M. Amino Acids, Peptides, and Proteins. In *Lehninger: Principles of Biochemistry*; W.H. Freeman: New York, 2004, ISBN 0-7167-4339-6.

[90] Bardaweel, S. K.; Abu-Dahab, R.; Almomani, N. F. An *In Vitro* Based Investigation into the Cytotoxic Effects of D-amino acids. *Acta Pharmaceutica* **2013**, *63(4)*, 467-478.

[91] Nudelman, A.; Bechor, Y.; Falb, E.; Fischer, B.; Wexler, B.A. Acetyl Chloride-Methanol as a Convenient Reagent for: A) Quantitative Formation of Amine Hydrochlorides B) Carboxylate Ester Formation C) Mild Removal of Nt-Boc-Protective Group. *Synthetic Communications* **1998**, *28*, 471-474.

[92] Puskas, J. E.; Castano, M.; Mulay, P.; Dudipala, V.; Wesdemiotis, C. Method for the Synthesis of γ-PEGylated Folic Acid and Its Fluorescein-Labeled Derivative. *Macromolecules* **2018**, *51(22)*, 9069-9077.

[93] Wang, S.; Luo, J.; Lantrip, D. A.; Waters, D. J.; Mathias, C. J.; Green, M. A.; Fuchs, P. L.; Low, P. S. Design and Synthesis of [^{111}In]DTPA-Folate for Use as a Tumor-Targeted Radiopharmaceutical. *Bioconjugate Chemistry* **1997**, *8*, 673-679.

[94] Cho, B. K.; Roy, E. J.; Patrick, T. A.; Kranz, D. M. Single-Chain Fv/Folate Conjugates Mediate Efficient Lysis of Folate-Receptor-Positive Tumor Cells. *Bioconjugate Chemistry* **1997**, *8*, 338-346.

[95] Schneider, R.; Schmitt, F.; Frochot, C.; Fort, Y.; Lourette, N.; Guillemin, F.; Muller, J. F.; Barberi-Heyob, M. Design, Synthesis, and Biological Evaluation of Folic Acid Targeted Tetraphenylporphyrin as Novel Photosensitizers for Selective Photodynamic Therapy. *Bioorganic & Medicinal Chemistry* **2005**, *13*, 2799-2808.

[96] Kohler, N.; Fryxell, G. E.; Zhang, M. A Bifunctional Poly(ethylene glycol) Silane Immobilized on Metallic Oxide-Based Nanoparticles for Conjugation with Cell Targeting Agents. *Journal of the American Chemical Society* **2004**, *126*, 7206-7211.

[97] Licciardi, M.; Tang, Y.; Billingham, N. C.; Armes, S. P.; Lewis, A. L. Synthesis of Novel Folic Acid-Functionalized Biocompatible Block Copolymers by Atom Transfer Radical Polymerization for Gene Delivery and Encapsulation of Hydrophobic Drugs. *Biomacromolecules* **2005**, *6*, 1085-1096.

[98] De, P.; Gondi, S. R.; Sumerlin, B. S. Folate-Conjugated Thermoresponsive Block Copolymers: Highly Efficient Conjugation and Solution Self-Assembly. *Biomacromolecules* **2008**, *9*, 1064-1070.

[99] Seo, K.S. Design and Synthesis of Multifunctional Poly(Ethylene Glycol)s using Enzymatic Catalysis for Multivalent Cancer Drug Delivery. Ph.D. Dissertation, The University of Akron, Akron, OH, 2012.

[100] Poe, M. Acidic Dissociation Constants of Folic Acid, Dihydrofolic Acid, and Methotrexate. *Journal of Biological Chemistry* **1977**, *252(11)*, 3724-3728.

[101] Mindt, T. L.; Muller, C.; Melis, M.; de Jong, M.; Schibli, R. "Click-to-Chelate": *In Vitro* and *In Vivo* Comparison of a $^{99m}Tc(CO)_3$-Labeled N(τ)-Histidine Folate Derivative with Its Isostructural, Clicked 1,2,3-Triazole Analogue. *Bioconjugate Chemistry* **2008**, *19*, 1689-1695.

[102] Mahou, R.; Wandrey, C. Versatile Route to Synthesize Heterobifunctional Poly(Ethylene Glycol) of Variable Functionality for Subsequent PEGylation. *Polymers* **2012**, *4(1)*, 561-589.

[103] Goessl, A.; Tirelli, N.; Hubbell, J.A. A Hydrogel System for Stimulus-Responsive, Oxygen-Sensitive In Situ Gelation. *Journal of Biomaterials Science, Polymer Edition* **2004**, *15*, 895-904.

[104] Buwalda, S.J.; Dijkstra, P.J.; Feijen, J. In Situ Forming Poly(Ethylene Glycol)-Poly(L-Lactide) Hydrogels via Michael Addition: Mechanical Properties, Degradation, and Protein Release. *Macromolecular Chemistry and Physics* **2012**, *213*, 766-775.

[105] Hiemstra, C.; van der Aa, L.J.; Zhong, Z.; Dijkstra, P.J.; Feijen, J. Novel In Situ Forming, Degradable Dextran Hydrogels by Michael Addition Chemistry: Synthesis, Rheology, and Degradation. *Macromolecules* **2007**, *40*.

[106] Yoshimoto, K.; Hirase, T.; Nemoto, S.; Hatta, T.; Nagasaki, Y. Facile Construction of Sulfanyl-Terminated Poly(Ethylene Glycol)-Brushed Layer on a Gold Surface for Protein Immobilization by the Combined use of Sulfanyl-Ended Telechelic and Semitelechelic Poly(Ethylene Glycol)s. *Langmuir* **2008**, *24*, 9623-9629.

[107] Hirase, T.; Nagasaki, Y. Construction of Mercapto-Ended Poly(Ethylene Glycol) Tethered Chain Surface for High Performance Bioconjugation. In Proceedings of the AIChE Annual Meeting, San Francisco, CA, USA, November 2006.

[108] Nie, T.; Baldwin, A.; Yamaguchi, N.; Kiick, K.L. Production of Heparin-Functionalized Hydrogels for the Development of Responsive and Controlled Growth Factor Delivery Systems. *Journal of Controlled Release* **2007**, *122*, 287-296.

[109] Belair, D.G.; Miller, M.J.; Wang, S.; Darjatmoko, S.R.; Binder, B.Y.; Sheibani, N.; Murphy, W.L. Differential Regulation of Angiogenesis using Degradable VEGF-Binding Microspheres. *Biomaterials* **2016**, *93*, 7-37.

[110] Yu, H.; Feng, Z.G.; Zhang, A.Y.; Sun, L.G.; Qian, L. Synthesis and Characterization of Three-Dimensional Crosslinked Networks Based on Self-Assemly of α-Cyclodextrins with Thiolated 4-arm PEG using a Three-Step Oxidation. *Soft Matter* **2006**, *2*, 343-349.

[111] Du, Y.J.; Brash, J.L. Synthesis and Characterization of thiol-terminated Poly(Ethylene Oxide) for Chemisorption to Gold Surface. *Journal of Applied Polymer Science* **2003**, *90*, 594-607.

[112] Wan, J. K. S.; Depew, M. C. Some Mechanistic Insights in the Behaviour of Thiol Containing Antioxidant Polymers in Lignin Oxidation Processes. *Research on Chemical Intermediate*s **1996**, *22*, 241-253.

[113] Yang, T.; Long, H.; Malkoch, M.; Kristofer Gamstedt, E.; Berglund, L.; Hult, A. Characterization of Well-Defined Poly(Ethylene Glycol) Hydrogels Prepared by Thiol-Ene Chemistry. *Journal of Polymer Science Part A: Polymer Chemistry* **2011**, *49*, 4044-4054.

[114] Zhang, H.J.; Xin, Y.; Yan, Q.; Zhou, L.L.; Peng, L.; Yuan, J.Y. Facile and Efficient Fabrication of Photoresponsive Microgels via Thiol–Michael Addition. *Macromolecular Rapid Communications* **2012**, *33*, 1952-1957.

[115] Zustiak, S.P.; Leach, J.B. Hydrolytically Degradable Poly(Ethylene Glycol) Hydrogel Scaffolds with Tunable Degradation and Mechanical Properties. *Biomacromolecules* **2010**, *11*, 1348-1357.

[116] Zustiak, S.P. Hydrolytically Degradable Polyethylene Glycol (PEG) Hydrogel: Synthesis, Gel Formation, and Characterization. In *Extracellular Matrix*; Leach, J., Powell, E., Eds.; Humana Press: New York, NY, USA, 2015; Vol. 93, ISBN 978-1-4939-2082-2.

[117] Arroyo, M.; Sinisterra, J. V. High Enantioselective Esterification of 2-Arylpropionic Acids Catalyzed by Immobilized Lipase from *Candida antarctica*: A Mechanistic Approach. *The Journal of Organic Chemistry* **1994**, *59*, 4410-4417.

[118] Patzek, T. W. A First Law Thermodynamic Analysis of Biodiesel Production from Soybean. *Bulletin of Science, Technology & Society* **2009**, *29(3)*, 194-204.

[119] Gooch, E. E. Determination of the Iodine Value of Selected Oils: An Experiment Combining FTIR Spectroscopy with Iodometric Titrations. *The Chemical Educator* **2001**, *6(1)*, 7-9.

APPENDICES

APPENDIX A

INTERNSHIP REPORT

A short summary of observations and tasks performed noted during the internship that I pursued at Philpott Rubber Company, Aurora, OH from July – December 2018 is described in the following report.

A.1. Training received for operating injection and compression molding machines

In my training period, I shadowed operators everyday who dealt with raw material, tooling, plastic injection molding, plastic secondary operation, rubber molding, cast urethane, and quality and inspection. My observations are listed below:

A.1.1 Orientation/Safety, Raw Material, Tooling

Operator: William James

Observation: The responsibility of the floor supervisor is to ready the injection molding machines every morning: Prepare the mix for molding, change the molds in the machine according to the requirement, set the extruder and nozzle temperature, fill the hopper with the raw material (dry it if necessary by starting the air dryer in the hopper). He performs secondary plastic operations and molding operations during break time of the operators. He also regrinds the thermoplastic elastomer waste produced by trimming the flashes off the molded parts.

Raw Material Mixing for Thermoplastic Elastomers (TPEs):

Regrinding of TPEs from previous batch (1 part) + New TPE (2 parts) + Pelletized/Powdered Dye (1 pound per 40 pound TPE). TPE raw material mixture was mixed on a drum mixer for 10 minutes and then loaded in the hopper using a suction pump. Nylon, Polyurethanes, and Rubber are never regrinded. All the materials are in the pelletized form, except the rubber for rubber compression molding and polyurethane for cast urethane process. Nylon is hot air dried overnight in the hopper to be molded the next day.

Tooling: I observed the mold changing process in the injection molding machine (Van Dorn 120) and also how to start the machine.

A.1.2 Plastic Injection Molding and Secondary Plastic Operations:

Task 1: Molding Nylon Blocks (215 parts to be made)

Operator: Morgan

Machine: Van Dorn

It is a thermoplastic injection molding machine.

Process Parameters:

Temperature: Nozzle = 540^{o} C, eventually reduced to 490^{o} C; Extruder = 510^{o} C.

Material Volume = Unknown to the operator, but the extruder pulls back 5.5 inches.

Injection time = 5 s, Material filling time in the extruder = 30 s

Boost Pressure = 820 psi

Procedure: Glass reinforced Nylon pellets (~38 pounds) were loaded in the hopper manually and were hot air dried overnight to remove moisture traces. An automatic timer was set to stop the hot air drying for 7 am the following morning. Molds were also replaced. They were sprayed with mold releasing agent. The machine was set to operation the following morning. The molded part was manually removed from the

machine and was transferred to a hot water bath (with electrical coil heating) for ~20 minutes. The nylon block was then removed from the bath, the flashes were cut off and the part was kept on a plate to be taken for drilling a hole in it.

Observation: The first molded parts were faulty, having cracks, so they had to be discarded. The first few parts had a lot of flash (extra material from molding) on it, therefore, the nozzle temperature was reduced to 490^{o} C. Also, a lot of parts cracked while drilling hole in them. 183 were parts made.

Figure A.1.1. Van Dorn Thermoplastic Injection Molding Machine

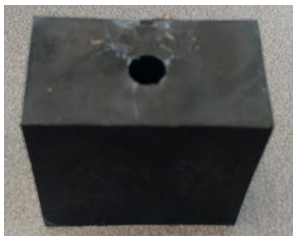

Figure A.1.2. Finished Product (Nylon Block)

Task 2: Molding Santoprene (TPE) Diaphgrams (to be used in Air Operated Double Diaphgram Pumps) (1200 parts/day)

Operator: Mike Morgan

Machine: Van Dorn 50

It is a 50 ton thermoplastic injection molding machine.

Process Parameters:

Temperature: Nozzle = 400^{o} C, eventually reduced to 390^{o} C; Extruder = 410^{o} C.

Material Volume = Unknown to the operator, but the extruder pulls back 1.5 inches?

Injection time = 5 s, Material filling time in the extruder = 12 s

Boost Pressure = 880 psi

Procedure: Santoprene pellets were loaded in the hopper using suction pump. The machine was set to operation in the morning. The molded part was manually removed from the machine and was air cooled for ~5 minutes. The flashes were trimmed off (this requires skills!) and the parts were stacked (20/stack). The parts were then sent for drilling holes in them (secondary plastic operation). Every 10^{th} piece was inspected by the operator for quality.

Observation: The first 4-5 pieces came out in a darker shade and were therefore discarded. The flashed material was collected and was regrinded in a regrinding machine.

Figure A.1.3. Van Dorn 50 Thermoplastic Injection Molding Machine

Figure A.1.4. Finished Product (Santoprene Diaphgram)

Figure A.1.5. Regrinder

Plastic Secondary Operation:

Task 3: Punching Hole in the TPE Diaphgram

Operator: Jannet

Machine: Bridgeport

Procedure: A complimentary mold (like a positive mold on which the molded can be kept such that the molded part does not move – hard to explain, I'll see if I get the pictures) was kept on the work desk. The molded part was fixed on the complimentary mold and a hole was punched on it with the help of the drilling machine. The drilled parts were then stacked and were packed 40 in a box. The boxes were then sealed and transferred to the shipping area.

Figure A.1.6. A Hole Punching Machine

Task 4: Removing Flashes from the Nylon Rings

These rings have applications as sealants for canisters used in the military.

Operator: Janette

Procedure: The molded white rings were investigated for flashes (extra material from molding) and for any dust particles on the white rings. The parts with dust particles were discarded. The rings with flashes were kept 6 on a tray and a torch was blown over them to melt the flashes. The rings were then packed (400/box).

A.1.3 Rubber Molding and Cast Urethane:

Rubber Molding:

Rubber Gasket:

Operator: Laurel

Machine: Pan Stone

It is a digitally controlled 800 ton rubber compression press.

Process Parameters:

Temperature: 325^{o} C

Compression Time = 120 s, then 2 times cool off with 1 s (the mold does not open, it just lowers to let some air in via the holes on the mold), then 540 s.

Procedure: The custom rubber blend was in the form of solid tubes. These tubes were cut to the required length for the mold. The tube was laid such that it exactly fits the mold, any extra material was cut off or if it was short of material, some material was cut off from the tube and was laid on the mold. The operation was started. The molded rubber gasket was then removed from the mold manually and was cooled for 3 minutes. The flashes were then trimmed off using a scissor. The molded parts were then packed in a box.

Figure A.1.7. Pan Stone Compression Molding Machine (Mold used was different than the picture)

Cast Urethane:

Operator: Tom

No machine as such, but the molds are kept heated on a heated table (200^{o} C). PU's are soft but have high Shore Hardness (meaning, they are tough).

Task 1: Yellow Coil Saddle

This product is used as an anti-slip base for keeping large metal coils over them.

Procedure: The raw materials are kept in digitally and pneumatically controlled dispensing machines, each raw material in a different dispensing machine. These machines keep the raw material at set temperatures. The raw materials are kept heated in these machines. The blend recipes are already saved in the controller. The recipe for the yellow Coil Saddle is selected and ~8kg polymer (PU with Polyether backbone) is dispensed in a bucket. A liquid yellow dye was added to the polymer (~18g) and this step was repeated for two more times in two separate buckets. The curing agent or the "curative" was then dispensed into each of the buckets (~1.2kg). And the mixture was homogenized by placing the bucket in a vortex mixer. Mixing time was approximately 10 s. This process was repeated with the other two buckets. A mold release agent was applied to the mold. The mold was fitted with nuts and bolts and also a washer (the final application demands a washer to be inside the mold to

later fix nuts and bolts through it). All the homogenized polymer mixture was poured onto the heated mold and it was cured for ~20 minutes. The casted material was removed from the mold by first removing the nuts and lifting the material from the cast. The bolts were then removed. The casted material was placed on a large tray and was then kept in a heated oven (200^{o} C) overnight.

Figure A.1.8. The Heated Polymer and Curative Dispensing Machine

Figure A.1.9. Mold for Yellow Coil Saddle

Figure A.1.10 Overnight Curing Ovens

Task 2: Red Gasket Ring

This product has application in pumps.

Procedure: A polymer blend was used to make this part (PU with Polyester backbone used) along with red dye and a curative. The mixture was homogenised on a vortex

mixer for 10 s and was then poured into the mold. The molds for these were circular in shape. They were cured for ~10 minutes and were then cured overnight. The parts were then pressed to obtain holes around the circumference.

Figure A.1.11. Cast for Red Gasket Ring kept over the heated table

A.1.4 Quality and Inspection:

Inspector: Peggy May

Performed Caliper Measurements on the molded parts taken for quality inspection. Measured the Shore A Hardness and Shore D Hardness for materials demanding these measurements. 3 molded parts from each operation were inspected every 2 hours. The measurements were documented.

A.1.5 3D scanning and Polyworks:

The 3D scanner along with its workstation software is shown in the figure A.1.12. In the first two months of my internship, I learned how to operate the Nikon ModelMaker MMDX – Handheld 3D scanner and developed an expertise in using PolyWorks software. The 3D laser scanner scans objects and creates its point cloud in the PolyWorks software. This scanner is useful in measuring dimensions on injection molded objects and screens them for defects. It is also used for reverse engineering parts to design custom molds. I used the 3D scanner primarily for measuring

dimensions on injection molded parts and evaluate the deviation from their nominal measurements obtained from their CAD model.

Figure A.1.12. 3D Scanner with Polyworks software running on the computer

A.2. Injection Molding of Rubber Bullets

We tried to mold 2018PFM-5 Batch#1 (called 'the material' henceforth) obtained from PolyFiberMatrix, LLC into small plastic caps on Arburg Allrounder 320C Injection Molding Machine (shown in Figure A.1.13) at Philpott Solutions, Aurora, OH.

Figure A.1.13. Arburg Allrounder 320C Injection Molding Machine

Procedure: The machine was switched on and set to conditions mentioned in the sheet from PolyFiberMatrix, LLC. The screw rotation rpm was set to 165 rpm and the nozzle temperature was set at 400F. The injection carriage was fed with strips of the material, but the throat was not taking in the strips. The strips were curling up in the throat (as shown in Figure A.1.14.B). Therefore, the material was cut into pieces

small enough for the throat to take in the material (as shown in Figure A.1.14.A). The machine had nylon material in the injection carriage form the previous molding. It had to be purged out; therefore, a purge material was fed to the screw to empty out the injection carriage. The nozzle was removed and the injection carriage was purged at a nozzle temperature of 520 F.

Figure A.1.14. (A) Small Pieces of the material that were fed to the machine. (B) Curled up material strips from the throat of the injection carriage.

After purging, the nozzle was fixed again to the injection carriage. The material was cut into thin strips (~1cm thickness and ~30cm length) and was tried to be fed to the throat of the injection carriage. The throat was allowing the passage of these strips into the injection carriage. The molding was set into operation. The machine was molding the leftover purge material for the first few pieces. The nozzle temperature was reduced to 450F and the Zone temperatures were set as shown in Figure A.1.15. The nozzle was removed to extrude out hold up material until our material was observed to fall out instead of the purge material. The nozzle was fixed again to the injection carriage and the molding was set to operation. The injection pressure was increased to 18000 psi. The molded parts are shown in Figure A.1.16.

Figure A.1.15. Injection Carriage temperatures

Figure A.1.16. Injection Molded Caps from 2018PFM-5Batch#1

After two days from the previous operation, the machine was switched on and set to previously established conditions. The nozzle was removed and the injection carriage was emptied of any previous material. The nozzle was fixed again and the machine was set to operation. The throat was fed with the cut pieces of the material. This time, there was no issue with accepting of the material, it readily went in the injection carriage. A mold release agent was sprayed on the mold. The temperature conditions are shown in Figure A.1.17, the nozzle temperature being 430F. The injection parameters are shown in Figure A.1.18.

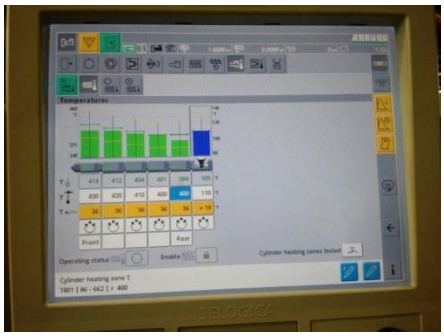

Figure A.1.17. Temperature conditions for molding 2018PFM-5Batch#1

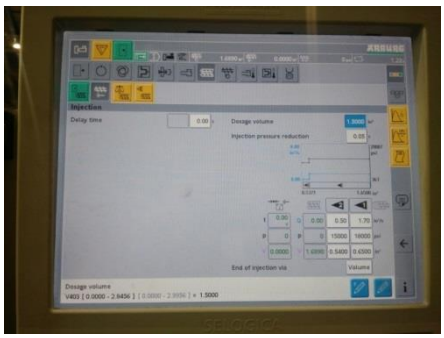

Figure A.1.18. Injection parameters for molding 2018PFM-5Batch#1

Spraying mold release agent is a must for injection molding this material. If the mold release is not sprayed, a difficulty in removing the parts from the mold were observed, which eventually deformed the parts as shown in Figure A.1.19.

Figure A.1.19. Appearance of molded parts from 2018PFM-5Batch#1 without using a mold release agent

The cooling time (time between injection and mold release) was decreased from 60s to 45s to save time on the operation. However, a difficulty was observed in removing the parts from the mold. It was observed that even at 60 s, there was a slight difficulty in removing the parts, therefore, the cooling time was increased to 70 s, and it was observed that all the 4 molded parts came out of the mold easily. The dosage volume was reduced from 1.5 in^3 to 1.2 in^3 because it was observed that the screw did not push the material all the way into the mold, therefore, there was some hold up. To avoid this hold up, the dosage volume was reduced. However, it was observed that complete parts were not molded, as shown in Figure A.1.20. The molded parts are shown in Figure A.1.21.

Figure A.1.20. Incomplete molded parts from 2018PFM-5Batch#1 due to low injection volume

Figure A.1.21. Molded parts from 2018PFM-5Batch#1

A.3 Rubber Bullet Polymer Compounding for Tacticity quantification

The material used for molding parts discussed in section A.2, that is 2018PFM-5Batch#1, was tacky. Strips of the material were sticking to each other; therefore, a mold release agent was constantly used to remove the caps from the mold after each operation. This prolongs the operation time. Therefore, it is desirable to add an anti-tack agent into the material while compounding such that the material exhibits non-tacky behavior.

In the following study, the tacticity of the material is attempted to be quantified using two kinds of anti-tack agents in the material. The anti-tack agent providing a more anti-tack behavior will then be used in the commercial blend of the material. SIBS and Butyl Rubber blends with varying compositions of Zinc Oxide, Carbon Black N550, and Anti-tack agent (HPS11 or WS180 from Struktol Company of America) were compounded in order to be compression molded into polymer strips which will be then used for tacticity quantification.

Blend Recipes:

1. In parts per hundred rubber (phr):

Fill Factor		76	76	76	76	76	76	76
Volume(cc):	SP.GR.	64.6	64.6	64.6	64.6	64.6	64.6	64.6
Exxon Butyl 268	0.92	50.00	50.00	50.00	50.00	50.00	50.00	50.00
SIBS 073T	0.95	50.00	50.00	50.00	50.00	50.00	50.00	50.00
ZnO	5.57	277.0	262.0	247.0	290.0	286.0	270.0	255.0
Carbon Black N550	1.82		5.00	10.00			5.00	10.00
HPS11 (3-5phr)	0.98				5.00			
WS180 (1-3phr}	0.95					5.00	5.00	5.00
Total PHR		377.0	367.0	357.0	395.0	391.0	380.0	370.0
SP.GR.		2.41	2.34	2.28	2.41	2.39	2.33	2.27

Compounding:

The compound blends' nanofillers were prepared with a Branbender Mixer (Brabender, Intelli-Torque Plasti-Corder, USA) with REE6 Mixing Bowl (Sigma) in addition to Banbury, Roller and CAM Blades. The mixer has a 40 - 80 g capacity and single screw extruder attachment with strand die. First, 10 minutes per batch, 60 RPM, and 120^{o}C were used as the mixing conditions. The compound was removed from the mixer maximum of 10 minutes and the filler was scraped off from the wall of the mixer. This procedure was repeated one additional time. After mixing, the compounds were subjected to milling involving the preparation of a thin (0.5 – 1 mm) film. The films were then folded and 20,000 PSI pressure was applied to prepare a thin film from the folded polymer. This folding and compression cycle was repeated 2-3 times to ensure good dispersion of polymer or compound matrix.

2. In grams:

STOCK ID:	PM_2018_08_14_1	PM_2018_08_14_3	PM_2018_08_14_4	PM_2018_08_14_5	PM_2018_08_14_7
Exxon Butyl 268 (g)	20.64	20.63	19.70	19.77	19.78
SIBS 073T (g)	20.64	20.63	19.70	19.77	19.78
ZnO (g)	114.35	101.89	114.28	113.09	100.88
Carbon Black N550 (g)		4.13			3.96
HPS11 (g)			1.97		
WS180 (g)				1.98	1.98

3. Filler Volume %:

	1	3	4	5	7
	PM_2018_08_14 1	PM_2018_08_14 3	PM_2018_08_14 4	PM_2018_08_14 5	PM_2018_08_14 7
V tot	64.6	64.6	64.6	64.6	64.6
V ZnO	20.5	18.3	20.5	20.3	18.1
V Carbon Black		2.3			2.2
V HPS11			2.0		
V WS180				2.1	2.1
Filler vol%	31.8	31.8	31.8	31.4	31.4

Figure A.1.22: Brabender Mixer

Mixing

Temperature 110.00 C

rpm 60.00

Mix time 3 minutes after everything is in.

Refining

Use large press. T=248 F

Use as low pressure as possible.

Fold and press three times.

Compression Molding:

Prior to molding, weights of polymer from mixing were obtained for processing yield of compounds. Press was first heated to 220˚F. Polymer batches were pressed between Teflon sheets to create flat uniform sheet of 1 mm thick. This sheet

was cut into strips, and then further cut and inserted into the mold (5.1 cm x 4.5 cm x 0.3 cm). Teflon was placed on top of circular punches and place system in hydraulic press platens. System was put under approximately 5000 PSI for 5 minutes. Molding system was then allowed to cool to room temperature (under a load) before opening mold. The flashes were removed from the molded material and the material was cut into strips of 2.25 cm x 5.1 cm. The strips were placed on top of each other such that the contact area has a dimension of 2.25 cm x 4 cm.

Specimen:

Specimens were prepared from the following mixes:

PM_2018_08_14_1: 2 specimens – 1A and 1B (No Carbon Black)

PM_2018_08_14_4: 1 specimen (No Carbon Black)

PM_2018_08_14_5: 1 specimen (No Carbon Black)

PM_2018_08_14_3: 1 specimen

PM_2018_08_14_7: 2 specimens – 7A and 7B**.**

Total 7 Specimens.

A specimen with dimensions (width = 2.25 cm and thickness ≅ 0.6 mm) was prepared and kept under a load of 12.4 kg (for 12 samples) for 72 h. An example is given in Figure A.1.23.

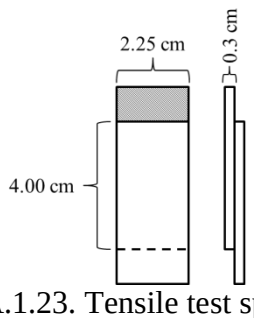

Figure A.1.23. Tensile test specimen

Instrumental:

Tensile testing was carried out on an Instron 5567 equipment with a 1000-N load cell using above described specimens (contact length = 40 mm, neck width = 22.5 mm and thickness = 0.6 mm) and a crosshead speed of 50 mm/min.

The specimen was mounted on the brackets. The distance between the brackets was measured as 44 mm.

The crosshead and the computer were started. The test was monitored until the two pieces came apart. The measurement was repeated the other 6 samples.

Results:

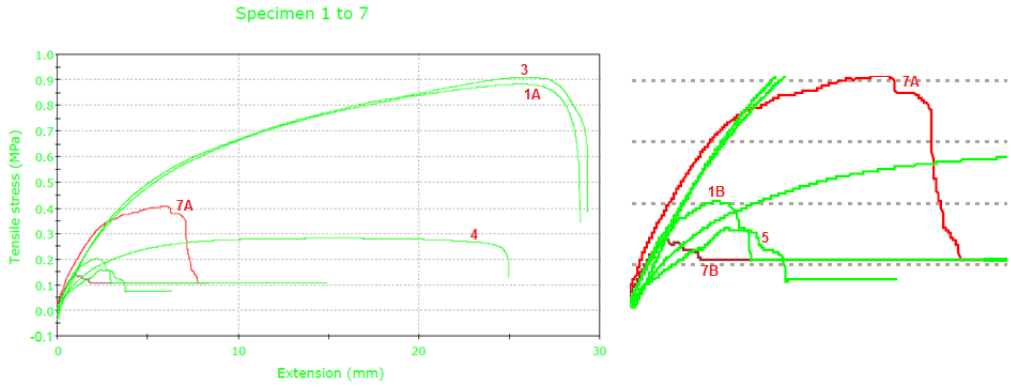

Figure A.1.24. Tensile Test Results

The results were inconsistent as seen in Figure A.1.24. The replicates (1A and 1B, 7A and 7B) did not demonstrate similar trend as seen from the figure. Therefore, redoing the compression molding and the experiment was suggested.

Compression Molding Part 2:

The mixes were again compression molded and specimens were prepared from them since results from the previous tensile test were not conclusive.

The mixes chosen for compression molding were:

PM_2018_08_14_1: 2 samples – 1A and 1B (No Carbon Black)

PM_2018_08_14_5: 2 samples – 5A and 5B (No Carbon Black)

PM_2018_08_14_3: 1 sample

PM_2018_08_14_7: 2 samples – 7A and 7B**.**

Total 7 Samples.

Prior to molding, weights of polymer from mixing were obtained for processing yield of compounds. Press was first heated to 220˚F. Polymer batches were pressed between Teflon sheets to create flat uniform sheet of 1 mm thick. This sheet was cut into strips, and then further cut and inserted into the mold (5.1 cm x 4.5 cm x 0.3 cm). Teflon was placed on top of circular punches and place system in hydraulic press platens. System was put under approximately 5000 PSI for 5 minutes. Molding system was then allowed to cool to room temperature (under a load) before opening mold. The flashes were removed from the molded material and the material was cut into strips of 2.25 cm x 5.1 cm. The strips were placed on top of each other such that the contact area has a dimension of 2.25 cm x 4 cm. An example is given in Figure 1.

These strips were laid over a steel plate and were covered with a steel plate of same dimension. A load of 12.4 kg was then kept on the steel plate. The experiment will continue for 72 hours. After 72 h, the load was removed. However, while attempting to remove the top steel plate that was stuck to the samples, specimen 5A and 7A came apart and therefore, were not used for tensile measurement.

Results:

The repeat results were consistent when compared with their original results. The samples that did not contain the anti-tack agent (1A R, 1B R, 3, 3R) demonstrated high tensile stress (> 100N) with long elongation that translates to high tacticity. Therefore, the strips did not come apart easily and were adhered to each other with a stronger force than that required for breaking the specimen. On the other hand, the samples containing the anti-tack agents (5B, 5B R, 7B, 7B R) demonstrated lower

tensile stresses with lesser extension of the sample than seen in samples without anti-tack agents. These samples came apart easily translating to a significantly lower tack. Therefore, it can be concluded that the addition of the anti-tack agent plays a significant role in reducing the tacticity of the thermoplastic elastomer.

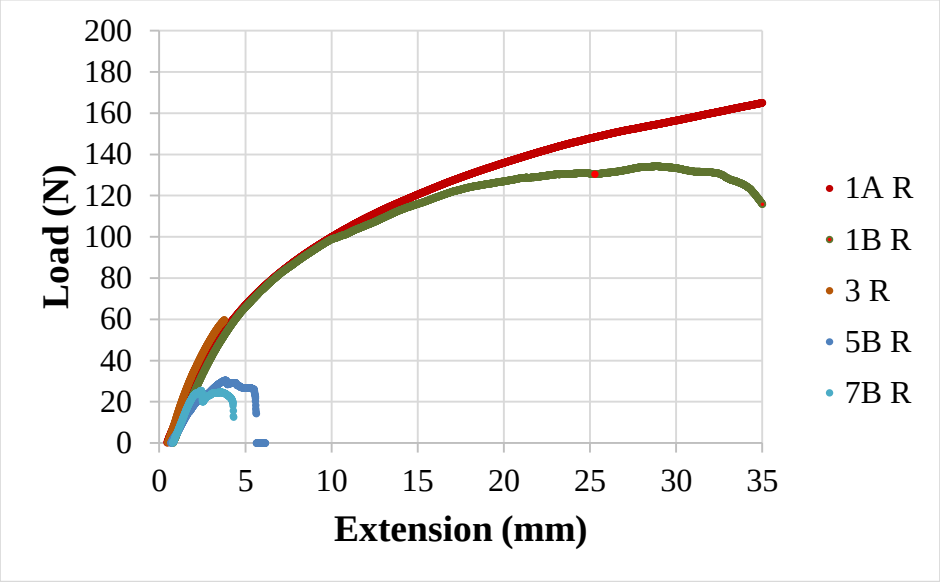

Figure A.1.25. Load vs. Extension plot for the repeat experiments (R represents Repeat) conducted on 2018_08_27

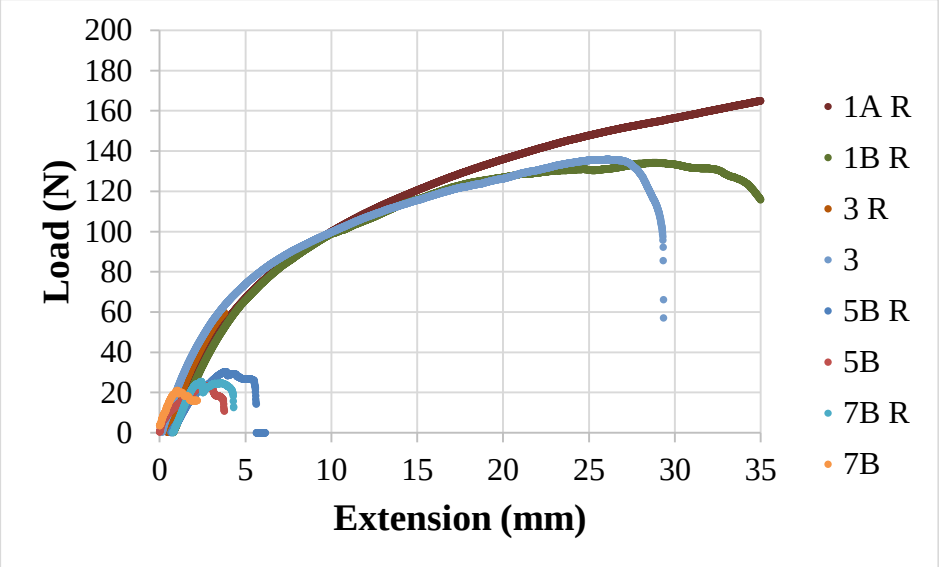

Figure A.1.26. Load vs. Extension plot for the original and the repeat experiments (R represents Repeat)

A.4 Injection Molding of a commercial part using Design of Experiments

The goals of this experiment were to injection mold Part #1-2520 (Figure A.1.27A) and optimize the process parameters. This part was already molded in the China facility of Philpott Rubber Solutions, however, the customer requirement was that the Part#1-2518 shown in Figure A.1.27(B) must easily fall and fit in to the grooved teeth present on Part#1-2520. With present injection molding parameters, the Part#1-2518 was fitting into Part#1-2520, however, it was not falling easily into it. Therefore, an experimental design was set up with varying levels of parameters as shown in Table A.1.

This part is made up of glass filled nylon; therefore, it hardens as soon as the nylon enters the mold. Therefore, the injection pressure is one of the key parameters. The Part#1-2520 was molded on VanDorn 230 Injection Molding Machine at Philpott Solutions, Aurora, OH. This machine has a capability of running at a maximum and minimum injection pressure of 2000 psi and 500 psi. However, the nylon did not fill the mold when the injection pressure was 500 psi as shown in Figure A.1.28. Therefore, the low injection pressure was set at 1000 psi. The hold time was set at a maximum and minimum of 10 s and 1 s respectively. Since the glass-filled nylon hardens quickly as it enters the mold, the hold time parameter does not affect the processing significantly. Therefore, to save processing time, this parameter was not varied beyond 10 s. The closing time is an influential parameter on the process; the glass fillers align and shrink in the mold during the closing time, therefore, affecting the process. The closing time was set at a maximum and minimum of 25 s and 5 s respectively. The molded parts require a cooling time of at least half an hour. Three parts were molded for each experiment mentioned in the design; therefore, three replicates were obtained.

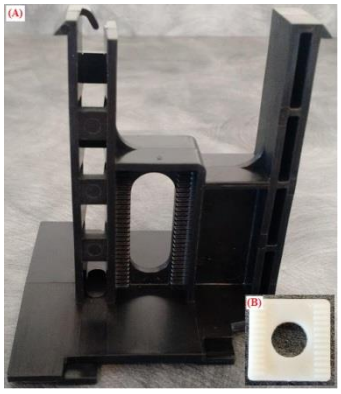

Figure A.1.27. (A) Part#1-2520 and (B) Part#1-2518

Table A.1. Experimental Design for Part#1-2520 Injection Molding

Experiment No.	Injection Pressure (psi)	Hold Time (s)	Closing Time (s)
1	2000	10	25
2	2000	10	5
3	2000	1	25
4	2000	1	5
5	1000	10	25
6	1000	10	5
7	1000	1	25
8	1000	1	5


Figure A.1.28. Injection molded part with 500 psi injection pressure

Results:

a. Splay was observed on the parts molded with parameters suggested in experiments 1-4. This was expected since the nylon was black in color and the injection carriage had traces of previously molded material in the machine that was white.

b. If the injection pressure was high, that is 2000 psi, flash was observed on the molded part.

c. If the closing time is short, that is 5 s, the molded part does not receive enough cooling time inside the mold, and therefore, it comes out of the mold at a higher temperature than the mold itself (150F).

d. For experiments with low injection pressure and low closing time, disproportionate warping was observed as shown in Figure A.1.29.

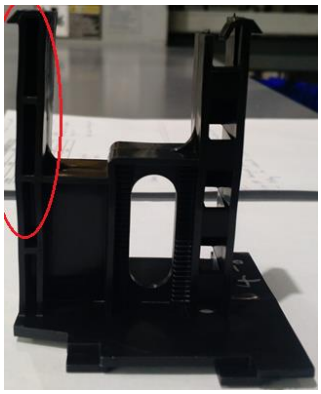

Figure A.1.29. A warped molded part

To determine the parameters that gave desired results, a preliminary test of fitting the Part#1-2518 into the cooled injection molded parts was performed. It was observed that none of the experiments yielded the desired outcome except for replicate #2 in experiment 1. The outcome is shown in Table A.2.

Experiment 1 and 3 did not show significant difference in the outcome, therefore, it can be concluded that hold time does not have a significant effect on the outcome.

Part#1-2518 had to be pushed with force to fit into the molded parts which were molded with parameters suggested in experiments with low injection pressure and low closing time. Therefore, a high injection pressure and high closing time are suggested with desirable outcome.

Table 2. Outcome Table

Experiment No.	Replicate #1	Replicate #2	Replicate #2
1	×	✓	×
2	×	×	×
3	×	×	×
4	×	×	×
5	×	×	×
6	×	×	×
7	×	×	×
8	×	×	×

The maximum injection pressure that the machine is capable of exerting is 2000 psi. It is not advisable to run the machine at its extreme. Therefore, for future optimization experiments, using an injection pressure of 1800 psi is suggested. The hold time did not significantly influence the outcome; therefore, using a hold time of 3 s is suggested to save on the processing time. The future optimization experiments are demonstrated in Table A.2. The closing time is varied as 25 s, 35 s, 45 s, and 55 s with three replicates molded in each experiment.

Table A.3. Experimental Design for Part#1-2520 Injection Molding

Experiment No.	Injection Pressure (psi)	Hold Time (s)	Closing Time (s)
9	1800	3	25
10	1800	3	35
11	1800	3	45
12	1800	3	55

Observations:

a. High injection pressure leads to formation of flash on the molded part.

b. As the closing time was increased, the nylon was hardening in the nozzle, therefore, increasing the process time.

To determine the parameters that gave desired results, the preliminary test was performed as discussed previously for the first experimental design. The outcome is shown in Table A.4.

Table A.4. Outcome Table

Experiment No.	Replicate #1	Replicate #2	Replicate #2
9	×	×	×
10	✓	✓	×
11	✓	×	✓
12	✓	✓	✓

Suggestions – Based on the outcome, it can be concluded that the closing time can be set to between 35 – 55 s depending on the allowable process time.

A.5 Injection Molding of a commercial part

The goals of this experiment were to injection mold Part #1-2516 (From Stahl Company) and optimize the process parameters. The client demanded the part to be hazy and not clear.

This part is made up of clear ABS (Figure A.1.30A). The Part#1-2516 was molded on VanDorn 120 Injection Molding Machine at Philpott Solutions, Aurora, OH. The nozzle temperature was set to 420 F. The hold pressure and hold time were reduced from 520 psi to 500 psi and 2 sec to 1 sec respectively to reduce the amount of flash obtained on the part. The cut off position time was reduced from 6 sec to 5 sec to prevent ABS from hardening at the nozzle. The shot size was increased from 1.1 in^2 to 1.5 in^2 since incomplete parts were molded at 1.1 in^2 injection volume. The boost speed was reduced from 2 in/s to 1.5 in/s and the boost pressure was increased from 800 psi to 900 psi in order to obtain a hazy part. However, after cooling, the part was not as hazy as required as seen in Figure A.1.31 (left). Therefore, the clear ABS

was mixed with an opaque ABS (Figure A.1.30B) in 80-20 wt% ratio to obtain the desired haziness, as seen in Figure A.1.31 (right).

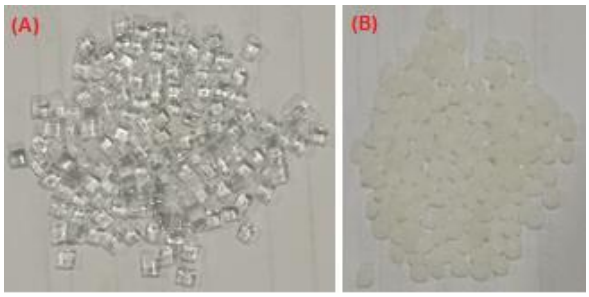

Figure A.1.30. (A) Clear ABS and (B) Opaque ABS

A.6 Vertical Injection Molding

The goal of this experiment was to injection mold putter heads for golf sticks on a vertical injection molding machine. The vertical injection molding machine has a polymer part is obtained. Coloured polyurethane pellets of 90 durometer shore hardness were used to make the putter heads. A low injection speed (2 in/min) was maintained to avoid attracting air bubbles inside the carriage and eventually the part. The nozzle temperature was maintained at 310 F.

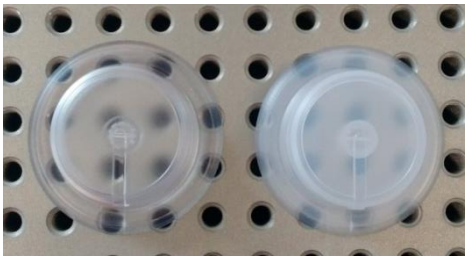

Figure A.1.31. Part# 1-2516. Left – Clear ABS, Right – Clear and Opaque ABS (80-20 wt% mixture)

A.7 3D scanning and PolyWorks

A.7.1 Scanning of a pump diaphragm

I used a 3D scanner to generate a point cloud of an object on PolyWorks software to obtain dimensions mentioned on the CAD model. My task was to figure out how to obtain all the dimensions on a pump diaphragm shown in Figure A.1.32.

Therefore, I first defined all the dimensions on the CAD Model in PolyWorks using "Features on cross-section" component (Figure A.1.33).

Figure A.1.32. A Pump Diaphragm – The Task Piece

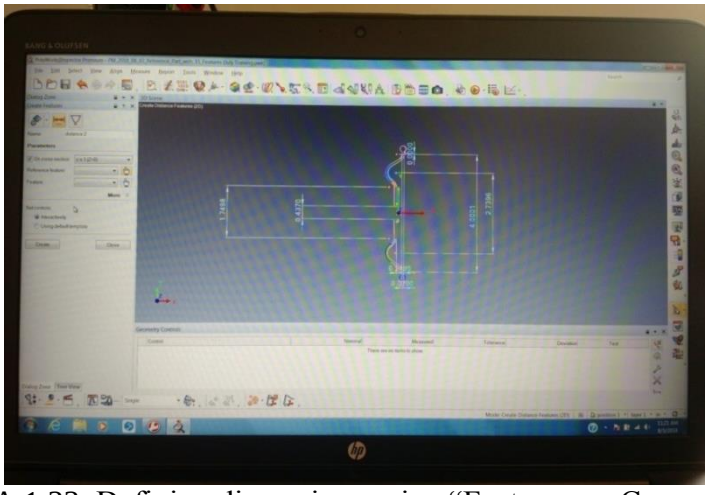

Figure A.1.33. Defining dimensions using "Features on Cross-section"

Then, I scanned the object (Pump Diaphragm) and fitted it over the CAD model and extracted all the measured components. The Figure A.1.34 shows the object fitted on the CAD Model.

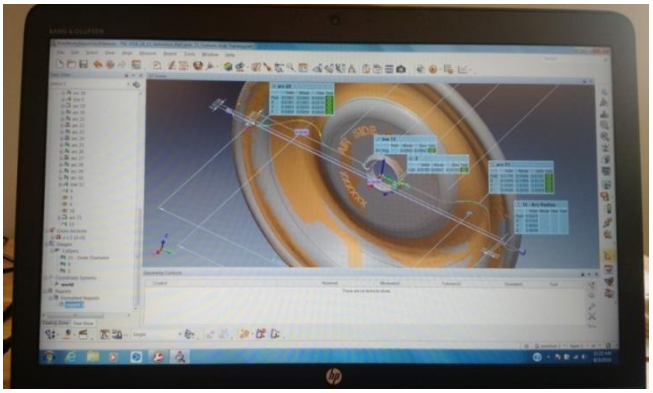

Figure A.1.34. Object (Data) fitted on the CAD model (Reference)

A source file which will extract the desired measurements from any given scan of the piece was created. All the components could not be measured from a single scan of the piece from one frame of reference. Therefore, 3 scans were obtained on a single piece with 3 different frames of references. These frames of references are presented in Figure A.1.35. 6 pieces were assigned to be inspected. Therefore, a total of 6 x 3 = 18 scans were generated with 18 detailed reports of the measurements. The measurements were tabulated in an attached excel file and were submitted to the company.

Few measurements at the curves were not able to extract from either scan 1, 2, and 3 on any piece. It was speculated that since the part 93465 and 93465-9 were shiny around the curved surface, the laser scanner was not able to construct a point cloud these surfaces which contributed to the curved surface measurements. Therefore, to mask the shine and mattify the surface of the pieces in order to obtain the measurements, all the pieces were spray coated with a thin layer of white paint on the insides. The outside surfaces of the pieces were not painted since it did not constitute the desired measurements. The pieces were air-dried for 30 minutes before obtaining their scan. Only scan 2 was obtained for all the coated 6 pieces; because the desired measurements could only be obtained through either scan 2 or 3, the easier to scan frame being scan 2, it was chosen. The measurements are tabulated in an attached excel file.

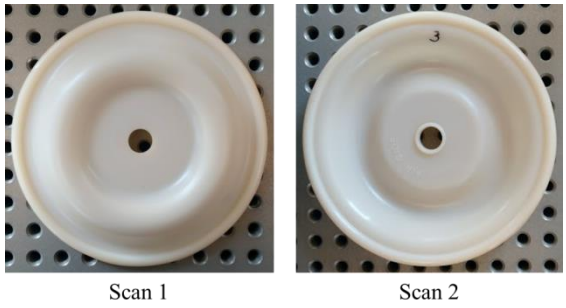
Scan 1

Scan 2


Scan 3

Figure A.1.35. Types of Scans obtained on piece 93465-9 (Santoprene Diaphragm)

A.7.2 Scanning of a commercial Part 1-2501:

I also worked on obtaining dimensions mentioned on the CAD model using PolyWorks software for parts on a portable t-shirt printing machine from Stahl's company (more information withheld due to privacy concerns). My task is to generate a file in PolyWorks with mentioned dimensions that can be extracted from a scanned object (using 3D Scanner).

I first defined all the dimensions on the CAD Model in PolyWorks using "Features on cross-section" component. Then, I scanned the object and fitted it over the CAD model and extracted all the measured components. A source file which will extract the desired measurements from any given scan of the piece was created. All the components could not be measured from a single scan of the piece from one frame of reference. Therefore, 2 scans were obtained on a single piece. These frames of references are presented in Figure A.1.36 and A.1.37.

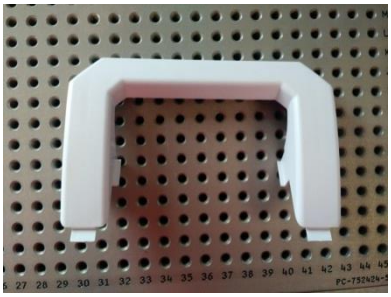

Figure A.1.36. Scan 1 obtained on the Heater Handle (Part #2501)

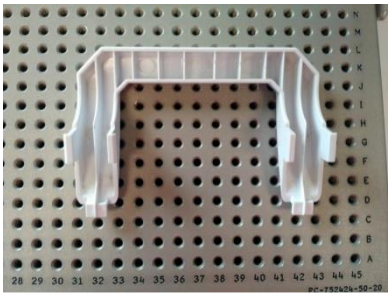

Figure A.1.37. Scan 2 obtained on the Heater Handle (Part #2501)

The objective of the next experiment was to obtain the scanned model of Stahl's part 1-2501 (Heater Handle), which is shown in Figure A.1.38, which was dyed in red color. It was previously observed that the laser scanner is unable to develop a scanned model for objects of red hue. During the current experiment, it was again observed that the laser scanner was not able to create a model for the red Part 1-2501.

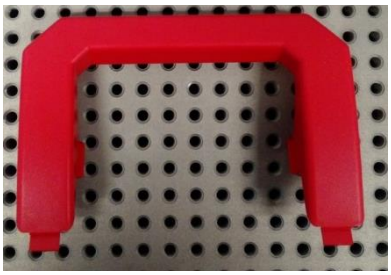

Figure A.1.38. Stahl's Part 1-2501 (Heater Handle)

A.7.3 Scanning of a commercial Part 1-2505

I used a 3D scanner to generate a point cloud of an object on PolyWorks software to obtain dimensions mentioned on the CAD model. My task was to figure out how to obtain all the dimensions on Part#1-2505. I cannot attach the CAD drawing due to privacy concerns. Therefore, I first defined all the dimensions on the

CAD Model in PolyWorks using “Features on cross-section” component. Then, I scanned the object and fitted it over the CAD model and extracted all the measured components. A source file which will extract the desired measurements from any given scan of the piece was created.

Only flatness measurement was desired from the scanned part, therefore, only one frame of reference was used to obtain the scan. These frames of references are presented in Figure A.1.39.

Fitting the data cloud on the CAD model could not measure the flatness. Therefore, “Extract Feature with Polygonal Model” feature was used through which a plane was defined on the cloud model. The flatness of this plane was measured to be

Figure A.1.39. Part #2505

0.0373” which is higher than the desired 0.01” flatness. This plane is shown in Figure A.1.40.

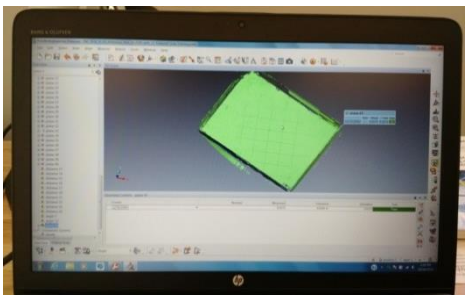

Figure A.1.40. Plane obtained on the cloud model Part #2505

A.7.4 Scanning of a commercial Part 1-2503 – Heater Latch

The objective of this experiment was to obtain the dimensions of Stahl’s Part 1-2503 (Heater Latch) using the laser scanner. Sample 1-4 were molded in China facility using nylon material (white dye) and sample 5 and 6 were molded in Aurora

facility. The China and Aurora samples were showing differences in fitting into the main prototype. The China samples were fitting easily and the Aurora samples were not. Hence, obtaining dimensions on both sets using calliper and laser scanner is desired. The samples are shown in Figure A.1.41 and their calliper measurements are shown in Table A.5. The scanner was also scanning the clipping plane along with the object. Therefore, the issue of eliminating clipping plane was also resolved. The clipping plane was scanned in entirety and was re-defined as the clipping plane in the

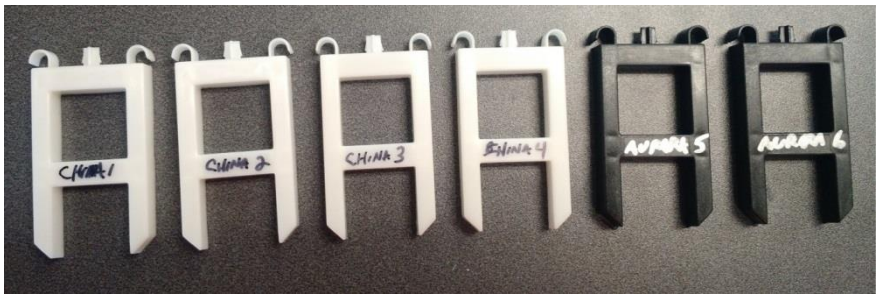

Figure A.1.41. Stahl's Part 1-2503

Table A.5. Measurements on Stahl's Part 1-2503

	Attribute	Dimension (in)	Lower Tolerance	Upper Tolerance	Sample 1 (China)	Sample 2 (China)	Sample 3 (China)	Sample 4 (China)	Sample 4 (China)	Sample 4 (China)
1	Length	2.52	2.51	2.53						
2	Recess	0.01	0.00	0.02						
3	Width	0.05	0.04	0.06						
4	Height	0.37	0.37	0.38	0.385	0.378	0.382	0.380	0.380	0.380
5	Length	2.71	2.70	2.72	2.728	2.718	2.735	2.729	2.739	2.739
6	Width	1.45	1.44	1.46	1.458	1.461	1.458	1.457	1.462	1.461
7	Width	0.95	0.94	0.96	0.967	0.965	0.960	0.961	0.967	0.967
8	Angle	45.0								
9	Width	1.580	1.570	1.590	1.564	1.566	1.579	1.578	1.575	1.579

program, in order for the scanner to avoid scanning the clipping plane while scanning the desired objects.

One of the key reasons that the black parts molded in Aurora facility is demonstrating difficulty in fitting in the black heater latch and keystone is that the material used for molding the white sample and the black sample have different shrink rates; the white dyed unfilled nylon material has a shrink rate of 1% while the glass filled black dyed nylon material has a shrink rate of 0.1%.

A.7.5 Calliper Measurement of Stahl's Part 1-2516

The objective of this experiment was to obtain the dimensions of Stahl's Part 1-2516 (Heater Cover) using a calliper. Sample 1 was molded in China facility using nylon material (white dye) and sample 2 was molded in Aurora facility. The China and Aurora samples were showing differences in fitting in the other parts (Part 1-2503, etc.). The China samples were fitting easily and the Aurora samples were not. Hence, obtaining dimensions on both sets using calliper and laser scanner is desired. The samples are shown in Figure A.1.42 and their calliper measurements are shown in Table A.6.

Figure A.1.42. Stahl's Part 1-2516

Table A.6. Measurements on Stahl's Part 1-2516

	Attribute	Sample 1 (China)	Sample 2 (Aurora)
1	Length (in)	13.525	13.605
2	Width (in)	10.491	10.572

A.7.6 Laser Scanning of commercial Part 1-2515 and 2522

Part 1-2515 (Frame Cover – Figure A.1.43A) is the cover for Part1-2522 (Swing Frame – Figure A.1.43B) in the Stahl's assembled prototype for the T-shirt printing machine. Both parts were injection molded at the Aurora facility. However, it was found that the cover fit loosely on the injection molded frame and it fit perfectly with a 3D printed frame. The frame was smaller for the cover. Therefore, the objective of this experiment was to determine the cause of this problem and offer a possible solution. In order to obtain an insight into the problem, both parts were scanned using a laser scanner and were fitted to the CAD models.

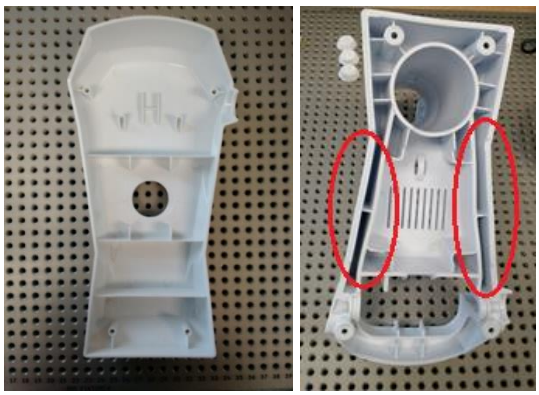

Figure A.1.43. (A) Stahl's Part 1-2515 (Frame Cover) and (B) Stahl's Part 1-2522 (Swing Frame – circled: observed warping) molded at the Aurora facility

Part 1-2515 was molded using ABS (acrylonitrile butadiene styrene) polymer and Part 1-2522 was molded using unfilled nylon polymer. One of the key reasons that the frame is demonstrating difficulty in fitting in the cover is that nylon and ABS

have different shrink rates. It can be observed from Figure A.1.43B that the frame has warped from the sides leading to shrinkage of the frame. Therefore, the frame fit loosely on the cover.

It was observed from the CAD model that the nominal angle for the side planes of the cover and the frame should be 17.081. The measured angle for the cover was determined as 17.000 and the measured angle for the frame was determined as 23.763 from their 3D scan presented in Figure A.1.44 and Table A.7. Therefore, the frame had side planes at a different angle confirming that the cover loosely fit on the frame due to non-uniform shrinkage.

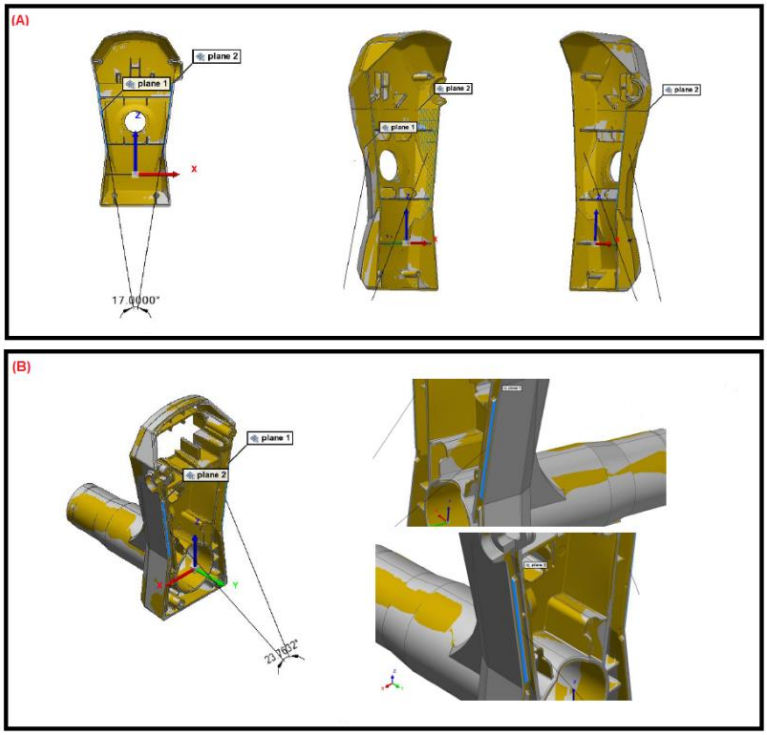

Figure A.1.44. 3D scanned and fit for (A) Stahl's Part 1-2515 and (B) Stahl's Part1-2522

Table A.7. Nominal and Measured Angle Values for the 3D scanned part

	Nominal Angle	**Measured Angle**
Part 1-2515 – Frame Cover	17.081	17.000
Part 1-2522 – Swing Frame	17.081	23.763

A.7.7 Laser Scanning of commercial Part 1-2502 and Part1-2521

The objective of this experiment was to obtain the dimensions of Stahl's Part 1-2502 (Heater Cover) using the 3D laser scanner. Sample 1 was molded in China facility using nylon material (white dye) and sample 2 was molded in Aurora facility. The China and Aurora samples were showing differences in fitting in the other parts (Heater Latch and Keystone). The China samples were fitting easily and the Aurora samples were not. Hence, obtaining dimensions on both sets using a laser scanner is desired. The Part 1-2502 was molded at different injection molding machines having different tonnage (440 and 220) and is shown in Figure A.1.45. The angle between the planes that are circled was calculated from the 3D scan since the fitting issue was felt along these planes. The keystone (Part 1-2521) was molded at the Aurora facility and is shown in Figure A.1.46 and was scanned using the laser scanner. The angle between the planes that are circled was calculated since the fitting issue was felt along these planes. Table A.8 provides the values of the measured angles calculated from these parts. Part 1-2521 was easily sliding into the Part 1-2502 molded with the 440T machine due to the wider angle between the planes of interest.

Figure A.1.45. Stahl's Part 1-2502 (Heater Cover)

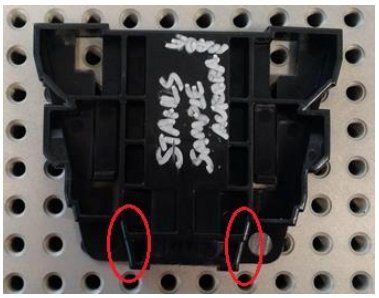

Figure A.1.46. Stahl's Part1-2521 (Keystone) molded at the Aurora facility

Table A.8. Nominal and Measured Angle Values for the 3D scanned parts molded at Aurora facility

	Nominal Angle	**Measured Angle**
Part 1-2502 – 440T	28.1422^{o}	36.1134^{o}
Part 1-2502 – 230T	28.1422^{o}	29.1481^{o}
Part 1-2502	28.1422^{o}	28.5004^{o}
Part 1-2521 – Keystone	28.1422^{o}	28.0139

One of the key reasons that the black parts molded in Aurora facility is demonstrating difficulty in fitting in the black heater latch and keystone is that the material used for molding the white sample and the black sample have different shrink rates; the white dyed unfilled nylon material has a shrink rate of 1% while the glass filled black dyed nylon material has a shrink rate of 0.1%.

APPENDIX B

LIST OF ABBREVIATIONS

2-HEDS	2-Hydroxyethyl disulphide
AcCl	Acetyl Chloride
Ac-FL-PEG-FL-Ac	Acrylated fluorescein labeled PEG
Br-PEG-Br	Poly(ethylene glycol)-dibromide/ bis(5-bromovalerate) poly(ethylene glycol)
Br-S-S-Br	bis(2-ethyl 4-bromobutanoate) disulfide
CALB	*Candida antartica* Lipase B
DCC	N,N'-Dicyclohexylcarbodiimide
DEE	Diethyl Ether
DMAP	4-dimethylaminopyridine
DMF	Dimethyl Formamide
DMSO	Dimethyl Sulfoxide
DODT	2,2'-(Ethylenedioxy)diethanethiol
DOE	Department of Energy
dPEG	Discreet Poly(ethylene glycol)
dPEG	Poly(ethylene glycol) (Đ = 1, M.W. = 898 g mol^{-1})
DTT	Dithiothreitol
EBB	Ethyl 4-bromobutyrate
EBV	Ethyl 5-bromovalerate

EDC	1-ethyl-3-(3-dimethylaminopropyl)carbodiimide
ESI	Electron Spray Ionization
EtOAc	Ethyl Acetate
FA	Folic Acid
FA-FL-PEG-FL-FA	Two-functional folate-targeted fluorescein-labeled poly(ethylene glycol) based conjugate
FA-Li	Lithiated Folic Acid
FA-SH	Thiol functionalized Folic Acid
FA-S-S-FA	FA-γ-bis(2-ethyl bromobutanoate) disulfide
FITC	Fluorescein isothiocyanate
FL	Fluorescein
FLA	Fluorescein-*o*-acrylate
FL-COOH	Fluorescin
FL-COOLi	Lithiated Fluorescin
FL-PEG-FL	Fluorescein-labeled Poly(Ethylene Glycol)
FR	Folate Receptor
H_2N-PEG-NH_2	Poly(ethylene glycol)-diamines/ bis(2-aminopropanoate) poly(ethylene glycol)/ bis(3-aminopropanoate) poly(ethylene glycol)
H_2O_2	Hydrogen Peroxide
HS-PEG-SH	Poly(ethylene glycol)-dithiol/ bis(3-mercaptopropionate) poly(ethylene glycol)
IgG	Immunoglobulin G
L-Al	L-Alanine
MALDI	Matrix Assisted Laser Desorption Ionization

MeOH	Methanol
MP-SH	Methyl 3-mercaptopropionate
n-BuLi	*n*-Butyllithium
NMR	Nuclear Magnetic Resonance
PAMAM	Poly(amido amine)
PEG	Poly(Ethylene Glycol)
R3P	Reversible Redox Ring Polymerization
SEFOSE	Sucrose Ester of Soybean Oil
*t*BOC	*tert*-Butyloxycarbonate
TEA	Triethylamine
TEG	Tetraethylene Glycol
THF	Tetrahydrofuran
TNBC	Triple Negative Breast Cancer
Tol	Toluene
UV	Ultra-Violet
β-Al	β-Alanine